2018

Improving efficiency of the load and resistance factor design of axially-loaded drilled shafts in bridge foundations

Philippe Kalmogo
Iowa State University

Improving efficiency of the load and resistance factor design of axially-loaded drilled shafts in bridge foundations

by

Philippe Kalmogo

A dissertation submitted to the graduate faculty

in partial fulfillment of the requirements for the degree of

DOCTOR OF PHILOSOPHY

Major: Civil Engineering (Structural Engineering)

Program of Study Committee:
Sri Sritharan, Co-major Professor
Jeramy Ashlock, Co-major Professor
Vernon Schaefer
Igor Beresnev
William Meeker

The student author, whose presentation of the scholarship herein was approved by the program of study committee, is solely responsible for the content of this dissertation. The Graduate College will ensure this dissertation is globally accessible and will not permit alterations after a degree is conferred.

Iowa State University

Ames, Iowa

2018

DEDICATION

The author would like to dedicate this dissertation to his parents and siblings for all their support, love, and continuous guidance, which were instrumental to the successful completion of this dissertation.

TABLE OF CONTENTS

Page

LIST OF FIGURES

Page

LIST OF TABLES

Page

ACKNOWLEDGMENTS

The research presented in this dissertation was conducted as part of two research projects funded by the Iowa Highway Research Board (IHRB) and the Midwest Transportation Center (MTC). I would like to express my sincere gratitude to Dr. Sri Sritharan and Dr. Jeramy Ashlock for providing me with this great opportunity to work on these projects and for their support, guidance, and advice along this learning journey. For agreeing to serve as members of my committee and for their assistance, I would like to thank Drs. Vernon Schaefer, Igor Beresnev, and William Meeker. Thank you also to the Iowa DOT Technical Advisory Committee including Ahmad Abu-Hawash, Dean Bierwagen, Lyle Brehm, Ken Dunker, Kyle Frame, Steve Megivern, Curtis Monk, Michael Nop, Gary Novey, John Rasmussen, and Bob Stanley. Finally, many thanks to Douglas Wood, Owen Steffens, and Zhao Cheng for their contribution to the successful completion of all the drilled shaft field load tests and Hasung Kim for his assistance with laboratory soil testing.

ABSTRACT

The Federal Highway Administration (FHWA) mandated utilizing the Load and Resistance Factor Design (LRFD) for all new bridges initiated in the United States after October 1, 2007. To achieve part of this goal, a database for Drilled SHAft Foundation Testing (DSHAFT) was developed and reported on by Garder, Ng, Sritharan, and Roling in 2012. Using the available data in DSHAFT, preliminary resistance factors were calibrated and proposed by Ng et al. (2014). Compared to the American Association of State Highway and Transportation Officials (AASHTO) LRFD Specifications, the preliminary locally-developed factors showed the potential for improved design efficiency. As additional load test data become available, resistance factors are expected to be recalibrated, thus the objective of this research was to utilize an expanded version of DSHAFT to refine and recommend final resistance factor values for implementation. To achieve this goal, the research examined recommendations given in AASHTO LRFD Bridge Design Specifications and the FHWA drilled shaft design guidelines and reviewed calibration studies conducted by Iowa and other states. Several challenges in the calibration process were identified, and it was found that a regional calibration can lead to resistance factors lower than code recommended values contrary to expectations. To overcome the main challenges in the resistance factor calibration associated with the lack of good quality load test data, the use of load test on small-scale drilled shafts as a cost-effective approach to predict load-deformation behavior of larger diameter shafts was investigated. A total of five instrumented reduced-scale drilled shafts were constructed and load tested to investigate scale effects and develop appropriate scaling relations. Test data seem to indicate that skin friction decreases with increasing shaft diameter. Additional research is needed to confirm the findings and develop a suitable methodology to extrapolate test results on smaller shafts to larger diameter shafts. The research also investigated the accuracy of the finite element method to predict load-deformation response of drilled shafts so that displacement criteria can be integrated in design. Simulation results showed that the Mohr-Coulomb is simple to implement using CPT data, and it can provide adequate predictions. Resistance factors were calibrated in accordance with AASHTO LRFD framework for various drilled shaft design methods

recommended by O'Neill and Reese (1999), Brown et al. (2010), and others. Two different procedures i.e., Approach I and Approach II were used in the calibration of skin friction resistance factors, with Approach II providing the highest resistance and efficiency factors.

CHAPTER 1. INTRODUCTION

Drilled shafts, also known as drilled piers, caissons, or bored piles, are a type of deep foundation constructed by excavating a cylindrical hole in the ground and constructing a cast-in place reinforced concrete column within the hole. They can be used in various type of structures including but not limited to bridges, buildings, retaining structures, and transmission lines. Drilled shafts offer several advantages over other types of deep foundation such as driven piles, micropiles, or continuous flight auger piles. Due to their relatively larger size, they provide much higher axial and lateral resisting forces through a combination of skin friction and end bearing. A single drilled shaft may oftentimes replace a group of several piles, thus eliminating the need for a pile cap. Under certain circumstances such as cohesive soils with deep groundwater, deep scour conditions, and sites with restricted access or low conditions, drilled shafts are easier to construct, and they can be very cost effective.

1.1 Design Approach

Uncertainties are inherent part of engineering designs. Over the years, engineers have developed various strategies to account for these uncertainties and incorporate them in the design process of man-made structures. In the geotechnical engineering field, designers have, in the past, used a factor of safety (FS) consistent with the traditional Allowable Stress Design (ASD) framework to account for design uncertainties and provide a margin of safety against adverse performance of substructure systems. In the ASD philosophy, both load and resistance uncertainties are lumped into a single factor of safety that is selected based on the design methodology, successful past practices, and the designer's subjective engineering judgment. However, various types of load and resistance have different levels of variability and uncertainty, and the ASD philosophy can lead to over-conservatism as well as inconsistent and unreliable structures performance. The limitations of the ASD approach have been long recognized, and the Load and Resistance Factor Design (LRFD) was developed to better quantify design uncertainties.

The introduction of the LRFD approach in the early 80's alleviated the shortcomings associated with the ASD philosophy. The LRFD approach recognizes that both load and

resistance are independent random variables with associated probability of occurrence. Therefore, anticipated foundation loads are multiplied by appropriate load factors usually greater than unity while the resistance components are multiplied by resistance factors less than unity such that the resulting design satisfies a given limit state. A limit state is defined as a condition beyond which the foundation no longer satisfies its intended function. While limit states that should be considered include service limit state, strength limit state, extreme limit state, and fatigue limit state, only the first two are involved in typical foundation design. Load factors and resistance factors are selected to achieve a target probability of failure depending on the foundation type and level of redundancy in the system. LRFD has several advantages compared to ASD. Contrary to ASD, LRFD separates load uncertainties from resistance uncertainties. Additionally, the use of load factors and resistance factors established from probability-based reliability analyses as opposed to a factor of safety results in more consistent levels of reliability in both substructure and superstructure designs.

In drilled shaft design, static design methods of empirical or semi-empirical nature are generally used to determine the shaft size, embedment length, and tip elevation required to transfer the superstructure loads to the ground. While some states have developed local design methods using load test data that better reflect local geologic conditions and construction practices, most design agencies routinely use the American Association of State Highway and Transportation Officials (AASHTO) LRFD Bridge Design Specifications recommended methods, which are based on the work of O'Neill and Reese (1999) and Brown et al. (2010). Several design methods are available depending upon the geomaterial type, and they require properties that may be determined from laboratory tests on field-collected soil/ rock samples or correlated to in-situ test results.

In a typical design process, the subsurface at the planned drilled shaft location is divided into several idealized geomaterial layers using appropriate soil boring logs from subsurface investigation, and the different layers are classified as either cohesive soil, cohesionless soil, Intermediate Geomaterial (IGM), or Rock. For drilled shaft design purposes, cohesive soils are geomaterials with undrained shear strength less than 5 ksf, and they include clayey sands and gravels, lean fat clay soils, and silts with liquid limit over 50. Cohesionless soils include gravels and sands with less than 5 percent fines, gravels and sands

with silty fines, and non-plastic silts. Rocks are defined as high strength cohesive cemented geomaterials with unconfined compressive strength greater than 100 ksf. IGMs are geomaterials with strength characteristics transitional between soil and rock. They can be categorized as either cohesive or cohesionless. Cohesive IGMs are geomaterials with unconfined compressive strength ranging between 10 ksf and 100 ksf while cohesionless IGMs are considered to be very dense granular geomaterials with Standard Penetration (SPT) blow count number between 50 and 100. After the subsurface profile has been discretized and strength properties assigned to each zone, appropriate design methods are selected to estimate the nominal side and base resistance of each geomaterial layer. Once nominal resistances are determined, the designer must select either the ASD or LRFD approach to account for uncertainties in the anticipated loads and resistances. Despite the advantages of LRFD over ASD, its adoption by the geotechnical engineering community has been extremely slow due to several reasons including but not limited to the reluctance to change from the community of practicing engineers accustomed to ASD and perhaps more importantly from the lack of quality load test databases necessary for the calibration of resistance factors.

To push for the transition from ASD to LRFD for foundation design, the Federal Highway Administration (FHWA) issued a mandate in 2000 that stipulated the use of LRFD for all federally-funded bridges designed after October 1, 2007. To facilitate this transition, LRFD design guidelines for deep foundations were developed and presented in AASHTO LRFD Bridge Design Specifications based on the work of Barker et al. (1991), Paikowsky et al. (2004), and Allen (2005). However, resistance factors recommended in previous and current editions of the AASHTO code suffer from a few limitations. Since the guidelines were established for use at a national scale, resistance factors were developed and recommended only for selected design methods. Local design methods used by some DOTs were not covered by the specifications. Moreover, resistance factors associated with some geomaterials and corresponding design methods were determined by fitting to ASD factor of safety due to the lack of proper load test data needed for a reliability-based calibration, which defeats the fundamental goal of LRFD to achieve consistent levels of reliability. Where sufficient reliable data was available for reliability analyses, the final selected values was adjusted using engineering judgment to reflect successful past practices, thereby modifying

the target reliability that the calibration was designed to achieve. Additionally, the load test database used for reliability analyses included test data from various regions with different soil conditions and construction practices. As a result of this variability, AASHTO recommended factors have led to unnecessary conservative designs at the local level as indicated by Moore (2007). Considering these shortcomings and to improve design efficiency, the use of higher resistance factors was allowed by the FHWA, on the condition that these higher values are supported by local load test data and determined in a manner consistent with the AASHTO LRFD framework.

1.2 Iowa Regional LRFD Calibration

The Iowa Department of Transportation's efforts to comply with the FHWA mandate to use LRFD procedures for bridge design was initiated with the regional calibration of resistance factors for driven piles. A database of 264 local load tests known as PILOT-IA (Pile Load Tests in Iowa) was developed in an IDOT research project and used in the calibration of resistance factors for clay, sand, and mixed soil conditions using various static design methods (Sritharan et al., 2010). Ten additional instrumented load tests were also performed to verify the calibrated resistance factors. Compared to code recommendations, the resulting driven-pile LRFD calibration resulted in higher resistance factors and efficiencies, and significant driven pile foundation cost savings. Given the success of the regional calibration of resistance factors for driven piles, a similar endeavor was initiated for drilled shafts in subsequent and ongoing IDOT research projects.

To overcome the deficiencies associated with code recommendations for LRFD of drilled shafts, a research plan composed of three phases was devised by researchers at Iowa State University. In phase I of the project, an electronic database of load tests collected from Iowa and several neighboring states was developed by Garder et al. (2012). Available information on 32 drilled shaft load tests were collected, reviewed, and integrated into a Microsoft Office Access™ based Database for Drilled SHAft Foundation Testing (DHSAFT). The resulting database included 29 Osterberg cell (O-cell) load tests and 3 statnamic load tests. Preliminary reliability analyses were then performed on the 13 load tests from Iowa by Ng et al. (2012), and the calibrated resistance factor is presented in Table 1.1 along with those recommended by AASHTO.

The calibrated resistance factor of 0.66 was higher than all values recommended by AASHTO. However, it should be noted that the resistance factor was calibrated based on a total resistance (skin friction + end bearing) scheme.

Table 1.1: Summary of AASHTO and Regionally Calibrated Resistance Factors (Ng et al. 2012)

Soil Type	Shaft/Toe Resistance	Resistance Factor (φ) for β_T=3.00	
		AASHTO	DSHAFT
Clay	Shaft	0.45	0.66 (based on total resistance)
	Toe	0.40	
Sand	Shaft	0.55	
	Toe	0.50	
Rock	Shaft	0.50-0.55	
	Toe	0.50	
Intermediate Geomaterial (IGM)	Shaft	0.60	
	Toe	0.55	

Additionally, no distinction was made between geomaterial types, thus the individual reliability of each design method is not reflected in the calibrated resistance factor. Nonetheless, the calibration results showed that a calibration at the regional level can potentially improve resistance factors for the design of drilled shafts in axial compression, thus resulting in safer, more reliable, and cost-effective designs.

To further investigate this potential during Phase II of the project, the database was expanded with 9 additional usable O-cell load tests for further calibration. Because of missing key information such as boring logs and soil/rock strength parameters, 13 additional load tests were deemed unusable in the statistical analyses. Additionally, the majority of the load tests in DSHAFT were terminated at relatively small shaft displacements or before full mobilization of the shaft resistance. Therefore, the ultimate resistance, or the shaft resistance at the chosen displacement failure criterion, could not be determined from Loadtest's procedure for constructing the equivalent top load-displacement curve.

To overcome this challenge, three different procedures for extrapolating the shaft top load-displacement curve were established by Ng. et al. (2014). These procedures were used

to generate complete load-displacement curves that allowed resistance factors to be calibrated at specific shaft top displacement criteria, including 1 inch which is used by IDOT as a strength limit state at 2.5 times the service load, and a top displacement equal to 5% of the shaft diameter which is recommended in AASHTO (2010) as an ultimate limit state. Resistance factors were determined for each geomaterial type and for individual resistance components, i.e. skin friction and end bearing.

Calibrated resistance factors for side resistance are presented in Table 1.2 along with those recommended by AASHTO (2010), NCHRP 343 (Barker et al. 1991), NCHRP 507 (Paikowsky et al. 2004) and NHI (Allen 2005). Resistance factors were calibrated at three different failure criteria including load test criterion, Iowa DOT 1 inch top displacement, and the AASHTO criterion of 5 % of the shaft diameter. Since resistance factors were only calibrated at the AASHTO criterion of 5 % of the shaft diameter in other studies, direct comparison could only be made for this particular case. The calibrated resistance factor for side resistance in clay using the α-method was much lower compared to other recommended values regardless of the failure criterion. At the AASHTO failure criterion, the calibration resulted in a 51% decrease compared to the AASHTO value. Calibrated factors for side resistance in sand using the β-method were also lower. Compared to AASHTO, a 17% decrease resulted from the calibration. For side resistance in IGM using the modified α-method, the calibration resulted in higher resistance factors compared to other recommended values, including an increase of 13% compared to AASHTO. The regional resistance factor for side resistance in rock was calibrated using the Horvath and Kenney (1979) method. The calibrated factor of 0.62 was higher than the AASHTO-recommended value of 0.55 which is based on a calibration by fitting to the ASD factor of safety. The efficiency factor value of 0.53 shows that the Horvath and Kenney (1979) method would result in a more economical design compared to the Carter and Kulhawy (1988) method used in NCHRP 507.

Because of insufficient data, a resistance factor could not be calibrated for end bearing in clay. For end bearing in sand, the calibration resulted in a resistance factor of 0.75 which is an improvement over the value of 0.50 recommended by AASHTO.

Table 1.2: Comparison of Resistance Factors for Unit Side Shear Resistance (Ng et al. 2014)

Geo material	Failure Criteria	Resistance Factors for β_T = 3.00, φ					φ/λ	
		NCHRP 343[e]	NCHRP 507[b]	NHI 05-052[a]	NHI 05-052[c]	AASHTO (2010)[d]	DSHAFT	DSHAFT
Clay	LTR	n/a	n/a	n/a	n/a	n/a	0.31	0.15
	1-in Δ	n/a	n/a	n/a	n/a	n/a	0.20	0.11
	5% D for Δ	0.65	0.36 (φ/λ: 0.41)	0.55	0.60	0.45	0.22	0.12
Sand	LTR	n/a	n/a	n/a	n/a	n/a	0.47	0.34
	1-in Δ	n/a	n/a	n/a	n/a	n/a	0.48	0.54
	5% D for Δ	n/a	0.31 (φ/λ: 0.28)	0.55	n/a	0.55	0.47	0.53
IGM	LTR	n/a	n/a	n/a	n/a	n/a	0.66	0.26
	1-in Δ	n/a	n/a	n/a	n/a	n/a	0.63	0.30
	5% D for Δ	n/a	0.51 (φ/λ: 0.41)	0.55	n/a	0.60	0.69	0.32
Rock	LTR	n/a	n/a	n/a	n/a	n/a	0.57	0.39
	1-in Δ	n/a	n/a	n/a	n/a	n/a	0.55	0.49
	5% D for Δ	0.65	0.38[f] (φ/λ: 0.32)	0.55	0.55	0.55	0.62	0.53

[a] – calibration by fitting to ASD; [b] – calibration performed using reliability theory (FORM); [c] – calibration performed using reliability theory (Monte Carlo Method); [d] – selected value among NCHRP 343, NCHRP 507 and Allen (2005); [e] – recommended value; [f] – based on Carter and Kulhawy (1988); LTR – load test report criterion; n/a – not available; Δ – shaft top displacement; D – shaft diameter.

The efficiency of 0.44 for this case was also higher than the maximum value of 0.32 achieved in NCHRP 507. Resistance factors for end bearing in IGM and rock are presented in Table 1.3 and Table 1.4, respectively. Resistance factors were calibrated for various design methods. In the case of IGM, the calibration resulted in unrealistic resistance factors for the Goodman (1980), Carter & Kulhawy (1988) and Sowers (1979) design methods. Because these methods consistently underestimated the actual measured resistance, their corresponding resistance factors were greater than unity. For the O'Neill & Reese (1999) method, the calibrated resistance factor of 0.20 and corresponding efficiency of 0.21 were much lower than the values recommended by NCHRP 507 and AASHTO. The Proposed Method of Ng et al. (2014) is an average of the Rowe and Armitage (1987) and Carter & Kulhawy (1988) methods, and was the most efficient design method with a calibrated resistance factor of 0.85 and efficiency of 0.62 at the AASHTO failure criterion.

Table 1.3: Comparison of resistance factors of end bearing in IGM (Ng. et al. 2014)

	Analytical Method	Resistance Factors for β_T = 3.00, φ				φ/λ
		NCHRP 507[(a)]	NHI 05-052[(b)]	AASHTO (2010)[(c)]	DSHAFT	DSHAFT
LTR	Rowe & Armitage (1987)	n/a	n/a	n/a	0.32	0.29
	Goodman (1980)	n/a	n/a	n/a	1.27	0.28
	Terzaghi (1943)	n/a	n/a	n/a	0.29	0.26
	Carter & Kulhawy (1988)	n/a	n/a	n/a	1.46	0.17
	Sowers (1979)	n/a	n/a	n/a	0.67	0.24
	O′Neill & Reese (1999)	n/a	n/a	n/a	0.15	0.18
	Proposed Method	n/a	n/a	n/a	0.59	0.47
1-in Δ	Rowe & Armitage (1987)	n/a	n/a	n/a	0.32	0.33
	Goodman (1980)	n/a	n/a	n/a	1.41	0.35
	Terzaghi (1943)	n/a	n/a	n/a	0.24	0.23
	Carter & Kulhawy (1988)	n/a	n/a	n/a	1.71	0.22
	Sowers (1979)	n/a	n/a	n/a	0.64	0.27
	O′Neill & Reese (1999)	n/a	n/a	n/a	0.17	0.22
	Proposed Method	n/a	n/a	n/a	0.64	0.58
5% D for Δ	Rowe & Armitage (1987)	n/a	n/a	n/a	0.44	0.36
	Goodman (1980)	n/a	n/a	n/a	1.86	0.36
	Terzaghi (1943)	n/a	n/a	n/a	0.49	0.39
	Carter & Kulhawy (1988)	n/a	n/a	n/a	3.04	0.30
	Sowers (1979)	n/a	n/a	n/a	1.06	0.33
	O′Neill & Reese (1999)	0.57 to 0.65 (φ/λ: 0.44 to 0.48)	0.55	0.55	0.20	0.21
	Proposed Method	n/a	n/a	n/a	0.85	0.62

(a) – calibration performed using reliability theory (FORM); (b) – calibration by fitting to ASD; (c) – selected value among NCHRP 343, NCHRP 507 and Allen (2005); LTR – load test report criterion; n/a – not available; Δ - shaft top displacement; D – shaft diameter.

For end bearing in rock, comparison could only be made for the Carter & Kulhawy (1988) design method. The calibrated resistance factor of 0.31 and corresponding efficiency of 0.31 were lower than other recommended values. Similar to end bearing in IGM, the Proposed Method of the Phase II study was the most efficient design method with a resistance factor of 0.71 and an efficiency of 0.68. Using the previous calibration results as a foundation consistent with the goal to continuously refine and improve the regionally-calibrated drilled shaft resistance factors, this project aims at further and more detailed calibrations by expanding the DSHAFT database with 8 additional usable O-cell load tests. The new calibrations will serve as a verification of the preliminary resistance factors, and will enable recommendation of adjustments or improvements where necessary. In addition to the new

calibrations, an alternative to the O-cell load test procedure for field verification of drilled shaft capacity will be investigated as part of this research.

Table 1.4: Comparison of resistance factors of end bearing in rock (Ng. et al. 2014)

Failure Criteria	Analytical Method	Resistance Factors for β_T = 3.00, φ				φ/λ
		NCHRP 507[a]	NHI 05-052[b]	AASHTO (2010)[c]	DSHAFT	DSHAFT
LTR	Rowe & Armitage (1987)	n/a	n/a	n/a	0.11	0.38
	Goodman (1980)	n/a	n/a	n/a	0.28	0.24
	Terzaghi (1943)	n/a	n/a	n/a	0.15	0.18
	Carter & Kulhawy (1988)	n/a	n/a	n/a	0.19	0.04
	Sowers (1979)	n/a	n/a	n/a	0.28	0.38
	O′Neill & Reese (1999)	n/a	n/a	n/a	0.25	0.39
	Proposed Method	n/a	n/a	n/a	0.11	0.18
1-in Δ	Rowe & Armitage (1987)	n/a	n/a	n/a	0.10	0.30
	Goodman (1980)	n/a	n/a	n/a	0.30	0.22
	Terzaghi (1943)	n/a	n/a	n/a	0.13	0.13
	Carter & Kulhawy (1988)	n/a	n/a	n/a	0.22	0.04
	Sowers (1979)	n/a	n/a	n/a	0.26	0.30
	O′Neill & Reese (1999)	n/a	n/a	n/a	0.22	0.29
	Proposed Method	n/a	n/a	n/a	0.36	0.41
5% D for Δ	Rowe & Armitage (1987)	n/a			0.16	0.38
	Goodman (1980)	n/a			0.42	0.25
	Terzaghi (1943)	n/a			0.22	0.19
	Carter & Kulhawy (1988)	0.45 to 0.49 (φ/λ: 0.37 to 0.38)	0.55[d]	0.50[d]	0.31	0.04
	Sowers (1979)	n/a			0.40	0.38
	O′Neill & Reese (1999)	n/a			0.35	0.40
	Proposed Method	n/a			0.71	0.68

(a) – calibration performed using reliability theory (FORM); (b) – calibration by fitting to ASD; (c) – selected value among NCHRP 343, NCHRP 507 and Allen (2005); (d) – based on Canadian Geotechnical Society (1985); LTR – load test report criterion; n/a – not available; Δ - shaft top displacement; D – shaft diameter.

1.3 Drilled Shaft Field Load Testing

Because of their high load carrying capacity, the number of drilled shafts required in a bridge foundation system is generally lower than that of other types of deep foundation such as driven piles. The loss of redundancy that results from using a single drilled shaft in place of a pile group requires a more precise and accurate prediction of drilled shaft foundation capacity. However, accurate prediction of drilled shaft performance under service and strength limit states using established static design methods is a difficult task due to the significant influences of local geology, resulting soil properties, and construction procedures

on drilled shaft behavior. To ensure that design requirements are met and that necessary adjustments can be made if needed, the Iowa DOT routinely performs a capacity verification through a load test on a full-scale demonstration shaft constructed at the actual bridge site. Field loading tests offer the potential to obtain detailed information on load transfer characteristics for both side and base resistance, reduce variabilities associated with drilled shaft design methods, and justify the use of higher resistance factors in the LRFD framework. Field verification of drilled shaft resistance can be accomplished using conventional top-down load tests, bi-directional pressurized O-cell tests, Statnamic (rocket propelled impulse) test, or high strain dynamic test.

Due to its popularity and advantages over conventional top down load tests, the bi-directional load test method has been the primary testing method for several DOTs including Iowa. The O-Cell is a bi-directional hydraulic jack-like device constructed at a predetermined depth inside the shaft. As hydraulic pressure inside the cell is increased, the cell expands and loads both portions of the shaft above and below the O-cell. The portion of the shaft above the load cell moves upward and is resisted by downward skin friction, while the portion below the shaft moves downward and is resisted by upward skin friction and upward end bearing. The skin friction and the end bearing can thus be measured separately if the O-cell is placed at the very end of the shaft. Instrumentation along the shaft allows the quantification of the resistance along different shaft segments. Compared to conventional top down load test, O-cell load testing can achieve much higher loads. Additionally, the use of an O-cell eliminates the need for a reaction frame which becomes increasingly expensive and impractical as the required load on the foundation increases.

Despite these advantages, bi-directional load testing has a few limitations. The goal to mobilize the full capacity in both portions of the shaft above and below the O-cell is almost never attained due to the difficulty of predicting the accurate location of the O-cell for a balanced failure. In most cases, full mobilization is only achieved either below or above the O-cell, which halts movement of the opposing shaft section thus limiting its mobilized resistance. Since drilled shafts are designed to limit the movement of the superstructure to a specific value, designers are generally more concerned in obtaining the top load-deformation characteristics of the entire shaft. Upward and downward load-displacement curves obtained

from O-cell load testing can be converted to an equivalent top-down load-displacement curve. However, because failure is rarely achieved in both loading directions, the Loadtest's procedure for constructing the equivalent top load-displacement curve requires extrapolation of the resistance in the non-failed region, which introduces some uncertainties. Additionally, the procedure cannot establish the resistance transferred in each soil layer along the shaft for a given shaft top displacement. Only t-z analyses using collected data from the strain gauges installed along the shaft can yield such information, which is highly valuable for resistance factor calibration studies.

Although bi-directional load testing has been a more cost-effective field verification method for drilled shaft performance compared to conventional top-down load testing, its inability to provide complete shaft load-displacement characteristics has been one of the major obstacles to the regional calibration of drilled shaft resistance factors. Resistance factor calibration requires known resistance at target shaft top displacements which are not always available from bi-directional load test results. Although extrapolation methods available in the literature can be used to alleviate this issue, they introduce additional uncertainties that may not be quantifiable into the calibration process. To overcome the limitations associated with bi-directional load testing for drilled shaft resistance factor calibration, a new alternative will be evaluated as part of this research. This alternative consists in conducting more economical conventional top down-load tests on small diameter shafts and developing scaling relations to predict the behavior of larger diameter shafts.

1.4 Scope of Research

A careful review of current code specifications for LRFD of drilled shafts was conducted for this study, and revealed several limitations associated with the recommended resistance factors. The procedure used to establish these resistance factors does not fully comply with the fundamental goal of LRFD to achieve a consistent target reliability across all substructure and superstructure designs. Additionally, resistance factors were calibrated for use at the national level, and they may not always result in efficient designs at the state level due to differences in local soil conditions and construction techniques. Several limitations of the bi-directional load test using O-cell as a field verification method for drilled shaft performance and for resistance factor calibration were also highlighted. Given the

shortcomings of the code current LRFD specifications for drilled shafts, the overall scope of the research herein is to improve the design efficiency of axially-loaded drilled shafts at Strength Limit State I by developing regional resistance factors using a database of local load tests. The regional factors should be consistent with the core goal of LRFD, and they should account for the effect of local soil conditions and construction practices. To accomplish this goal, the proposed research focuses on the following objectives:

1. Conduct a thorough investigation of the history of AASHTO-recommended resistance factors for LRFD of drilled shafts in axial compression. The review will help to provide an understanding of the origins of the resistance factors provided in previous and current editions of the AASHTO Bridge Design Specifications. Assumptions made in the LRFD calibration of these factors will be highlighted to illustrate their limitations and to emphasize the need for regionally calibrated resistance factors. The review will also cover regional calibration studies conducted by other States.
2. Identify major challenges in the resistance factor calibration process that may prevent full realization of expected outcomes.
3. Evaluate new load test data and expand DSHAFT.
4. Evaluate acceptable means of extrapolating and using load test data.
5. Devise and execute conventional top-down load tests on five reduced-scale drilled shafts to investigate the dependency of skin friction on drilled shaft diameter.
6. Develop a more economical drilled shaft field testing method that will provide more conclusive results compared to O-cell load tests by fully mobilizing shaft resistance. This objective will be achieved by developing scaling relations from the reduced-scale shaft test outcomes that will allow prediction of the load-deformation behavior of larger size shafts.
7. Investigate the accuracy of the finite element method at predicting drilled shaft load-deformation response in order to enable incorporation of a displacement criteria in design.
8. Using an expanded version of DSHAFT, perform a calibration consistent with the current LRFD framework to refine preliminary resistance factors previously established by Ng. et al. (2014). Where appropriate, the calibrated factors will be

compared to those recommended in current AASHTO LRFD Specifications and other studies, and final values will be recommended for implementation.

1.5 Thesis Outline

Following the introduction, a comprehensive review of both ASD and LRFD philosophies and their underlying basic principles is presented in Chapter 2 of this thesis. Steps necessary for the regional resistance factor calibration are discussed along with available reliability analyses methods. Analytical methods available for drilled shaft capacity prediction and field capacity verification are also detailed. Finally the review is concluded with a discussion of calibration studies conducted by other states.

The next four chapters constitute a series of articles to be submitted for publication in peer-reviewed journal papers in the field of geotechnical engineering. Chapter 3 discusses the practicability of drilled shaft resistance factor calibration at the regional level and challenges that are likely to be encountered. Chapter 4 details the construction and load testing of five small-scale drilled shafts for the experimental investigation of the effect of scale on drilled shaft skin friction. Chapter 5 investigates the use of the finite element method to predict load-deformation response of drilled shafts and facilitate displacement-based design. In Chapter 6, the LRFD framework is implemented to develop regional resistance factors using the expanded version of DSHAFT. Chapter 7 provides a summary of the different tasks accomplished, major results, and recommendations for future work.

1.6 References

AASHTO LRFD Bridge Design Specifications (2007). Customary U.S. Units, 4th edition, 2008 Interim, Washington, D.C.

AbdelSalam, S. S., K. W. Ng, S. Sritharan, M. T. Suleiman, and M. Roling. (2012). *Development of LRFD Procedures for Bridge Pile Foundations in Iowa, Volume III: Recommended Resistance Factors with Consideration of Construction Control and Setup*. TR-584, Iowa Highway Research Board, Ames, IA.

Allen, T. M. (2005). *Development of Geotechnical Resistance Factors and Downdrag Load Factors for LRFD Foundation Strength Limit State Design*. FHWA-NHI-05-052, Federal Highway Administration, U.S. DOT, Washington, DC.

Barker, R. D., J. K. Rojiani, O. P. Tan, and S. C. Kim. (1991). *NCHRP Report 343: Manuals for the Design of Bridge Foundations*. Transportation Research Board, National Research Council, Washington, D.C.

Brown, D. A., J. P. Turner, and R. J. Castelli (2010). *Drilled Shafts: Construction Procedures and LRFD Design Methods*. NHI Course No. 132014, Geotechnical Engineering Circular No. 10, National Highway Institute, U.S. Department of Transportation, Federal Highway Administration, Washington, D.C.

Garder, J., K. W. Ng, S. Sritharan, and M. Roling (2012). *An Electronic Database for Drilled Shaft Foundation Testing (DSHAFT)*. Final Report to Iowa Department of Transportation. Institute for Transportation, Iowa State University, Ames, IA.

Paikowsky, S. G. with contributions from B. Birgisson, M. McVay, T. Nguyen, C. Kuo, G. Baecher, B. Ayyub, K. Stenersen, K. O'Malley, L. Chernauskas, and M. O'Neill. (2004). *Load and Resistance Factor Design (LRFD) for Deep Foundations*. National Cooperative Highway Research Program (NCHRP) Report number 507, Transportation Research Board, Washington D.C.

Schmertmann, J. H., J. A. Hayes. (1997). The Osterberg Cell and Bored Pile Testing- A Symbiosis. *The Third International Geotechnical Engineering Conference,* Cairo University, Egypt.

CHAPTER 2. LITERATURE REVIEW

The following sections provides a comprehensive review of the principles underlying ASD and LRFD approaches in foundation design as well as their major differences. A complete description of the resistance factor calibration including available reliability methods is also presented. The review also covers the various static design and load testing methods used for drilled shaft capacity prediction and field verification.

2.1 ASD vs. LRFD in Foundation Design

Uncertainties are inherent part of drilled shafts design. They stem from various sources and may lead to variability in the drilled shafts anticipated loads and resistances. Consequently, engineers have, over the years, developed various strategies to account for the unknowns and provide a margin of safety against undesired performance defined whether in terms of excessive settlement or complete geotechnical failure. Historically, a factor of safety was used in the ASD framework to ensure that drilled shafts applied loads were always less than the available resistance regardless of any variation during the design life of the structure as shown in Figure 2.1. The factor of safety used in the ASD framework was selected based on the design method used, successful past practices, and the designer's engineering judgment. Despite its simplicity, this approach could not guarantee a consistent level of reliability across designs due its inability to accurately and quantitatively account for the different levels of uncertainty associated with the load and resistance variable.

LRFD overcomes the major limitation associated with ASD by providing a more rational approach to quantify and account for all sources of uncertainty involved in the design process. As illustrated by the basic LRFD Eq. (2.1), uncertainties associated with various types of load and resistance at a given limit state can be taken into account by load and resistance factors, respectively. In LRFD, the load and resistance are treated as independent random variables with some probability of occurrence (Figure 2.2). Using their known variabilities, the load and resistance factors can be calibrated to ensure that the probability of factored loads exceeding the available resistance is at an acceptable level. This failure region, represented by the shaded area in Figure 2.2, is related to a reliability index, β, which value must be specified in the calibration process.

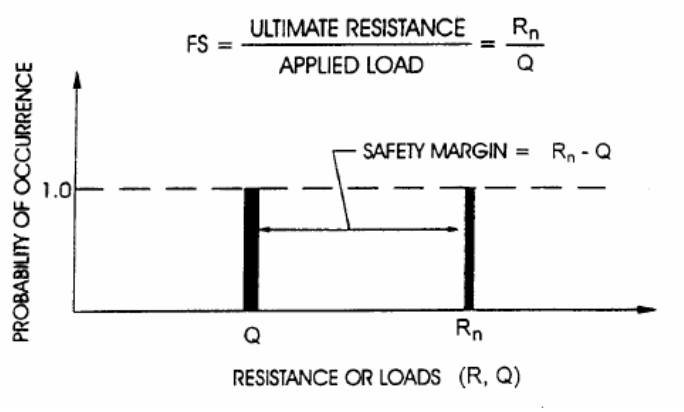

Figure 2.1: ASD Principle (Withiam et al., 1998)

$$\sum \gamma_i Q_i \leq \varphi R_n \tag{2.1}$$

where,

Q_i = Load type i (e.g. dead load, live load etc.)

γ_i = Factor for load type i

R_n = Nominal resistance

φ = Resistance factor

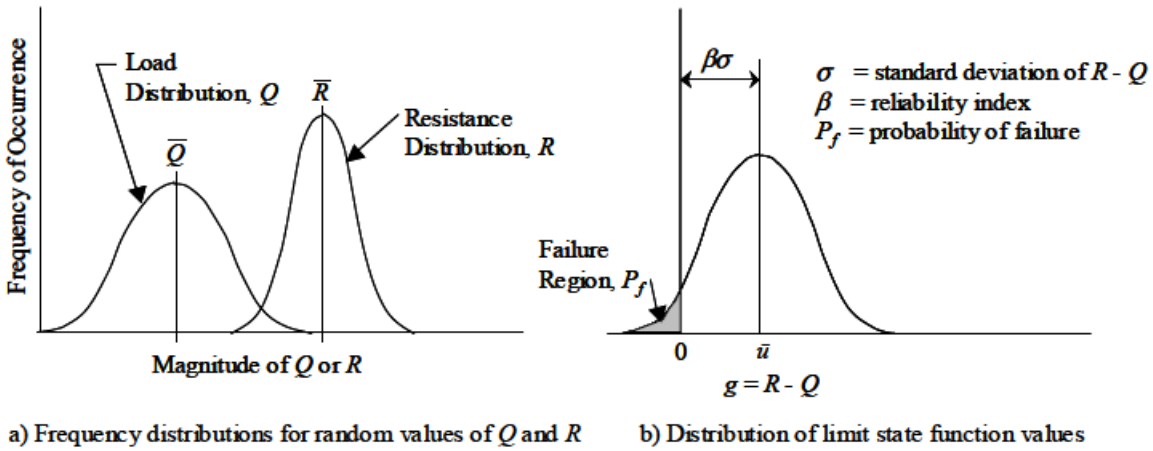

Figure 2.2: Load and resistance distribution and reliability Index (Withiam et al., 1998)

2.2 Resistance Factor Calibration Approach

Resistance factor calibration can be accomplished by judgment, fitting to ASD, reliability theory, or a combination of the above, but only calibration using reliability theory can fulfill the true goal of LRFD to ensure more uniform and consistent levels of safety across designs. In calibration by judgment, experience, which includes records of past satisfactory and poor performance, is relied upon to select appropriate values for the resistance factors.

Calibration by fitting to ASD is simply a format change consisting in the selection of resistance factors that would result in the same designs as ASD factors of safety. This approach can be used when insufficient load test data prevents the development of resistance factors through reliability-based statistical analyses. It only eliminates the discrepancy between load values used for substructure and superstructure designs, thereby reducing possible miscommunications between structural and geotechnical engineers. Considering only dead load (Q_D) and live load (Q_L), resistance factor determined from calibration by fitting is expressed as:

$$\varphi = \frac{\gamma_{Q_D}\frac{Q_D}{Q_L} + \gamma_{Q_L}}{\left(\frac{Q_D}{Q_L} + 1\right) FS} \tag{2.2}$$

where,

φ = Resistance factor

γ_{Q_D} = Load factor for Dead Load

γ_{Q_L} = Load factor for Live Load

The ratio of Q_D to Q_L is dependent upon the type of structures, span length, and other factors, and several recommendations regarding its value has been made in the literature. Barker et al. (1991) suggested a value of 3.0 for bridge structures, while Paikowsky et al. (2004) recommended values between 2.0 and 2.5 to be more reasonable and applicable to long span bridges.

Calibration by reliability theory involves the application of probabilistic methods of varying levels of complexity. Level III method (fully probabilistic) is the most accurate, but

it is rarely used in LRFD calibration because of the difficulty to obtain the required load and resistance information. Level II includes approximate probabilistic methods such as the first order second moment (FOSM) method, and it only requires the first two moments (i.e. mean and standard deviation) of the load and resistance variables to define the probability distributions associated with each variable. This approach, through an iterative procedure, can determine the safety or reliability index associated with a combination of selected values of load and resistance factors. Level I probabilistic methods are the least accurate, and they also use a second moment reliability method. The difference between Level I and Level II methods, however, lies in the limit state function being linearized at the mean values of the load and resistance rather than at the design point on the nonlinear failure surface. The use of any of these probabilistic methods requires the existence of an extensive record of load test data to statistically characterize the different variables involved in the limit state function. The general steps involved in a calibration based on reliability theory can be summarized as follows:

- Develop a sufficiently large database of high quality load tests. The database should include complete test data and all relevant subsurface characteristics and construction details at each test shaft. Importantly, the tests should have been conducted to complete geotechnical failure or sufficiently large displacements such that extrapolation of the measured resistance does not become a necessity.
- Depending on the quantity of available data, categorize based on the type of geomaterials present along the shafts and construction methods. Each category should have sufficient data from a statistical point of view for the analysis.
- For each category and selected strength criterion, determine the measured shaft resistance from load test data and calculate the predicted shaft resistance using the appropriate static design method.
- Calculate the resistance bias, λ, as the ratio of the measured to predicted resistances.
- Calculate the resistance bias statistical parameters including the mean, standard deviation, and coefficient of variation (COV).

- Determine the most suitable distribution type (e.g., normal, lognormal) for the resistance bias using probability density functions (PDFs), cumulative distribution functions, (CDFs), or statistical tests such as the Anderson Darling or the Chi-squared tests.
- Select desired the reliability method for the calibration based on the desired degree of sophistication.
- Adopt the load variable statistical characteristics recommended by the design code.
- Select the desired target reliability, and calibrate the resistance factors.
- Verify the reliability of the calibrated resistance factors using full-scale load tests and establish regional LRFD guidelines for drilled shafts foundations.

Because of the lack of research on superstructure loads transfer to the foundation and the difficulty to obtain such information, the characteristics of the load uncertainties used in superstructure analysis are also used for substructures. Consequently, load factors associated with the Strength I limit state condition recommended by AASHTO are commonly used. The dead and live load random variables are assumed to follow a lognormal distribution with probabilistic characteristics presented in Table 2.1 (Nowak, 1999).

Table 2.1: Statistical Parameters of Dead Load and Live Load

Load (Q)	Load Factor (γ)	Load Bias (λ)	Coefficient of Variation (COV_Q)
Dead (D)	1.25	1.05	0.1
Live (L)	1.75	1.15	0.2

The selection of a target reliability is a function of several factors including but not limited to the desired failure probability, the amount of redundancy present in the foundation system, the level of reliability inherent in past ASD practices, the extent of damage and potential human loss in the event of undesired structure performance, and the design life of the structure. Maintaining a uniform level of reliability across all limit states is also an important aspect to be considered. While resistance factors for bridge structural components have been calibrated to achieve a reliability index of 3.5, reliability analyses by Barker et al. (1991) have shown that the previously used factors of safety for foundation design in the ASD framework resulted in reliabilities less than 3.5. Based on their findings, target

reliabilities of 3.5, 2.5 to 3.0, and 2.0 to 2.5 were recommended for single shaft supported foundations, non-redundant systems, and highly redundant systems, respectively. Paikowsky et al. (2004) define a foundation system with five or more shafts in a group as redundant. Otherwise, it is classified as non-redundant. The higher reliability associated with highly redundant systems such as driven pile groups stem from the fact that failure of a single component in a larger group may not automatically result in the collapse of the entire foundation. In contrast, a foundation composed of fewer components has a higher probability of failure in the event that a single element fails or is overloaded. AASHTO resistance factors were developed based on these recommendations.

To achieve a calibration by reliability theory, the performance function that incorporates all random variables describing the failure mechanism of a drilled shaft must be developed. Rearranging the LRFD limit state Eq. (2.1) and considering only dead load and live load consistent with Strength I limit state leads to:

$$\varphi R_n - \left(\gamma_{Q_D} Q_D + \gamma_{Q_L} Q_L\right) \geq 0 \tag{2.3}$$

If the load and resistance are assumed to be random variables, then the performance limit function corresponding can be written as:

$$g(R, Q) = R_m - Q_m \tag{2.4}$$

where, g is a random variable representing the margin of safety, and Q_m and R_m are random variables representing the actual loads and resistance.

The parameters necessary to statistically characterize these random variables include the mean (μ), standard deviation (σ), and coefficient of variation (COV) defined by Eq. (2.5), Eq. (2.6), and Eq. (2.7), respectively.

$$\mu = \frac{1}{N}\sum x_i \tag{2.5}$$

$$\sigma = \sqrt{\frac{\sum(x_i - \mu)^2}{N - 1}} \tag{2.6}$$

$$\mathrm{COV} = \frac{\sigma}{\mu} \tag{2.7}$$

where, N is the total number of data values and x_i the individual value of the random variable being considered.

The variation of actual load and resistance values from predicted values can be expressed in terms of the bias λ, defined as the ratio of the measured to predicted values.
Using this relationship between measured and predicted values, Eq. (2.4) can be rewritten as:

$$g(R, Q) = \lambda_R R_n - \left(\lambda_{Q_D} Q_D + \lambda_{Q_L} Q_L\right) \tag{2.8}$$

The minimum R_n required to satisfy the limit state design equation is obtained when Eq. (2.3) is equated to zero, which represents the boundary line between satisfactory structure performance and adverse performance.

$$R_n = \frac{\gamma_{Q_D} Q_D + \gamma_{Q_L} Q_L}{\varphi} \tag{2.9}$$

Substituting Eq. (2.9) into (2.8) yields:

$$g(R, Q) = \lambda_R \frac{\gamma_{Q_D} Q_D + \gamma_{Q_L} Q_L}{\varphi} - \left(\lambda_{Q_D} Q_D + \lambda_{Q_L} Q_L\right) \tag{2.10}$$

Factoring out Q_L from each term in Eq. (2.10) gives:

$$\frac{g(R, Q)}{Q_L} = \lambda_R \frac{\gamma_{Q_D} \frac{Q_D}{Q_L} + \gamma_{Q_L}}{\varphi} - \left(\lambda_{Q_D} \frac{Q_D}{Q_L} + \lambda_{Q_L}\right) \tag{2.11}$$

Redefining $g(R, Q)/Q_L$ as $g(R, Q)$, the performance function can be written as:

$$g(R, Q) = \lambda_R \frac{\gamma_{Q_D} \frac{Q_D}{Q_L} + \gamma_{Q_L}}{\varphi} - \left(\lambda_{Q_D} \frac{Q_D}{Q_L} + \lambda_{Q_L}\right) \tag{2.12}$$

Eq. (2.12) can be solved using the various reliability methods described previously. If both the load and resistance random variables are assumed to follow a perfect lognormal distribution as consistent with current AASHTO specifications, then a closed-form solution relating the resistance factor, φ, to the reliability index β developed by Withiam et al. (1998) using the FOSM reliability method can be expressed as:

$$\varphi = \frac{\lambda_R\left(\frac{\gamma_D Q_D}{Q_L} + \gamma_L\right)\sqrt{\left[\frac{(1 + COV_D^2 + COV_L^2)}{1 + COV_R^2}\right]}}{\left(\frac{\lambda_D Q_D}{Q_L} + \lambda_L\right)\exp\left\{\beta_T\sqrt{\ln[(1 + COV_R^2)(1 + COV_D^2 + COV_L^2)]}\right\}} \quad (2.13)$$

where,

COV_R = Coefficient of variation of resistance,

COV_D = Coefficient of variation of dead load

COV_L = Coefficient of variation of live load

β_T = Target reliability index

λ_R = Resistance bias factor

λ_D = Dead load bias factor

λ_L = Live load bias factor

γ_D = Dead load factor

γ_L = Live load factor

Q_D = Dead load

Q_L = Live load

A modified version of Eq. (2.13) was developed by Bloomquist et al. (2007) to minimize the difference between the results obtained from all three reliability methods, and it is represented by Eq. (2.14). As the actual distribution of the load and resistance bias factors deviate from the lognormal, Eq. (2.13) and (2.14) become approximations, and the more sophisticated Monte Carlo simulation should be used to provide more accurate results. The Monte Carlo simulation is a numerical technique that utilizes a given variable mean value, standard deviation, COV, and distribution type to randomly generate a chosen number of virtual observations of the variable allowing extrapolation of the cumulative density function values.

$$\varphi = \frac{\lambda_R\left(\frac{\gamma_D Q_D}{Q_L}+\gamma_L\right)\sqrt{\left(1+\frac{\frac{Q_D^2}{Q_L^2}\lambda_D^2 COV_D^2+\lambda_L^2 COV_L^2}{\frac{Q_D^2}{Q_L^2}\lambda_D^2 COV_D^2+2\frac{Q_D}{Q_L}\lambda_D\lambda_L+\lambda_D^2}\right)\frac{1}{1+COV_R^2}}}{\left(\frac{\lambda_D Q_D}{Q_L}+\lambda_L\right)\exp\left\{\beta_T\sqrt{\ln\left[(1+COV_R^2)\left(1+\frac{\frac{Q_D^2}{Q_L^2}\lambda_D^2 COV_D^2+\lambda_L^2 COV_L^2}{\frac{Q_D^2}{Q_L^2}\lambda_D^2 COV_D^2+2\frac{Q_D}{Q_L}\lambda_D\lambda_L+\lambda_D^2}\right)\right]}\right\}} \quad (2.14)$$

It is able to deal with a variety of functions and can be easily implemented on a computer using EXCEL or MATLAB. The steps necessary to implement a Monte Carlo Simulation can be described as follows:

- Use the statistical parameters of each random variables to generate N random numbers for each variable. The value of N is a function of the desired accuracy, the target probability of failure, and the coefficient of variation.
- Assume a trial resistance factor, φ and evaluate the performance function for each set of randomly generated load and resistance values.
- Calculate the probability of failure, p_f, as the ratio of the number of failures ($g \leq 0$) to the total number of simulations N, and determine the corresponding reliability index.
- Iterate until the calculated reliability index converges to the desired target value.

As reported by Paikowsky et al. (2004) and Allen (2005), the difference between the resistance factors calculated from these methods is within 10% with FORM and Monte Carlo simulation providing the highest values.

A calibration using a combination of any of the approaches previously detailed i.e., by judgement, fitting, or reliability theory, is warranted when the data required for a proper reliability-based calibration is not available, or when the quality of the data at hand is questionable. As Allen (2005) stated, "if the adequacy of the input data is questionable, the final load and resistance factor combination selected should be more heavily weighted

toward a level of safety that is consistent with past successful design practice, using the reliability theory results to gain insight as to whether or not past practice is conservative or non-conservative."

2.3 Drilled Shaft Capacity Prediction Methods

Over the years, various analytical methods have been developed to estimate the nominal axial resistance of drilled shafts. These methods were developed empirically or semi-empirically from correlation of drilled shaft measured performance to known soil parameters and may not have been developed using a consistent strength criterion. To ensure selection of the most appropriate methods for reliable estimate of drilled shaft resistance, several factors must be considered including site subsurface conditions, extent of available soil parameters, anticipated load conditions, construction technique, and local practice. Soil parameters required by these methods can be determined directly from in-situ or laboratory soil sample testing or from correlation to other soil properties. Drilled shaft ultimate axial capacity can be expressed as:

$$Q_u = Q_b + Q_s = q_b A_b + \sum_{i=1}^{n} q_{si} A_{si} \tag{2.15}$$

where,

q_b = Unit end bearing resistance,

A_b = Base cross sectional area,

q_{si} = Unit side resistance of soil layer i,

A_{si} = Shear area of soil layer i,

n = Number of soil layers along shaft length

It is important to note that the maximum side resistance and end resistance are mobilized at different magnitudes of shaft movement. As shown in Figure 2.3, side resistance is fully mobilized at relatively much smaller tip movement compared to base resistance. In situations where the soil is prone to softening, side resistance may have reduced to a residual value by the time end bearing is significantly mobilized. This major difference must be considered in design to avoid overestimating either component of the total resistance.

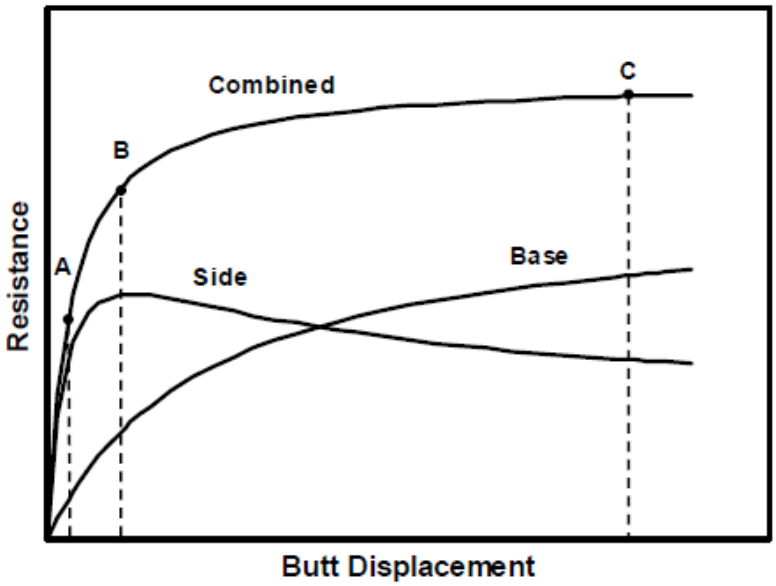

Figure 2.3: Side and base resistance load-displacement characteristics (Brown et al. 2010)

In fact, some agencies choose to neglect the end bearing component in practice due to this reason coupled with uncertainties associated with construction.

2.3.1 Side Resistance Prediction Methods

2.3.1.1 Cohesive soil

Side resistance of drilled shafts in cohesive soil is commonly evaluated in terms of undrained shear strength consistent with short-term loading conditions using the α-method. The α-method, developed by Tomlinson (1971) based on back-analysis of load test results on timber, pipe, and precast concrete piles in cohesive soils, suggests that the unit skin friction is related to the undrained shear strength by an empirical factor α, which varies with depth and the strength of the cohesive soil. This relationship is expressed as:

$$q_s = \alpha S_u \qquad (2.16)$$

where,

S_u = Undrained shear strength (ksf)

α = 0 from the ground surface to a depth of 5 ft or to the depth of seasonal moisture change whichever is greater

α = 0.55 for $\frac{S_u}{P_a} \leq 1.5$,

α = $0.55 - 0.1\left(\frac{S_u}{P_a} - 1.5\right)$ for $1.5 \leq \frac{S_u}{P_a} \leq 2.5$; and

P_a = Atmospheric pressure (2.12 ksf).

In previous practice, the side resistance was neglected over a distance of one diameter above the base of the shaft based on numerical modeling that predicted the development of a zone of tension near the base. However, this recommendation has been discarded from current practice because of the lack of evidence from field load test data. The undrained shear strength parameter should ideally be determined in the laboratory from triaxial tests (consolidated undrained, unconsolidated undrained) on undisturbed soil samples or in-situ from tests including vane shear test (VST) and cone penetration test (CPT). The undrained shear strength can also be estimated using various correlations available in the literature. Examples of such correlations include but are not limited to those developed by Bjerrum (1972) and Bowles (1982) as follows:

$$S_u = \frac{f_1 N_{60} P_a}{100} \tag{2.17}$$

where,

f_1 = Empirical factor (4.5 for PI = 50 and 5.5 for PI = 15),

PI = Plasticity index,

N_{60} = SPT blow count corrected for hammer efficiency, and

P_a = Atmospheric pressure (2.12 ksf).

Table 2.2: Undrained Shear Strength Correlation to SPT Blow Count Number (Bowles, 1982)

S_u, ksf	0	0.25	0.5	1	2	4
N, standard penetration resistance	0	2	4	8	16	32

2.3.1.2 Cohesionless soil

The unit side resistance of a drilled shaft in cohesionless soils is a function of the normal stress acting on the shaft-soil interface, and it can be estimated by the β-method expressed as:

$$q_s = K \tan \delta \sigma'_V = \beta \sigma'_V \quad (2.18)$$

where,

K = Lateral earth pressure coefficient at shaft-soil interface

δ = Effective stress angle of friction at shaft-soil interface

σ'_v = Vertical effective stress at mid-depth of soil layer (ksf)

β = Side resistance coefficient

To calculate the vertical effective stress as a function of depth, the soil unit weight was estimated from Table 2.3 and Table 2.4 based on the uncorrected SPT blow count number.

Table 2.3: Unit weight correlation to SPT blow count for granular soils (Bowles, 1982)

SPT N-Value (blows/foot)	γ (lb/ft^3)
0 – 4	70 – 100
4 – 10	90 – 115
10 – 30	110 – 130
30 – 50	110 – 140
> 50	130 – 150

Table 2.4: Unit weight correlation to SPT blow count for cohesive soils (Bowles, 1982)

SPT N-Value (blows/foot)	γ_{sat} (lb/ft^3)
0 – 4	100 – 120
4 – 8	110 – 130
8 – 32	120 – 140

In previous AASHTO recommendations, the β coefficient was determined as a function of depth below the ground surface. Based on back-analysis of load test data, O'Neill and Hassan (1994) developed the following expressions:

$$\beta = 1.5 - 0.135\sqrt{z} \text{ for sandy soils and } N_{60} \geq 15 \quad (2.19)$$

$$\beta = \frac{N_{60}}{15}\left(1.5 - 0.135\sqrt{z}\right) \text{ for all cohesionless soils and } N_{60} < 15 \quad (2.20)$$

$$\beta = 2.0 - 0.06(z)^{0.75} \text{ for gravelly sands and gravels and } N_{60} \geq 15 \quad (2.21)$$

where,

N_{60} = Average SPT blow count in the design zone under consideration and corrected for hammer efficiency.

z = Depth below ground surface a soil mid-depth (ft)

A limit of 4 ksf was imposed on the unit side resistance calculated using this approach based on the maximum value observed in the load test database that served as the basis for the development of the expressions. Rollins et al. (2005) developed and proposed an additional expression for β as follows:

$$\beta = 3.4 \times e^{(-0.085z)} \text{ for gravels with } N_{60} \geq 50 \quad (2.22)$$

where,

z = Depth below ground at soil layer mid depth (ft)

N_{60} = Average SPT blow count in the design zone under consideration and corrected for hammer efficiency.

β calculated from Eq. (2.27) is limited to a minimum of 0.25 and maximum value of 3.0. Although this approach to estimating the β coefficient has been found to be conservative in practice, it fails to account explicitly for the in-situ state of stress and soil shear strength, which is necessary for proper modeling of the mechanisms of soil-structure interaction controlling side resistance. A more rational approach that overcomes this major limitation was developed by Chen and Kulhawy (2002). In this approach, the β coefficient is determined as function of in-situ lateral earth pressure and interface friction angle as follows:

$$\beta = K_0 \left(\frac{K}{K_0}\right) \tan\varphi' = (1 - \sin\varphi') \left(\frac{\sigma'_p}{\sigma'_v}\right)^{\sin\varphi'} \tan\varphi' \leq K_p \tan\varphi' \quad (2.23)$$

where,

φ' = Soil effective stress friction angle

σ'_p = Effective vertical preconsolidation stress

σ'_v = Vertical effective stress at mid-depth of soil layer (ksf)

K_p = Passive earth pressure coefficient

K_p = Passive earth pressure coefficient

K_0 = At rest earth pressure coefficient

Depending on the type of cohesionless soils, the effective vertical preconsolidation stress can be estimated using the following correlations:

$$\frac{\sigma'_p}{P_a} \approx 0.47(N_{60})^m \quad \text{for sands, silty sands and silts} \quad (2.24)$$

$$\frac{\sigma'_p}{P_a} = 0.15N_{60} \quad \text{for gravelly soils} \quad (2.25)$$

where m is 0.6 for clean quarzitic sands and 0.8 for silty sands to sandy silts.

When the subsurface information is limited to the SPT blow count numbers, the drained friction angle can be estimated using the following correlations proposed by Sabatini et al. (2002) and Kulhawy and Chen (2007):

$$\varphi' = \tan^{-1}\left[\frac{N_{60}}{12.2 + 20.3\left(\frac{\sigma'_{vo}}{p_a}\right)}\right]^{0.34} \quad (2.26)$$

$$\varphi' = \sqrt{15.4(N_1)_{60}} + 20 \quad (2.27)$$

$$\varphi' = 27.5 + 9.2\log[(N_1)_{60}] \quad (2.28)$$

where,

N_{60} = Field measured SPT blow count number corrected to 60% hammer efficiency

$(N_1)_{60}$ = N_{60} normalized for effects of overburden pressure

σ'_{vo} = Vertical effective stress at the sample depth

p_a = Atmospheric pressure (2.12 ksf)

When cone penetration resistance, q_c, are available from Cone Penetration Test (CPT) data, the effective friction angle can be determined as:

$$\varphi' = \tan^{-1}\left[0.1 + 0.38\log\left(\frac{q_c}{\sigma'_{vo}}\right)\right] \quad (2.29)$$

Other correlations are also available in the literature. The characteristics of the database and the assumptions used in developing these correlations should be known to ensure that the correlations are appropriately used.

2.3.1.3 Intermediate Geomaterials

2.3.1.3.1 Cohesive intermediate geomaterials

The intermediate geomaterial category was introduced by O'Neill and Reese (1999) to describe materials that are transitional between soil and rock. The cohesive type include argillaceous geomaterials such as heavily overconsolidated clays, clay shales, saprolites, and mudstones that are prone to smearing during drilling and calcareous rocks such as limestone, limerock and argillaceous geomaterials that are not prone to smearing during drilling. From an engineering perspective, IGM are classified as materials with unconfined compressive strength ranging between 10 and 100 ksf. Based on the design methodology developed by Hassan et al. (1997), the unit side resistance of drilled shafts in cohesive IGM is given by:

$$q_s = \alpha\, \phi\, q_u \quad (2.30)$$

where,

α = Empirical factor determined from Figure 2.4

q_u = Uniaxial compressive strength of intact rock (ksf), and

ϕ = Correction factor to account for the degree of jointing (see Table 2.5).

The method was developed assuming an interface friction angle (ϕ_{rc}) of 30 degrees, a ratio of modulus of rock mass (E_m) to q_u between 115 and 500, and a total vertical displacement required to mobilize the full side resistance of 1 inch. If the interface friction angle differs from the assumed value, then α can be adjusted using the following expression:

$$\alpha = \alpha_{\text{Figure 2.1}} \frac{\tan \phi_{rc}}{\tan 30^{\circ}} \tag{2.31}$$

The magnitude of α depends also on the pressure exerted by the freshly placed concrete. Assuming a minimum concrete slump of 7 in. and a placement rate of 40 ft per hour or greater, the concrete pressure σ_n, at a given depth z_i^* below the cut-off elevation is given by:

$$\sigma_n = 0.65 \gamma_c z_i^* \tag{2.32}$$

where,

γ_c = Concrete unit weight (kcf), and

z_i^* = Depth below the selected cutoff elevation to the middle of a material layer i, which is limited to 40 ft.

The φ parameter accounts for the effect of joints on the unit skin resistance of cohesive IGMs. This effect can be estimated from Table 2.5 based on the Rock Quality Designation (RQD) and the joint characteristics (i.e., either closed joints or open/gouge-filled joints). No recommendations are made for RQD values less than 20%, and load tests are recommended to determine the side resistance in these circumstances.

2.3.1.3.2 Cohesionless intermediate geomaterials

O'Neill and Reese (1999) described cohesionless intermediate geomaterials as very dense granular tills or granular residual materials with SPT N_{60} value ranging between 50 and 100 blows per foot. As previously recommended by the 1999 FHWA drilled shaft manual,

unit side resistance in cohesionless IGMs was estimated using the rational β-method detailed in section 2.2.1.2. In current practice, this approach is recommended for both cohesionless soils and IGMs.

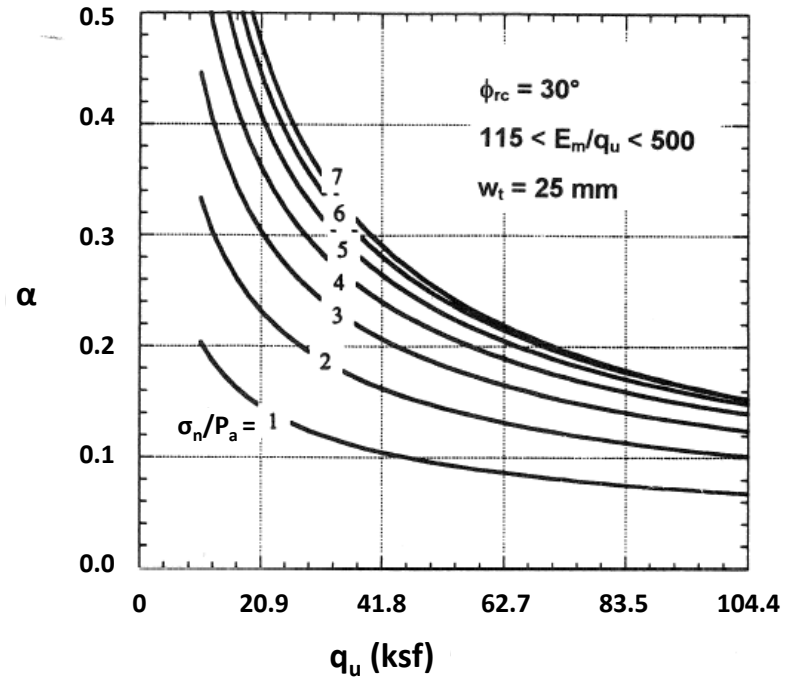

Figure 2.4: Factor α for cohesive IGM (adapted from O'Neill et al. 1996)

Table 2.5: Side resistance reduction factor for cohesive IGM

Rock Quality Designation, RQD (%)	Joint Reduction Factor, ϕ	
	Closed Joints	Open or Gouge-Filled Joints
100	1.00	0.85
70	0.85	0.55
50	0.60	0.55
30	0.50	0.50
20	0.45	0.45

2.3.1.4 Rock

For drilled shaft design purposes, rock are geomaterials such as shales, sandstone, limestone, and mudstone with uniaxial compressive strength greater than 100 ksf or SPT blow count larger than 100. The unit side resistance of drilled shafts in rock can be evaluated based on the compressive strength of the rock as:

$$q_s = C \cdot p_a \sqrt{\frac{q_u}{p_a}} \tag{2.33}$$

where,

q_u = Mean uniaxial compressive strength for the rock layer in ksf

p_a = Atmospheric pressure (2.12 ksf)

C = Regression coefficient based on load test results

The value of q_u should be limited to the 28-day compressive strength of the drilled shaft concrete(f_c'). Different values of C have been proposed by various studies including but not limited to those of Horvath and Kenney (1979), Rowe and Armitage (1987), and Kulhawy and Phoon (1993). Based on their analyses, Horvath and Kenney (1979) recommended a value of 0.65, which was adopted by O'Neill and Reese (1999) and previous versions of AASHTO LRFD specifications. An empirical reduction factor α_E was added by O'Neill and Reese (1999) to account for the degree of jointing in the rock resulting in the following expression:

$$q_s = 0.65\alpha_E P_a \sqrt{\frac{q_u}{P_a}} \tag{2.34}$$

The reduction factor α_E is a function of the ratio of the of rock mass modulus to intact rock modulus (E_m/E_i), which depends on the RQD, and it can be estimated from Table 2.6 and Table 2.7. Most recent studies by Kulhawy et al. (2005) suggests that, as shown in Eq.(2.35), a regression coefficient C of 1.0 is appropriate for the design of "normal" rock sockets that are not prone to smearing during drilling and that can be constructed without support, special equipment or procedures.

Table 2.6: Estimation of α_E (O'Neill and Reese 1999)

E_m/E_i	α_E
1.0	1.0
0.5	0.8
0.3	0.7
0.1	0.55
0.05	0.45

Table 2.7: Estimation of E_m based on RQD (O'Neill and Reese 1999)

Rock Quality Designation, RQD (%)	E_m/E_i	
	Closed Joints	Open Joints
100	1.00	0.60
70	0.70	0.10
50	0.15	0.10
20	0.05	0.05

The reduction factor α_E is only recommended where artificial support such as casing would be required during construction of the rock socket.

$$q_s = 1.0\ P_a \sqrt{\frac{q_u}{P_a}} \tag{2.35}$$

A significant increase of the drilled shaft side resistance can be achieved by artificial roughening of the rock socket using grooving tools. In this case, the unit side resistance can be estimated using the following expression proposed by Horvath et al. (1983):

$$q_s = 0.80 \left[\frac{\Delta r}{r}\left(\frac{L'}{L}\right)\right]^{0.45} q_u \tag{2.36}$$

where,

q_u = Uniaxial compressive strength of rock (ksf),

Δr = Height of asperities or grooves in rock sidewall (ft),

r = Radius of drilled shaft (ft),

L' = Distance along surface of rock socket (ft), and

L = Depth of rock socket (ft).

The geometric terms in Eq. (2.36) are illustrated in Figure 2.5. An accurate geometry of the socket must therefore be known for proper use of Eq. (2.36).

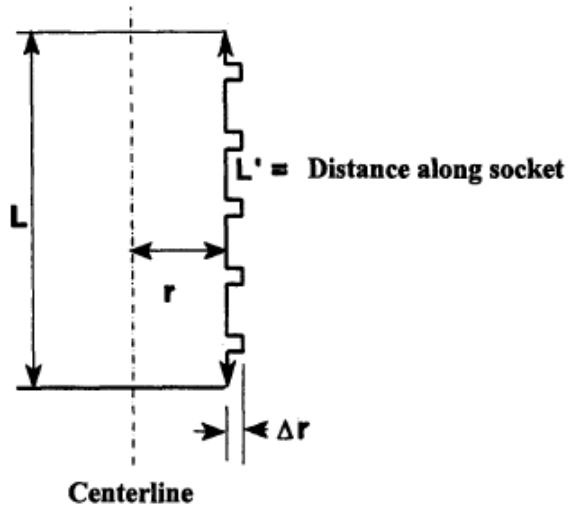

Figure 2.5: Definition of geometric terms in Eq. (2.36) (O'Neill and Reese 1999)

2.3.2 End Resistance Prediction Methods

2.3.2.1 Cohesive soil

End bearing of drilled shafts in cohesive soils is determined from bearing capacity theory in terms of total stress analysis as:

$$q_p = N_c S_u \leq 80.0 \text{ ksf} \tag{2.37}$$

where,

N_c = Bearing capacity factor

S_u = Mean undrained shear strength of the cohesive soil over a depth of 2B below base

If the rigidity index of the soil is known, then N_c can be calculated as:

$$N_c = 1.33(\ln I_r + 1) \tag{2.38}$$

where,

I_r = Rigidity index = $\frac{E_s}{3S_u}$

E_s = Young's modulus

S_u = Undrained shear strength

If the rigidity index cannot be estimated, N_c can be determined as a function of the undrained shear strength as shown in Table 2.8.

Table 2.8: Bearing capacity factor

S_u (ksf)	$I_r = E_s/3S_u$	N_c
0.5	50	6.5
1	150	8.0
2	250-300	9.0

For cases where the shaft embedment length is at least three times the shaft diameter and the average shear strength is greater or equal to 2 ksf, N_c can be taken as 9.0. For embedment depth smaller than three times the shaft diameter, a reduction factor applies to the bearing capacity factor and the end bearing is calculated as:

$$q_p = \frac{2}{3}\left[1 + \frac{1}{6}\left(\frac{Z}{B}\right)\right] N_c S_u \tag{2.39}$$

where,

Z = Embedded depth of shaft in cohesive soil (ft), and

B = Diameter of drilled shaft (ft).

2.3.2.2 Cohesionless soil

Due to soil disturbance resulting from the construction process, end resistance in cohesionless soils cannot be reliably determined from bearing capacity theory. Rather, direct empirical correlations developed from actual load tests data are relied upon to estimate drilled shaft base resistance. For routine design, the end resistance in cohesionless soils can be estimated using the following correlation proposed by Reese and O'Neill (1989):

$$q_p = 1.2\ N_{60} \leq 60 \text{ ksf} \tag{2.40}$$

where, N_{60} = Average SPT blow count between the base and two diameters below the base.

The end resistance calculated using Eq. (2.40) is limited to a maximum value of 60 ksf based on the largest value observed in the load tests database used to develop the correlation.

Eq. (2.40) is not applicable to situations where the average SPT value exceeds 50. Load testing is recommended in this case. Otherwise, the upper bound value of 60 ksf can be used for design. End bearing in cohesionless soil can be improved via base grouting, a mechanical process of injecting a water-cement mixture under pressure at the base of the shaft. Mullins (2000) proposed the following expression to estimate the additional end resistance that may result from base grouting:

$$q_{p,total} = (TCM) \times q_{p,un-grouted}[Eq.\ (2.21)] \tag{2-41}$$

where,

TCM = tip capacity multiplier = $0.713 \times GPI \left(\frac{\delta_t}{B}\%\right)^{0.364} + \left[\frac{\frac{\delta}{B}\%}{0.4\left(\frac{\delta}{B}\%\right)+3}\right]$,

δ_t = tolerable settlement of the shaft (ft),

B = shaft diameter (ft),

GPI = grout pressure index = $\frac{GP_{max}}{q_{p,\ un\text{-}grouted}}$,

GP_{max} = anticipated maximum grout pressure (ksf) = $\frac{R_s}{A_{shaft}}$,

R_s = nominal side resistance for the total length of embedded shaft (kip), and

A_{shaft} = cross-sectional area of the shaft (ft^2).

2.3.2.3 Cohesionless intermediate geomaterial

Unit end bearing in cohesionless IGM can be determined in accordance with O'Neill and Reese (1999) recommendations using the following the expression:

$$q_p = 0.59\left[N_{60}\left(\frac{P_a}{\sigma'_v}\right)\right]^{0.8}\sigma'_v \tag{2-42}$$

where,

σ'_v = vertical geostatic effective stress at the base elevation of the shaft (ksf),

P_a = atmospheric pressure (2.12 ksf), and

N_{60} = Average SPT blow count between base and two diameters below base corrected for hammer efficiency, limited to 100.

The end bearing shall be limited to a maximum value as determined by Eq. (2.46) for drilled shafts with diameter greater or equal to 4.17 ft when serviceability limit state conditions are not verified.

$$q_{p,max} = \left(\frac{4.17}{B}\right) 0.59 \left[N_{60}\left(\frac{P_a}{\sigma'_v}\right)\right]^{0.8} \sigma'_v \quad (2\text{-}43)$$

where, B is the diameter of the drilled shaft base.

2.3.2.4 Cohesive intermediate geomaterial and rock

End resistance in cohesive IGM and rock is affected by a variety of rock mass conditions such as rock mass strength, discontinuities, as well as the spacing, condition and orientation of the discontinuities. Depending on these conditions, rock mass can be classified as intact or massive, jointed, layered, or fractured. Consequently, end bearing capacity may be controlled by various failure modes as illustrated in When the joints spacing and condition below the shaft base can be characterized, the unit end resistance for rock mass with steeply dipping open joints and joint spacing smaller than the shaft diameter proposed by Sowers (1976) can be expressed as:

$$q_p = q_u \quad (2.46)$$

For rock mass characterized by steeply dipping closed joints with joint spacing smaller than the shaft diameter or rock mass with moderate dipping angles between 20° and 70°, Terzaghi (1943) bearing capacity equation for circular cross sections can be used to estimate the unit end bearing.

$$q_p = c'N_c s_c + B2\gamma N\gamma s\gamma + \gamma D N q s q \quad (2.47)$$

where,

c' = Rock mass cohesion,

Nc = $2\sqrt{N_\phi}(N_\phi + 1)$,

N

N = N_ϕ^2,

=

$N\phi N\phi 2-1$

$\tan 245o+\phi'2$,

ϕ' = Rock friction angle,

sc $= 1 + \frac{N_q}{N_c}$,

$s\gamma$ = 0.6,

sq = 1 + tan (ϕ'),

B = Shaft rock-socket diameter,

D = Foundation depth,

γ = Effective unit weight of the rock mass

Table 2.9.Various expressions have been developed to predict end resistance for various rock mass conditions. However, some of these correlations require information related to rock conditions that is usually not available in routine drilled shaft design. When the available parameters are limited to the unconfined compressive strength (q_u) of the intact rock and the RQD, unit end resistance in rock or IGM can be expressed as:

$$q_p = N_{cr}^* q_u \tag{2.44}$$

where, N_{cr}^* is an empirical bearing capacity factor.

The value of N_{cr}^* is a function of the rock mass condition below the shaft base. Based on the work of Rowe and Armitage (1987), a N_{cr}^* value of 2.5 can be used for intact rock when the following criteria are satisfied:

- The rock from the shaft base to a depth of two times the shaft diameter is either intact or tightly jointed with visible joint spacing much greater than the shaft diameter
- The depth of the rock socket is greater than one and one-half diameters
- Solution cavities or voids are not present below the shaft base
- The shaft base can be adequately cleaned using conventional clean-out equipment

For routine design, the rock can be considered to be intact when the RQD is equal to 100%. When the RQD is between 70% and 100% and the joints are closed and approximately horizontal, O'Neill and Reese (1999) proposed the following expression for end resistance:

$$q_p(\text{MPa}) = 4.83[q_u(\text{MPa})]^{0.51} \tag{2.45}$$

When the joints spacing and condition below the shaft base can be characterized, the unit end resistance for rock mass with steeply dipping open joints and joint spacing smaller than the shaft diameter proposed by Sowers (1976) can be expressed as:

$$q_p = q_u \tag{2.46}$$

For rock mass characterized by steeply dipping closed joints with joint spacing smaller than the shaft diameter or rock mass with moderate dipping angles between 20° and 70°, Terzaghi (1943) bearing capacity equation for circular cross sections can be used to estimate the unit end bearing.

$$q_p = c'N_c s_c + \frac{B}{2}\gamma N_\gamma s_\gamma + \gamma D N_q s_q \tag{2.47}$$

where,

c' = Rock mass cohesion,

N_c = $2\sqrt{N_\phi}(N_\phi + 1)$,

N_γ = $\sqrt{N_\phi}(N_\phi^2 - 1)$,

N_q =N_ϕ^2,

N_ϕ = $\tan^2\left(45^o + \frac{\phi'}{2}\right)$,

ϕ' = Rock friction angle,

s_c = $1 + \frac{N_q}{N_c}$,

s_γ = 0.6,

s_q = 1 + tan (ϕ'),

B = Shaft rock-socket diameter,

D = Foundation depth,

γ = Effective unit weight of the rock mass

Table 2.9: Bearing capacity failure modes in rock (U.S. Army Corps of Engineers 1994)

Rock Mass Condition			Failure	
Type	**Joint Dip Angle from Horizontal**	**Joint Spacing**	**Illustration**	**Mode**
INTACT/MASSIVE	N/A	S >> B	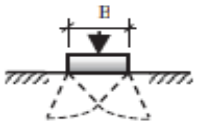	(a) Brittle Rock: Local shear failure caused by localized brittle fracture
			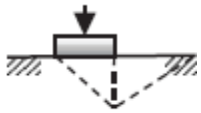	(b) Ductile Rock: General shear failure along well-defined shear surface
STEEPLY DIPPING JOINTS	70° < α < 90°	S < B	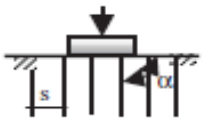	(c) Open Joints: Compression failure of individual rock columns
			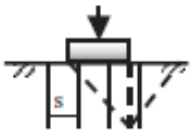	(d) Closed Joints: General shear failure along well defined failure surfaces; near vertical joints
		S > B	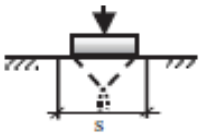	(e) Open or Closed Joints: Failure initiated by splitting leading to general shear failure; near vertical joints
JOINTED	20° < α < 70°	S < B or S > B if failure wedge can develop along joints	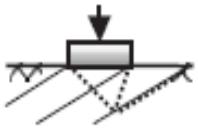	(f) General shear failure with potential for failure along joints; moderately dipping joint sets
LAYERED	0° < α < 20°	Limiting value of H wrt B is dependent upon material properties	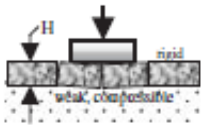	(g) Rigid layer over weak compressible layer: Failure is initiated by tensile failure caused by flexure of rigid upper layer
			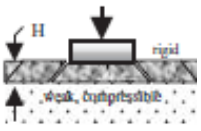	(h) Thin rigid layer over weak compressible layer: Failure is by punching shear through upper layer
FRACTURED	N/A	S << B	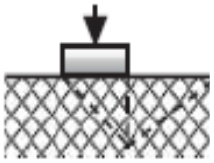	(i) General shear failure with irregular failure surface through fractured rock mass; two or more closely spaced joint sets

The rock effective stress friction angle and cohesion needed to calculate the unit end bearing using Eq. (2.47) can be determined from laboratory triaxial tests on rock core samples or estimated using the following expressions developed by Hoek et al. (2002):

$$\phi' = \sin^{-1}\left[\frac{6\,a\,m(s + m\sigma_3')^{a-1}}{2(1+a)(2+a) + 6\,a\,m(s + m\sigma_3')^{a-1}}\right] \tag{2.48}$$

$$c' = \frac{q_u[(1+2a)s + (1-a)m\sigma_3'](s + m\sigma_3')^{a-1}}{(1+a)(2+a)\sqrt{\frac{1 + 6\,a\,m(s + m\sigma_3')^{a-1}}{(1+a)(2+a)}}} \tag{2.49}$$

where,

q_u = Rock uniaxial compressive strength,

a = Empirical parameter = $\frac{1}{2} + \frac{1}{6}\left(e^{\frac{-GSI}{15}} - e^{\frac{-20}{3}}\right)$,

m = Empirical parameter = $m_i \exp\left(\frac{GSI-100}{28-14D}\right)$,

m_i = Empirical parameter for intact rock by rock group given in Table 2.10,

s = Empirical parameter = $\exp\left(\frac{GSI-100}{9-3D}\right)$,

σ_3' = Minor principal effective stresses,

GSI = Geological strength index = RMR−5 for RMR greater than 23 or $(9 \log_e Q' + 44)$ for RMR less than 23,

D = Damage factor caused by blast damage and stress relaxation ranging from zero for undisturbed in situ rock masses to 1.0 for very disturbed rock masses (Note: no work has been published relating D to drilled shaft construction),

RMR = Rock mass rating by summing all relative ratings determined in Table 2.13

Q′ = Modified tunneling quality index = $\frac{RQD}{J_n} \times \frac{J_\gamma}{J_a}$,

RQD = Rock quality designation as described in Section 2.3.4,

J_n = Joint parameter based on no. of sets of discontinuities (refer to Table 2.11),

J_γ = Joint parameter based on roughness of discontinuities (refer to Table 2.11), and

J_a = Joint parameter based on discontinuity condition & infilling (refer to Table 2.11).

Table 2.10: Values of the constant m_i by rock group (Hoek et al. 1995)

Rock Type	Class	Group	Texture			
			Coarse	Medium	Fine	Very Fine
Sedimentary	Clastic		Conglomerate (22)	Sandstone 19 Graywacke (18)	Siltstone 9	Claystone 4
	Non-clastic	Organic		Chalk 7 Coal (8-21)		
		Carbonate	Breccia (20)	Sparitic limestone (10)	Micritic limestone 8	-
		Chemical	-	Gypstone 16	Anhydrite 13	-
Metamorphic	Non-foliated		Marble 9	Hornfels (19)	Quartzite 24	-
	Slightly foliated		Migmatite (30)	Amphibolite 31	Mylonites (6)	-
	Foliated*		Gneiss 33	Schists (10)	Phyllites (10)	Slate 9
Igneous	Light		Granite 33	-	Rhyolite (16)	Obsidian (19)
			Granodiorite (30)	-	Dacite (17)	-
	Dark		Diorite (28)	-	Andesite (19)	-
			Gabbro 27	Dolerite (19)	Basalt (17)	-
			Norite 22	-	-	-
	Extrusive pyroclastic type		Agglomerate (20)	Breccia (18)	Tuff (15)	-

* – Value of m_i will be significantly different if failure occurs along a foliation plane; Values in parentheses are estimates.

This approach to estimating the unit end bearing is rather complex, and the following simplified bearing capacity equation proposed by Goodman (1980) can be used to obtain an approximate value:

$$q_p = q_{u,design}(N_\phi + 1) \tag{2.50}$$

where, the rock unconfined compressive strength used for design is taken as one-fifth of the unconfined compressive strength measured in the laboratory.

Table 2.11: Joint parameters used to determine Q′

No. of Sets of Discontinuities	Joint Parameter J_n
Massive	0.5
One set	2
Two sets	4
Three sets	9
Four or more sets	15
Crushed rock	20

Roughness of Discontinuities	Joint Parameter J_γ
Noncontinuous joints	4
Rough, wavy	3
Smooth, wavy	2
Rough, planar	1.5
Smooth, planar	1
Slick and planar	0.5
Filled discontinuities	1

Discontinuity Condition & Filling	Joint Parameter J_a
Unfilled cases:	
Healed	0.75
Stained, no alteration	1
Silty or sandy coating	3
Clay coating	4
Filled Discontinuities:	
Sand or crushed rock infill	4
Stiff clay infilling < 0.2 in.	6
Soft clay infill < 0.2 in. thick	8
Swelling clay < 0.2 in.	12
Stiff clay infill > 0.2 in. thick	10
Soft clay infill > 0.2 in. thick	15
Swelling clay > 0.2 in.	20

A reduction in the value obtained from laboratory uniaxial compression tests is necessary since the strength of a small diameter rock specimen does not include scale effects and may overestimate the compressive strength of a larger rock mass with discontinuities.

For rock mass with steeply dipping open or closed joints and joint spacing smaller than the shaft diameter, the unit end bearing may be estimated using Kulhway and Goodman (1980) as:

$$q_p = J\, c\, N_{cr} \tag{2.51}$$

where,

J = Correction factor that depends on the ratio of horizontal discontinuity spacing to socket diameter (H/B) as shown in Figure 2.6

c = Rock mass cohesion can be approximated as $0.1q_u$ suggested by Kulhawy and Cater (1992) or using Eq.(2.49) for fractured rock masses (ksf)

N_{cr} = Bearing capacity factor= $\frac{2N_\phi^2}{1+N_\phi}(\cot\phi)\frac{S}{B}\left(1-\frac{1}{N_\phi}\right)-N_\phi(\cot\phi)+2\sqrt{N_\phi}$,

B = Shaft rock socket diameter (ft)

S = Joint spacing (ft)

N_ϕ = $\tan^2\left(45^o+\frac{\phi}{2}\right)$

ϕ = Rock friction angle estimated using Eq. (2.48) for fractured rock masses

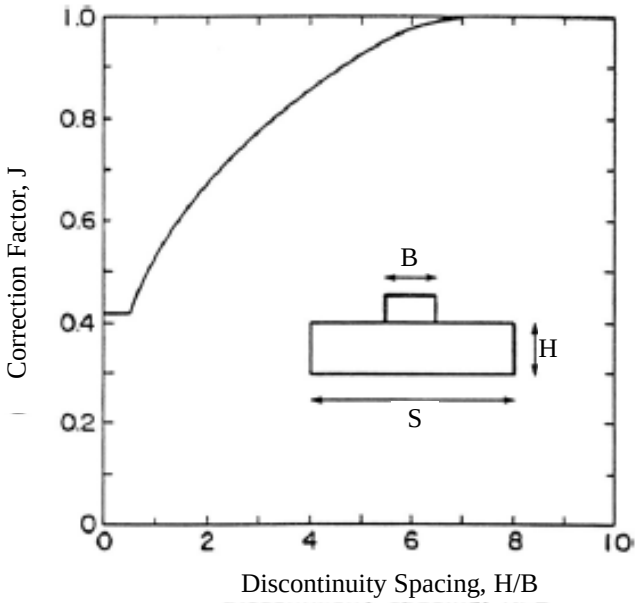

Figure 2.6: Correction factor for discontinuity spacing (Kulhawy and Carter 1992)

When the joint spacing is greater than 1 foot and the aperture of the discontinuity is as large as 0.25 inch, the Canadian Geotechnical Society (1995) illustrated by Eq. (2.52) can be used.

$$q_p = 3q_u K_{sp} d \tag{2.52}$$

where,

K_{sp} $= \frac{3+\frac{s_v}{B}}{10\sqrt{1+300\frac{t_d}{s_v}}}$

d $= 1 + 0.4\frac{D_s}{B} \leq 3.4$

s_v = vertical spacing between discontinuities

t_d = aperture (thickness) of discontinuities

B = socket diameter

D_s = socket embedment depth.

For fractured rock mass where the joint spacing is significantly smaller than the shaft diameter, Carter and Kulhawy (1988), based on Hoek-Brown (1988) strength criterion, suggested that end resistance can be expressed as:

$$q_p = \left[\sqrt{s} + \sqrt{\left(m\sqrt{s} + s\right)}\right] q_u \qquad (2.53)$$

where, s and m are the fractured rock mass parameters.

The s and m parameters are presented in Table 2.12, and they are function of the rock type as well as the Rock Mass Rating (RMR). As illustrated in Table 2.13, the Rock Mass Rating is influenced by five parameters including the strength of intact rock, RQD, joints spacing, joints condition, and groundwater conditions. The RMR is determined as the sum of the relative rating associated with each parameter.

Due to limited test data and studies, no analytical methods are currently available to estimate the end resistance of drilled shafts bearing on a rigid rock layer overlying more compressible rock layers.

Table 2.12: Approximate relationship between rock-mass quality and fractured rock-mass parameters used in defining nonlinear strength (Hoek and Brown 1988)

Rock Quality	Parameters	Rock Type A = Carbonate rocks with well-developed crystal cleavage: dolomite, limestone and marble B = Lithified argrillaceous rocks: mudstone, siltstone, shale and slate (normal to cleavage) C = Arenaceous rocks with strong crystals and poorly developed crystal cleavage: sandstone and quartzite D = Fine grained polymineralic igneous crystalline rocks: andesite, dolerite, diabase and rhyolite E = Coarse grained polymineralic igneous & metamorphic crystalline rocks: amphibolite, gabbro gneiss, granite, norite, quartz-diorite				
		A	B	C	D	E
INTACT ROCK SAMPLES Laboratory size specimens free from discontinuities. RMR = 100	m s	7.00 1.00	10.00 1.00	15.00 1.00	17.00 1.00	25.00 1.00
VERY GOOD QUALITY ROCK MASS Tightly interlocking undisturbed rock with unweathered joint at 3 to 10 ft. RMR = 85	m s	2.40 0.082	3.43 0.082	5.14 0.082	5.82 0.082	8.567 0.082
GOOD QUALITY ROCK MASS Fresh to slightly weathered rock, slightly disturbed with joints at 3 to 10 ft. RMR = 65	m s	0.575 0.0029 3	0.821 0.0029 3	1.231 0.0029 3	1.395 0.0029 3	2.052 0.0029 3
FAIR QUALITY ROCK MASS Several sets of moderately weathered joints spaced at 1 to 3 ft. RMR = 44	m s	0.128 0.0000 9	0.183 0.0000 9	0.275 0.0000 9	0.311 0.0000 9	0.458 0.0000 9
POOR QUALITY ROCK MASS Numerous weathered joints at 2 to 12 in.; some gouge. Clean compacted waste rock. RMR = 23	m s	0.029 3×10^{-6}	0.041 3×10^{-6}	0.061 3×10^{-6}	0.069 3×10^{-6}	0.102 3×10^{-6}
VERY POOR QUALITY ROCK MASS Numerous heavily weathered joints spaced < 2 in. with gouge. Waste rock with fines. RMR = 3	m s	0.007 1×10^{-7}	0.010 1×10^{-7}	0.015 1×10^{-7}	0.017 1×10^{-7}	0.025 1×10^{-7}

Table 2.13: Geomechanics classification of rock-masses (AASHTO, 2010)

	Parameter		Ranges of Values						
1	Strength of intact rock material	Point load strength index	> 175 ksf	85 – 175 ksf	45 – 85 ksf	20 – 45 ksf	For this low range, uniaxial compressive test is preferred		
		Uniaxial compressive strength, q_u	> 4320 ksf	2160 – 4320 ksf	1080 – 2160 ksf	520 – 1080 ksf	215 – 520 ksf	70 – 215 ksf	20 – 70 ksf
	Relative Rating		15	12	7	4	2	1	0
2	Drill core quality RQD		90% to 100%	75% to 90%		50% to 75%	25% to 50%		< 25%
	Relative Rating		20	17		13	8		3
3	Spacing of joints		> 10 ft	3 – 10 ft		1 – 3 ft	2 in – 1 ft		< 2 in
	Relative Rating		30	25		20	10		5
4	Condition of joints		• Very rough surface • Not continuous • No separation • Hard joint wall rock	• Slightly rough surfaces • Separation < 0.05 in • Hard joint wall rock		• Slightly rough surface • Separation < 0.05 in • Soft joint wall rock	• Slicken-sided surface or • Gouge < 0.2 in thick or • Joints open 0.05 – 0.2 in • Continuous joints		• Soft gouge > 0.2 in thick or • Joints open > 0.2 in • Continuous joints
	Relative Rating		25	20		12	6		0
5	Ground water conditions (use one of the three) evaluation criteria as appropriate to the method of exploration	Inflow per 30 ft tunnel length	None	< 400 gal./hr		400 – 2000 gal./hr			> 2000 gal./hr
		Ratio = joint water pressure/ major principal stress	0	0.0 – 0.2		0.2 – 0.5			> 0.5
		General conditions	Completely Dry	Moist only (interstitial water)		Water under moderate pressure			Severe water problems
	Relative Rating		10	7		4			0

2.4 Drilled Shaft Field Load Testing

Although the literature provides a wide array of analytical methods correlating geomaterials properties to drilled shaft field performance, drilled shaft capacity prediction is subject to various uncertainties. Potential sources of errors in the anticipated drilled shaft resistance include errors associated with the method utilized to determine relevant geomaterial properties (correlations, laboratory testing, or field testing), errors due to sampling disturbance and improper testing techniques, influence of local soil conditions and construction practices. To date, the most reliable approach to determining drilled shaft resistance has been to perform load tests at the actual project site. For design purposes, field load tests are performed to either obtain load transfer characteristics of the side and end bearing resistance components for design optimization of the production shafts (load transfer test) or to verify that the as-built test shaft is capable of withstanding the anticipated superstructure loads without excessive deformation (proof test). Load tests can be performed at various stages of a given project. They can be conducted either during the design phase, at the start of construction, or on the production shaft. Performing field load tests during the design phase of the project is almost always more beneficial. By doing so, the foundation design can be refined to achieve the highest efficiency based on tests results. Results from load tests performed at the start of construction can also be used to make shaft length adjustments, although radical design changes could be impractical. Potential cost savings associated with this option are reduced due to higher bids and increased contingency from the contractor. Load tests on production shafts can assure quality and improve reliability of the constructed shafts. However test results cannot be used to make design changes to the already built foundation. Therefore, the production shaft design is more conservative and costly to accommodate for unfavorable test results. Furthermore, the load tested production shafts can experience permanent displacements or structural damages that may negatively impact the future performance of the shafts. Because of the significant amount of time and money necessary to perform field load tests, meticulous planning is required to achieve maximum benefits.

2.4.1 General Considerations in Planning Axial Load Tests

To maximize the benefits of conducting field load tests, the most important objectives of the testing program must be clearly defined in the initial phase of planning. To ensure the successful completion of these objectives, they should be included in the contract documents to inform all participants involved in the project. In general, the most important goals are associated with identifying and quantifying design parameters that control the foundation performance. The focus of the load test can then be shifted depending upon which resistance components (rock socket vs. overburden, side shear vs. end bearing on rock) are expected to contribute the most to the overall drilled shaft axial resistance. The test shaft can thus be instrumented properly to determine load transfer characteristics along the shafts and to refine the design as needed. As listed by Brown et al. (2010), possible objectives of a drilled shaft axial load test include but are not limited to the following:

- Determine base resistance at a representative location in the bearing stratum
- Determine base resistance using a specific construction method and level of bottom-hole cleanliness
- Determine side resistance in a rock socket at a representative location in the bearing formation
- Determine side resistance with a specific construction method and drilling fluid
- Determine side resistance after the maximum allowed exposure time to drilling fluid
- Determine side resistance after the maximum allowed exposure time of an open hole in a rock which is prone to weathering and degradation
- Determine the benefits of sidewall grooving to side resistance (might include tests with and without grooving, for instance)
- Determine the distribution of side resistance in various strata, each of which may contribute to the total resistance
- Determine the side resistance at large axial displacement to verify that strain softening and brittle behavior does not occur
- Determine the contribution to side resistance of a portion of the shaft within permanent casing

- Determine the axial resistance below the scour zone by separating the portion of resistance above the design scour elevation
- Determine shaft load versus displacement relationships for both side and base resistance

Other secondary objectives might include assessment of constructability issues, assessment of installation method, effect of construction on nearby structures, concrete mix, etc. Once the objectives of the load test program have been identified, the number and location of test shafts must be determined. For a given project site, they are controlled by five main considerations including the variability of the subsurface geology, objectives of the test program, characteristics of the supporting structures, variability of the geomaterial properties, and the type of construction procedures. Depending on the variability of the subsurface geology and stratigraphy, it might be necessary to divide the project area into more than one "site" for field load test purposes. Although this task is left to the designer's discretion, the following guidelines can be considered when evaluating whether a particular location should be considered a different site:

- The geologic character of the predominant bearing formation is different; e.g., sandstone instead of shale, sand instead of clay, etc.
- The average calibrated resistance (unit load transfer in side shear or end bearing) in the zone providing the majority of the axial resistance varies from the test location by a factor of two or more,
- The location is more than 2,000 ft from the test shaft location,
- At each of the main piers of a long span bridge where there is a large number of drilled shafts in each pier foundation, particularly where the geology may differ on either side of a natural drainage feature.

The number of load tests is dependent upon the number of identified sites. A single load test would generally be performed at each site. Multiple tests could be conducted at a given site depending on the objectives of the testing program. Once the number and specific location of load tests have been determined, a confirmation boring should be performed at the location of each test to develop a subsurface stratigraphy and determine geomaterial properties.

The properties of geomaterials at the test location must be determined so that load test results can be properly interpreted and static resistance prediction methods and design parameters correctly calibrated for production shafts. Geomaterial properties can be determined from in-situ testing performed in combination with site investigation techniques such as borings or soundings prior to the test shaft construction and careful observation of the test shaft excavation during construction. A detailed log of the excavation during construction will ensure consistency with the stratigraphy observed in the boring and highlight any differences that could appear useful in interpreting test results. The excavation can also reveal important geological features such as boulders, irregular rock surface, cemented layers, and soft or weathered layers that cannot be identified from small diameter borings or rock core. Soil and rock samples should also be collected and taken to the laboratory for classification and testing.

Differences in overburden conditions between the test shaft and production shafts due to grade changes or scour should also be considered. This difference can significantly affect the axial resistance as a result of the loss of some bearing layers and confining stresses. Load tests must, therefore, be conducted under the same conditions as those of the production shafts. Otherwise, appropriate measures should be taken to ensure that resistance from strata susceptible to scour and stress changes are evaluated and accounted for in the interpretation of test results and final design.

Because of the influence of construction techniques on drilled shaft axial resistance, test shafts and production shafts must be constructed using the same methods to ensure similar performance. If possible, a technique shaft should be performed before the test shaft is installed to evaluate the effects of the selected drilling fluids, use of casing, drilling and base clean out tools in order to anticipate and resolve any potential construction issues. The as-built dimensions of the test shaft should also be determined and utilized to appropriately interpret load test results. These dimensions can be estimated from concrete volume measurements as a function of depth or more precisely from sonic caliper measurements.

2.4.2 Field Load Test Methods

Drilled shaft field capacity verification can be conducted using conventional top-down load test, bi-directional load test, rapid load test, or high strain dynamic load test. Advantages and limitations associated with each of these methods are presented in the following sections.

2.4.2.1 Conventional top-down load test

In a conventional top-down load test, the axial performance of a drilled shaft is measured by applying a downward static load on top of the shaft using a hydraulic jack that reacts against a properly designed reaction system. The reaction system is generally composed of a main reaction beam and an anchorage system that may consist of drilled shafts with threaded rods, micropiles, grouted anchors, or driven piles. Sufficient clear spacing must be provided between the anchorage system and the test shaft to avoid impacting the test shaft performance. As recommended by the Standard Test methods for Deep Foundations Under Static Axial Compressive Load (ASTM D-1143), the anchor piles should be installed at a minimum clear distance of five times the diameter of the test shaft or anchor piles, whichever is the greater. When large diameter shafts make this requirement impractical, a spacing of 3.5 diameters can be used instead, as long as the test shaft performance is not affected. It is also crucial to design the reaction system to prevent twisting or eccentric loading in the reaction beam, which could lead to safety issues as well as inaccurate measurements from damaged equipment (i.e. jack and load cell). The reaction frame should be appropriately instrumented so that any unexpected behavior can be detected and appropriate measures taken to guarantee safe progress and conclusion of the test. The loading procedure should follow the ASTM D-1143 “Procedure A: Quick Test” method, which requires load increments corresponding to 5% of the “anticipated failure load” to be maintained at the same time interval ranging between 4 and 15 minutes. Shaft instrumentation readings should be recorded at various periods including 0.5, 1, 2, and 4 minutes up and 8 and 15 minutes for longer intervals. Unloading should be completed in 5 to 10 equal decrements using the same time intervals. ASTM D-1143 provides other alternate loading procedures including the Maintained Test, Loading in Excess of Maintained Test, Constant Rate of Penetration Test, Constant Movement Increment Test, and the Cyclic

Loading Test. Conventional top-down load tests are time consuming and can become expensive and impractical as the drilled shafts size and capacity gets larger.

2.4.2.2 Bi-directional load test

Bi-directional load tests have grown to become the preferred testing method for several state DOT's. As a result of its loading mechanism, the embedded sacrificial jack(s) is/are capable of subjecting drilled shafts to large magnitudes of load without the need of reaction systems, which can become increasingly expensive and impractical in the realm of typical drilled shaft loads. A typical bi-directional load test setup using an Osterberg load cell (O-cell) is illustrated in Figure 2.7.

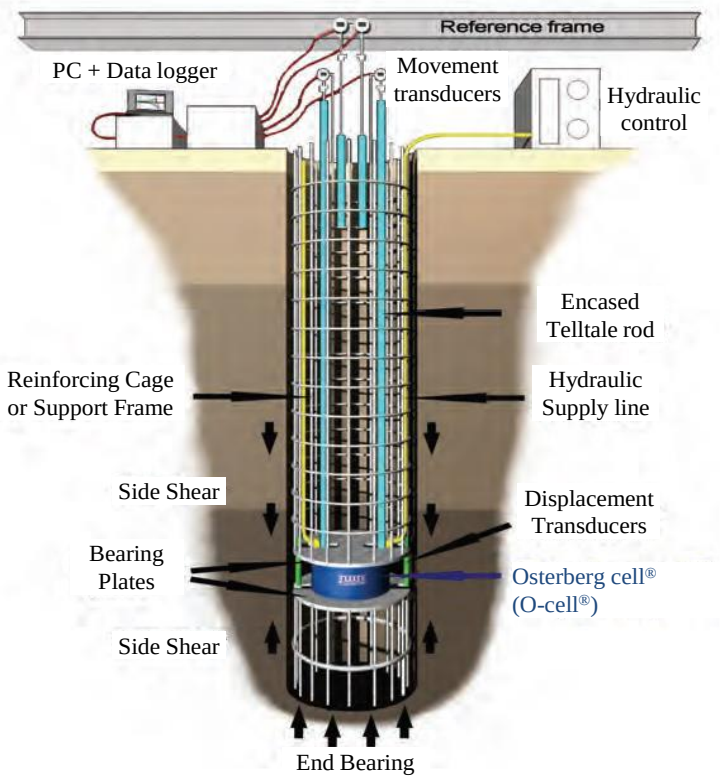

Figure 2.7: Bi-directional load test schematic using O-cell (Loadtest, Inc.)

The O-cell assembly, composed of an O-cell placed between an upper and lower steel bearing plates, is installed at a predetermined location within the shaft reinforcing cage. Single O-cells range between 9 and 34 inches in diameter and are able to subject drilled

shafts to bi-directional loads ranging between 800 and 12,000 kips. Depending on the cross-sectional space available between the steel bearing plates, it may be possible to use multiple O-cells in combination to deliver more than 12,000 kips of bi-directional loads.

After the concrete has been cast and allowed to cure sufficiently, the test is initiated by pressurizing the O-cell just enough to break the tack welds that hold the cell together dividing the shaft into an upper and lower portion as a result. The O-cell is typically pressurized using water or a combination of water and biodegradable vegetable oil. After breaking the tack welds, the internal pressure of the O-cell is increased incrementally to load the upper and bottom sections of the shaft. Movement of the segment above the cell is resisted by downward side shear while movement of the segment below the cell is resisted by a combination of upward side shear and end bearing. Instrumentation installed at various locations along the shaft length provide data on the strains and movements taking place during the test. Movements of the top and bottom bearing plates of the O-cell assembly as well as shaft compression are measured by telltale rods extending to the top of the shaft while displacement transducers located between the O-cell plates measure the O-cell expansion. Load transfer in various strata along the shaft is measured by strain gauges installed at carefully selected elevations.

The test is conducted until one of the following outcomes: failure in side shear of the upper segment, failure in side shear and end bearing of the lower segment, simultaneous failure of both upper and lower segments, maximum capacity or stroke of load cell reached. The load cell assembly should ideally be located at a depth above and below which the axial resistances are approximately equal so that the side shear and base resistances are fully mobilized. Otherwise, the test will terminate as soon as either section reaches its ultimate resistance as shown in Figure 2.8 and Figure 2.9. In cases where the O-cell is undersized, neither portion of the shaft will reach its maximum capacity at the end of the test as illustrated in Figure 2.10. O-cell load testing can be conducted in multiple stages by using multiple cells embedded at different levels along the shaft in order to obtain separate resistance measurements of various segments.

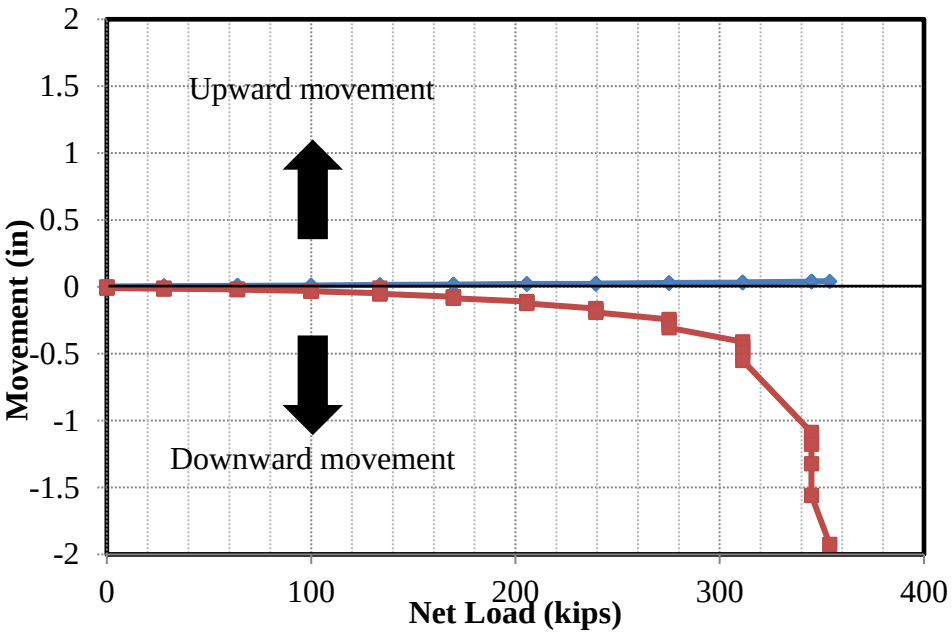

Figure 2.8: Example of O-cell test with failure of lower section

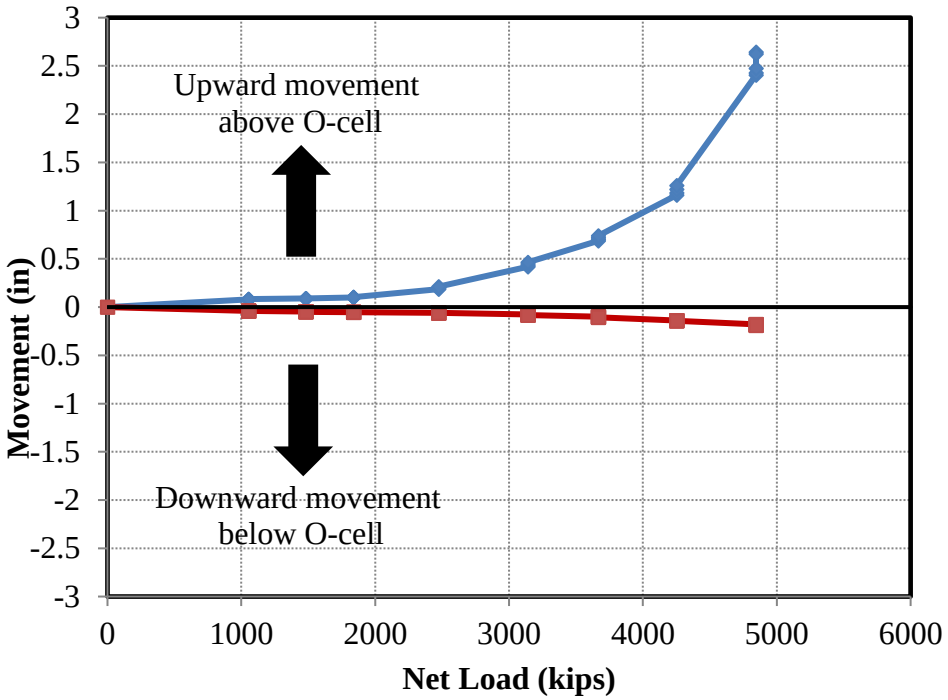

Figure 2.9: Example of O-cell test with failure of upper section

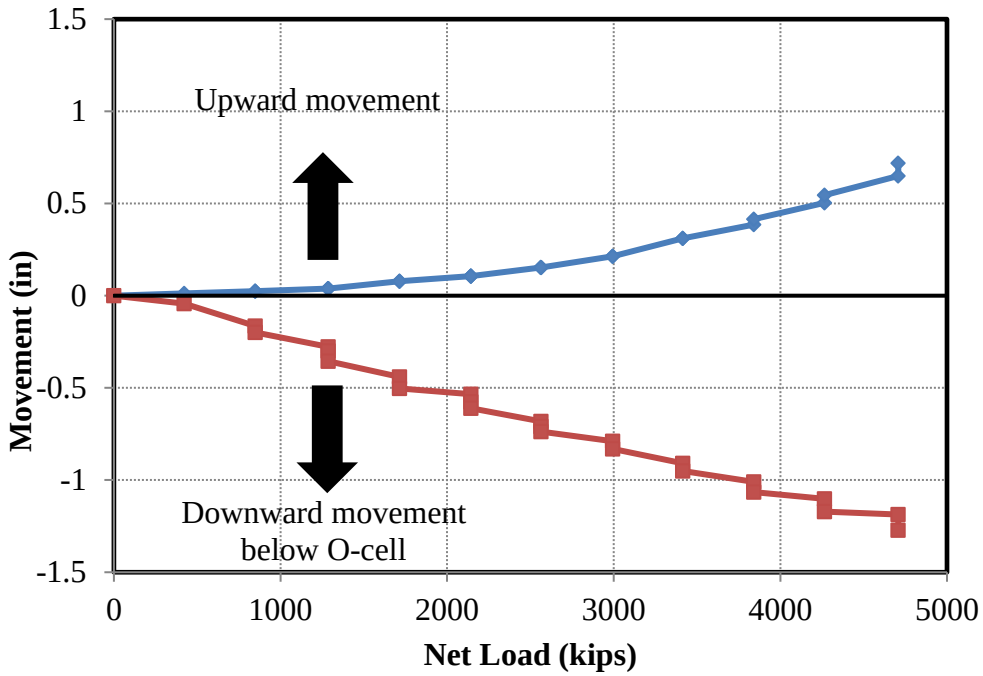

Figure 2.10: Example of O-cell test in which neither upper nor lower resistance reach ultimate capacity

This multi-stage loading approach can also overcome the difficult task of determining the correct depth of a single O-cell assembly to achieve a balanced failure condition. Schematics of such test setup is illustrated by Figure 2.11.

Since production shafts are loaded at the top, O-cell load test results which, provide two separate load-displacement responses for the upper and lower segments of the shaft, are usually combined into an equivalent top-load displacement curve following a two-part procedure developed by Loadtest, Inc. The construction procedure includes the following assumptions:

- The drilled shaft is initially considered as a rigid element, then the additional elastic compression that would occur in a top loaded shaft is estimated and included
- The load-displacement response of the segment below the O-cell is identical as when top loading the entire shaft

- When the O-cell is placed near or at the bottom of the shaft, the net end bearing load-movement response developed by the bottom of the O-cell is the same as the end bearing load-movement response in a top loaded shaft
- The side resistance-displacement curve in a top loaded shaft is equivalent to the same net side shear multiplied by an adjustment factor 'F' for a given downward movement as occurred in the O-cell test for that same movement at the top of the cell in the upward direction. The adjustment factor F is 1.00 for all rock sockets and primarily cohesive soils in compression, 0.95 for primarily cohesionless soils, and 0.80 for all soils in top load tension tests.

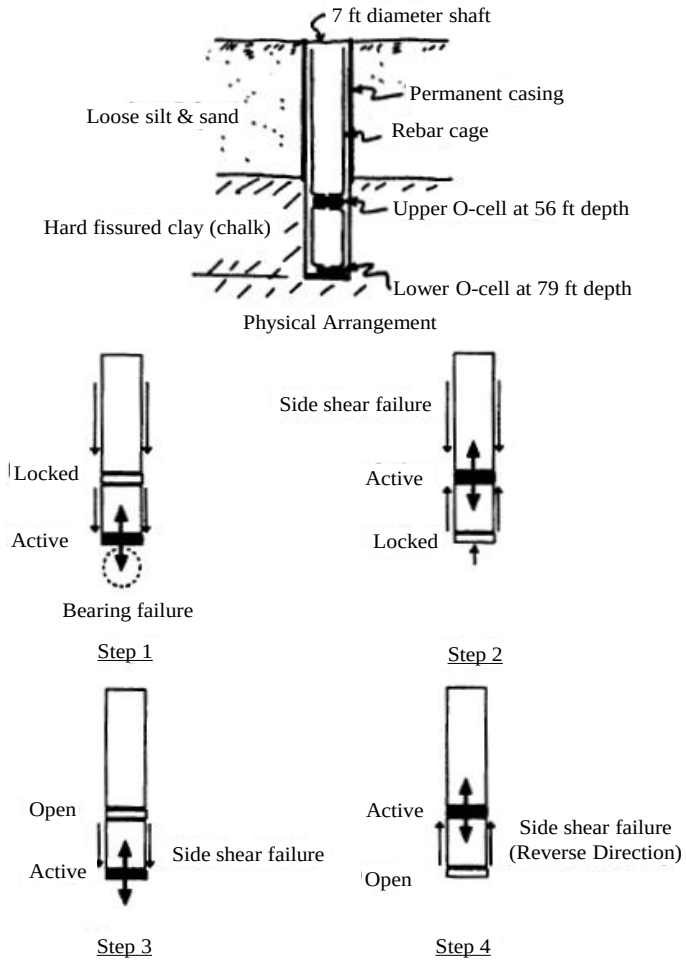

Figure 2.11: Multi-level O-cell testing arrangement (O'Neill et al. 1996)

In part I of the procedure, the equivalent top-load displacement curve for the rigid shaft resulting from the upper and lower sections is obtained by selecting arbitrary displacement values, and determining and summing the upward and downward net loads corresponding to the same displacement as shown in Figure 2.12 and Figure 2.13. In doing so, it may be necessary to extrapolate resistance of the portion which displaced the least. However, extrapolation beyond the maximum measured value may be unconservative if side shear is susceptible to strain softening. After the equivalent top-load displacement curve of the rigid shaft is constructed, the additional elastic compression of the top-loaded shaft is estimated in part II of the procedure and included to the shaft response as shown in Figure 2.14.

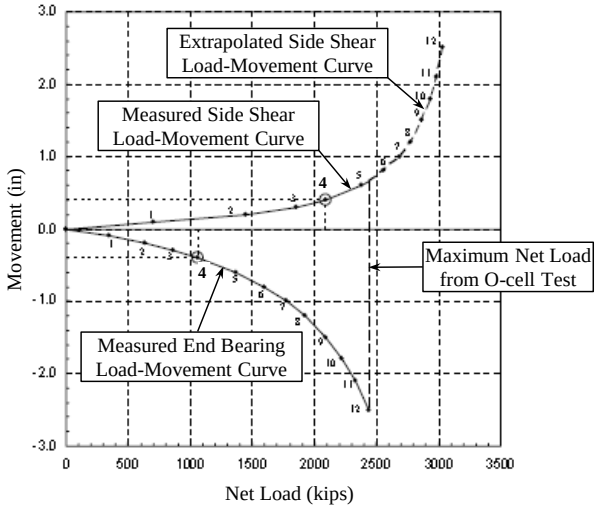

Figure 2.12: Example of measured and extrapolated O-cell load-displacement curves (Loadtest, Inc.)

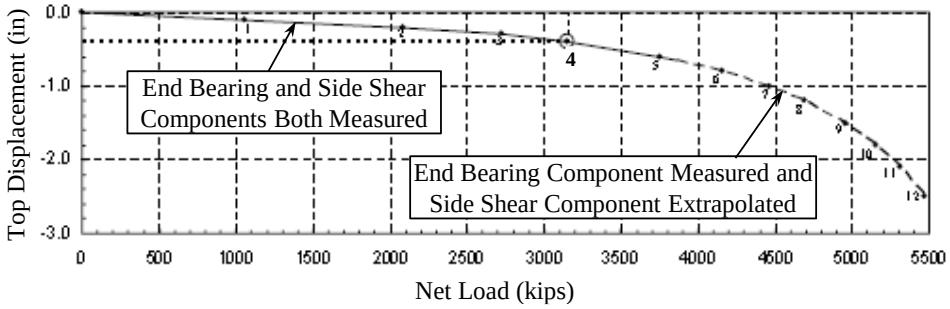

Figure 2.13: Equivalent top-load displacement curve based on O-cell data in Figure 2.12 (Loadtest, Inc.)

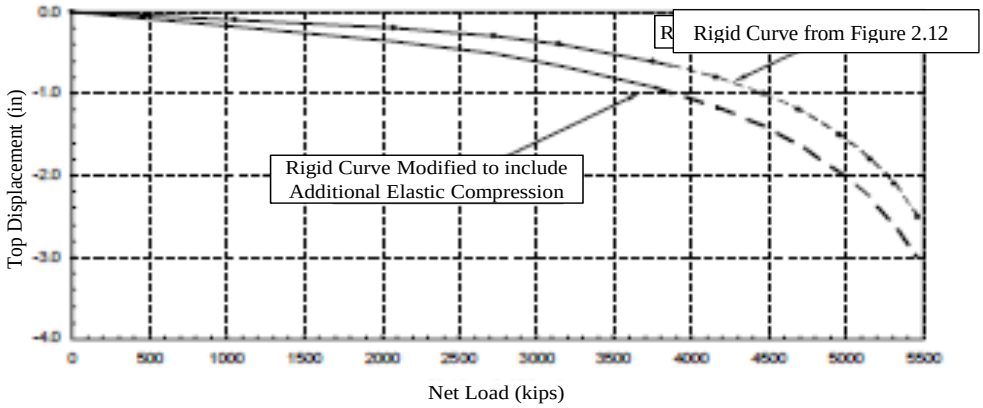

Figure 2.14: Equivalent top-loaded displacement curve including elastic compression (Loadtest, Inc.)

An important difference between O-cell load test and actual loading condition as simulated by top-down load test is the resistance distribution with depth. As shown in Figure 2.15, axial load decreases in the downward direction for top loaded shaft whereas it decreases in the upward direction in an O-cell test. Due to the lack of evidence suggesting otherwise, it is usually assumed that drilled shaft axial resistance in soil is the same regardless of the loading direction. For drilled shafts in rock, however, the combined effect of dilatancy at the shaft/rock interface and radial strains due to Poisson's effect is more significant in a top-down test compared to an O-cell test. Consequently, differences in side resistance distribution with depth as well as differences in total resistance of the rock socket may arise.

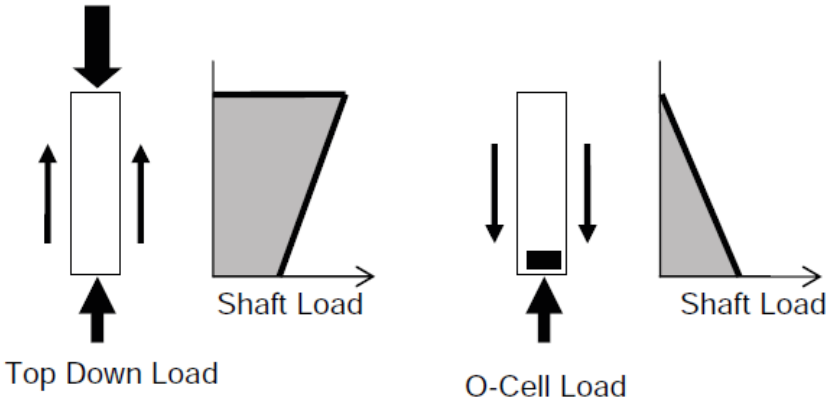

Figure 2.15: Load distribution with depth during top down and O-cell test

Based on finite element modeling, Shi (2003) suggests that the equivalent top-down curve from O-cell test is conservative at higher displacements due to differences in normal stresses at the shaft/rock interface, which increase with increasing rock mass modulus and interface friction angle. These differences should be considered when interpreting results from O-cell load tests. A summary of advantages and limitations associated with O-cell load testing is presented in Table 2.14.

Table 2.14: Advantages and limitations of O-cell load tests

Advantages	Limitations
• Ability to test high capacity production or test shafts • Ability to test at select segments of a drilled shaft • Allows investigation of creep effects	• Pre-arrangement of test setup is required • Does not allow testing on existing drilled shafts • The accuracy of the equivalent top-load displacement response may depend how the data interpretation • Construction of equivalent top load-displacement curve may require data extrapolation is some cases • Discrepancy in skin resistance associated with upward loading vs. downward loading is not completely known, but treated with adjustment factors

2.4.2.3 Rapid load test

Rapid load test is performed in accordance with ASTM D-7383-08 and can be accomplished in two different ways. The first method consists in dropping a heavy mass on top of the drilled shaft, which is covered with a soft cushion that reduces the acceleration of the mass over the desired time interval. This method can be used to apply up to 1000 kips of load on drilled shafts. The more commonly used method follows Newton's 2nd Law and involves the use of combustion gas pressure to accelerate a heavy mass positioned on top of the shaft in the upward direction thereby producing an equal and opposite downward force on the shaft. The reaction mass weighs approximately between 5% and 10% of the test load, and the load pulse is applied over a sufficient duration of time to minimize the effects of wage propagation (80 ms to 300 ms). The test is performed using the Statnamic loading device

developed by Berminghammer and Janes (1989), which is capable of applying loads as large as 10,000 kips. Depending on the load capacity of the Statnamic device used, a catch frame mechanism or a gravel containment system is used to contain the reaction mass. A schematic of a Statnamic loading device and test setup is shown in Figure 2.16. Gas pressure, generated by combustion of pelletized fuel held in the fuel chamber, produces upward acceleration of the reaction mass. A calibrated load cell positioned on top of the shaft measures the applied force over time during the test while the shaft displacement is measured using a photo-voltaic sensor mounted with the load cell. The shaft downward acceleration is also monitored via servo-accelerometers. Examples of measurements from rapid load testing are presented in Figure 2.17. Shown are the Statnamic applied force, F_{stn}, the shaft inertial force, Fa, and the shaft displacement. The load transferred to the soil is calculated as the difference between the Statnamic applied force and the shaft inertial force. The overall soil resistance has two components including a static resistance, F_s, and a dynamic resistance F_d. The static axial resistance of the shaft can be determined from the test data using the unloading point method (UPM) or the segmental unloading point method (SUPM) depending on the shaft length.

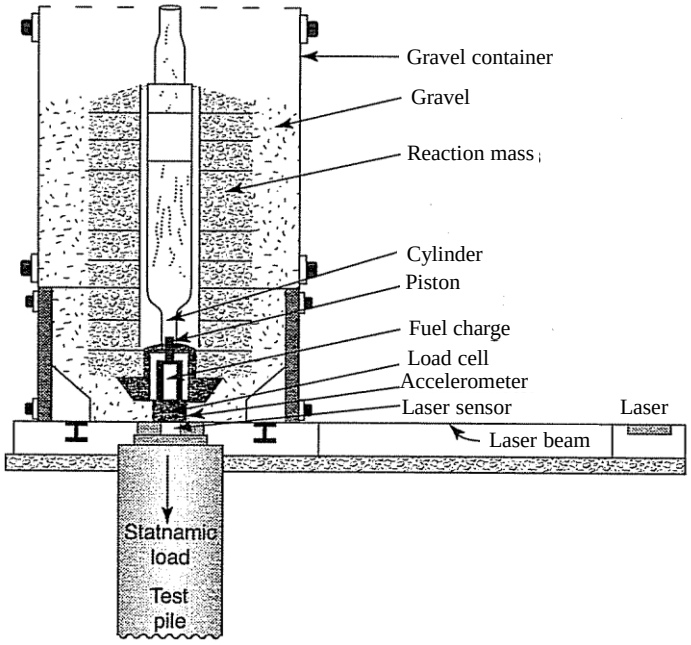

Figure 2.16: Schematic of Statnamic loading apparatus

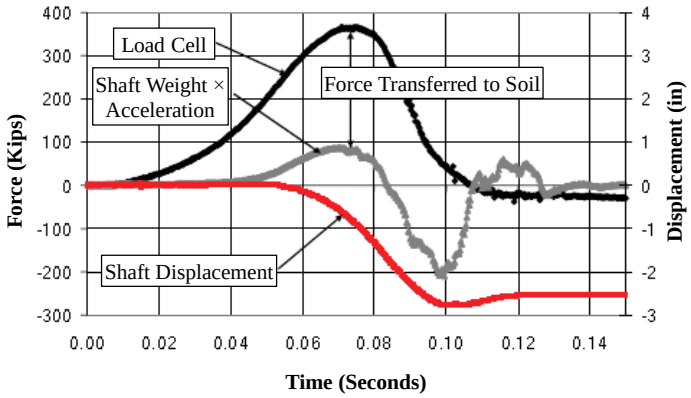

Figure 2.17: Example of force, acceleration and displacement measurements during a rapid load test (Brown et al. 2010)

Following the UPM procedure, equilibrium of the forces acting on the shaft can be written using the simple single degree of freedom model shown in Figure 2.18 as:

$$F_{stn} = F_a + F_d + F_s = m\,a(t) + c\,v(t) + k\,u(t) \tag{2.54}$$

where,

c = Damping coefficient

v(t) = Shaft velocity

k = Soil-pile stiffness

u(t) = Shaft displacement

By rearranging Eq. (2.54), the soil static resistance can be determined as:

$$F_s = F_{stn} - (F_a - F_d) = F_{stn} - m\,a(t) - c\,v(t) \tag{2.55}$$

At the unloading i.e. point 2 in Figure 2.19, the soil dynamic resistance is zero as the result of the velocity being equal to zero. The static resistance can thus be calculated from Eq. (2.55) since the statnamic force and the shaft inertial force are known values. Then, the damping coefficient can be calculated at any point between 1 and 2 using Eq. (2.56) and assuming that the maximum static resistance is fully mobilized and constant between point 1 and point 2 in Figure 2.19.

$$c(t) = \frac{F_{stn}(t) - F_a(t) - F_{s\,max}}{v(t)} \tag{2.56}$$

Once a best estimate average of the damping coefficient is selected, Eq. (2.55) can be used to develop the complete static load-displacement curve.

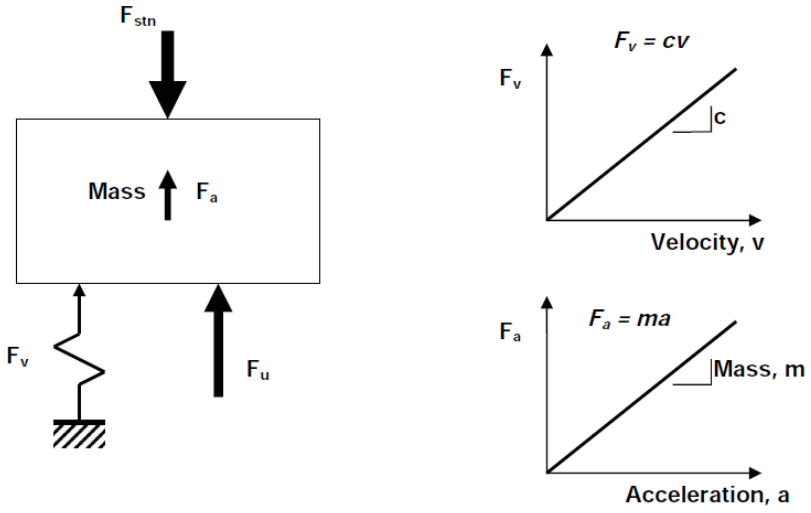

Figure 2.18: Statnamic test single degree of freedom model (Brown et al. 2010)

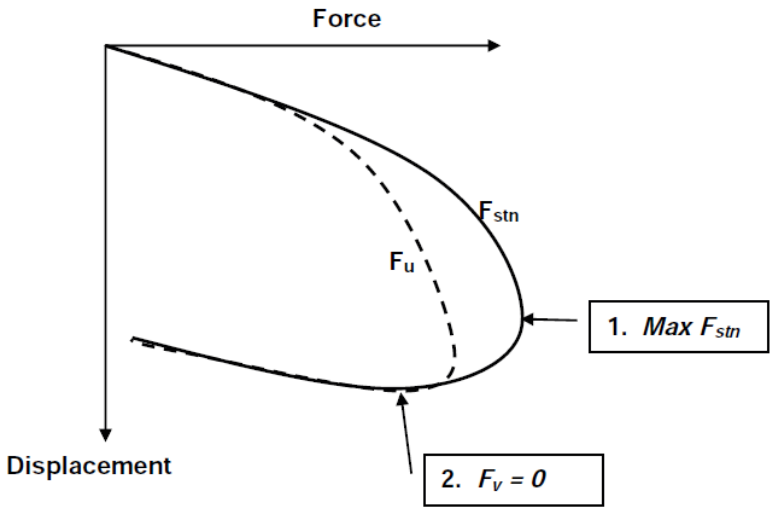

Figure 2.19: Statnamic load-displacement curve (Brown et al. 2010)

The SUPM is used for shafts with length greater than 80 ft to 100 ft, and it follows the same procedure as the UPM. The shaft in this approach, however, is treated as a series of multiple segments, therefore instrumentation is necessary along the shaft to determine the magnitude of load transferred between segments. Once the static resistance is determined following either procedure, loading rate effects are accounted for using the soil-dependent rate factors given in Table 2.15. A summary of the advantages and limitations associated with rapid load testing is presented in Table 2.16.

Table 2.15: Rate factors

Rock	Sand	Silt	Clay
0.96	0.91	0.69	0.65

Table 2.16: Rapid load testing advantages and limitations

Advantages	Limitations
• Ability to test existing or production shafts with relatively high capacity • Able to replicate actual top loading conditions • Economies of scale for multiple tests • Eliminates need for reaction system	• Cost of reaction weights mobilization • Test load is limited to 5000 tons • Rate effects must be considered in the resistance estimation

2.4.2.4 High strain dynamic test

In high strain dynamic testing, the shaft is subjected to the impact of a falling mass using either a custom fabricated drop weight test apparatus or a large pile driving hammer. To prevent significant compression and tension forces from developing, the shaft top must be properly cushioned, and the weight of the falling mass should not exceed 1% to 2% the desired test load. Force and velocity at the shaft top are measured using strain transducers and accelerometers linked to a device such as the Pile Driving Analyzer (PDA). The applied force at a given time can be obtained either from the strain transducer measurements using Eq. (4) or from the accelerometer data using Eq. (5).

$$F = \varepsilon EA \tag{2.57}$$

$$F = \left(\frac{EA}{C}\right) v = Z\, v \tag{2.58}$$

where,

F = Force in a uniform shaft

ε = Measured strain

E = Elastic modulus of a uniform shaft

A = Cross-sectional area of a uniform shaft

v = Particle velocity in a uniform shaft

C = Wave speed of a uniform shaft = $\sqrt{\frac{E}{\rho}}$

ρ = Mass density of a uniform shaft

Z = Shaft impedance

Shaft displacement over time is calculated by double integration of the measured acceleration. To ensure reliable measurements, the top of the shaft must be exposed to provide the appropriate area for the strain gauges and accelerometers. These gauges should ideally be mounted directly on the concrete at four points 90° apart around the shaft and at a distance of 1 to 1.5 diameters below the top of the shaft.

The soil static resistance can be determined from the test data using the Case Method (Eq. (2.59), which uses wave propagation theory and assumes that the dynamic soil resistance is a linear function of viscous damping and pile toe capacity (Rausche, 1985).

$$R_s = \frac{1}{2}\left\{(1 - J_c)\left[F_T(t_m) + \frac{EA}{C} v_T(t_m)\right] + (1 + J_c)\left[F_T\left(t_m + \frac{2L}{C}\right) - \frac{EA}{C} v_T\left(t_m + \frac{2L}{C}\right)\right]\right\} \tag{2.59}$$

where,

R_s = Maximum static soil resistance

t_m = Time when maximum total resistance occurs

$F_T(t_m)$ = Measured force near pile top at time t_m

$v_T(t_m)$ = Measured velocity near pile top at time t_m

J_c = Dimensionless Case damping factor,

C = Pile wave speed

E = Modulus of elasticity of a pile material

A = Cross-sectional area of a pile (in^2)

L = Pile length below gauges

This method may not always be accurate since the dynamic soil resistance is assumed to be related to the pile toe capacity, and a more sophisticated analysis involving a signal matching process may be required to derive reliable static resistance from the test data. In this process, the shaft is discretized into several segments as shown in Figure 2.20. Each segment is assigned a mass, a stiffness, and a soil model composed of an elastic-plastic spring and a linear viscous damper. For a given input force and velocity, the response of the model is computed and compared to the actual test shaft response. The model parameters are adjusted until convergence is achieved between the computed and measured shaft responses. The distribution of side and end resistances obtained from this signal matching process is not a unique solution but is generally considered to be a good approximation. Various computer programs such as CAPWAP have been developed and are available to facilitate this rigorous analysis. Interpretation of the test data by signal matching is significantly influenced by several factors including damping and the shaft impedance. Therefore, the soil conditions and the impedance profile of the shaft must be known and carefully considered during the analysis to avoid underestimating or overestimating the different resistance components. High strain dynamic testing should be performed in accordance with ASTM D 4945, and its advantages and limitations are presented in Table 2.17.

2.4.2.5 Uplift test

Uplift load testing may be necessary for projects with foundations subjected to significant uplift loads from earthquake or wind induced overturning moments. The test loading system generally requires high strength steel rods to be embedded into the full length of the shaft as shown in the test setup example in Figure 2.21. When these rods are anchored to the concrete, the shaft is subjected to tensile stresses. The reduction of normal stresses at the shaft/soil interface as a result of Poisson's effect will tend to reduce the shaft side shear. Otherwise, the steel rods can be isolated from the concrete using adequate sleeves, and

anchored to a steel plate at the bottom of the shaft. In this case, the shaft will be subjected to compression, and normal stresses at the interface may tend to increase.

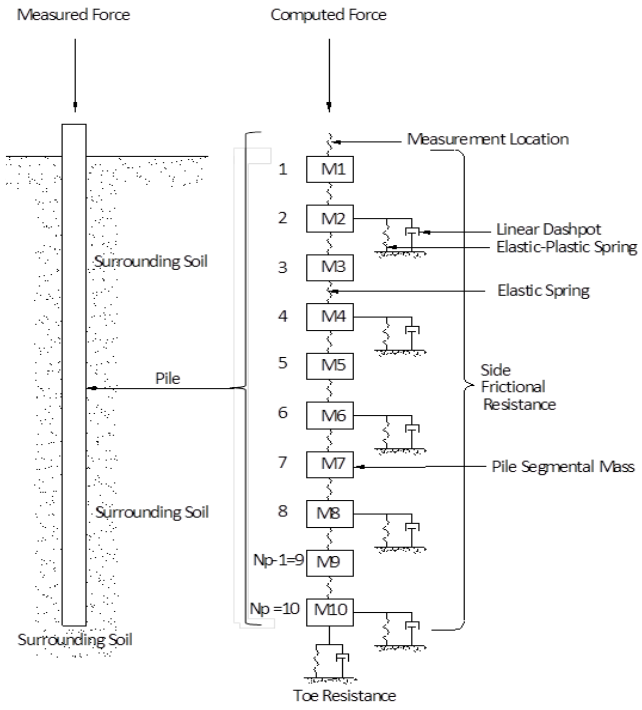

Figure 2.20: CAPWAP model of shaft/soil system (Hannigan et al. 1998)

Table 2.17: High strain dynamic testing advantages and limitations

Advantages	Limitations
• Ability to test existing or production shafts with relatively high capacity • Able to replicate actual top loading conditions • Relatively cheap compared to other types of testing • Test can be performed with minimal setup • Does not require reaction system	• Limited capacity compared to bi-directional testing • Signal matching analysis produces non-unique resistance distribution • Potential damage of shaft top from driving stresses • Estimation is highly dependent on soil damping and elastic characteristics • Data interpretation requires accurate knowledge of shaft structural properties and surrounding soil parameters

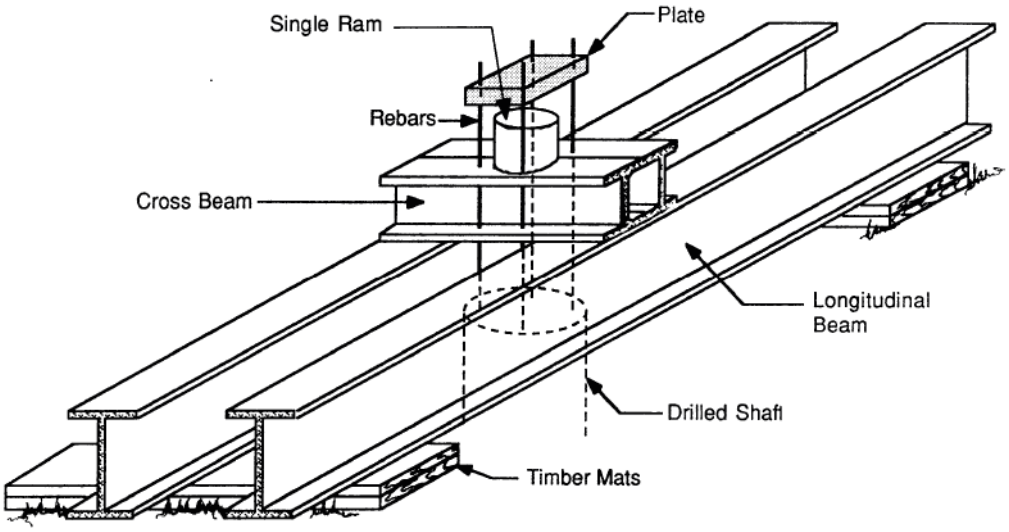

Figure 2.21: Uplift test setup

It is important to consider these different conditions in selecting the best approach to evaluate the desired loading condition. The reaction foundation may consist of mats or shafts depending on the ground conditions. The reaction foundation must be carefully selected and placed at sufficiently large distance from the test shaft to avoid creating stresses in the test shaft zone of influence.

2.5 Structural Design

From a structural point of view, drilled shafts are treated as reinforced concrete beam-columns, and their design is performed according to AASHTO LRFD Bridge Design Specifications. Details on the minimum and maximum required longitudinal and transverse reinforcement are provided by the AASHTO (2016). Drilled shaft resistance to compressive axial load is calculated as:

$$R_p \leq R_{sp} = \beta\left[0.85f'_c\left(A_g - A_s\right) + A_s f_y\right] \quad (2\text{-}60)$$

where,

β = Reduction factor, 0.85 for spiral reinforcement and 0.80 for tie reinforcement,

f'_c = Specified minimum 28-day compressive strength of concrete,

A_g = Gross area of drilled shaft section,

A_s = Total area of longitudinal steel reinforcement, and

f_y = Specified yield strength of steel reinforcement.

2.6 AASHTO Drilled Shafts LRFD Resistance Factors

Specifications for the design of drilled shafts in axial compression at Strength I limit state in accordance with LRFD are recommended by AASHTO (2016) based on the work of Brown et al (2010) and Allen (2005). Slight changes were made to these specifications to reflect a departure from O'Neill and Reese (1999) design methods, which served as the basis of previous editions of AASHTO. Current recommended design methods and their corresponding resistance factors are presented in Table 2.18. With the exception of resistance factors for skin friction prediction in sand and rock, all other resistance factors remain unchanged from the previous edition. Resistance factors for skin friction prediction in sand and rock were updated to reflect the transition of design methods from O'Neill & Reese (1999) to Brown et al. (2010). These resistance factors are recommended based on a calibration by fitting to current factors of safety until reliability analyses can be conducted for the new methods. A 20% reduction in all resistance factors is recommended when a single drilled shaft is used to support a bridge pier. A resistance factor of 1.0 is recommended for serviceability limit state to ensure that the drilled shaft settlement does not exceed a tolerable value.

2.7 States Regional LRFD Calibration

Given the limitations associated with resistance factors recommended by AASHTO for drilled shaft design, local jurisdiction have, in recent years, dedicated significant efforts to research studies designed to develop and implement resistance factors that better 1) reflect local soil conditions and construction practices; 2) cover design methods other than those recommended by AASHTO; and 3) improve drilled shaft design efficiency thereby reducing foundation cost.

Table 2.18: AASHTO (2016) drilled shaft resistance factors for axial compression

Method/Soil/Condition			Resistance Factor
Nominal Axial Compressive Resistance of Single-Drilled Shafts, φ	Side resistance in clay	α-method (Brown et al., 2010)	0.45
	Tip resistance in clay	Total Stress (Brown et al., 2010)	0.40
	Side resistance in sand	β-method (Brown et al., 2010)	0.55
	Tip resistance in sand	Brown et al. (2010)	0.50
	Side resistance in cohesive IGM	Brown et al. (2010)	0.60
	Tip resistance in cohesive IGM	Brown et al. (2010)	0.55
	Side resistance in rock	Kulhawy et al. (2005) Brown et al. (2010)	0.55
	Side resistance in rock	Carter and Kulhawy (1988)	0.50
	Tip resistance in rock	Canadian Geotechnical Society (1985) Pressuremeter Method (Canadian Geotechnical Society, 1985) Brown et al. (2010)	0.50

2.7.1 Louisiana

A series of several calibration studies were conducted in order to develop resistance factors consistent with the region's soil conditions and construction practices. The first calibration was conducted by Abu-Farsakh et al. (2010) considering a collection of sixty-six top down and O-cell load tests from Louisiana and Mississippi. Only twenty-six load tests were used in the actual calibration to maintain consistency in the soil conditions and to minimize excessive extrapolation of load test data when necessary. The majority of the load tests was conducted using the O-cell load testing method. The second calibration study, conducted by Abu Farsakh et al. (2013), used an expanded database that included eight additional tests obtained from LADOT. All shafts were constructed and tested in soil types that included silty clay, clay, sand, clayey sand, and gravel. The shaft lengths range from 35.1 to 138.1 feet with diameters ranging from to 2 to 6 feet. The Monte Carlo simulation

technique was implemented to evaluate skin friction and end bearing resistance factors associated with drilled shaft design methods recommended by O'Neill and Reese (1999) and Brown et al. (2010) for a settlement corresponding to 5% of the shaft diameter (AASHTO criterion) or the plunging load whichever occurred first. The exponential curve fitting method was selected to extrapolate a small number of drilled shafts that did not meet the 5% of the shaft diameter settlement criterion that was used in this study. Presented in Table 2.19 are the results from that calibration. On one hand, the regionally calibrated factors of 0.39 and 0.26 were far less than AASHTO recommended values of 0.45 for clay and 0.55 for sand or any average that would result from these two values. The calibrated values of 0.52 and 0.53 for tip resistance, on the other hand, showed some improvement compared to AASHTO values of 0.40 for clay and 0.50 for sand. If resistance factors for the combination of side and tip resistance are considered, the calibrated values either show some improvement or close agreement with AASHTO recommended values.

Table 2.19: Calibrated resistance factors (Abu-Farsakh et al. 2013)

Design Method	φ, side resistance	φ, tip resistance	φ, total resistance
O'Neill & Reese (1999)	0.39	0.52	0.60
Brown et al. (2010)	0.26	0.53	0.48

Following similar analysis procedures and using an updated database of sixty-nine O-cell load tests, the latest calibration study was conducted by Fortier et al. (2016). In addition, to the Monte Carlo simulation technique, the FOSM reliability method was used to calibrate the resistance factors for comparison purposes. An additional strength criterion i.e. 1-inch top displacement was also considered. Table 2.20 illustrates the calibrated resistance factors obtained from the Monte Carlo simulation. A direct comparison between the values shown in Table 2.19 and Table 2.20 shows that all resistance factors at the AASHTO criterion decreased significantly between the two calibration studies and compared to AASHTO. Another important observation in the two studies relates to the difference in the uncertainty involved with predicting the total resistance and the uncertainty associated with separate side and tip resistance prediction.

From the higher resistance factors obtained for total resistance prediction compared to side and tip resistance in both studies, it is safe to conclude that the uncertainty in predicting the total resistance is less than that associated with predicting either side or tip.

Table 2.20: Side and end bearing resistance factors after (Fortier et al. 2016)

Design Method	1-inch criterion			AASHTO criterion		
	φ, side resistance	φ, tip resistance	φ, total resistance	φ, side resistance	φ, tip resistance	φ, total resistance
O'Neill & Reese (1999)	0.30	0.19	0.34	0.35	0.16	0.38
Brown et al. (2010)	0.15	0.15	0.31	0.29	0.11	0.27

2.7.2 Kansas

Calibration of resistance factors for drilled shafts in weak rocks in the state of Kansas was conducted by Yang et al. (2010). According to the study, the use of AASHTO LRFD specifications by KDOT engineers led to designs that were often inconsistent with their past ASD practice. Thus, the calibration was justified by the need to develop regional factors that would resolve this issue and be reflective of the state's experience. To evaluate the uncertainty associated with O'Neill and Reese (1999) design method for intermediate geomaterials (IGM), a database including twenty-five O-cell load tests collected from Kansas, Colorado, Missouri, Ohio, and Illinois was developed. Using the Monte Carlo simulation technique, resistance factors for skin friction and end bearing were calibrated at the AASHTO strength criterion and at a serviceability criterion corresponding to 0.25 inch. Resistance factors associated with skin friction were calibrated following a total side resistance and layered unit side resistance approach. In addition to the target reliability of 3.0 commonly recommended for drilled shafts, the study also considered a target reliability of 2.3. Table 2.21 presents the resistance factors obtained from the calibration. Considering the total side resistance approach, the calibrated factor of 0.50 represents a decrease from AASHTO recommended value of 0.60. Following the layered side resistance approach, the regional resistance factor of 0.70 shows some improvement compared to AASHTO. This difference highlights the effect of the resistance bias calculation method on the calibrated

resistance factor (uncertainty in total resistance prediction vs. uncertainty in one or multiple layers resistance prediction), which is not covered in the AASHTO LRFD calibration framework. For end bearing, the calibration did not result in any improvement.

Table 2.21: Calibrated resistance factors modified after (Yang et al. 2010)

Situation			φ (β_t=3.0)	AASHTO φ (β_t=3.0)
Side resistance	Strength Limit State	Total	0.50	0.60
		Layered	0.70	
	Service Limit State	Total	0.35	1.00
		Layered	0.40	
Base resistance	Strength Limit State	-	0.25	0.55
	Service Limit State	-	0.15	1.00

2.7.3 Nevada

In Nevada, Motamed et al. (2016) used a database of 41 load tests to calibrate resistance factors for axially loaded drilled shafts constructed in interbedded layers of silty clay and sand with seams of caliche. With the exception of one case, all load tests used in the calibration were O-cell load tests. The shafts diameter ranged from 2 to 8 ft with lengths between 31.6 and 128 ft. Following the scoring system specifically developed for the study and illustrated in Table 2.22, the load tests were classified in 3 groups including 1) all data, 2) load tests with mean score > 2, and load tests with mean score > 3. As can be seen from the scoring system, load test quality ranges from 1 to 4 and is a function of the extent of available details on the site subsurface exploration as well as the amount of extrapolation of load test data necessary. Four design methods including M1, M2, M3, and M4 were investigated in the calibration. M1 treats caliche as very dense sand with unit weight of 140 pcf, effective friction angle of 40°, and SPT blow count of 50. M2 treats caliche as cohesive IGM with unconfined compressive strength of 100 ksf unless lower values are suggested from site specific data. M3 treats caliche as rock with unconfined compressive strength of 729 ksf and RQD of 70% unless other values are suggested by site-specific data. M4 represents an approach proposed by the author base on the following assumptions:

- The skin friction is estimated using the following: $\frac{f_{SN}}{p_a} = 0.85\sqrt{\frac{q_u}{p_a}} \leq 15.8$
- Caliche layers with lack of information on their compressive strength are assigned a value of 729 ksf
- End bearing corresponds to the rock model or 100 ksf whichever is lower
- Strongly cemented materials with SPT blow count > 50 are assigned a skin friction of 6 ksf
- Treat moderately cemented materials with SPT blow count < 50 the same as the parent material.

Table 2.22: Load test quality scoring system (Motamed et al. 2016)

Score	Scoring Criteria	
	Load Test Data	**Geotechnical Investigation Data**
1 (worst)	Extrapolation > 2% of the shaft diameter is required for both components of bi-directional movement or > 3% is required for a top-down test.	Incomplete boring logs with little to no SPT data or proper visual-manual classifications. No lab data.
2	Extrapolation > 2% of the shaft diameter is required for one component of bi-directional movement (second component may require < 2%) or > 2.5% but ≤ 3% is required for a top-down test.	Boring logs with minimal SPT data (i.e. missing for some geologic units) and useful visual-manual classifications. No lab data.
3	Extrapolation < 2% of the shaft diameter is required for both components of bi-directional movement or > 2% but ≤ 2.5% is required for a top-down test.	Boring logs are complete with SPT data, visual-manual classification and possibly torvane or pocket pen data. Limited lab data and/or additional in situ data is available.
4 (best)	Either no extrapolation is needed or extrapolation ≤ 2% of the shaft diameter is required for only one component of load-cell movement or in total for a top-down test.	Complete boring logs with detailed material classifications, SPT data and possibly other data such as CPT or shear wave velocity measurements. Thorough lab data covering soil strengths is available.

Due to the inability to separate end bearing from skin friction based on the available data, the resistance factors were calibrated for total resistance only. The Monte Carlo simulation was implemented in two approaches i.e. L1 and L2 to calibrate the resistance factors in this study.

The resistance factors calibrated using L1 relate to the uncertainty of the overall resistance predicted using the best estimate of the geomaterial properties based on available data, while those calibrated from L2 approach capture the uncertainty associated directly with the testing method and interpretation used to determine the geomaterial properties. Following the general calibration procedure, resistance factors were calibrated at a target reliability of 3.0 for a strength criterion corresponding to shafts settlement equal to 5% of the shaft diameter or plunging failure whichever occurred first. As illustrated in Table 2.23, the calibrated resistance factors ranged from 0.66 to 1.09 depending on the calibration level and the design method. The results also show that the influence of the data quality on the calibrated resistance factors was a function of the design method considered. For a given calibration level and design method, the lowest resistance factor was selected as the governing value.

Table 2.23: Total resistance factors (Motamed et al. 2016)

Calibration Level	Caliche Model	ϕ at $\beta = 3$		
		All data	Mean Score >2	Mean Score > 3
L1	M1	1.05	0.78	0.79
	M2	0.81	0.85	0.85
	M3	0.90	0.91	0.91
	M4	0.73	0.77	0.72
L2	M1	1.09	0.86	1.02
	M2	0.84	0.87	0.76
	M3	0.90	0.91	0.77
	M4	0.71	0.74	0.66

2.7.3 New Mexico

A database of ninety-five drilled shaft O-cell cell and top down load tests collected from New Mexico and other states was developed by Ng and Fazia (2012) to assist in the calibration of resistance factor for skin friction in cohesionless soils. Among the available data, only twenty four tests were selected for the calibration. It is important to also note that only five of the load tests considered were performed in New Mexico. The shafts diameter ranged from 1.5 ft to 7 ft with lengths ranging from 24.3 ft to 134.5 ft. The study investigated the reliability of three methods for predicting skin friction in cohesionless soils including O'Neill and Reese (1999) β-method, Brown et al. (2010) β-method, and Chua et al. (2000) Unified Design Equation. The resistance bias corresponding to each method were calculated

and statistically characterized. Assuming a lognormal or polynomial distribution for the resistance bias, the Monte Carlo simulation technique was used to calibrate the resistance factor associated with each design method for a reliability of 3.0. As seen from the results presented in Table 2.24, the use of a fitted polynomial regression model to characterize the resistance bias results in higher resistance factors compared to those obtained based on the assumption of a lognormal distribution. Nonetheless, all calibrated factors were lower than AASHTO recommended value of 0.55.

Table 2.24: Calibrated resistance factors (Ng and Fazia 2012)

Design Method	Lognormal	Polynomial
O'Neill & Reese (1999)	0.32	0.45
Chua et al. (2000)	0.26	0.49
Brown et al. (2010)	0.37	0.47

2.8 References

Abu-Farsakh, M. Y., X. Yu, and Z. Zhang. 2012. Calibration of Side, Tip, and Total Resistance Factors for LRFD of Drilled Shafts. 91th Transportation Research Board Annual Meeting, Washington, D.C., 2012.

Abu-Farsakh, M., Q. Chen, and M. Haque. 2013. Calibration of Resistance Factors of Drilled Shafts for the New FHWA Design Method. FHWA/LA Publication 12/495, Louisiana Transportation Research Center, Baton Rouge, LA.

Allen, T. M., A. S. Nowak, and R. J. Bathurst. 2005. *Calibration to determine load and resistance factors for geotechnical and structural design*. Circular E-C079. Transportation Research Board, Washington, D.C.

Allen, T. M. 2005. Development of Geotechnical Resistance Factors and Downdrag Load Factors for LRFD Foundation Strength Limit State Design. FHWA-NHI-05-052, Federal Highway Administration, U.S. DOT, Washington, D.C.

Barker, R. D., J. K Rojiani, O. P. Tan, S. C. Kim. 1991. *NCHRP Report 343: Manuals for the Design of Bridge Foundations*. Transportation Research Board, National Research Council, Washington, D.C.

Brown, D. A., J. P. Turner, and R. J. Castelli. 2010. *Drilled Shafts: Construction Procedures and LRFD Design Methods*. NHI Course No. 132014, Geotechnical Engineering Circular No. 10 National Highway Institute, U.S. Department of Transportation, Federal Highway Administration, Washington, D.C.

Fortier, A. R. 2016. Calibration of resistance factors needed in the LRFD Design of drilled shafts. Master thesis, Louisiana State University, Baton Rouge, LA.

Motamed, R., K. Stanton, and S. Elfass. 2016. *LRFD Resistance Factor Calibration for Axially Loaded Drilled Shafts in the Las Vegas Valley*. NDOT Research Report No. 515-13-803, Nevada Department of Transportation, Carson City, NV.

Ng, T., and S. Fazia. 2012. Development and Validation of a Unified Equation for Drilled Shaft Foundation Design in New Mexico. Report No. 456A, New Mexico Department of Transportation, Albuquerque, NM.

Ng, W. K., S. Sritharan, and J. C. Ashlock. 2014. *Development of Preliminary Load and Resistance Factor Design of Drilled Shafts in Iowa.* Project 11-410, Institute of Transportation, Ames, IA.

O'Neill, M. W. and L. C. Reese. 1999. Drilled Shafts: Construction Procedures and Design Methods, Publication FHWA-IF-99-025, FHWA, Washington, D.C.

Paikowsky, S. G. 2004. *Load and Resistance Factor Design (LRFD) for Deep Foundations*. Publication NCHRP-507. Transportation Research Board, Washington D.C.

Withiam, J. L., E. P.Voytko, R. M. Barker, J. M. Duncan, B. C. Kelly, S. C. Musser, and V. Elias. 1998. *Load and Resistance Factor Design (LRFD) for Highway Bridge Substructures*. Publication No. FHWA HI-98-032, Federal Highway Administration, Washington, DC.

Yang, X., J. Han, and R. L. Parsons. 2010. *Development of Recommended Resistance Factors for Drilled Shafts in Weak Rocks Based on O-cell Tests*. K-tran: KU-07-4, Kansas Department of Transportation, Topeka, KS.

CHAPTER 3. REGIONAL CALIBRATION OF RESISTANCE FACTORS FOR LRFD OF DRILLED SHAFTS – IS IT PRACTICABLE?

A paper to be submitted to the ASCE Journal of Geotechnical and Geoenvironmental Engineering

Philippe Kalmogo, Sri Sritharan, Jeramy Ashlock

3.1 Abstract

The Federal Highway Administration (FHWA) mandated implementation of the Load and Resistance Factor Design (LRFD) method for all federally-funded bridges initiated after 2007. This call for adoption of the LRFD philosophy was driven by the need to achieve uniform and consistent levels of reliability in the design of all components of the substructure and superstructure, which cannot be ensured in the traditional Allowable Stress Design (ASD) framework. Although the American Association of State Highway and Transportation Officials (AASHTO) specifies resistance factors to be used with its recommended design methods, it also permits the use of higher values provided they can be justified by "substantial statistical data combined with calibration or substantial successful experience." Galvanized by the potential benefits that could be achieved, local jurisdictions have poured much effort into regional calibrations of resistance factors using locally available load test data. In this endeavor, the state of Iowa has dedicated significant effort towards developing local databases for driven piles and drilled shafts and using these databases for calibration of regional resistance factors. While regional calibration for driven piles in Iowa has led to the use of higher resistance factors as well as increased design efficiency compared to AASHTO's recommendations, calibration of resistance factors for drilled shafts has been met with various challenges, most of which are likely to be encountered by other states. The challenges are discussed in this paper, and it is shown that a regional reliability-based calibration for drilled shafts may not always achieve the same level of success as has been realized for driven piles.

3.2 Introduction

Since the FHWA-issued mandate for the adoption of the Load and Resistance Factor Design (LRFD) philosophy for all bridges designed after October 1, 2007, Departments of

Transportation (DOTs) and other local jurisdictions across the United States have made considerable efforts to transition from the traditionally used Allowable Stress Design (ASD) to the more reliable LRFD approach. Although the benefits of LRFD over ASD have been recognized for years, its adoption by the geotechnical engineering community had been relatively slow for bridge design prior to the FHWA mandate. Contrary to the traditional ASD method, which combines all uncertainties into a single factor of safety, LRFD uses load and resistance factors to ensure that various sources of uncertainty and their respective statistical properties are properly accounted for in design. A transition from the conventional ASD to the more robust LRFD not only minimizes the probability of overly conservative designs that can result from the use of a single factor of safety, but more importantly, it leads to a consistent and uniform level of reliability in the design of all components of substructures and superstructures.

On the basis of various research studies conducted by Barker et al. (1991), Paikowsky et al. (2004), and Allen et al. (2005), the current AASHTO LRFD specifications for drilled shafts were developed and recommended for implementation by state DOTs and other local jurisdictions in their respective design practices. As stated by Allen (2005), AASHTO resistance factors were developed through a combination of calibration by fitting to previously used ASD factors of safety, calibration using reliability theory on a general load test database, and engineering judgment. Several limitations associated with these recommendations have been identified in the literature. For example, some investigators have reported that the recommended resistance factors were found to be overly conservative and resulted in designs that differed from expectations based on past experience (e.g., Moore 2007). The conservativeness of the AASHTO resistance factors relative to local experience was attributed to the characteristics of the load test databases used in the various studies that formed the foundation for AASHTO recommendations. It was hypothesized that those databases included load test data from a variety of locations having a wide range of geological conditions, testing methods, and construction practices, leading to conservative resistance factors to accommodate such large variability. As a result, designs at the regional level based on the nationally recommended specifications led to larger size foundations and increased cost relative to prior ASD designs. Additionally, since engineering judgment was exercised in some cases to adjust the resistance factors determined by reliability based-

calibration and fitting, the safety level that the reliability based-calibrations initially aimed to achieve is no longer satisfied and is in fact unknown for such cases.

Another shortcoming associated with the current AASHTO LRFD specifications relates to the fact that they were meant to establish design recommendations at the national level, and therefore resistance factors were only provided for a selected number of design methods. No resistance factors were recommended for the various local in-house design methods developed and used by several state DOTs.

Recognizing that AASHTO recommended specifications have some limitations when implemented at the regional level, state DOTs have been allowed to use higher regionally calibrated resistance factors, provided that they are developed in a manner consistent with the AASHTO LRFD framework. If implemented successfully, a regional reliability-based calibration using only load test databases that encompass soil conditions, testing methods, and construction practices specific to a given region or state can be expected to achieve the following:

- Resistance factors that satisfy a consistent and uniform target level of reliability required for foundation design
- Calibration of resistance factors associated with design methods other than those covered by AASHTO specifications, such as in-house DOT design methods
- Increased design efficiency and therefore reduced foundation cost

Motivated by these potential benefits, research teams at Iowa State University, with the support of the Iowa DOT, have spent considerable effort on development of local load test databases for the ultimate goal of regional calibration of resistance factors. This research has generated the Pile Load Test (PILOT) (Roling et al. 2010) and Drilled Shaft Foundation Testing (DSHAFT) (Garder et al. 2012) databases for driven piles and drilled shafts, respectively.

Using the PILOT database, resistance factors for driven piles were developed and successfully implemented in the Iowa DOT LRFD bridge design guidelines. As envisioned, the regional calibration led to resistance factors that satisfy a given and known probability of

failure (i.e., a reliability of 2.3), improved design efficiency, and significantly reduced overall foundation costs in comparison to designing the same foundation using the AASHTO recommended resistance factors (AbdelSalam et al. 2011). The quality and extent of the collected data facilitated integration of setup into the design process (AbdelSalam et al. 2012). Following this success, the DSHAFT database was used to develop regional resistance factors for drilled shafts (Ng et al. 2014). However, several issues have made the calibration challenging, and preliminary resistance factors determined thus far have not always shown significant improvements over those recommended by AASHTO. Given that these challenges are universal for any group attempting to improve upon the AASHTO recommended resistance factors for drilled shafts using regional data, they are demonstrated in this paper along with potential solutions to overcome these challenges. To better understand which variables can affect resistance factor calibration at the regional level, the major differences between ASD and LRFD as well as the various steps required in the AASHTO LRFD calibration framework are first presented. The difficulties encountered are then discussed, and it is finally shown that the expected benefits of a regional calibration may not always be fully realized.

3.3 Fundamental Principles of ASD and LRFD

Historically, foundations were designed following the traditional ASD procedure, whereby a global factor of safety was used to account for all uncertainties associated with both load and resistance. Although this approach provided some margin of safety against undesired performance, it failed to accurately quantify the different reliability levels associated with various sources of uncertainty. The chosen safety factors were somewhat subjective and a function of several parameters including past successful practice, project type, design methods, and judgment on the part of the designer. This was generally held to result in unnecessary conservatism and costly foundation designs with varying safety levels. As illustrated in Figure 3.1, the primary flaw in the ASD approach resides in its inability to recognize that load and resistance are not deterministic in nature. Since the single factor of safety cannot account for the different sources of uncertainty in a quantitative manner, ASD generally leads to designs with unknown and varying probabilities of failure.

LRFD overcomes the deficiencies associated with ASD by providing a more rational approach to quantify and account for all sources of uncertainty involved in the design process. As illustrated by the basic LRFD Eq. (3.1), uncertainties associated with various types of loads and resistances for a given limit state can be taken into account by the load and resistance factors, respectively.

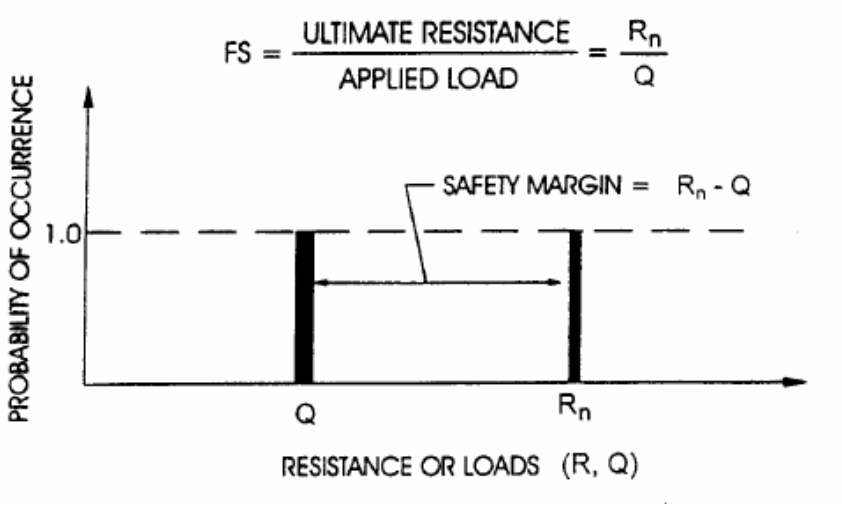

Figure 3.1: ASD approach (Withiam et al., 1998)

$$\sum \gamma_i Q_i \leq \varphi R_n \tag{3.1}$$

where,

Q_i = Load type i (e.g. dead load, live load etc.)

γ_i = Factor for load type i

R_n = Nominal resistance

φ = Resistance factor

In LRFD, the load and resistance are treated as independent random variables whose probability of occurrence has a specific distribution (Figure 3.2). Using their known variabilities, the load and resistance factors can be calibrated to ensure that the probability of the factored loads exceeding the available resistance is at an acceptable target level of risk. This failure region, represented by the shaded area in Figure 3.2, is related to the reliability

index β, whose value must be specified in the calibration process. The reliability index can be selected based on cost-benefit analyses or failure rates estimated from actual case histories Typical design values of probability of failure for foundations of structures range from 1:100 to 1:1000, for which the AASHTO LRFD framework recommends the corresponding target reliabilities of β =2.3 and 3.0 for redundant and non-redundant systems, respectively.

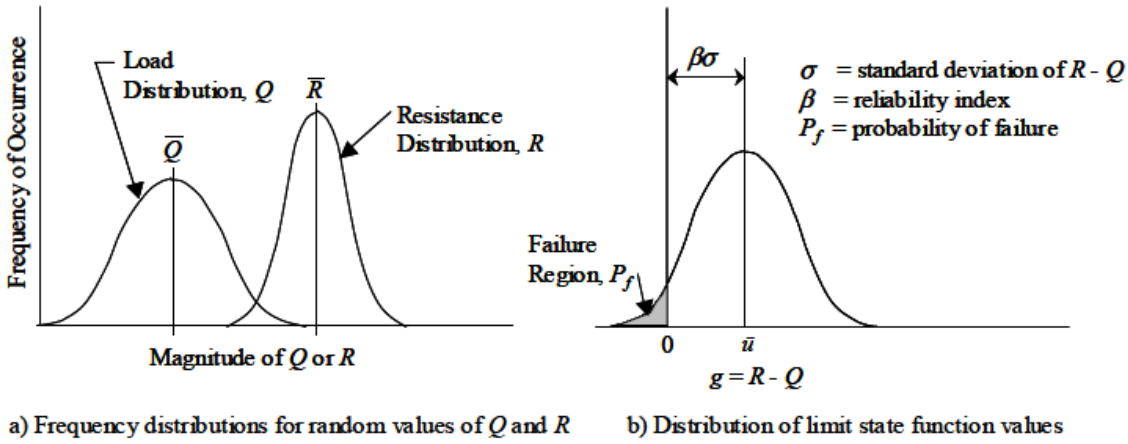

Figure 3.2: Load and resistance distributions and reliability index (Withiam et al., 1998)

As discussed above, resistance factor calibration completed by for AASHTO was accomplished by judgment, fitting to ASD, reliability theory, or a combination of these approaches. However, only calibration using reliability theory can fulfill the true goal of LRFD to ensure more uniform and consistent levels of safety across designs. In calibration by judgment, past experience, which includes records of prior satisfactory and poor performance, is relied upon to select appropriate values for the resistance factors. Calibration by fitting to ASD is simply a format change consisting of selecting resistance factors that would result in the same designs as the ASD factors of safety. This approach only eliminates the discrepancy between load values used for substructure and superstructure designs, thereby reducing possible miscommunications between structural and geotechnical engineers.

Calibration by reliability theory involves applying probabilistic methods with varying levels of complexity. The Level III method (fully probabilistic) is the most accurate, but it is rarely

used in LRFD calibration because of the difficulty in obtaining the required load and resistance information. Level II includes approximate probabilistic methods such as the first order second moment (FOSM) method, and it requires only the first two moments (i.e. the mean and standard deviation) of the load and resistance variables to define the probability distributions associated with each variable. Through an iterative procedure, this approach can be used to determine the safety or reliability index associated with a combination of selected values of load and resistance factors. Level I probabilistic methods are the least accurate, and they also use a second moment reliability method. The difference between Level I and Level II methods lies in the limit state function being linearized at the mean values of the load and resistance for Level I, rather than at the design point on the nonlinear failure surface for Level II.

The use of any of these probabilistic methods requires the existence of an extensive record of test data to statistically characterize the different variables involved in the limit state function. Unlike the driven piles data sets, drilled shaft data sets have relatively fewer points because of the much higher costs of conducting these tests. A calibration using a combination of any of the approaches previously detailed is warranted when the data required for a proper reliability-based calibration is not available, or when the quality of the data at hand is questionable. As Allen (2005) stated, "if the adequacy of the input data is questionable, the final load and resistance factor combination selected should be more heavily weighted toward a level of safety that is consistent with past successful design practice, using the reliability theory results to gain insight as to whether or not past practice is conservative or non-conservative."

3.4 Regional Resistance Factor Calibration: Expectation vs. Reality

As detailed in the preceding discussion, LRFD represents a superior approach to foundation design compared to ASD, but its application, with respect to its true end goal, has not always been a straightforward process. It has been shown that only calibration using reliability theory can lead to resistance factors that fully embrace the fundamental concepts of LRFD. Considering the limitations associated with AASHTO recommended resistance factors, it is believed by many that regional calibrations using local load test databases would logically lead to greater resistance factors due to a reduced variability in soil conditions and

construction practices. However, this expectation is often not realized, as will be illustrated below using two regional calibration studies from Louisiana and Kansas.

3.4.1 Louisiana Resistance Factor Calibration for Drilled Shafts in Mixed Soils

Citing the facts that AASHTO LRFD specifications were not specifically developed for any particular region, and their implementation in Louisiana or Mississippi could lead to a reduction in design efficiency and larger foundation sizes, a series of calibration studies was conducted to develop resistance factors consistent with the region's soil conditions and construction practices. The first calibration conducted in 2010 featured sixty-six top down and O-cell load tests from Louisiana (16 tests) and Mississippi (50 tests). Only twenty-six load tests produced data that could be used in the actual calibration because they met the FHWA's settlement criterion of 5% of the shaft diameter. The data included 22 O-Cell tests and 4 top-down tests. Using the Monte Carlo simulation method, resistance factors were calibrated for the O'Neill and Reese (1999) α and β-methods to achieve a target reliability of 3.0. Presented in Table 3.1 are the calibrated factors. Calibration using either dataset led to a total resistance factor of 0.50. Considering O-cell data only where it was possible to differentiate between side and tip resistance, the calibrated side resistance factor decreased by 56% and 64% compared to the recommended values of 0.45 and 0.55. For tip resistance, the calibrated factor increased by 88% and 50% compared to AASHTO recommended values of 0.40 and 0.50. It is worth noting that the calibration did not differentiate between clay and sand, and it is likely that the actual resistance factor for each separate geomaterial could be different from the calibrated values.

Table 3.1: Calibrated resistance factors from Abu-Farsakh et al. (2010)

Dataset	Regionally Calibrated φ			AASHTO	
	φ, side resistance	φ, tip resistance	φ, total resistance	φ, side resistance	φ, tip resistance
O-cell data	0.20	0.75	0.50	0.45 for clay 0.55 for sand	0.40 for clay 0.50 for sand
All data	-	-	0.50	0.45 for clay 0.55 for sand	0.40 for clay 0.50 for sand

The second calibration included eight additional tests obtained from the Louisiana DOT. All shafts were constructed and tested in soil types that included silty clay, clay, sand, clayey sand, and gravel. The Monte Carlo simulation technique was implemented to evaluate the reliability of the AASHTO drilled shaft design methods recommended by O'Neill and Reese (1999) and Brown et al. (2010). Presented in Table 3.2 are the results from that calibration. For the O'Neill and Reese (1999) method, the calibrated side resistance factor was 13% and 29% lower than AASHTO values of 0.45 and 0.55. For tip resistance, the calibration led to 30% and 4% increase compared to AASHTO. Compared to the previous calibration, side and total resistance factors increased while the tip resistance factor decreased. For the Brown et al. (2010) method, the calibrated side resistance factor was 42% and 53% smaller than AASHTO values. For tip resistance, the calibration led to increase of 33% and 6%.

Table 3.2: Calibrated resistance factors from Abu-Farsakh et al. (2013)

Design Method	Regionally Calibrated φ			AASHTO	
	φ, side resistance	φ, tip resistance	φ, total resistance	φ, side resistance	φ, tip resistance
O'Neill & Reese (1999)	0.39	0.52	0.60	0.45 for clay 0.55 for sand	0.40 for clay 0.50 for sand
Brown et al. (2010)	0.26	0.53	0.48	0.45 for clay 0.55 for sand	0.40 for clay 0.50 for sand

Following similar analysis procedures and using an updated database of sixty-nine O-cell load tests, the latest calibration study was conducted by Fortier et al. (2016). In addition to the Monte Carlo simulation technique, the FOSM reliability method was used to calibrate the resistance factors for further comparisons. An additional strength criterion of 1-inch top displacement was also considered. Table 3.3 details the calibrated resistance factors obtained from the Monte Carlo simulation. As shown, the regionally calibrated factors at the 1-inch strength criterion were lower than those at the AASHTO criterion, with the exceptions of tip resistance for both design methods and total resistance for Brown et al. (2010). Compared to the previous calibration results shown in Table 3.2, the latest calibration by Fortier et al. (2016) resulted in lower resistance factors at the AASHTO criterion except for side

resistance using Brown et al. (2010). Tip and total resistance factors decreased by as much as 79% and 44%, respectively. More importantly, the refined resistance factors were all lower than any of the values recommended by AASHTO. Comparison of the calibrated factors at the 1-inch top displacement strength criterion could not be made since that criterion was not considered in the calibration by Abu Farsakh et al. (2013).

Table 3.3: Side and end resistance factors from Monte Carlo simulation (Fortier et al. 2016)

Design Method	Regionally Calibrated φ						AASHTO	
	1-inch criterion			AASHTO criterion				
	φ, side resistance	φ, tip resistance	φ, total resistance	φ, side resistance	φ, tip resistance	φ, total resistance	φ, side resistance	φ, tip resistance
O'Neill & Reese (1999)	0.30	0.19	0.34	0.35	0.16	0.38	0.45 for clay 0.55 for sand	0.40 for clay 0.50 for sand
Brown et al. (2010)	0.15	0.15	0.31	0.29	0.11	0.27	0.45 for clay 0.55 for sand	0.40 for clay 0.50 for sand

Another important observation from the three studies is the different uncertainty in predictions of total resistance compared to those of separate side and tip resistances. From the higher resistance factors obtained for total resistance prediction compared to side and tip resistance in both studies, it can be concluded that the uncertainty in predicting the total resistance is less than that associated with predicting either side or tip resistances. Although these resistance factors will ensure that the drilled shaft design meet the targeted reliabilities chosen for the design methods, their implementation would result in larger and costlier foundations compared to AASHTO specifications, which are believed to be overly conservative in the first place. However, no discussion regarding this issue was offered in the studies. These calibration studies provide a good example of why a regional calibration study, while achieving resistance factors that comply with LRFD concepts, may be seen as unproductive as it will more often not lead to improved design efficiency compared to AASHTO recommendations. Therefore, the regional calibration exercise should be viewed as

improving the reliability of foundation design, which is not fully satisfied by AASHTO specifications due to including judgment and fitting to ASD in selecting the recommended values. As more tests data become available, the regionally calibrated factors will likely satisfy both the reliability requirements and provide resistance factors with high design efficiency.

3.4.2. Kansas Resistance Factor Calibration for Drilled Shafts in Weak Rock

Calibration of resistance factors for drilled shafts in weak rocks in the state of Kansas conducted by Yang et al. (2010) provide another evidence of the dilemma identified above in the calibration studies. According to the study, the use of AASHTO LRFD specifications by Kansas DOT engineers led to designs that were often inconsistent with their past ASD practice. Thus, the calibration was justified by the need to develop regional factors that would resolve this issue and be reflective of the state's experience. To evaluate the uncertainty associated with the O'Neill and Reese (1999) design method for intermediate geomaterials (IGM), a database was developed including twenty-five load tests from Kansas, Colorado, Missouri, Ohio, and Illinois. Using the Monte Carlo simulation technique, resistance factors for side resistance and tip resistance were calibrated at the AASHTO strength criterion. Resistance factors for side resistance were calibrated by two approaches, the first considering total side resistance, and the second considering segmental side resistance. In addition to the target reliability of 3.0 commonly recommended for drilled shafts, the study also considered a target reliability of 2.3.

Table 3.4 presents the resistance factors obtained from the calibration. For the total resistance approach, the calibrated side resistance factor of 0.50 represents a 17% decrease from the AASHTO recommended value of 0.60. For the segmental resistance approach, the regional resistance factor of 0.70 offers a 17% improvement. This difference highlights the effect of the different methods of calculating the resistance bias on the calibrated resistance factors and corresponding efficiency factors (or the uncertainties in prediction of total side resistance vs. those of a given shaft segment), which is not covered in the AASHTO LRFD calibration framework. For tip resistance, the calibration led to a decrease of 55%.

Table 3.4: Calibrated resistance factors modified after Yang et al. (2010)

Situation		φ (β_t=3.0)	AASHTO φ (β_t=3.0)
Side resistance	Total	0.50	0.60
	Layered	0.70	
Tip resistance		0.25	0.55

3.5 State of Regional LRFD Calibration in Iowa

3.5.1 Driven Piles

Regional calibration of resistance factors for driven piles was initiated with the development of PILOT, a collection of 264 pile static load tests conducted in Iowa between 1966 and 1989. Information in the database includes subsurface conditions, pile types, hammer characteristics, end-of-driving blow counts, and load test results. Pile types include steel H-shaped, timber, pipe, monotube, and concrete. Of the 264 piles, 207 were deemed reliable and utilized for LRFD calibration. Following a preliminary calibration based on the 207 reliable piles, 10 additional load tests were conducted on steel H-piles with the goals of verifying the preliminary resistance factors and providing data for development of resistance factors for Pile Driving Analyzer (PDA) as well as Case Pile Wave Analysis Program (CAPWAP) analyses.

Additional details on the calibrated resistance factors developed for various static analysis methods can be found in AbdelSalam et al. (2012). These regional resistance factors provided a significant improvement over AASHTO's recommended resistance factors. For static methods in sandy soils, the regional calibration resulted in a 40% increase for the SPT-Meyerhof method and a 3% increase for the β-method. For clay soils, a 55% increase was achieved for the β-method. For mixed soils, a 60% increase was realized for the β-method. Resistance factors were also calibrated for various dynamic analysis methods and dynamic formulas, similarly resulting in significant improvements. Compared to AASHTO's recommended resistance factors for the Wave Equation Analysis Program (WEAP) SA-based method, a 10% increase was achieved for sandy soils while a 30% increase was achieved for clay and mixed soils. A similar improvement for dynamic formulas was also observed as attested by an increase ranging between 100% and 140% for the ENR formula.

In this case, the regional calibration fulfilled the expected potential benefits by developing resistance factors that not only satisfy a known probability of failure but also improve design efficiency. The regional calibration also permitted evaluation of resistance factors associated with the Iowa DOT "Blue Book" design method. This method, which was used in the Iowa DOT past ASD practice, was found to be more efficient than all other nationally used static design methods, therefore it was recommended for implementation.

3.5.2 Drilled Shafts

Similar to PILOT, DSHAFT was developed during the initial phase of the drilled shaft resistance factor calibration studies in Iowa. The uniqueness of the database is that it ensures high quality information, including soil parameters that are routinely collected at the test site and therefore DSHAFT can be assumed to contain the best drilled shaft test information available at a regional level. The initial DSHAFT database was developed using forty-one load tests from 11 different states. Unlike driven piles which have an extensive record of load tests in Iowa, drilled shaft load tests are very limited. Thus, it was necessary to include load tests from other states so that a proper statistical characterization of the resistance variables could be accomplished. Load test data along with available site investigation, construction details, and field records were collected and integrated into an easy to use Microsoft Office Access-based electronic file. The database primarily includes O-cell load tests and three statnamic tests. The diameter of the shafts ranges from 0.76 m (2.5 ft) to 2.44 m (8 ft), and the length ranges between 3.44 m (11.3 ft) and 49.07 m (161 ft). Drilling under polymer slurry is the predominant type of construction method. Geomaterials along the shafts include sand, clay, IGM, and rock.

After an analysis of the gathered data, thirteen load tests were discarded from the calibration due to the absence of key information. Following the resistance factor calibration framework consistent with AASHTO recommendations, Ng et al (2014) used the database to determine resistance factors associated with various static design methods for skin friction and end bearing. In addition to the end bearing design methods covered by AASHTO, the calibration investigated several other methods proposed in the literature. Resistance factors were calibrated for three different strength criteria, the results of which are shown in Table 3.5. In the case of skin friction, the calibration led to an improvement of the resistance

factors associated with IGM and rock only. For end bearing, a higher resistance factor was achieved for sand only. The tip resistance factor for clay could not be calibrated due to insufficient data. The results from the preliminary study showed some partial success with regards to the benefits of a regional calibration. In the present study, the database was expanded with 7 additional usable load tests from Iowa for a new calibration and refinement of the resistance factors established in the preliminary study.

Table 3.5: Iowa preliminary drilled shaft resistance factors, modified after Ng. et al (2014)

Geomaterial	Failure Criterion	AASHTO		DSHAFT	
		φ, side resistance	φ, tip resistance	φ, side resistance	φ, tip resistance
Clay	LTR	n/a	n/a	0.31	n/a
	Δ =1 in.	n/a	n/a	0.20	n/a
	Δ = 5% of D	0.45	0.40	0.22	n/a
Sand	LTR	n/a	n/a	0.47	0.57
	Δ =1 in.	n/a	n/a	0.48	0.76
	Δ = 5% of D	0.55	0.50	0.47	0.75
IGM	LTR	n/a	n/a	0.66	n/a
	Δ =1 in.	n/a	n/a	0.63	n/a
	Δ = 5% of D	0.60	0.55	0.69	0.20
Rock	LTR	n/a	n/a	0.57	n/a
	Δ =1 in.	n/a	n/a	0.55	n/a
	Δ = 5% of D	0.55	0.50	0.62	0.31

LTR – load test report criterion; n/a – not available; Δ - shaft top displacement; D – shaft diameter.

3.5.3 Challenges during Calibration Studies

Despite significant efforts to collect and integrate good quality load test data into DSHAFT, the database still presents several challenges that can prevent full realization of the benefits of a regional calibration as accomplished for driven piles. Similar challenges are likely to be experienced by others interested in accomplishing the same. The first issue relates to the size of DSHAFT, which is due to the cost of drilled shaft load tests being fairly

high. The DSHAFT today includes a total of thirty five usable load tests, which is only 17% of the number of load tests used for calibration and verification of driven pile resistance factors in Iowa. This relatively small number of load tests may prevent the appropriate statistical characterization of the resistance variables, which can lead to resistance factors that are not truly reflective of past local experience. Perhaps the biggest challenge lies in the fact that the majority of the load tests in the database are not taken to complete geotechnical failure due to the difficulty of predetermining the appropriate depth of the O-cell to achieve a balanced failure both above and below the O-cell. Sometimes, only the portion of the shaft above or below the O-cell experiences complete failure, and the other does not. In other cases, O-cell capacity is reached prior to the test shaft experiencing failure. While these tests are sufficient to confirm the design capacity of drilled shafts at the specific location, they have limited values in calibration studies. This is because these tests are often terminated at relatively small shaft displacements, before full mobilization of the resistance of the different geomaterial layers along the shaft. This poses a major problem in the calibration of resistance factors at ultimate resistance or at target displacements at which the actual load resistances are not captured.

For example, an O-cell load test result from DSHAFT is presented in Figure 3.3. This test was performed on a 3.87 m (12.7 ft) long rock socket with a 0.91 m (3 ft) diameter, constructed in dolomite. At the end of the test, the shaft segment above the O-cell displaced 63.5 mm (2.5 in.) while the segment below the O-cell only displaced 5.08 mm (0.2 in.). Despite the upper portion of the shaft undergoing a significant displacement, it did not reach its ultimate capacity. The construction of an equivalent top-down load-displacement curve according to Loadtest's procedures would require extrapolation of the O-cell downward load-displacement curve to the displacement of 63.5 mm (2.5 in.) achieved in the upper portion of the shaft or to the displacement assumed at the ultimate limit state. Although undesirable for the purposes of LRFD calibration, extrapolation is relied upon to construct complete equivalent top load-displacement curves from O-cell load test results. Fitting functions that have been used and recommended in the literature to extrapolate load test results include the Ratio Function, the Chin-Kondner Hyperbolic Function, the Hansen 80% Function, and the Zhang Function, among others. However, extrapolating test data beyond measured values is not without risk of being unconservative and introducing additional bias that can negatively

affect the calibration of resistance factors. This challenge has been encountered in regional calibrations conducted by other states including but not limited to Louisiana and Nevada. In Louisiana, the exponential curve fitting method was used to extrapolate few of the load tests that did not meet the AASHTO strength criterion corresponding to 5% of the shaft diameter for top displacement (Abu-Farsakh et al. 2010, Abu-Farsakh et al. 2013, and Fortier et al. 2016). As noted in the studies, load tests that required excessive extrapolations were discarded from the calibration to reduce the probability of introducing unrealistic extrapolated values in the calibration. In the Nevada study, the Chin-Kondner hyperbolic curve fit was used where extrapolation of test data was necessary (Motamed et al. 2016). Although no load tests were discarded in the Nevada LRFD calibration, load tests that required large extrapolation were included in the category of low-quality data based on the scoring system established by Motamed et al. (2016). In Iowa, Ng et al. (2014) developed three different extrapolation procedures to estimate the required load information.

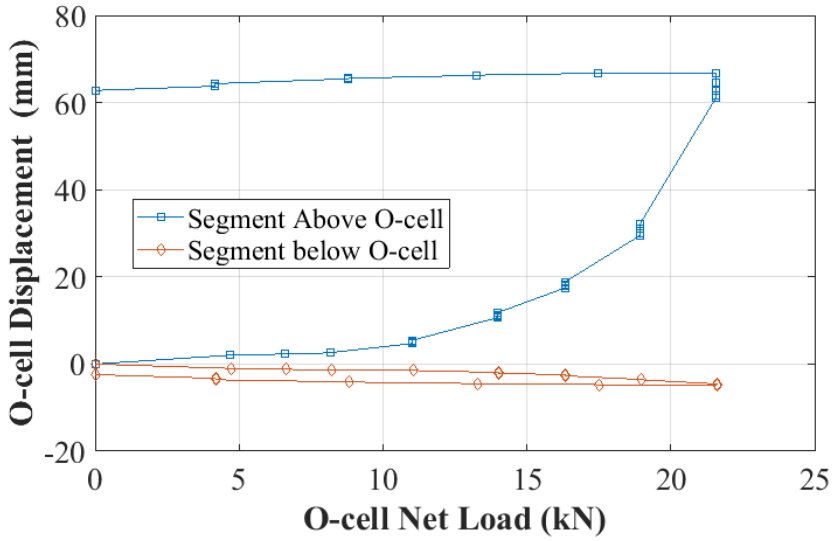

Figure 3.3: Example of O-cell load-displacement curve from DSHAFT (Test ID 2)

Another limitation of DSHAFT is lack of laboratory-measured soil and rock properties. With the exception of unconfined compressive tests performed on rock core samples, no other laboratory are routinely performed to estimate additional key soil parameters for most of the soil profiles in DSHAFT. The available information is generally limited to the in-situ SPT blow count number, which has to be correlated to typically used

soil parameters such as unit weight, undrained shear strength, and soil friction angle. However, correlations of the blow count number to soil properties are not always reliable, and their use can introduce additional uncertainties into the calibration process.

An additional difficulty encountered in the calibration process relates to sorting the load tests in DSHAFT according to geomaterial type. This categorization step must be done so that resistance factors can be calibrated for each geomaterial type and its corresponding design method. Most of the test shafts in DSHAFT, however, are constructed in mixed geomaterial profiles composed of a combination of clay, sand, IGM, and/or rock layers. Therefore, the usual approach of categorizing load tests based on an average soil profile (as used in the PILOT calibration for driven piles) has a limitation. It would not allow the evaluation of the uncertainty associated with each geomaterial type and corresponding design method. This approach would only allow the calibration of a single resistance factor associated with the total resistance derived from a combination of all soil types along the shaft and their corresponding design methods. Such a resistance factor would not recognize the different levels of reliability associated with the various design methods used for different soil types.

A segmental approach is, therefore, necessary in order to establish the resistance factor corresponding to each geomaterial layer or type. In the average soil profile approach, the soil profile surrounding the shaft is classified as either clay, sand, mixed (clay and sand), IGM, or rock based on some pre-established rules (e.g., 70% rule). The total resistance of the shaft is then estimated using the appropriate design methods for the determined average soil type and compared to the total measured resistance from the load test. The layered resistance approach uses strain gauge data to determine the load transferred between two given sets of strain gauge levels. Strain gauges are typically installed at geomaterial layer interfaces allowing the skin friction of the different geomaterial layers around the shaft to be quantified.

Two different procedures can be used to calculate the resistance bias in the layered approach, and they will be referred to as the local and global approaches. The two approaches will be illustrated using a load test from DSHAFT. As shown in Figure 3.4, the site for the load test considered is composed of clay shale bedrock overlain by silty and glacial clay.

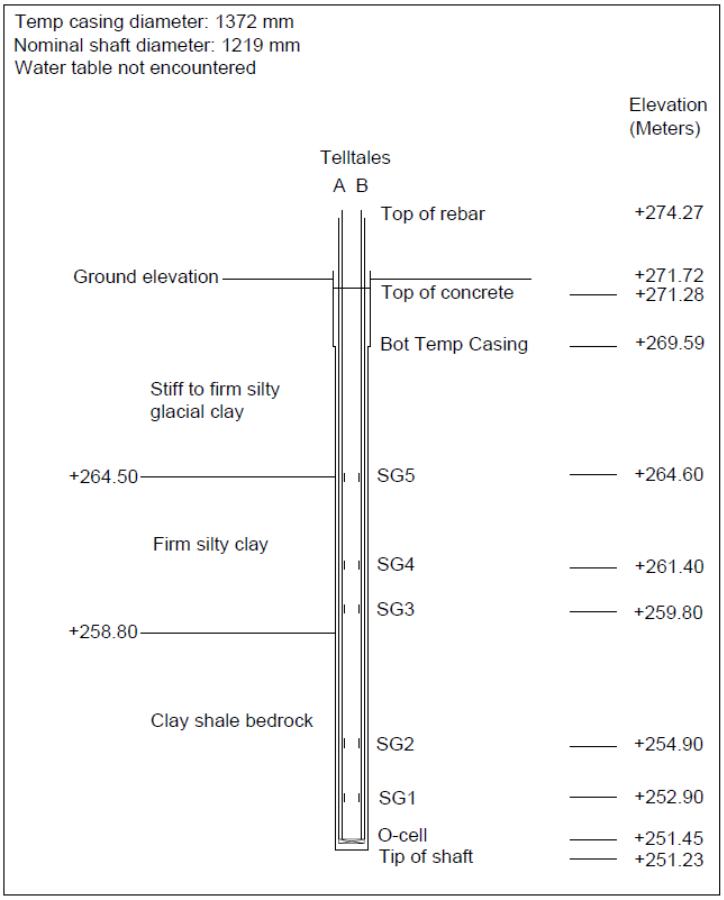

Figure 3.4: Example of load test soil profile from DSHAFT (Test ID 3)

The test was conducted as part of the I-235/28th Street Overpass project in Des Moines, Iowa. The shaft is instrumented with five levels of strain gauges resulting in six shear zones. Based on the geomaterial properties, three of these zones are classified as cohesive soil and the other three as cohesive IGM. In the local layered approach, three different resistance bias values, i.e. λTop-SG5, λSG5-SG4, λSG4-SG3, can be calculated for the cohesive soil category by computing the ratio of the measured resistance to the predicted resistance for each individual shear zone. A similar procedure for the three remaining zones will result in three different resistance bias values for the cohesive IGM category. In contrast, the global approach to calculating the resistance bias uses the sum of the resistances from shear zones of the same geomaterial category. For instance, rather than calculating three different resistance bias values for the cohesive soil layers in the example shown in Figure 3.4, a single resistance bias value is calculated by taking the ratio of the sum of the three measured resistances to the sum of the predicted resistances in these zones.

Both of these methods are repeated across all load tests in DSHAFT. The resulting resistance biases for each soil category and design method can then be used to determine the distribution type and corresponding statistical parameters needed for the calibration. Several important observations can be made regarding the characteristics of the resistance bias obtained from the two procedures. First, the local approach clearly provides a larger resistance bias sample size compared to the global approach. Furthermore, the statistical characteristics established by use of these two methods are unlikely to be identical. In the present study, the resistance bias from the local approach was found to be highly variable, resulting in greater uncertainty in predicting side resistance of individual shear zones. The global approach, however, is characterized by a lower coefficient of variation as result of a lower standard deviation, indicating that the design methods considered are generally more accurate at predicting the sum of soil resistances from multiple shaft segments. Histograms of resistance biases for side resistance prediction in cohesionless soils using O'Neill and Reese β-method at the 25.4 mm (1 in.) displacement strength criterion are presented in Figure 3.5 and Figure 3.6 for the local and global approach, respectively. Lognormal distribution fits based on Maximum Likelihood Estimation (MLE) are also included in these figures. Resistance bias values below unity indicate that the method overestimates the actual resistance while values above unity indicate that the method is conservative. When the local approach is used, the method over predicts side resistance in 28% of the shaft segments considered, whereas in the global approach shaft resistance is overestimated in only 11% of the segments. Additionally, the figures show that the measured resistance can be as low as 39% and 77% of the predicted resistance in a single shaft segment when using the local approach and global approach, respectively. These values illustrate that prediction errors are likely to be much larger when considering a single shaft segment. In the global, prediction errors are reduced due to compensation of errors resulting from the summation of side resistance of multiple segments. Consequently, resistance factors calibrated using statistical parameters estimated from the local approach will be smaller to ensure that the probability of the resistance design values exceeding the actual resistance in a given shaft segment is below the target value.

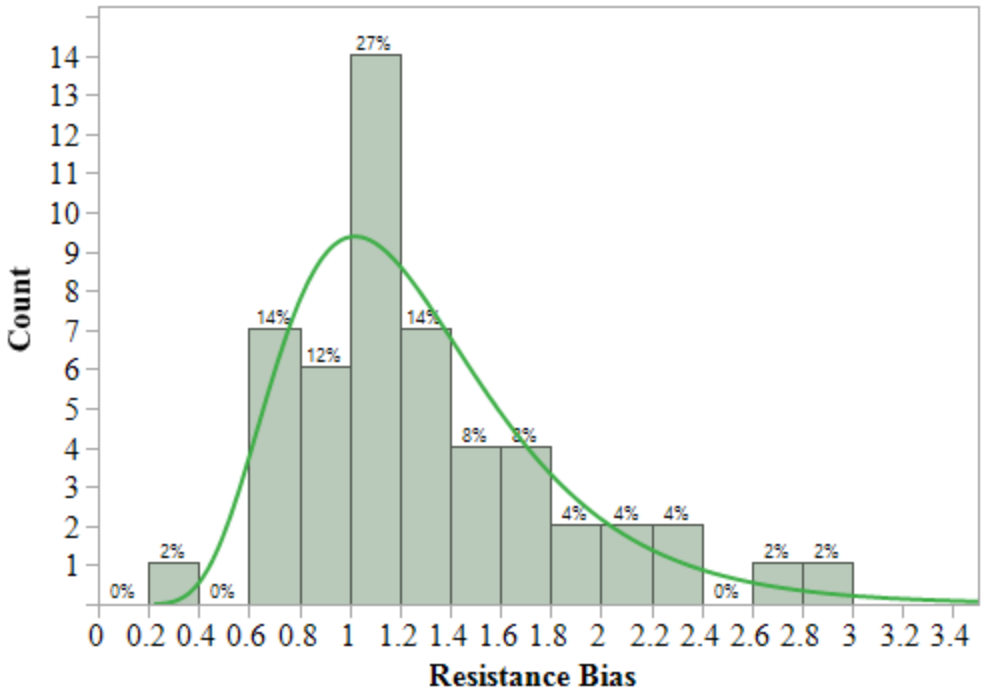

Figure 3.5: O'Neill and Reese β-method at 1 inch strength criterion-local approach

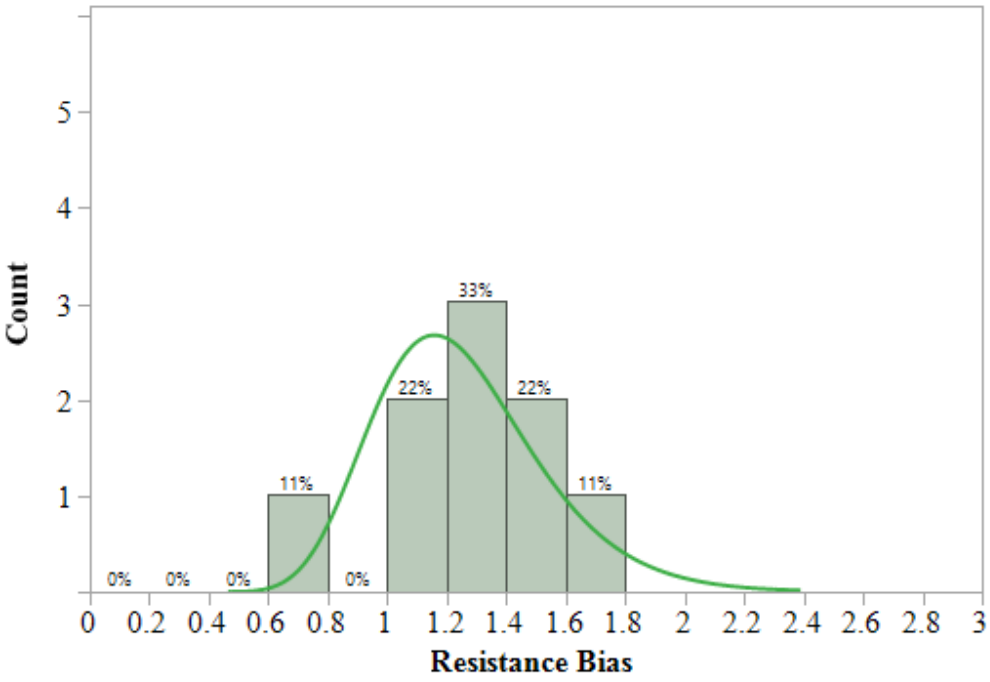

Figure 3.6: O'Neill and Reese β-method at 1 inch strength criterion-global approach

Resistance factors resulting from both local and global analysis approaches are presented in. A few important observations can be made from the values presented in these tables. At the AASHTO strength criterion of displacement equal to 5%D, the local approach generally results in lower resistance factors than the AASHTO recommended values, except for the O'Neill & Reese (1999) modified α-method. Using the global approach, the regionally calibrated resistance factors show significant improvement over both the local approach and the AASHTO-recommended values in all cases, with the exception of the Kulhawy et al. (2005) method for skin friction in rock. For instance, at the AASHTO strength criterion, the global calibration approach achieved increases in resistance factors of 56% and 47%, respectively, over the AASHTO values for side resistance in sand using the O'Neill and Reese (1999) β-method and Brown et al. (2010) β-method. Similarly, resistance factor increases of 18% and 33% were achieved for the O'Neill and Reese (1999) modified α-method and the Horvath and Kenney (1979) method, respectively. From the data presented herein, it is evident that following the global approach results in higher resistance factors for side resistance than the local approach.

Since the magnitude of the resistance factors alone do not indicate the efficiency of the design methods, efficiency factors corresponding to the regionally calibrated factors were also calculated for each approach, as shown in Table 3.6 and Table 3.7. This factor is calculated as the ratio of the resistance factor to the mean of the resistance bias, and its value ranges between 0 and 1, with higher values indicating higher efficiency. It is a better indicator of the true economy of the design method, and can be utilized to select the most cost-effective methods among two or more design methods for the same geomaterial. It can also more clearly illustrate when design methods provide poor resistance predictions at the regional level, so that more efficient design method alternatives can be developed accordingly. The efficiency factors from the global calibration approach were higher than those from the local approach, indicating that larger size drilled shafts will result from implementing resistance factors developed from the latter. For side resistance in sand, efficiency factors indicate that the O'Neill and Reese (1999) β-method is more efficient than the Brown et al. (2010) β-method, with the exception of efficiency factors at the AASHTO criterion in the local approach.

Table 3.6: Summary of side resistance factors from local approach

Design Method	Failure Criteria	Resistance Factors at $\beta_T = 3.00$, φ				Efficiency, φ/λ
		NCHRP 343	NCHRP 507	AASHTO (2016)	This Study	This Study
O'Neill & Reese (1999) α-method	Δ=1 in.	n/a	n/a	n/a	0.30	0.21
	Δ = 5% of D	0.65	0.36 (φ/λ=0.41)	0.45	0.26	0.19
O'Neill & Reese (1999) β-method	Δ=1 in.	n/a	n/a	n/a	0.49	0.44
	Δ = 5% of D	n/a	0.31 (φ/λ=0.28)	0.55	0.50	0.35
Brown et al. (2010) β-method	Δ=1 in.	n/a	n/a	n/a	0.45	0.40
	Δ = 5% of D	n/a	n/a	0.55	0.54	0.39
O'Neill & Reese (1999) modified α-method	Δ=1 in.	n/a	n/a	n/a	0.51	0.20
	Δ = 5% of D	n/a	0.51 (φ/λ=0.41)	0.60	0.64	0.22
Horvath & Kenney (1979)	Δ=1 in.	n/a	n/a	n/a	0.54	0.25
	Δ = 5% of D	0.65	n/a	0.55	0.54	0.21
Kulhawy et al. (2005)	Δ=1 in.	n/a	n/a	n/a	0.25	0.22
	Δ = 5% of D	n/a	n/a	0.55	0.26	0.20

Table 3.7: Summary of side resistance factors from global calibration approach

Design Method	Failure Criteria	Resistance Factors at $\beta_T = 3.00$, φ				Efficiency, φ/λ
		NCHRP 343	NCHRP 507	AASHTO (2016)	This Study	This Study
O'Neill & Reese (1999) α-method	Δ=1 in.	n/a	n/a	n/a	0.48	0.37
	Δ = 5% of D	0.65	0.36 (φ/λ=0.41)	0.45	0.45	0.35
O'Neill & Reese (1999) β-method	Δ=1 in.	n/a	n/a	n/a	0.71	0.62
	Δ = 5% of D	n/a	0.31 (φ/λ=0.28)	0.55	0.86	0.60
Brown et al. (2010) β-method	Δ=1 in.	n/a	n/a	n/a	0.56	0.47
	Δ = 5% of D	n/a	n/a	0.55	0.81	0.57
O'Neill & Reese (1999) modified α-method	Δ=1 in.	n/a	n/a	n/a	0.60	0.26
	Δ = 5% of D	n/a	0.51 (φ/λ=0.41)	0.60	0.71	0.24
Horvath & Kenney (1979)	Δ=1 in.	n/a	n/a	n/a	0.79	0.40
	Δ = 5% of D	0.65	n/a	0.55	0.73	0.33
Kulhawy et al. (2005)	Δ=1 in.	n/a	n/a	n/a	0.44	0.46
	Δ = 5% of D	n/a	n/a	0.55	0.39	0.37

For side resistance in rock, the Horvath and Kenney (1979) is slightly more efficient than the Kulhawy et al. (2005) in the local approach, while the contrary is true in the global approach.

Finally, it is important to recognize that the nationally-used AASHTO design methods for shaft capacity prediction were developed based on different displacements or failure criteria. However, to avoid inconsistencies in resistance factor calibration, the resistance bias should be calculated using predicted and measured resistances corresponding to the same failure criterion. The generalized set of normalized load-displacement curves for shafts in sands and clays provided in by O'Neill and Reese (1999) can be used to obtain estimates of the predicted resistance corresponding to different desired shaft displacements. However, such similar curves are not presently available for IGM and rock.

3.5.4 Conclusions and Recommendations

This study detailed several challenges that are likely to be encountered in the regional calibration of resistance factors for drilled shafts. Results from studies conducted by Louisiana, Kansas, and Iowa were utilized to demonstrate that resistance factor calibration at the regional level may not always be able to achieve the expected benefits immediately, and a continuous assessment would be required as more test data become available. Based on the completed study, the following conclusions can be drawn:

- The number of drilled shaft load tests having sufficiently good quality data, as observed in DSHAFT, which may be considered to represent a typical regional database, is relatively smaller than that of driven piles, influencing the appropriate statistical characterization of the resistance variable in the calibration. Therefore, the calibration often has to include load tests from other states, which can lead to increased variability in resistance prediction and thus lower resistance factors.
- Drilled shaft load tests rarely achieve complete geotechnical failure or sufficiently large shaft displacements. Thus, extrapolation of load test data is almost always required to estimate measured resistances at the selected strength criteria for resistance factor calibration. This adds additional uncertainty into the calibration process, and may lead to resistance factors that are not truly representative of actual

conditions. The resulting resistance factors may be unnecessarily conservative or conservative depending on the extrapolation method used.

- Soil parameters needed for shaft resistance prediction are primarily determined from correlations to in-situ SPT blow counts, which have been shown to be unreliable for some geomaterial types.
- A segmental rather than a total resistance calibration approach is needed to appropriately develop resistance factors corresponding to each geomaterial type and corresponding design method. Two segmental approaches for side resistance factor calibration can be used, namely the local and global approaches. The local approach provided a larger sample population size than the global approach. However, resistance factors and efficiency factors obtained from the global approach are higher than those from the local approach, due to presumably to compensation of errors occurring with the global approach. While the resistance factors established from the global approach may be used from the time being, it is important to continue to collect more regional data and revise the resistance factors appropriately in the future to ensure that the required reliability in foundation design are achieved.

Given that the LRFD of drilled shaft research needs to be continued at the national and regional levels, the following recommendations are provided:

- To help improve the quality of database, it is important that drilled shaft tests are taken to sufficiently large displacements for full mobilization of the shaft capacity to enable calibration without extrapolation. Data from these load tests are the primary foundation for development of statistically based resistance factors, and eliminating the need for extrapolation in the calibration process would increase reliability as well as efficiency. Provided that achieving a balanced failure in O-cell tests can be challenging, the tests should be designed to guarantee failure of the segment providing the most critical test data (side shear in Iowa).

- Though it would add incremental costs, future tests should include additional subsurface investigations at the test shaft locations, which will minimize the use of empirical correlations in determining the necessary soil parameters.

These investigations should include in-situ tests such as Cone Penetrometer Testing (CPT) as well as laboratory strength and deformation tests on adequate soil samples.

- Field tests should consider varying size of drilled shafts, typically in the range of 0.91 to 1.83 m (3 to 6 ft). With the shaft diameter changing, the side resistance could be impacted by size effects, which should be given attention to minimize the scatter in the data.

- It is crucial that the test shafts are instrumented adequately so that load transfer characteristics in the different geomaterials surrounding the test shafts can be developed and the corresponding resistance factors appropriately calibrated. The set of guidelines provided in the appendix can be used for this purpose.

3.7 References

AASHTO. (2004). LRFD *Bridge Design Specifications*, 3rd Ed, American Association of State Highway and Transportation Officials, Washington, D.C.

AASHTO. (2007). LRFD *Bridge Design Specifications*, 4th Ed, American Association of State Highway and Transportation Officials, Washington, D.C.

AASHTO. (2012). LRFD Bridge Design Specifications, 6th Ed, American Association of State Highway and Transportation Officials, Washington, D.C.

AASHTO. (2014). LRFD Bridge Design Specifications, 7th Ed, American Association of State Highway and Transportation Officials, Washington, D.C

AbdelSalam, S. S. 2010. Behavior characterization and development of LRFD resistance factors for axially-loaded steel piles in bridge foundations. PhD Dissertation, Iowa State University, Ames, IA.

AbdelSalam, S. S., K. W. Ng, S. Sritharan, M. T. Suleiman, and M. Roling. 2012. *Development of LRFD Procedures for Bridge Pile Foundations in Iowa, Volume III: Recommended Resistance Factors with Consideration of Construction Control and Setup*. TR-584, Iowa Highway Research Board, Ames, IA.

Abu-Farsakh, M. Y., X. Yu, S. Yoon, and C. Tsai. 2010. *Calibration of resistance factors needed in the LRFD design of drilled shafts*. FHWA/LA Publication 10/470, Louisiana Transportation Research Center, Baton Rouge, LA.

Abu-Farsakh, M. Y., X. Yu, and Z. Zhang. 2012. Calibration of Side, Tip, and Total Resistance Factors for LRFD of Drilled Shafts. 91th Transportation Research Board Annual Meeting, Washington, D.C., 2012.

Abu-Farsakh, M., Q. Chen, and M. Haque. 2013. Calibration of Resistance Factors of Drilled Shafts for the New FHWA Design Method. FHWA/LA Publication 12/495, Louisiana Transportation Research Center, Baton Rouge, LA.

Allen, T. M., A. S. Nowak, and R. J. Bathurst. 2005. *Calibration to Determine Load and Resistance Factors for Geotechnical and Structural Design*. Circular E-C079. Transportation Research Board, Washington, D.C.

Barker, R. D., J. K Rojiani, O. P. Tan, S. C. Kim. 1991. *NCHRP Report 343: Manuals for the Design of Bridge Foundations*. Transportation Research Board, National Research Council, Washington, D.C.

Brown, D. A., J. P. Turner, and R. J. Castelli. 2010. *Drilled Shafts: Construction Procedures and LRFD Design Methods*. NHI Course No. 132014, Geotechnical Engineering Circular No. 10 National Highway Institute, U.S. Department of Transportation, Federal Highway Administration, Washington, D.C.

Fortier, A. R. 2016. Calibration of Resistance Factors Needed in the LRFD Design of Drilled Shafts. Master thesis, Louisiana State University, Baton Rouge, LA.

Garder, J., K. Ng, S. Sritharan, and M. Roling. 2012. *Development of a Database for Drilled Shaft Foundation Testing (DSHAFT).* InTrans Project 10-366, Iowa Department of Transportation, Ames, IA.

Motamed, R., K. Stanton, and S. Elfass. 2016. *LRFD Resistance Factor Calibration for Axially Loaded Drilled Shafts in the Las Vegas Valley*. NDOT Research Report No. 515-13-803, Nevada Department of Transportation, Carson City, NV.

Nichols, S. C., and J. E. Nicks. 2015. Load and Resistance Factor design-Past, Present and Future. *Load and Resistance Factor Design: An Update on the Geotechnologies.* Deep Foundation Institute, Special Issue: LRFD, pp. 12-15.

Ng, W. K., S. Sritharan, and J. C. Ashlock. 2014. *Development of Preliminary Load and Resistance Factor Design of Drilled Shafts in Iowa.* Project 11-410, Institute of Transportation, Ames, IA.

O'Neill, M. W. and L. C. Reese. 1999. Drilled Shafts: Construction Procedures and Design Methods, Publication FHWA-IF-99-025, FHWA, Washington, D.C.

Paikowsky, S. G. 2004. *Load and Resistance Factor Design (LRFD) for Deep Foundations*. Publication NCHRP-507. Transportation Research Board, Washington D.C.

Turner, J. P. 2015. LRFD Practice for Drilled Shafts. *Load and Resistance Factor Design: An Update on the Geotechnologies*. Deep Foundation Institute, Special Issue: LRFD, pp. 59-62.

Withiam, J. L., E. P.Voytko, R. M. Barker, J. M. Duncan, B. C. Kelly, S. C. Musser, and V. Elias. 1998. *Load and Resistance Factor Design (LRFD) for Highway Bridge Substructures*. Publication No. FHWA HI-98-032, Federal Highway Administration, Washington, DC.

Yang, X., J. Han, and R. L. Parsons. 2010. *Development of Recommended Resistance Factors for Drilled Shafts in Weak Rocks Based on O-cell Tests*. K-tran: KU-07-4, Kansas Department of Transportation, Topeka, KS.

3.6 Appendix: Proposed Criteria for Strain Gauge Layout Plan for Drilled Shaft Load Testing

1. Use 4 strain gages per elevation throughout the shaft.
2. Place the strain gages at each soil layer interface below the bottom of permanent casing if the thickness of either soil layer is greater than 1.22 m (4 ft). A set of gages at the interface may be ignored if the layers above and below are 1.22 m (4 ft) or smaller.
3. If the layer thickness is greater than or equal to 4.57 m (15 ft), place gages at additional elevations equally spaced within the layer, with a vertical spacing between gages not to exceed 4.57 m (15 ft).
4. Place a set of gages approximately 0.91 m (3 ft) or one shaft diameter whatever is greater above and below the O-cell if possible.
5. Place the uppermost level of gages no higher than 0.61 m (2 ft) above the lowest soil interface above the tip off any permanent casing.
6. Place one set of gages at a distance of 0.61 m (2 ft) from the tip and a minimum of ½ shaft diameter below an O-cell near the tip.
7. Along the shaft length below the permanent casing, ensure placement of gauges at a spacing not to exceed 4.57 m (15 ft) regardless of the locations of the soil layers.

CHAPTER 4. EXPERIMENTAL INVESTIGATION OF THE EFFECT OF DIAMETER SIZE ON DRILLED SHAFT SKIN FRICTION

A paper to be submitted to the Journal of the Deep Foundations Institute

Philippe Kalmogo, Sri Sritharan, Jeramy Ashlock

4.1 Abstract

As the need for a more rational approach to account for uncertainty in foundation design grew in recent years, significant efforts have been devoted to the development of regional Load and Resistance Factor Design (LRFD) guidelines for deep foundation particularly for driven piles and drilled shafts. Such endeavors, which not only include regional calibrations of resistance factors but oftentimes the development of more efficient local design methods, are necessary to overcome the shortcomings associated with current national design specifications recommended by the American Association of State Highway and Officials (AASHTO). Following the successful development and implementation of regional LRFD guidelines for driven piles, recent regional calibration studies have been directed towards drilled shafts. However, the success of these calibrations has been hindered primarily by the lack of high quality load test data. The current approach of using bi-directional static load testing of full-scale shafts for design verification and optimization is costly and often unable to provide conclusive results regarding the ultimate geotechnical capacity or the shaft capacity at displacement values of interest. To overcome this challenge and supplement drilled shaft load test databases with additional data in a rapid and cost-effective manner, load testing on reduced-scale drilled shafts is investigated as a cost-effective alternative in this paper. Implementation of such testing method could rapidly improve the size and quality of drilled shaft load test databases by reducing cost and increasing the number of tests and more importantly by providing conclusive results on the ultimate geotechnical capacity of the test shafts. To explore the viability of such testing approach for the intended purpose, scale effects on drilled shaft skin resistance is investigated in this paper through a series of load tests. Results from the conducted tests do not clearly indicate a consistent trend regarding the influence of shaft diameter on skin resistance, and additional work is needed to reach definite conclusions.

4.2 Introduction

Because of their advantages over other types of deep foundations, the use of drilled shafts on bridge projects has significantly increased in recent years. Drilled shafts are able to carry much higher axial and lateral loads, thus they can be used in smaller numbers thereby eliminating the need for pile caps. They are also less susceptible to scour, and their construction produces much less noise and vibrations. However, the loss of redundancy that occurs as a result of using a smaller number or a single drilled shaft in place of a pile group requires that the drilled shaft foundation capacity be predicted more accurately. To verify the predicted capacity, which is susceptible to the variable nature of soil deposits, and ensure satisfactory field performance of the shaft, load tests are routinely performed on full-scale prototype shafts at the actual project site. Field load tests have several benefits. They offer the potential to obtain detailed information on the load transfer characteristics for both side and base resistance, and justify the use of higher resistance factors in the LRFD framework thereby optimizing the final design. More importantly, they are necessary for statistical analyses involved in the development of local design methods as well as resistance factors that improve efficiency at the regional level.

Bi-directional load tests have grown to become the preferred testing method in several states for drilled shaft field capacity verification. As a result of its loading mechanism, the embedded load cells are capable of subjecting drilled shafts to great magnitudes of loads without the need of reaction systems, which can become increasingly expensive and impractical in the realm of high capacity drilled shafts. A typical bi-directional load test using an Osterberg load cell (O-cell) is illustrated in Figure 4.1. As the internal pressure of the cell is increased, the cell expands and loads both segments of the shaft above and below the load cell. Movement of the segment above the cell is resisted by downward side shear, while movement of the segment below the cell is resisted by a combination of upward side shear and end bearing. Instrumentation installed at carefully selected locations along the shaft length provides data on the load transfer occurring in the various soil layers surrounding the shaft. The possible outcomes of a typical bi-directional load test involve the following: failure in side shear of the upper segment, failure in side shear and end bearing of the lower segment, simultaneous failure of both upper and lower segments, maximum

capacity of load cell reached. The desired outcome to reach a balanced failure condition in both shaft segments is seldom attained, therefore extrapolation of the non-failed portion is generally necessary to estimate its ultimate resistance and also assist in constructing an equivalent top load-displacement curve. Such a curve is important to designers since it represents actual foundation loading condition, and it can be constructed using the Loadtest's approximate procedure. Recourse to extrapolation in estimating the non-failed shaft segment resistance at ultimate or higher displacement needed to develop an equivalent top load-displacement curve introduces additional uncertainty into the actual shaft's capacity and partially defeats the purpose of the expensive test. Because of the relatively high cost of conducting load tests on full-scale shafts coupled with the inability to achieve significantly large displacements or complete geotechnical failure, the quantity of good quality drilled shaft load tests available in databases is usually limited and sometimes insufficient for proper calibrations of regional LRFD guidelines. In light of these shortcomings, an alternative method involving load tests on small-scale drilled shafts is explored in this paper.

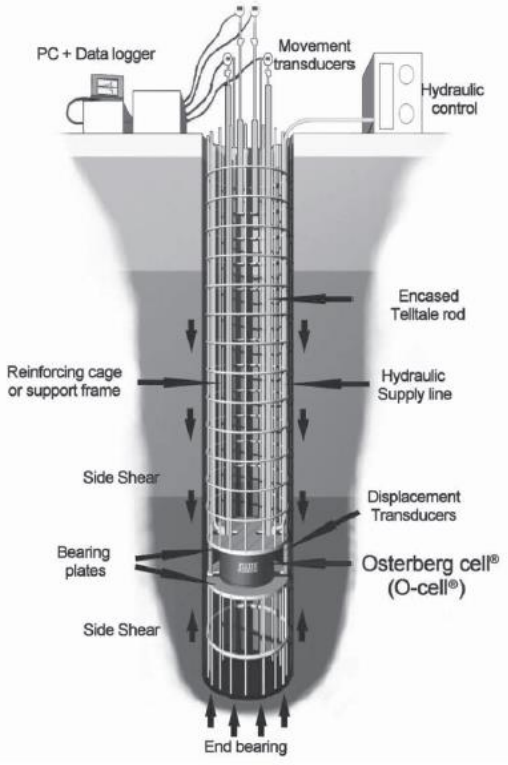

Figure 4.1: Typical bi-directional load test setup using O-Cell (Loadtest, Inc.)

To evaluate the feasibility of using such method, a literature review on the current state of knowledge on the phenomena contributing to scale effect in shear resistance is conducted accompanied by a review of the current state of knowledge on the applicability of small-scale load testing to full-scale specimens. Load tests available in the Drilled Shaft Foundation Testing (DSHAFT) database as well as load tests found in the literature relevant to the investigation are then analyzed to identify and highlight the influence of drilled shaft size on side shear. Finally, details and results of a load test program devised to investigate scale effects on drilled shaft side shear are presented.

4.3 Scale Effect in Side Shear

The effect of scale on shaft skin friction in soil as it relates to laboratory testing of small diameter models has long been recognized and investigated. Although no systematic approach or scaling relations have been developed to extrapolate small-scale test results to full-scale specimens thus far, tests results conducted by several researchers seem to indicate an inverse relationship between skin friction and shaft diameter. In other words, studies have shown that shaft skin friction tends to increase as the shaft diameter decreases. Using Mohr-Coulomb failure criterion and assuming a negligible cohesion, drilled shaft skin friction can be expressed as:

$$\tau_s=(\sigma'_{nc}+\Delta\sigma'_n)\tan\delta \qquad (4.1)$$

where σ'_{nc} is the normal effective stress at the pile-soil interface prior to loading, $\Delta\sigma'_n$ is the change in normal effective stress during loading, and δ is the pile-soil interface friction angle.

Upon loading, skin friction develops within a thin shear band adjacent to the shaft. The thickness of the shear band was found to be a function of several factors including the mean sand particle size, D_{50}, the shaft surface roughness, the sand relative density, and the stress level. Reports by Wernick (1978), Yoshimi and Kishida (1981), Boulon (1988), Hoteit (1990), and Desrues (1991) indicate that shafts with a smooth surface develop a shear band thickness ranging between 2 and 5 times D_{50} while those with a rough surface have a shear band thickness varying between 10 and 15 times D_{50}. For D_{50} less than 0.75 mm, Frost et al.

reported that the shear band thickness is about 2 mm and does not depend on D_{50}. Normal stress change at the pile-soil interface arises from the tendency of the shear band to increase or decrease in volume during loading. Dilation of the shear band in dense and over-consolidated soils results in an increase of normal stress at the interface while contraction in loose and normally consolidated soils leads to a decrease in normal stress. Using cavity expansion theory, Boulon and Foray (1986) found that the change in normal effective stress could be expressed as:

$$\Delta\sigma'_n = k_n \Delta u = \frac{4G}{D}\Delta u \qquad (4.2)$$

where, k_n is the equivalent normal stiffness, Δu is the radial expansion or contraction in the shear band, G is the equivalent linear shear modulus, and D is the shaft diameter.

As implied by Eq. (2), the change in normal effective stress and consequently effective shear stress becomes significant as the shaft diameter reduces.

Several experimental studies were conducted to investigate the dependence of shear stress on shaft diameter. Foray et al. (1998) used centrifuge testing to study the effect of pile diameter and mean gain size on shaft skin friction. Tension tests were conducted in two quartz sands of different density (D50 = 0.32 mm and 0.7 mm) on four instrumented piles (D = 16 mm, 27 mm, 35 mm, and 55 mm) with rough interfaces created by gluing sand grains onto the pile shafts. As expected, test results indicate a higher skin friction in the smaller diameter piles for a given sand density. For a given pile diameter, higher skin friction was observed in the coarser sand. This second observation was attributed to the formation of a greater shear band thickness in the coarser soil, thus it was concluded that there is a better correlation between skin friction and the ratio D/D_{50}. Results from centrifuge testing of three piles with varying roughness in silica sands conducted by Fioravante indicate that the effect of D/D_{50} becomes negligible for values greater than 30 to 50.

Lehane et al. (2005) conducted a series of centrifuge tension tests to further investigate scale effects on skin friction of rough piles buried in dense sand. Four 130 mm long piles with diameters of 3, 5, 10, and 18 mm piles were subjected to centrifuge acceleration levels of 30g, 50g, 100g, and 180g resulting in a total of 16 tension tests. Results

from these tests indicate that shear stress reduces with increasing pile diameter. Moreover, test data showed that the increase in normal effective stress during loading is responsible for much of the shear strength developed in small diameter piles. The scale effects were found to be decreasingly significant with increasing stress levels as observed by Foray (1991).

Balachowski (2006) used direct shear interface test with constant normal stiffness to study scale effects for dilative and contractive interfaces. The dilative interface was produced in the shear box using a rough plate at the bottom and Hostun dense coarse sand at the top. For the contractive interface, loose Hotsun quartz sand and loose carbonated Quiou sand were used in combination with a smooth plate. The test results showed that the scale effect is greater than unity for dilative interfaces and smaller than unity for interfaces that tend to contract upon shearing.

Analytical models have also been used to investigate scale effects on skin friction. For instance, using the software ROCKET 95, Baycan (1996) determined that the unit side shear of rock sockets with moderate roughness decreases as the socket diameter increases due to reduced dilatancy effects. Analytical data showed that the scale effect becomes negligible at diameters ranging between 1500 mm and 2000 mm. Experimental studies by Hassan and O'Neill (1997), however, suggest a lower diameter limit of 610 mm.

Other studies particularly related to driven piles did not provide conclusive results regarding scale effects on skin friction as expected from Eq. (2). Al-Mhaidib and Edil (1998) conducted a series of tension tests on smooth steel piles with diameters of 45, 89, and 178 mm in loose and dense saturated sands. A direct relationship between skin friction and pile diameter could not be established from the test data. Similarly, results from tension tests conducted by Alawneh et al. (1999) were inconclusive. The tests involved two different pile sizes (D = 41 mm and 61 mm) with intermediate to rough surfaces installed in medium dense and dense dry sands. Test data showed that the unit skin friction was higher for the larger diameter pile for intermediate roughness regardless of sand density. For the rough piles, the unit skin friction reduced as the shaft diameter increased for the dense sand. A similar trend was not observed in the medium sand.

A testing program including uplift load testing on six drilled shafts was conducted by Lutenegger et al. (1994) to evaluate the reliability of the borehole shear test and pressuremeter test at estimating the uplift capacity of drilled shafts in stiff soils. The subsurface at the testing site included a thick deposit of Connecticut Valley varved clay overlain by 1 m of mixed cohesive and cohesionless random compacted fill. The test shafts included diameters of 76 mm and 152 mm with lengths of 1.52 m, 3.05 m, and 4.57 m. A layout of the shafts and load test arrangement is shown in Figure 4.2. Although the tests were not conducted with the purpose of investigating scale effects, the results presented in the study were analyzed in order to identify any effect of the diameter size on the shaft skin friction. The unit skin friction-displacement curves were developed using the available data, and they are shown in Figure 4.3, Figure 4.4, and Figure 4.5. As observed, the larger diameter shaft appears to have a higher unit skin friction compared to the smaller diameter shaft for a given length. It is also interesting to note that the difference in unit skin friction between the two diameters is not consistent and decreases as the shaft length increases. While most of the studies in the literature tend to indicate an increasing skin friction with decreasing shaft diameter, test results from other studies either indicated the opposite or they were inconclusive.

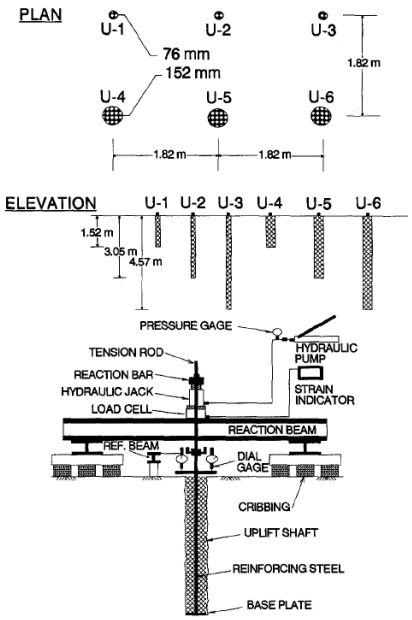

Figure 4.2: Shaft layout and test setup (Lutenegger et al. 1994)

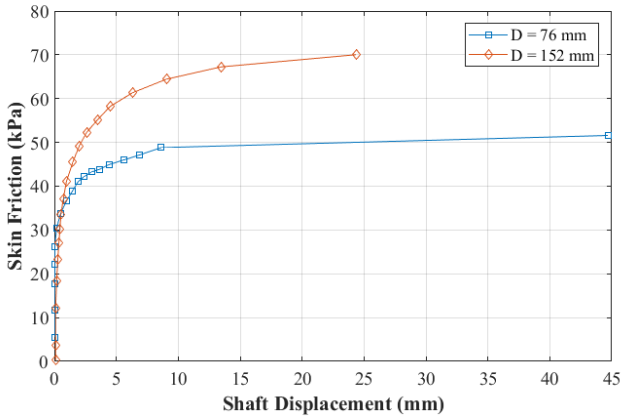

Figure 4.3: Side shear displacement curves for 1.52 m long shafts

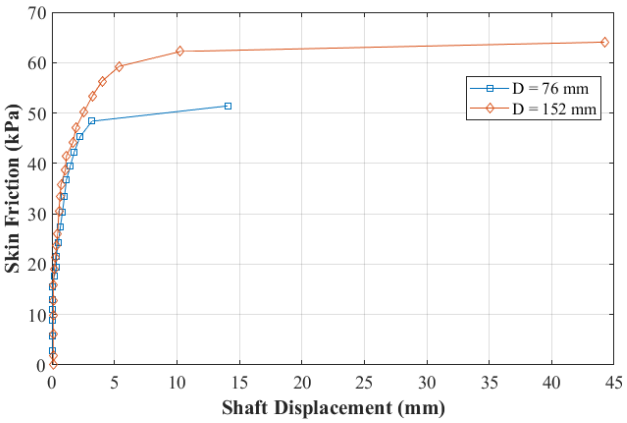

Figure 4.4: Side shear displacement curves for 3.05 m long shafts

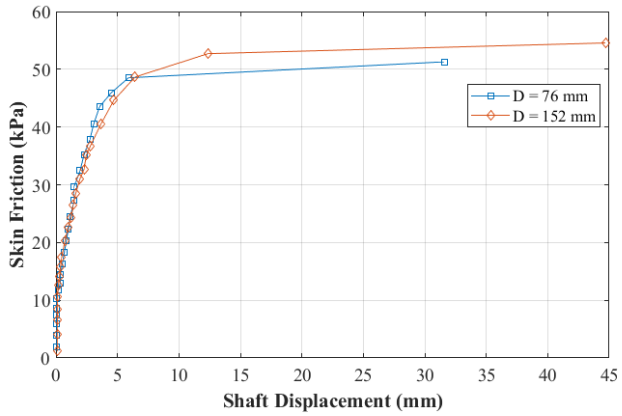

Figure 4.5: Side shear displacement curves for 4.57 m long shafts

Due to the fact that the dependency of skin friction on drilled shaft diameter is not fully understood, there has been little attempt to develop suitable methods to extrapolate results from load tests on small prototype shafts to full scale shafts in the literature. One of the few examples of such attempt include the studies conducted by Lizzi (1980). Arguing that the existing design methods for cast-in-place piles at the time were subject to large uncertainties and that more accurate capacity prediction methods using load tests on full-scale shafts were costly, Lizzi (1980) developed an experimental approach to using small diameter shaft load test results to predict the capacity of any larger diameter shafts of the same length and construction material that derive their resistance primarily from skin friction. The approach, known as the similitude method, is based on the compatibility of stress-strain conditions that exist on the shaft side surface and the pile cross section. For a given shaft segment as shown in Figure 4.6, the set of Eq. (4.3) termed "congruence equations" must be satisfied.

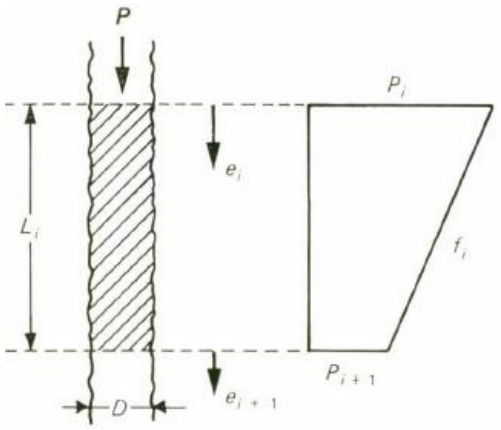

Figure 4.6: Shaft Segment

$$\frac{P_i - P_{i+1}}{\pi D L_i} f_i = \frac{e_i + e_{i+1}}{2}$$
$$\frac{P_i + P_{i+1}}{2EA} L_i = e_i - e_{i+1} \qquad (4.3)$$

where,

D = Pile diameter

A = Pile cross-sectional area including steel reinforcement

E = Concrete modulus of elasticity

L_i = Segment length

P = Total axial load on top of the pile

P_i = Axial forces along shaft segment

e_i = Settlements along shaft segment

f_i = Skin factor

The approach requires instrumentation along the shaft length to determine the load transfer occurring in various segments of the shaft. Using test data along with the congruence equations, skin factor vs. settlement charts are developed for each shaft segment of the small diameter shaft. These charts are subsequently utilized in combination with the congruence equations to determine the load transfer in shafts segments of a larger diameter shaft. A simpler approach that does not require instrumentation of the smaller diameter pile was proposed by Lizzi (1983) for situations where the ultimate bearing capacity was the sole information needed. This approach relied on simple linear extrapolation of the top load-displacement curve of a prototype shaft to a full scale shaft using the ratio of diameters. Application of the procedure to three case studies showed satisfactory accuracy.

More recently, Bradshaw et al. (2016) investigated the feasibility of small-scale pile load testing for the design of drilled foundations. The approach known as Borehole Plug Test consists in a pull-out test of a short concrete section constructed by placing a threaded bar with a steel end plate and casting a short concrete section within a typical borehole obtained during standard subsurface exploration. The measured load transfer behavior of the grout plug is then used in an appropriate finite element program to simulate the load-deformation behavior of the full scale foundation. The proposed method was evaluated in a field trial using results of load tests on full-scale micropiles constructed in a layer of very dense silty fine sand. The Borehole Plug Test was conducted at a distance of 15.2 m from one of the micropiles, and the measured load transfer curve was used to simulate the load test of the full scale micropile. A comparison of the actual and simulated tests showed identical behavior at low load levels. Beyond a load magnitude of 400 kN, the simulated load-displacement curve

was stiffer than the actual curve. This divergence was attributed to various reasons including the assumption of a linear elastic pile stiffness in the simulation and inaccuracies in the load transfer curves used in the simulation that may have resulted from differences in geometry, scale effect, and level of soil disturbance.

4.4 Scale Effect in DSHAFT

To facilitate the calibration of regional resistance factors for LRFD design of drilled shafts in Iowa, an electronic database of drilled shaft load tests was developed by Garder et al. (2012) using Microsoft Office Access. DSHAFT include load test data and all available subsurface investigation and construction details from Iowa and several neighboring states including Colorado, Illinois, Kansas, Kentucky, Minnesota, Missouri, Nebraska, Nevada, South Dakota, and Tennessee. The current version of the database contains 51 load tests and can be found at http://srg.cce.iastate.edu/dshaft. Geomaterial types include cohesive soils, cohesionless soils, cohesive and cohesionless intermediate geomaterials (IGM) and rock. The majority of the load tests was performed using the bi-directional load testing method with O-cell. DSHAFT includes drilled shafts of different diameter size, thus it was used to conduct a preliminary assessment of the influence of shaft diameter on skin friction.

The available data was categorized based on the type of geomaterial along shaft segments. Since the load tests were conducted in soils conditions with different strength conditions, the measured skin friction was normalized so that appropriate comparison could be made. The shaft resistance was normalized by the predicted resistance using O'Neill and Reese (1999) α-method and β-method for cohesive soils and cohesionless soils, respectively. For IGM and rock, the shaft resistance was normalized by the unconfined compressive strength, f'_c. The measured resistance was selected at a common shaft movement of 0.5 inch to ensure that the shaft resistance was nearly or fully mobilized and to obtain sufficient data for comparison. Plots of the variation of normalized resistance with respect to shaft diameter are shown in Figure 4.7 through Figure 4.10 for all geomaterial types in DSHAFT. As can be seen, a clear relationship between the diameter and the shaft resistance is not shown by the data. Although the measured resistance was normalized, the variability associated with the different soil conditions at the test locations could be significant enough to obscure any relationship between skin friction and diameter.

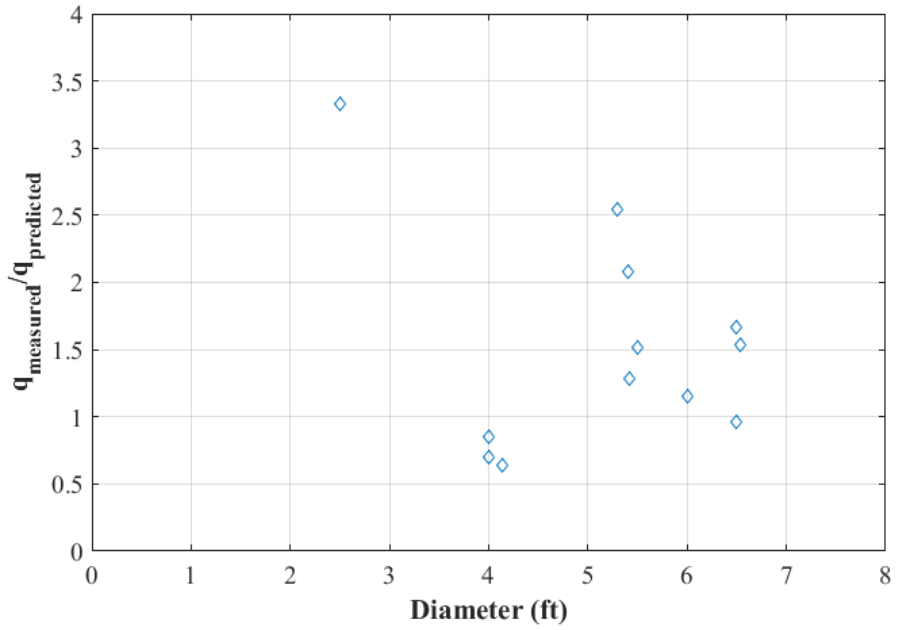

Figure 4.7: Normalized resistance variation with respect to diameter for cohesive soil

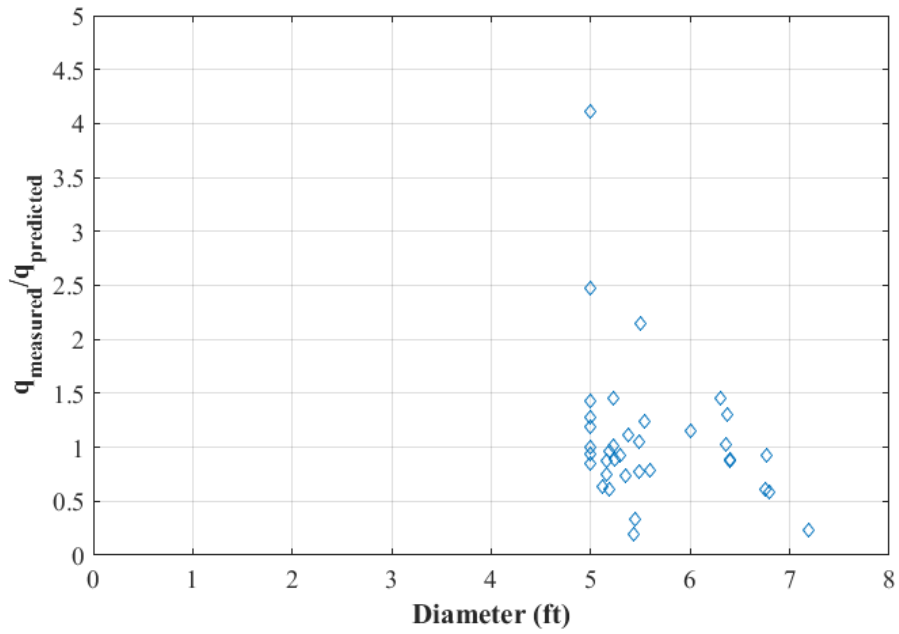

Figure 4.8: Normalized resistance variation with respect to diameter for cohesionless soil

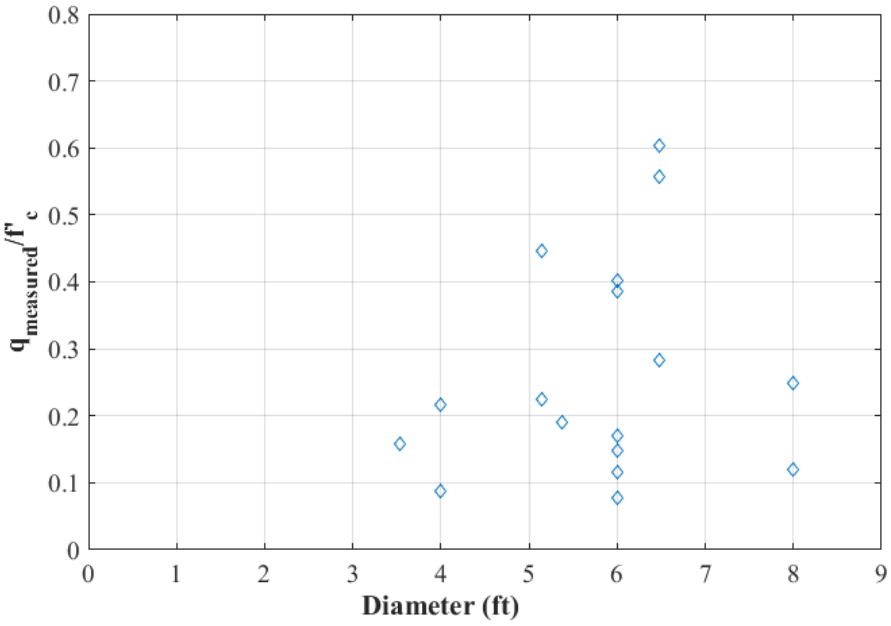

Figure 4.9: Normalized resistance variation with respect to diameter for cohesive IGM

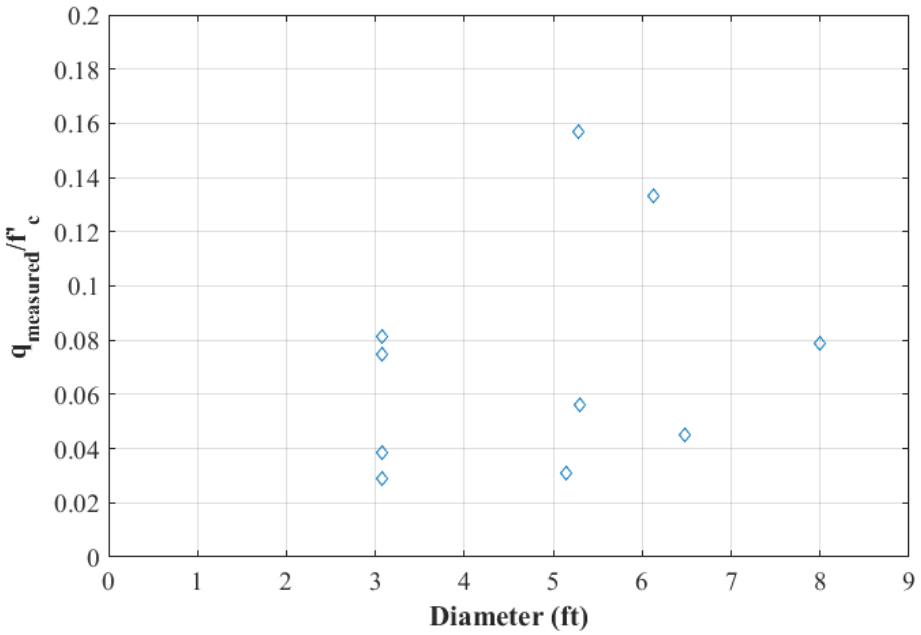

Figure 4.10: Normalized resistance variation with respect to diameter for rock

4.5 Field Investigation at Pottawattamie County

Review of the phenomena contributing to scale effects as well as current knowledge on the scalability of small-scale test results to full-scale shafts illustrated the need for further research to understand the phenomena and develop proper scaling relations. For this purpose, two field study involving conventional top down load tests on two small diameter shafts and a bi-directional load test of a full scale demonstration shaft was carefully conducted. The full scale demonstration shaft was performed by the Iowa DOT as part of a project involving the replacement of an existing bridge. The demonstration shaft had a nominal diameter of 5 ft and a length of 94.8 ft. The reduced scale shafts with nominal diameters of 1.5 ft (termed DS18) and 2 ft (termed DS24) were separated by a distance of 5 ft and installed at approximately 13 ft from the full scale shaft. Due to the limitations imposed by the testing equipment, the lengths of the reduced scale shafts were limited to 39.25 ft for and 38 ft for DS18 and DS24, respectively.

4.5.1 Test Site Subsurface Condition

Subsurface investigation to characterize the geomaterials underlying the testing site included a borehole at the center of the full-scale shaft and another at the center of DS24. The borehole at the full scale shaft location was 114.5 ft deep revealing a soil profile consisted of 5 ft of lean clay, 8 ft of fat clay, 7 ft of lean clay, 5 ft of silty sand, 48 ft of fine sand, 5 ft of coarse sand, 5 ft of fine sand and 31.5 ft of coarse sand. The ground water table was located at +966.1 ft during drilling. Laboratory testing and characterization of the collected soil samples at the full-scale shaft location was conducted by Terracon. Variations of SPT blow count number, moisture content, undrained shear strength and dry unit weight with depth are presented in Figure 4.11 and Figure 4.12. While the moisture content decreases with depth, the blow count numbers show an increasing trend with some scatter occurring between 25 ft and 70 ft below ground surface. Undrained shear strength was measured from torvane test on only two soil samples while the unit weight was determined for only three samples. The borehole at the center of DS24 was 45 ft deep and the subsurface at that location included 5 ft of lean clay, 8 ft of fat clay, 11.5 ft of lean clay, and 20.5 ft of poorly graded sand with silt.

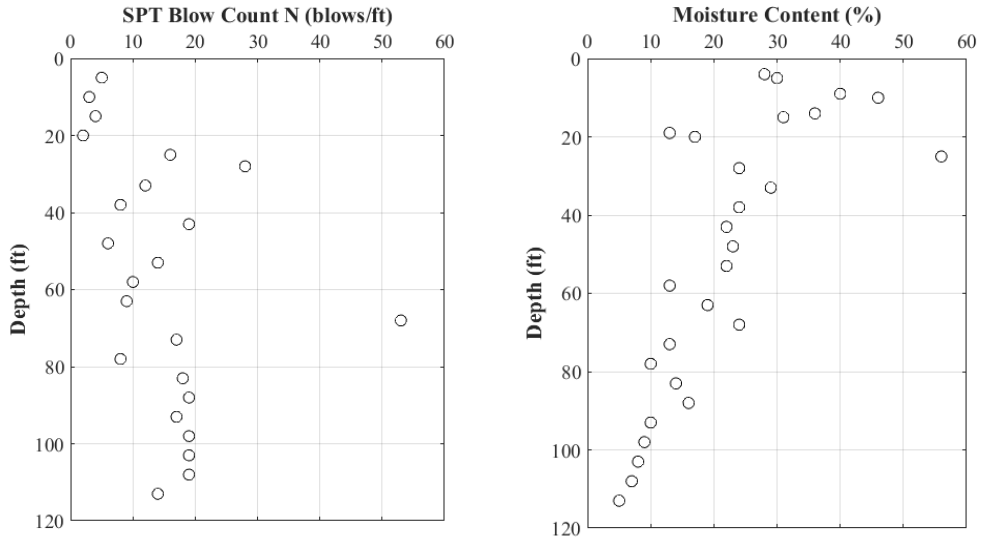

Figure 4.11: Variation of SPT N and moisture content with depth at full-scale shaft

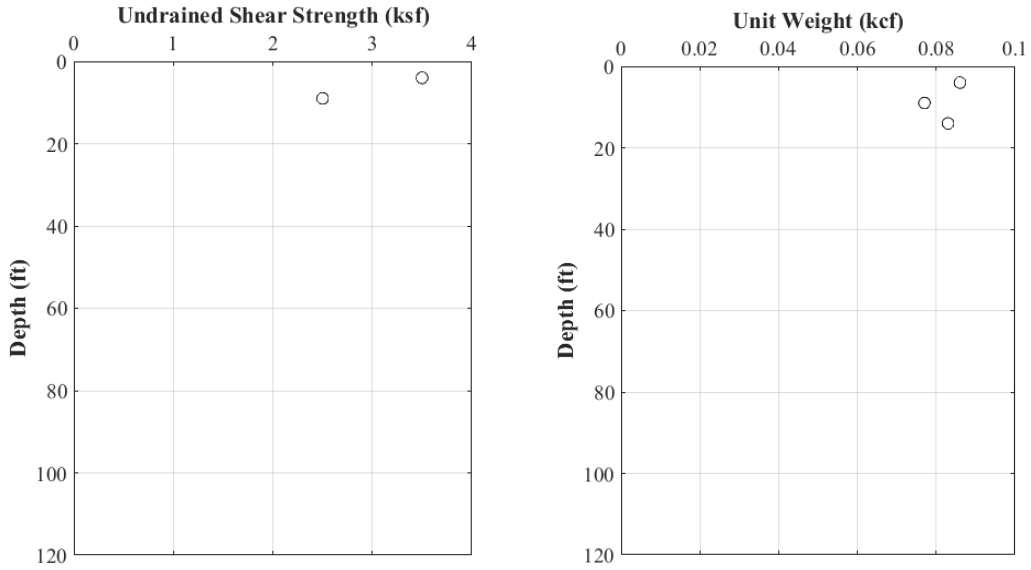

Figure 4.12: Variation of undrained shear strength and unit weight content with depth at full-scale shaft

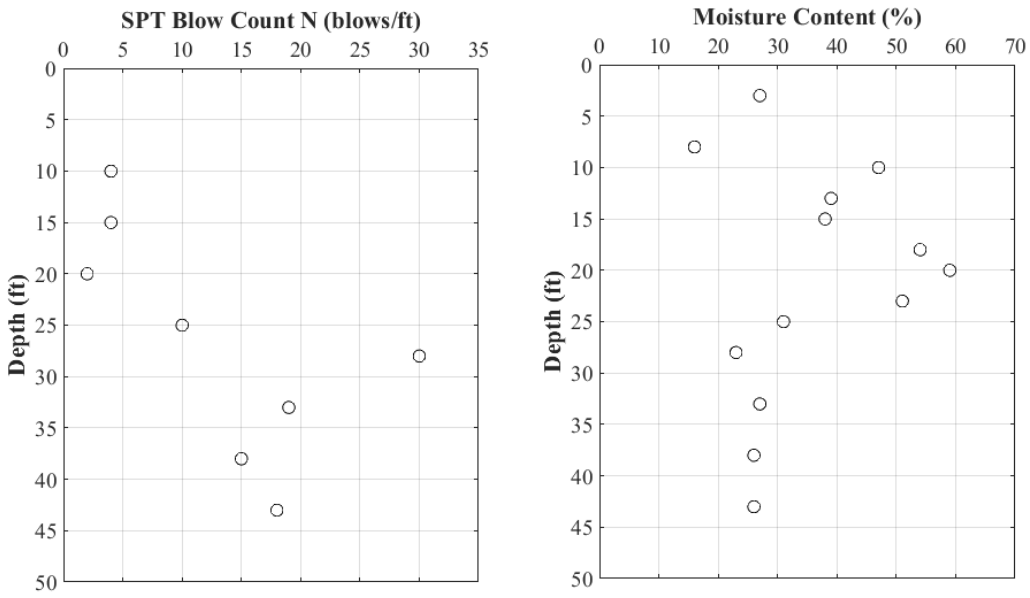

Figure 4.13: Variation of SPT N and moisture content with depth at DS24

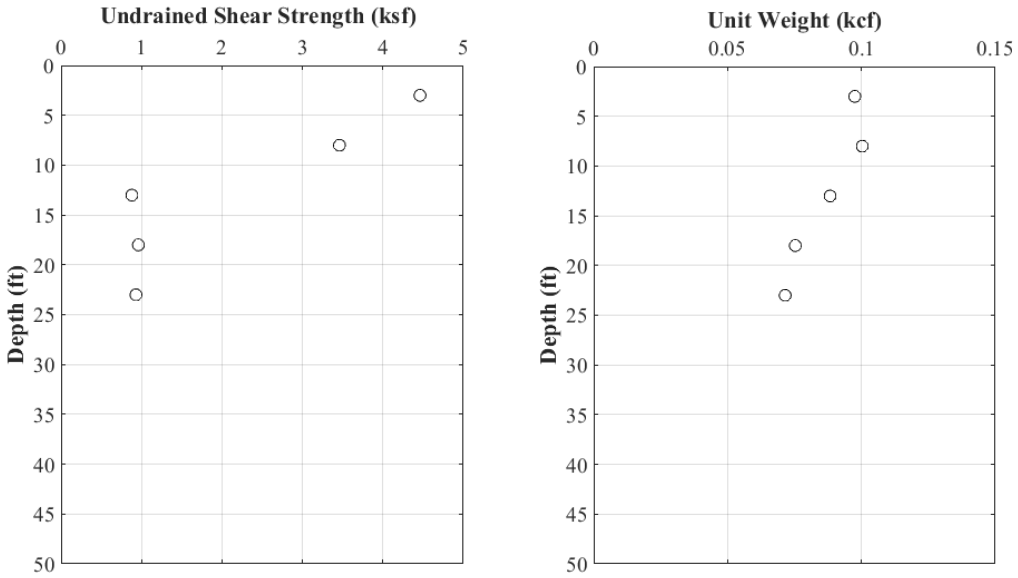

Figure 4.14: Variation of undrained shear strength and unit weight content with depth

The ground water table was located at +966.5 ft during drilling Shelby tube and split spoon soil samples retrieved during drilling were brought back to Iowa State University for laboratory testing. Soil USCS classification, moisture content and unit weight measurements

were conducted per ASTM standards. The undrained shear strength was estimated from unconfined compression tests on undisturbed samples from the Shelby tubes. Variations of SPT blow count number, moisture content, undrained shear strength and dry unit weight with depth are presented in and. The SPT blow count numbers increase with depth similar to the full-scale shaft location. The moisture content shows an increasing trend down to a depth of 25 ft and a relatively constant value between 25 ft and 45 ft. The estimated undrained shear strength, taken as half of the unconfined compressive strength, was determined for five samples and showed a decrease trend with depth similar to the measured unit weights.

4.5.2 Full Scale Test Shaft

Construction of the full-scale test shaft spanned over two days starting on August 1, 2016 and ending on August 2, 2016. The construction began with dry excavation of an 11 ft deep hole in the uppermost clay layers. A temporary casing with an outer diameter of 65 inch was placed into the drilled hole, and excavation of the shaft continued under polymer slurry to a base elevation of +883.7 ft. The construction was paused at the end of the first day subsequent to completion of the excavation. Upon resuming the next day, debris were removed from the shaft base utilizing a clean-out bucket to a final base elevation of +882.8 ft, and the excavation was profiled using the SONICALIPER. The instrumented reinforcing cage was then placed into the excavation supported by the temporary casing, and concrete was pumped through a tremie from the shaft base to an elevation of +977.1 ft. The temporary casing was removed following concrete placement to end the construction. Strain gauges were installed at selected elevations along the shaft so that load transfer characteristics of the various soil layers surrounding the shaft could be developed. Additional instrumentation included telltales and Linear Vibrating Wire Displacement Transducers (LVWDTs) to measure compression and movements of the shaft. The concrete was allowed to cure for 14 days before the load test. At this time, the unconfined compressive strength of the concrete had reached a value of 4.27 ksi.

Following ASTM D1143, the shaft was subjected to a bi-directional load of 1489 kips from the 24 inch diameter O-cell installed 26.8 ft above the shaft base. At this point further load increment was unsuccessful because the upper side shear could not sustain additional load. The load was then removed in five decrements to complete the test. Figure 4.15 shows

O-cell-load displacement responses of the shaft sections above and below the O-cell. Maximum displacements of 3.12 in. and 1.31 in. were achieved for the upper and lower sections, respectively. The load distribution along the shaft calculated from strain gauge data is shown in Figure 4.16 for all successful load increments. Unit side shear-displacement responses of the various shear zones were calculated from this load distribution using the as-built shaft dimensions obtained from SONICALIPER soundings and the resulting curves are presented in Figure 4.17.

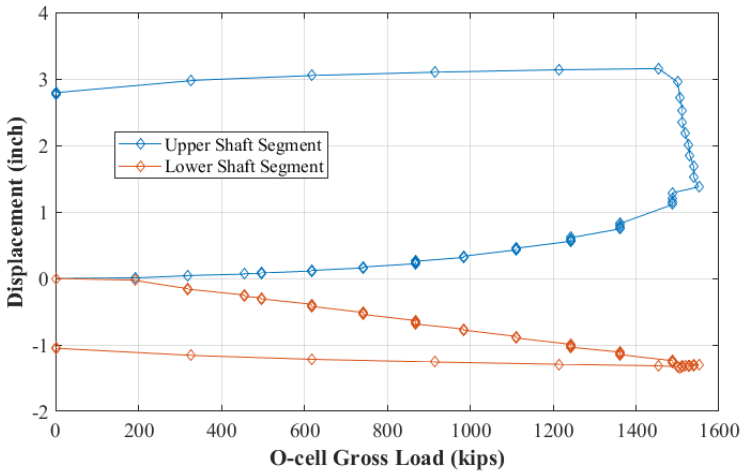

Figure 4.15: Full-scale shaft upper and lower segment load-displacement responses

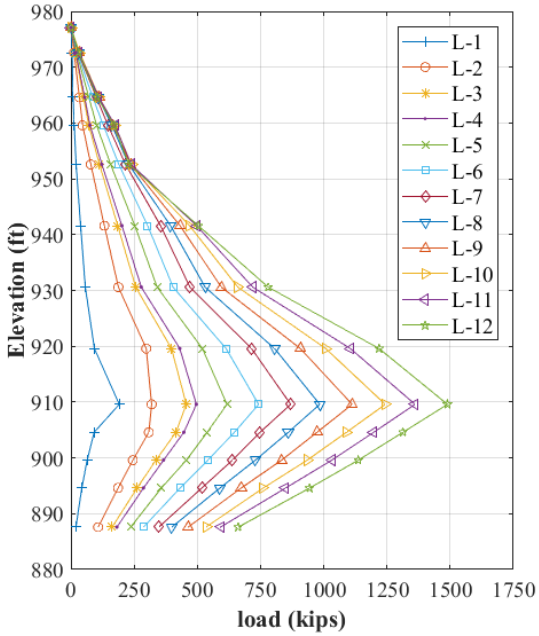

Figure 4.16: Full-scale shaft strain gauge load distribution

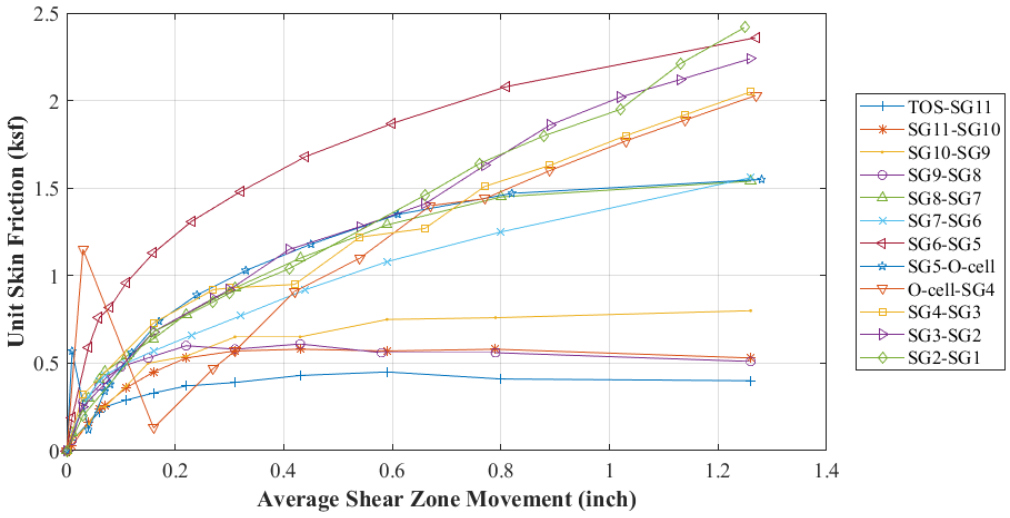

Figure 4.17: Full-scale shaft unit side shear

4.5.3 Reduced Scale Test Shafts

4.5.3.1 Capacity Prediction and Instrumentation Plan

Based on the subsurface conditions and the capabilities of the testing equipment available at the ISU testing laboratories, it was decided to limit the small-scale shaft lengths to 38 ft in order to ensure complete geotechnical failure and subject the shafts to significantly large displacements. The ultimate geotechnical capacity of the shafts was determined following O'Neill and Reese (1999) and Brown et al. (2010) recommended static design methods. Unit side shear in the uppermost cohesive soil layers were estimated using the α-method while the unit side shear in the cohesionless soils was estimated using the depth dependent β-method and the more rational β-method. As shown in Table 4.1, shaft resistance estimates that include the depth-dependent approach are conservative compared to those obtained that include the rational approach. Based on the subsurface profile established from the boring log at DS24, both small-scale shafts were instrumented with eight levels of strain gauges. The selected gauge locations were grinded to provide a flat surface and smooth finish for proper bonding.

Table 4.1: Reduced-scale shafts capacity prediction

Shaft diameter (ft)	Shaft Length (ft)	Shaft Capacity (kips)					
		O'Neill & Reese (1999)			Brown et al. (2010)		
		Side shear	End bearing	Sum	Side shear	End bearing	Sum
1.5	38	242	42	284	265	42	307
2	38	293	75	368	323	75	398

Upon completing surface preparation, the strain gauges were bonded to the rebar using an adequate adhesive. The gauges were then coated with some air drying solvent-thinned polyurethane to provide protection against moisture. Finally, the gauges were covered with butyl rubber to finish the installation process. Above ground, the shafts were instrumented with three string potentiometers to measure shaft movements and two magnetic mounted Direct Current Differential Transformers (DCDTs) to measure shaft compression from telltale movements. Shaft movements were also monitored via a digital survey level and barcode staff mounted on top of the shafts. Moreover, the reaction frame was equipped with two string potentiometers so that any unexpected behavior could be detected and appropriate corrective measures taken. A 400 kip load cell was also used to monitor the applied load during the test.

4.5.3.2 Construction and Testing

The shafts were constructed following a procedure similar to that of the full-scale shaft. Upon allowing the concrete to gain sufficient strength, both shafts were tested using the reaction system setup shown in Figure 4.18 and following ASTM D1143. Using 15 kips load increments, DS18 was initially loaded to 285 kips with a corresponding top displacement of 4.99 in. The next load step i.e. 300 kips, could not be completed because the string potentiometers monitoring shaft displacements had reached their maximum stroke of 5.6 in. thereby necessitating the need to unload the shaft in five equal decrements, re-setup, and reload the shaft. The shaft was successfully reloaded to a maximum load of 300 kips at which point the top displacement was in excess of 8 in. and additional load increment could not be sustained. The shaft was then unloaded to end the test. Following a similar procedure and using 20 kips load increments, DS24 was loaded to the maximum capacity of the

actuator i.e. 415 kips, for a corresponding top displacement of 2.12 in. Top load-displacement responses corresponding to the strain gauge data 8-minute readings obtained from both tests are shown in Figure 4.19.

Load distribution along the shaft length corresponding to the 8-minute readings was calculated from the measured strains and shaft composite stiffness, and they are shown in Figure 4.20 and Figure 4.21. Strain gauges located at elevations +974.5 ft and +941.5 ft appear to provide abnormal readings in both shafts. Additionally, readings from strain gauges located at elevation +953 ft i.e. level 3, in DS18 seem suspect. Unit skin friction curves developed from the load distribution obtained from the strain gauge data are shown in Figure 4.22 and Figure 4.23. As can be seen from Figure 4.22, two of the unit side shear-displacement curves associated with DS18 have unusual characteristics. These curves are associated with the shaft segment located between strain gauge level 4 and level 3 and the segment located between level 3 and level 2.These unusual load transfer characteristics indicate that the initial suspicions about the reliability of strain readings from level 3 gauges are justified. Thus, strain gauge data from level 3 were not considered in further analyses.

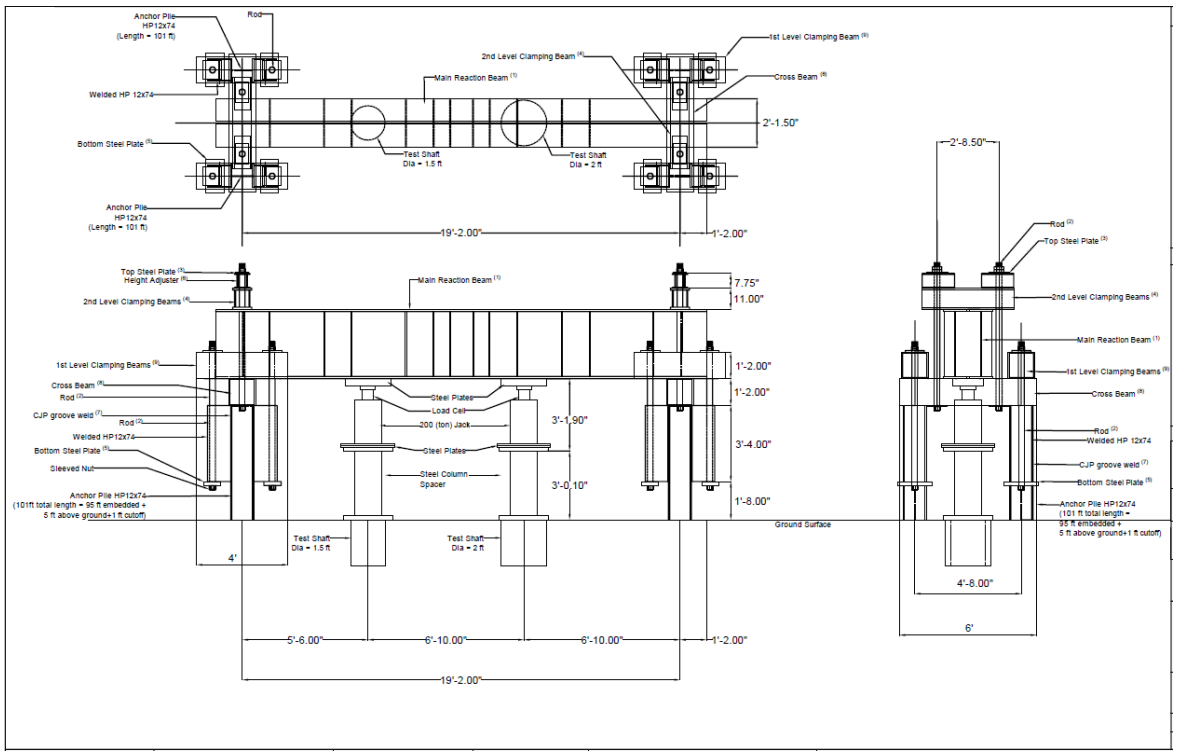

Figure 4.18: Reaction system details

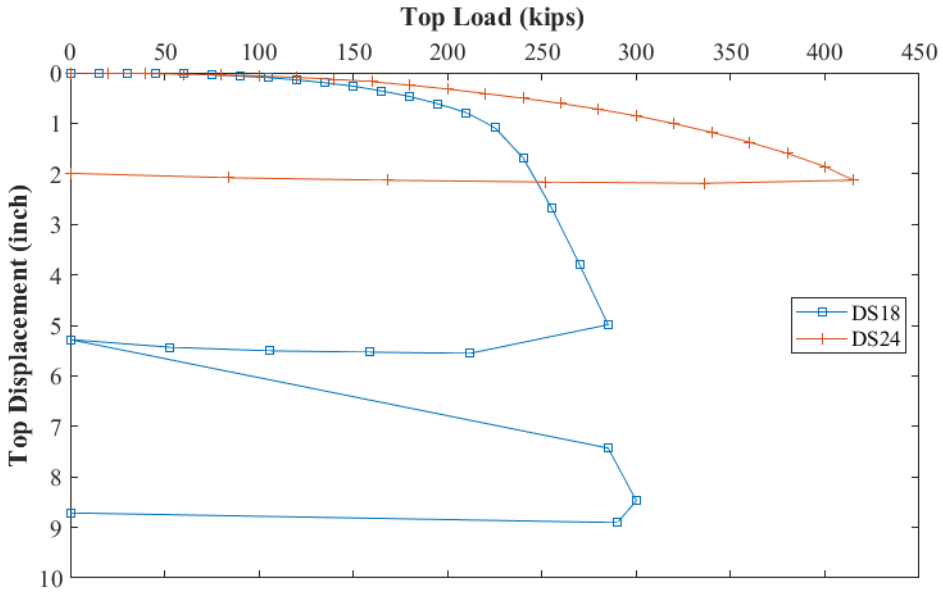

Figure 4.19: DS18 and DS24 top load-displacement curves

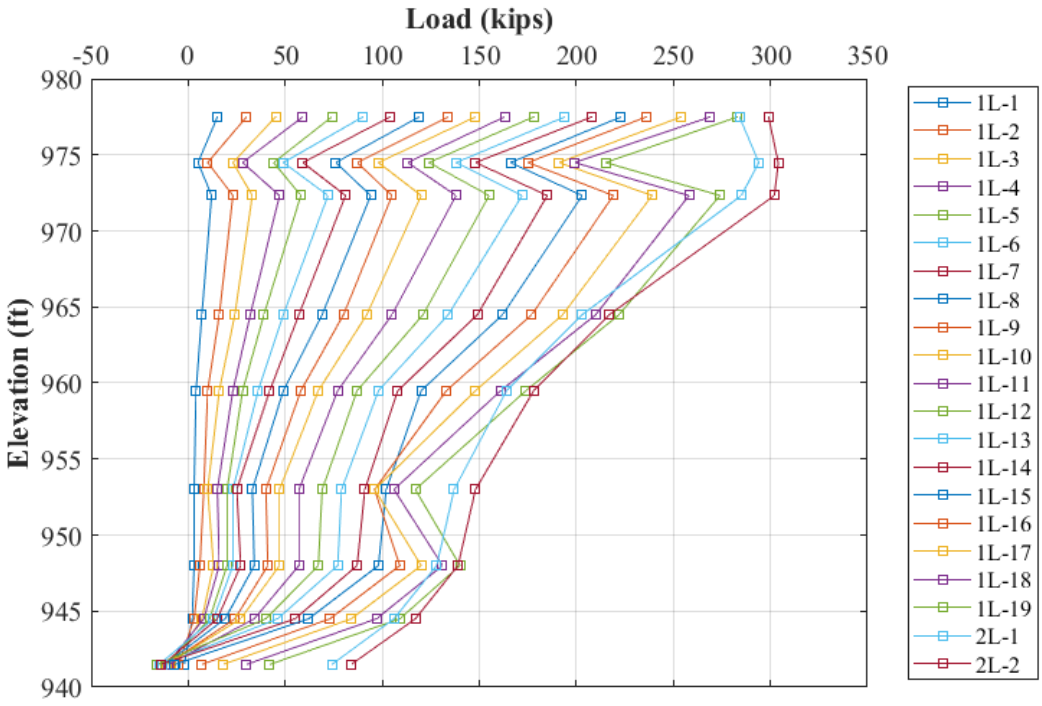

Figure 4.20: DS18 8-minute reading load distribution

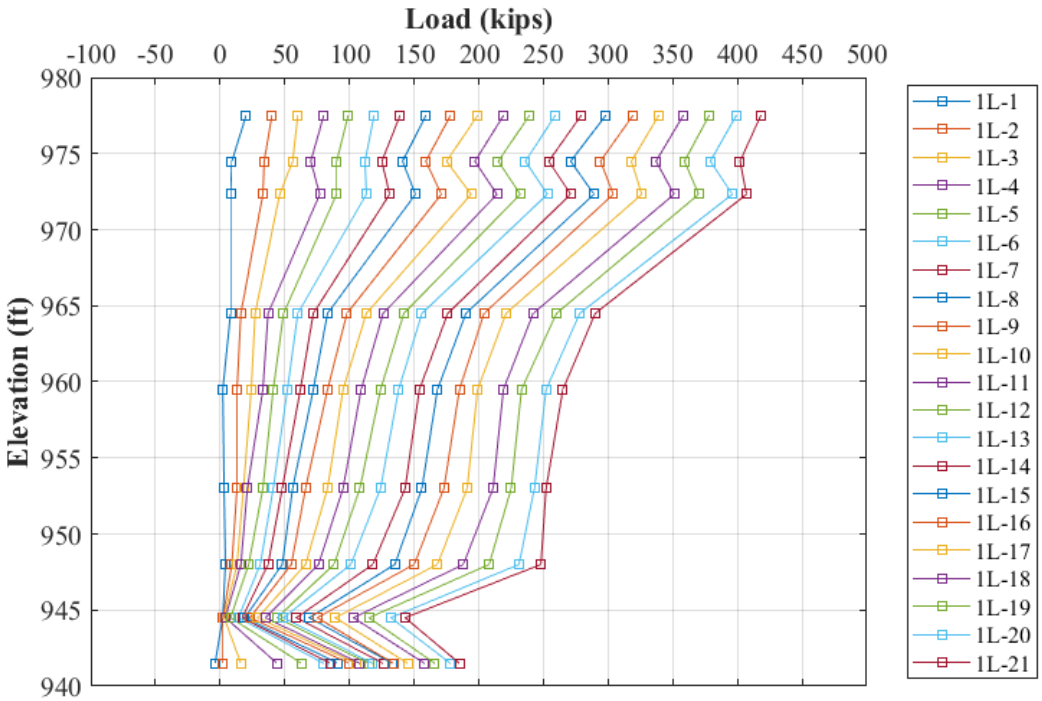

Figure 4.21: DS24 8-minute reading load distribution

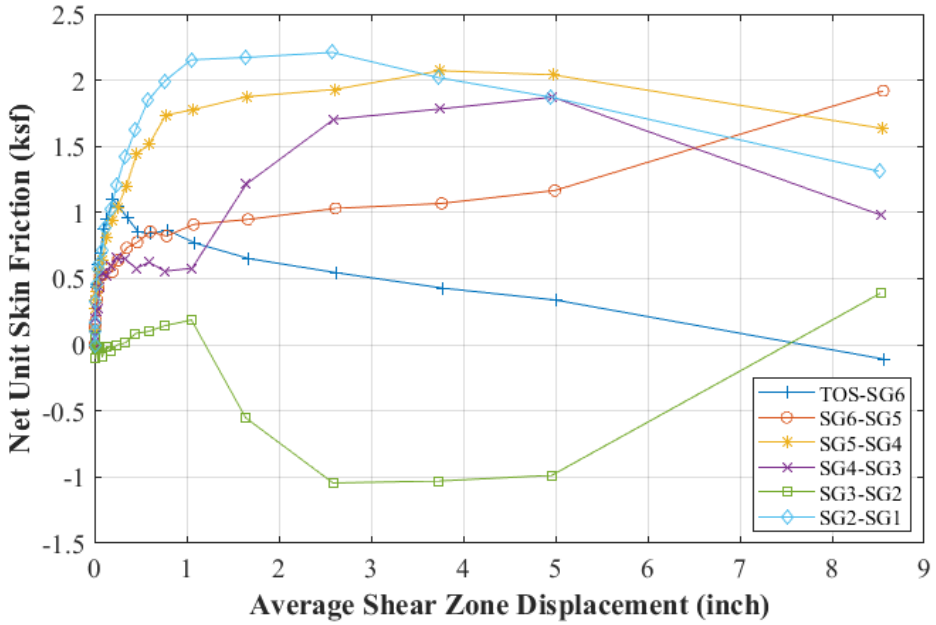

Figure 4.22: DS18 unit friction curves

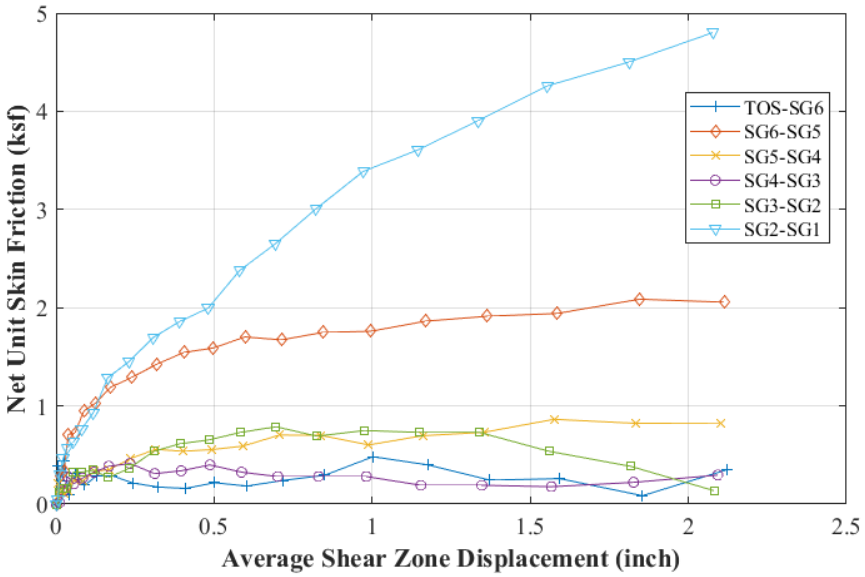

Figure 4.23: DS24 unit friction curves

4.5.4 Discussion of Tests Results

After establishing load transfer characteristics occurring in the different soil layers surrounding the small-scale shafts from strain gauge data, unit side shear-displacement curves were compared to those of the full-scale shaft so that any similarities and differences could become apparent. Comparisons are shown in Figure 4.24 for the top lean clay layer, Figure 4.25 for the fat clay layer, Figure 4.26 for lower lean clay layer, and Figure 4.27 for the sand layer. Due to the unreliable nature of the readings obtained from DS18 strain gauge level 3, the magnitude of load transferred in the lean clay layer above and sand layer below level 3 could not be determined. Thus, the lean clay and sand layers located between level 4 and level 2 were excluded from the comparison. In the uppermost lean clay layer, DS18 unit skin friction appears to be higher than that of the full scale shaft. Moreover, DS18 appears to have a stiffer response at low shaft displacements, reaching its maximum skin friction at a lower displacement compared to the full scale shaft. Comparison with DS24 unit side shear curve is rather difficult due to the unusual characteristic of the curve shape, which may be attributed to noise in the strain readings. Nevertheless, DS24 appears to have the lowest skin friction in that soil layer. In the fat clay layer, both DS18 and DS24 have higher unit skin friction compared to the full scale shaft with DS24 unit skin friction being the highest.

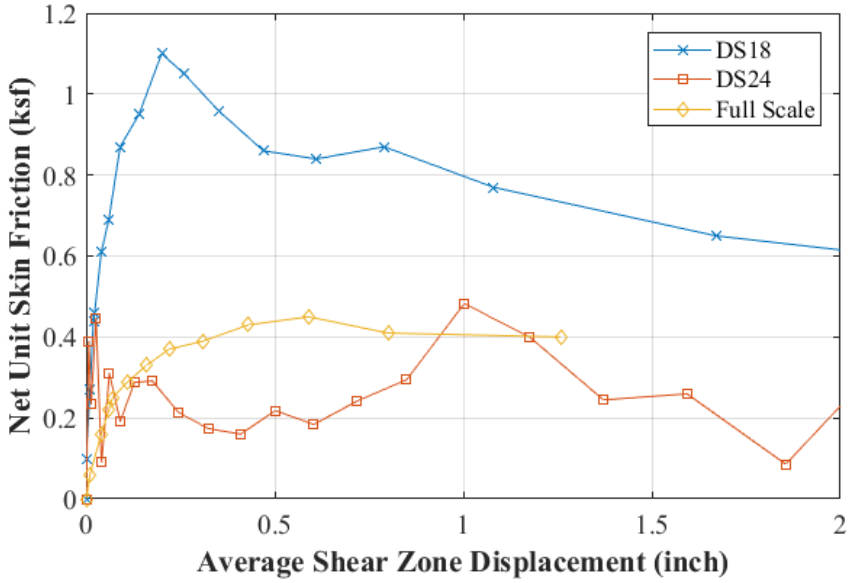

Figure 4.24: Unit side shear comparison in uppermost lean clay layer

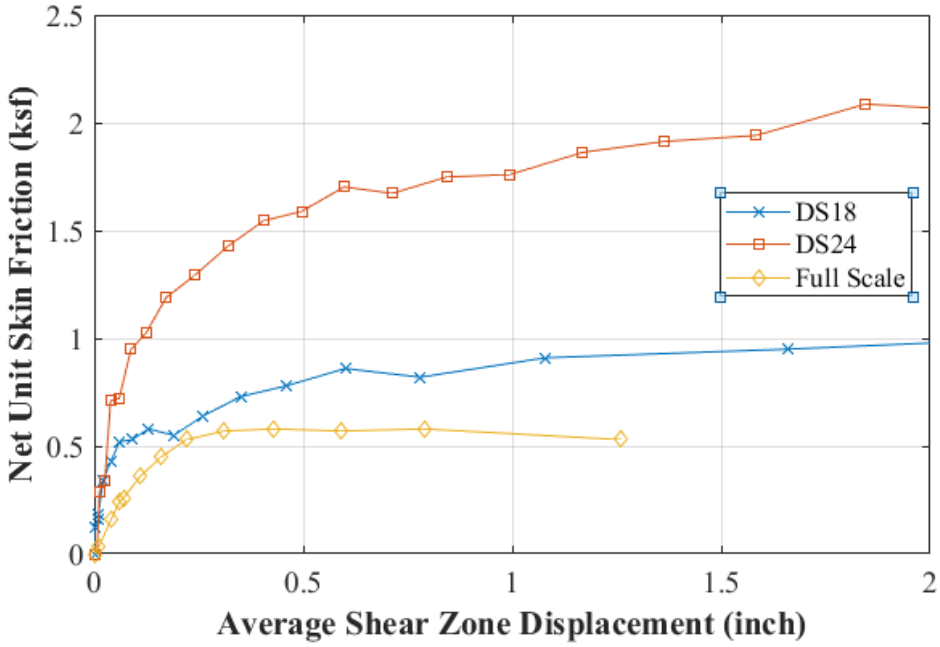

Figure 4.25: Unit side shear comparison in fat clay layer

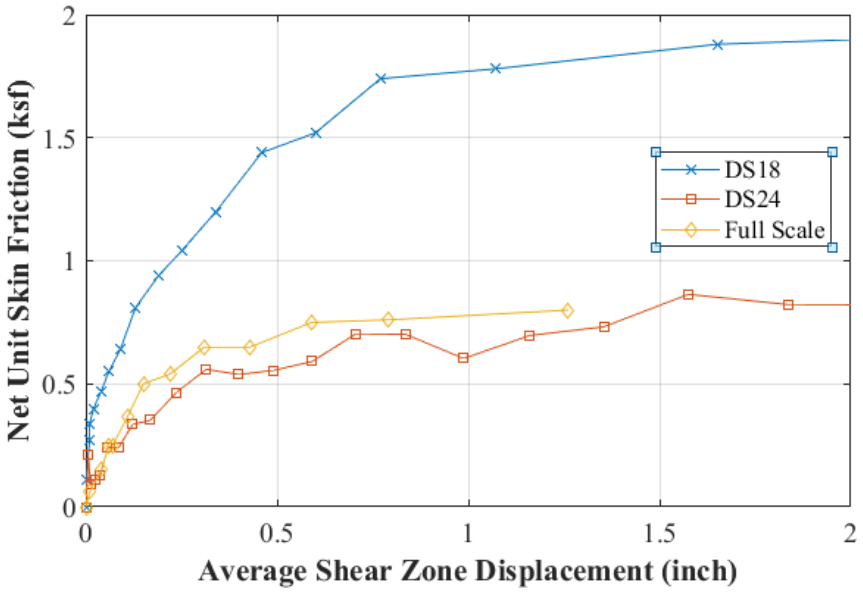

Figure 4.26: Unit side shear comparison in lowermost lean clay layer

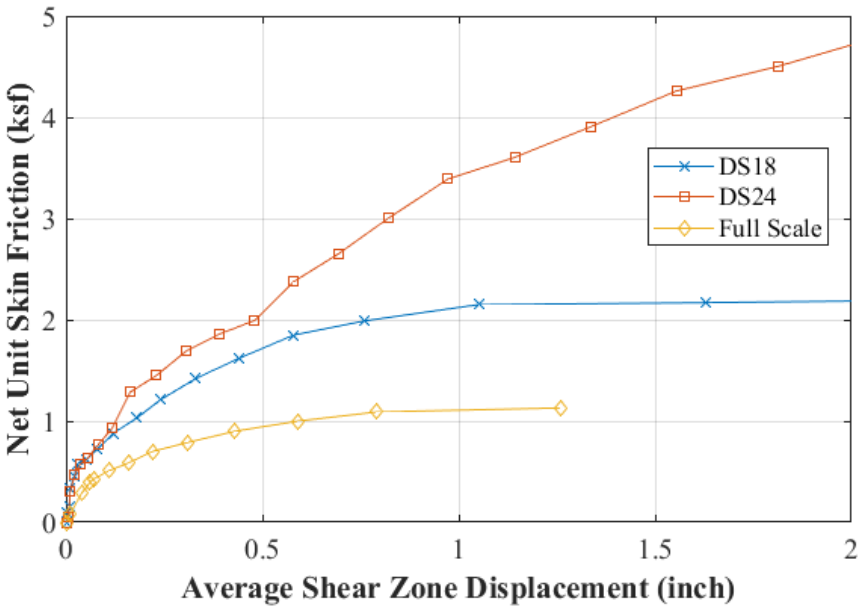

Figure 4.27: Unit side shear comparison in sand layer

Both DS18 and DS24 have a stiffer response at low displacements but reach their peak strength at higher displacements compared to the full scale shaft. In the lower lean clay layer, DS18 unit skin friction is the highest while DS24 side shear-displacement curve lies slightly

below that of the full-scale shaft. In the sand layer, both DS18 and DS24 have higher unit skin friction compared to the full scale shaft with DS24 being the highest. Both small-scale shafts, as observed in other layers, have a stiffer response at low displacements and reach their peak at higher displacements compared to the full scale shaft. DS24 in this case does not appear to have reached its peak at the maximum achieved displacement.

Based on the available data, plots of unit skin friction at 1 in. shaft movement with respect to shaft diameter were developed for all four soil layers. The shaft movement of 1 in. was selected to ensure that shaft resistance was almost or fully mobilized and to provide a common basis for comparison. As can be seen from the fitted trend lines in Figure 4.28 and Figure 4.29, the unit skin friction seems to decrease as the shaft diameter increases. The coefficient of determination, R^2, varies between 0.24 and 0.57. Plots of the unit skin friction ratio at 1 inch shaft movement as a function of the ratio of the diameters were developed and are shown in Figure 4.30 and Figure 4.31. In both lean clay layers the fitted trend line does not show a strong correlation between the skin friction and the diameter as evidenced by the low R2 value. In the fat clay and sand layers, the high R^2 values indicate a good correlation between the diameter and the skin friction. The trend lines in the fat clay and sand layer have a positive slope while those in the lean clay layers have a negative slope.

The close proximity of DS18 and DS24 may have played a significant role in the scatter observed in the data. To ensure that the soil conditions were similar for both reduced-scale shafts and to allow the same reaction system to be used for both tests, the reduced-scale shafts were designed and constructed with a clear spacing of approximately five feet, which violates ASTM D1143 minimum clear distance requirements. Moreover, the use of a temporary steel casing during construction resulted in a larger cross section in the upper ten feet of both shafts creating an end bearing condition at the zone of diameter change. The unanticipated end bearing condition may have affected the skin friction within the zone of influence beneath the upper ten foot section. Finally, it is hypothesized that the state of stresses around DS24 may have been altered following the load test on DS18. Since the initial conditions between the two shafts were not similar, a scatter in the data should be expected.

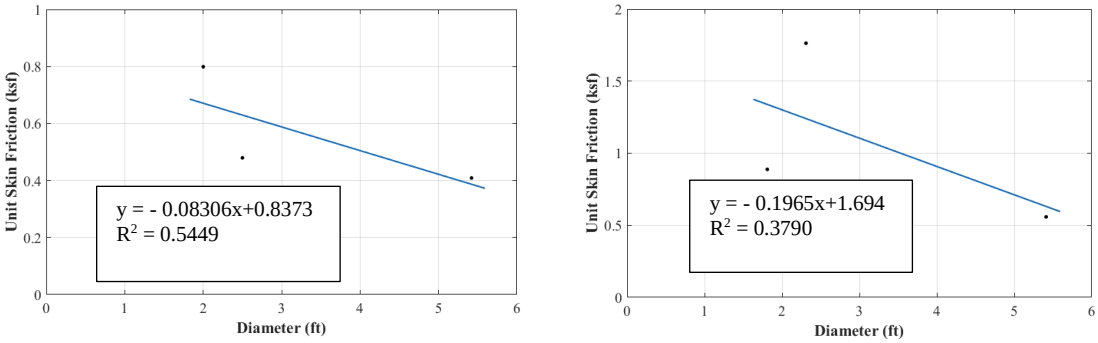

(a) **(b)**

Figure 4.28: Upper lean clay layer skin friction vs. diameter (a); fat clay layer skin friction vs. diameter (b)

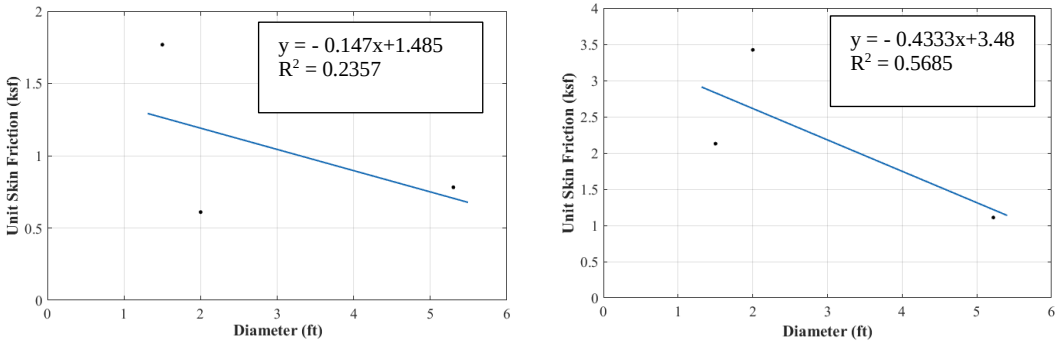

(a) **(b)**

Figure 4.29: Lower lean clay layer skin friction vs. diameter (a); sand layer skin friction vs. diameter (b)

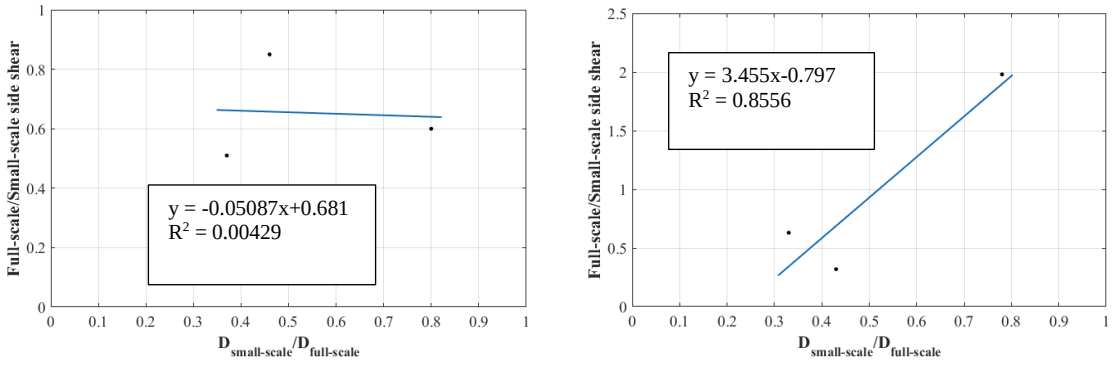

(a) **(b)**

Figure 4.30: Scaling relations for (a) upper lean clay layer and (b) fat clay layer

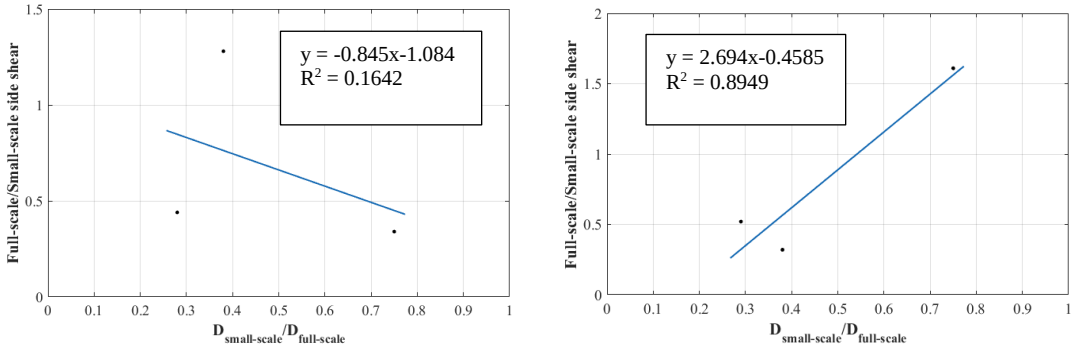

(a) **(b)**

Figure 4.31: Scaling relations for (a) lower lean clay layer and (b) sand layer

4.6 Field Investigation at Spangler

Additional field load testing that overcome the shortcomings of the previous study was considered at the Spangler test site on the Iowa State University campus to further investigate scale effect on drilled shaft unit skin friction. The testing plan included three drilled shafts with diameters of 1.5 ft, 1.75 ft, and 2 ft. Adequate clear spacing between the shafts was provided to minimize any potential interaction. To exclude the end bearing component from consideration, the tests were designed for uplift loading condition resulting from compressive loads applied at the shaft tip.

4.6.1 Test Site Subsurface Condition

Subsurface investigation at the site included two conventional borings and three Cone Penetrometer Test (CPT) soundings. The boring logs revealed a soil profile primarily composed of clay with occasional gravels and a 5 ft sand layer at 33.5 ft below ground surface in one of the borings. SPT blow count numbers and undrained shear strength variation with depth at the borings location are shown in Figure 4.32 and Figure 4.33. At both locations, the blow count numbers showed an increasing trend with depth. The undrained shear strength, estimated as half of the pocket penetrometer unconfined compressive strength, ranged between 3.25 ksf and 4.5 ksf. At end of drilling, the groundwater table was located at depths of 57.5 ft and 10.5 ft in boring hole 1 (BH1) and boring hole 2 (BH2), respectively. The CPT soundings showed interbedded layers of clay, clay and silty clay, silty sand and sandy silt, and sand. Undrained shear strength variation

with depth obtained from the CPT soundings are shown in Figure 4.34. The groundwater table was located at depths of 17 ft, 12 ft, and 7.5 ft for CPT-1, CPT-2, and CPT-3c, respectively.

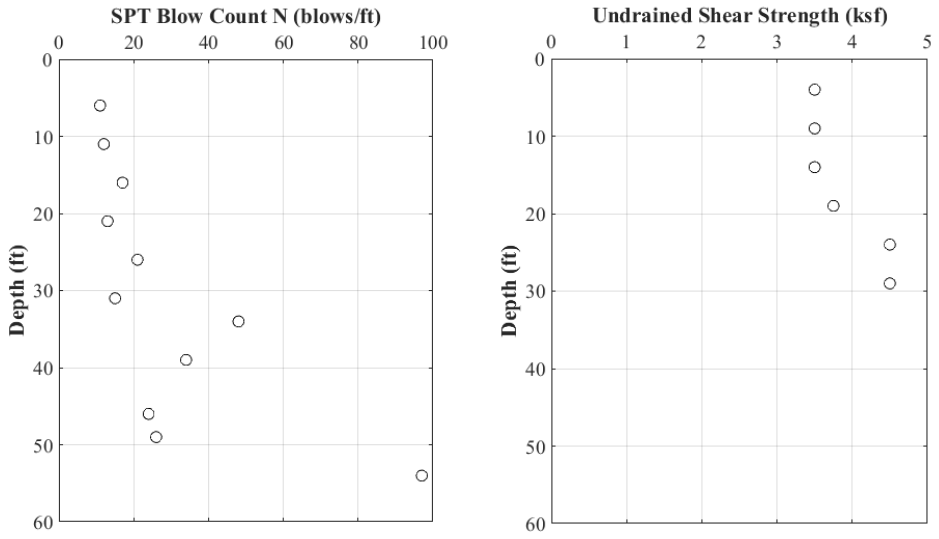

Figure 4.32: SPT blow count and undrained shear strength variation at BH1

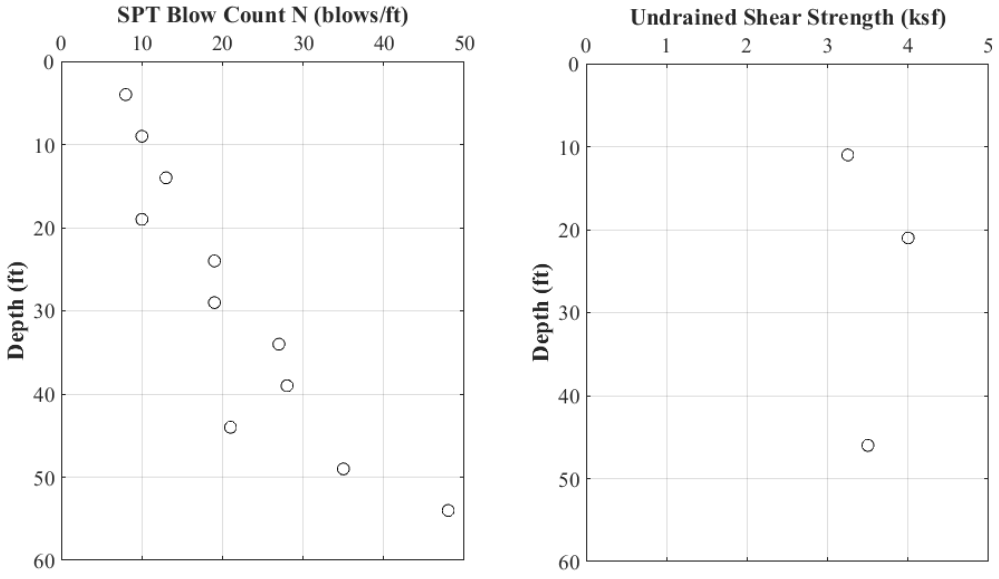

Figure 4.33: SPT blow count and undrained shear strength variation at BH2

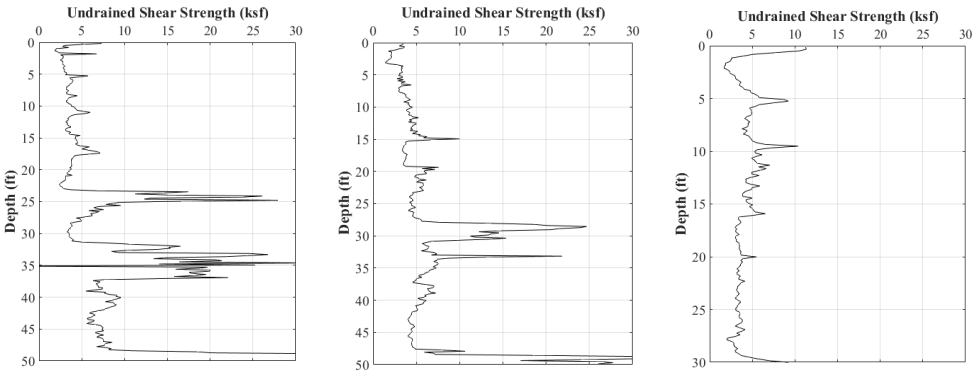

Figure 4.34: CPT soundings peak undrained shear strength

4.6.2 Capacity Prediction and Instrumentation Plan

Based on the available soil properties from the subsurface investigation, the length of the three shafts were limited to 17 ft below ground surface to ensure complete geotechnical failure. A summary of the estimated side shear using the α-method is shown in Table 4.2.

Table 4.2: Spangler test shafts capacity

Shaft Diameter (ft)	Side Shear Capacity (kips)
1.5	159
1.75	186
2	212

The instrumentation plan included eight levels of strain gauges to capture unit skin friction at different depths. The shafts reinforcing cages were instrumented following the same procedure used for the test shafts in Pottawattamie County. Above ground, the shafts were instrumented with four string potentiometers and two magnetic mounted DCDTs for shaft top displacement and compression measurements. Applied loads were monitored using a 200 kip load cell for each of the two hollow core hydraulic jacks used in the tests.

4.6.3 Construction and Testing

All shafts were excavated to the desired elevation using the dry method. Upon completing excavation, the reinforcing cages were lifted and placed into the holes, and concrete was placed from the ground surface using the free-fall method. Since construction of the test shafts was completed shortly before the start of winter season, testing was not

initiated until the following summer when weather conditions became favorable. All tests were completed using the reaction system setup shown in Figure 4.35. While monitoring all strain gauge signals prior to the beginning of the test, several strain gauges appeared to be out of range and were discarded. Furthermore, readings from several of the remaining gauges seemed unreasonable, and they appeared to drift over time. Various grounding strategies were attempted to resolve the unexplained drifting issue without success. It was then decided to proceed with the tests and rely on the data from the above ground instrumentation.

All shafts were loaded following ASTM D1143 similar to the load tests in Pottawattamie County. Using 15 kips load increments, the 2 ft diameter shaft was loaded to 120 kips with a corresponding average top displacement of 0.90 in. Further load increments could not be sustained since the shaft had reached its ultimate capacity. The 1.75 ft diameter shaft was subjected to a maximum load of 85 kips using 5 kips load increments. The corresponding average displacement at the top of the shaft was 0.91 in. The 1.5 ft diameter shaft was loaded to a maximum of 135 kips using 5 kips load increments. At this point the average shaft top movement was 1.54 in. The shafts load-displacement curves are presented in Figure 4.36. With respect to the measured side shear capacities, the predicted resistances presented in Table 4.1 were off by 17.78%, 118.82%, and, 76.67% for the 1.5 ft diameter shaft, 1.75 ft diameter shaft, and 2 ft diameter shaft, respectively.

4.6.4 Discussion of Tests Results

Load distribution with respect to depth could not be reliably determined due to the unreasonable nature of the strain gauge readings. The net side shear, calculated as the total applied load minus the buoyant shaft weight over the shaft side surface area, is plotted with respect to displacement for all shafts in Figure 4.37. The stiffest response and highest unit skin friction were observed in the 1.5 ft diameter shaft while the lowest stiffness and unit skin friction were observed in the 1.75 ft diameter shaft. Unit skin friction as a function of shaft diameter is shown in Figure 4.38. As observed, the unit skin friction seems to decrease with increasing shaft diameter. Since unit skin friction values at the previously used 1 in. shaft movement could not be obtained for all shafts, the common displacement of 0.90 in. was chosen.

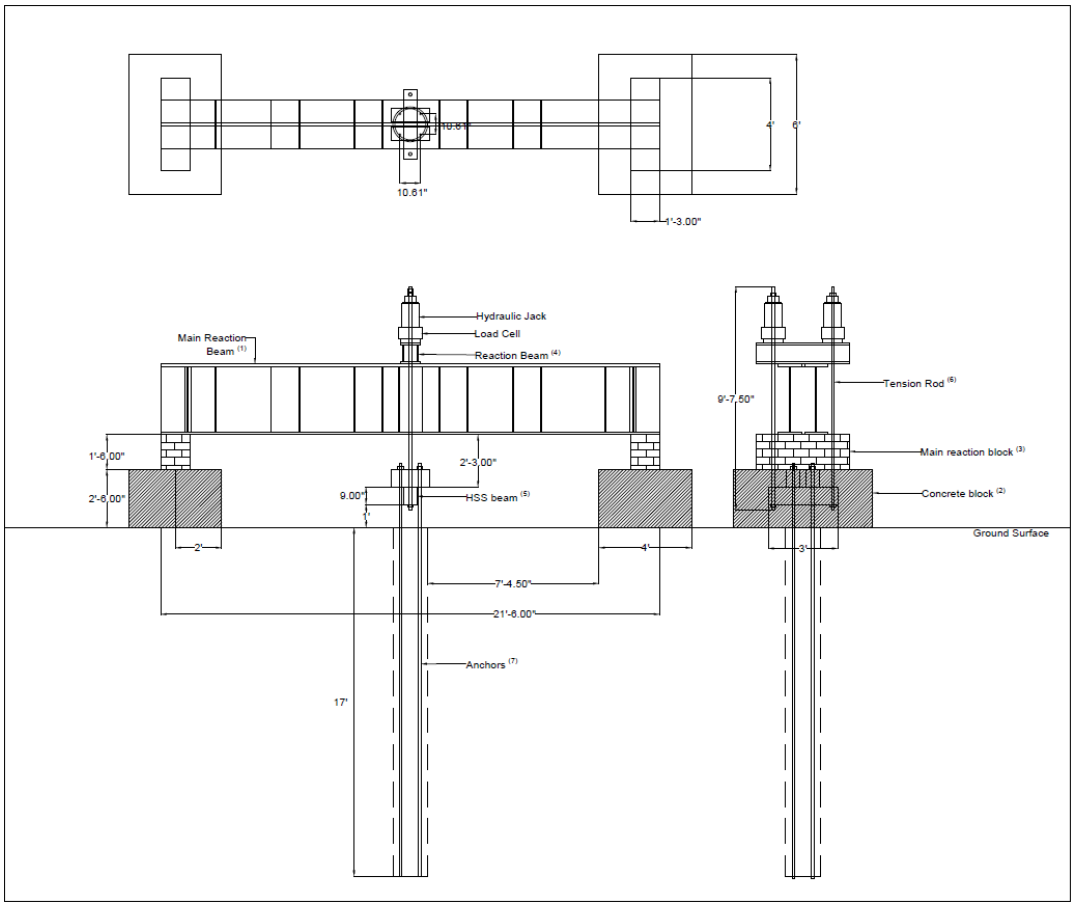

Figure 4.35: Spangler tests reaction frame details

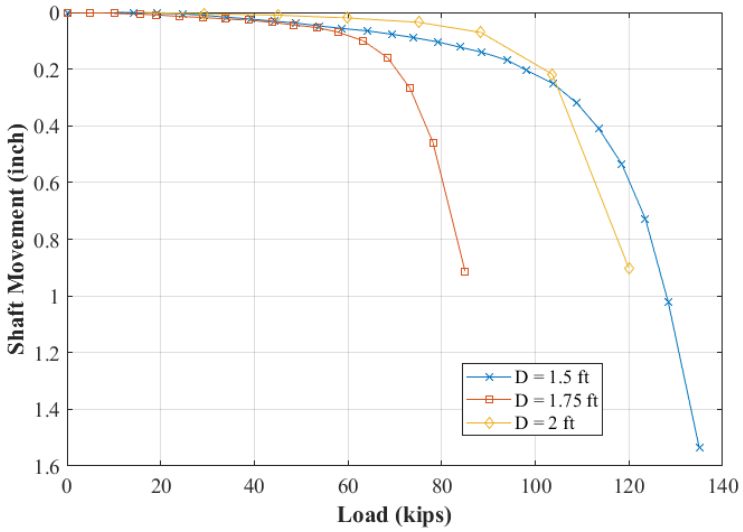

Figure 4.36: Spangler test shafts load-displacement curves

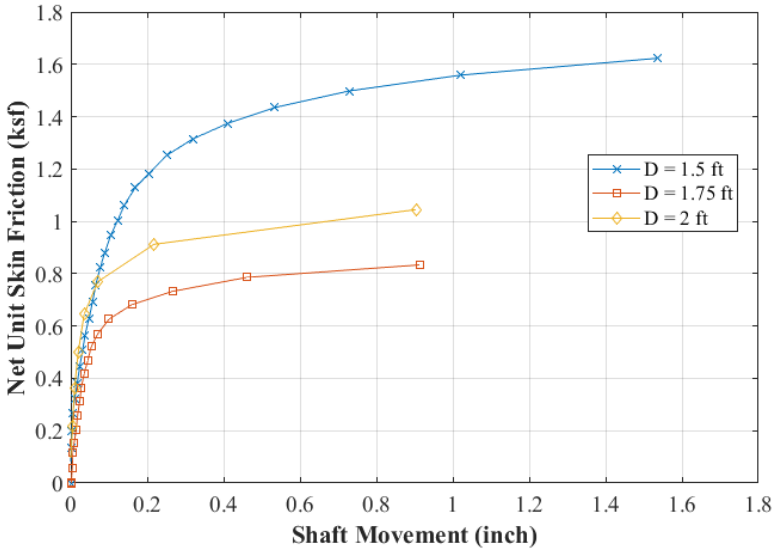

Figure 4.37: Spangler test shafts net unit skin friction curves

Scaling factors developed from the test data and shown in Figure 4.39 do not seem to correlate well with the diameter as evidenced by the low R^2 value of 0.0985. The scatter could have been caused by the difference in weather conditions preceding the tests. The first two tests i.e. 2 ft and 1.75 ft diameter shaft, were performed early in the summer during a time when rainy days were frequent while the third test was performed in dryer weather conditions. This difference in soil moisture content and groundwater table could have led to differences in soil strength.

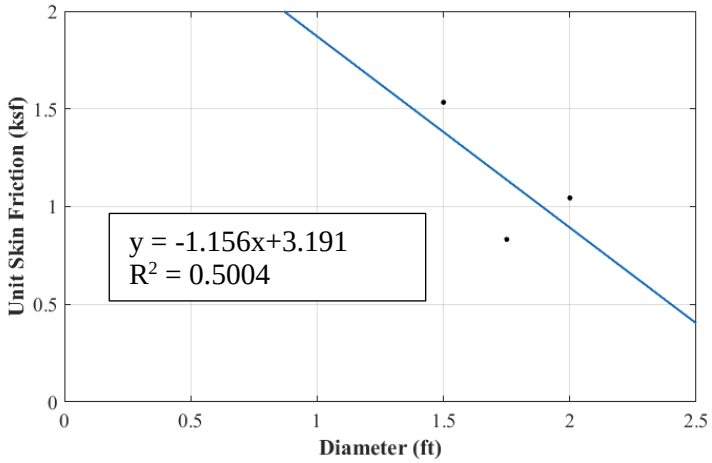

Figure 4.38: Spangler unit skin friction vs. diameter

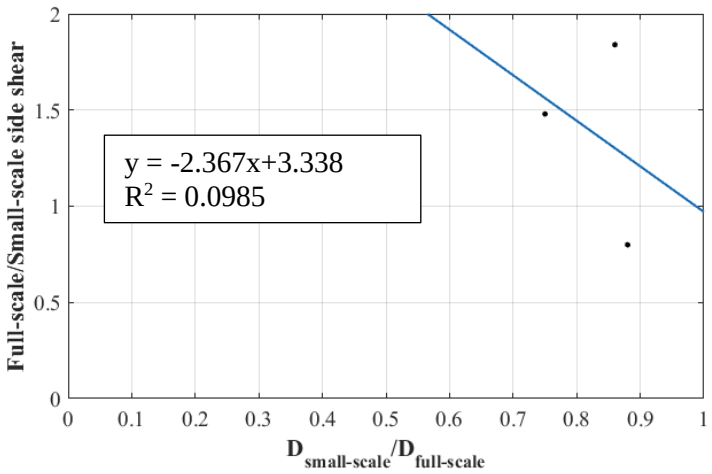

Figure 4.39: Scaling relation from Spangler tests

The assumption of similar soil conditions around the shafts may not also be completely accurate. Since subsurface investigation was not performed at each of the drilled shafts location, it is possible that the actual soil conditions could differ from the assumed condition and that the soil strength could be significantly different within a few distance from the locations where subsurface investigation was completed.

Since additional data was obtained from the Spangler tests for the cohesive soil category, a comparison including all previous data from the Pottawattamie county study in cohesive soil is presented in Figure 4.40. The measured resistance was selected at a common shaft movement of 0.90 in., and was normalized by the undrained shear strength. The shaft skin friction appears to decrease with increasing shaft diameter, and a power function fit to the data results in a high coefficient of determination of 0.81. However, since the field investigation only included four different diameter size, data on skin friction variation is not available for diameter size ranging between 2.5 ft and 5.5 ft. Therefore it is difficult to evaluate the accuracy of the fit within that range.

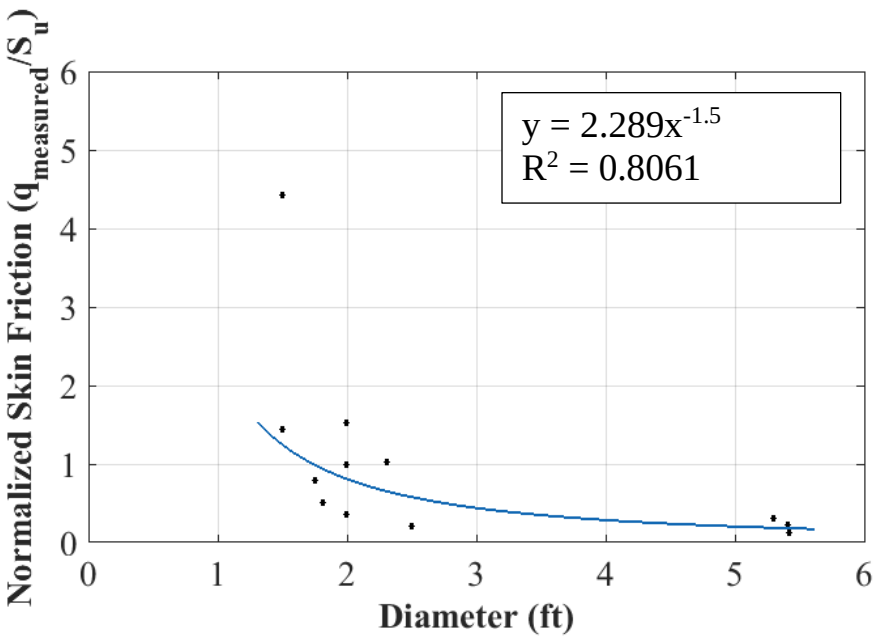

Figure 4.40: Normalized resistance variation with respect to diameter for all small scale tests and full-scale O-cell test in cohesive soil

4.6 Conclusions and Recommendations

The overall goal of this study was to evaluate the feasibility of a cost-effective drilled shaft load testing approach that uses reduced-scale drilled shafts. Following a review of current understanding of the influence of shaft diameter on skin resistance, a series of load tests on reduced-scale drilled shafts of various diameters was conducted at two sites in order to capture scale effects and to develop appropriate scaling relations that would enable the resistance prediction of larger diameter drilled shafts. The major conclusions of the study can be summarized as follows:

- Test data in cohesive soil seem to show decreasing skin friction in increasing shaft diameter. A power function fit to the data shows a strong correlation with a coefficient of determination of 0.81. Additional data including diameter size between 2.5 ft and 5.5 ft is needed to assess and confirm accuracy of the fit.

- Due to the unreliable readings from some of the strain gauges, test data in cohesionless soil is limited to three data points only. A linear fit to the available data shows decreasing skin friction with increasing shaft diameter with a coefficient of determination of 0.57. However, considering the scatter and the limited data, this fit may not be appropriate.
- Additional data is needed to further investigate the correlation between skin friction and shaft diameter and confirm the findings of this study so that accurate scaling relations can be developed. Additional testing should ensure that test specimens are constructed with adequate clear space to prevent interaction and change in initial soil conditions. The tests should also be conducted within a small timeframe so that weather conditions do not lead to differences in initial conditions and scatter in the test data.

4.7 References

Alawneh, A.S., A.I.H. Malkawi, and H. Al-Deeky. 1999. Tension tests on smooth and rough model piles in dry sand. *Canadian geotechnical journal*, Vol. 36, No. 4, pp 746-753.

American Association of State Highway and Transportation Officials (AASHTO). 2009. *AASHTO LRFD Bridge Design Specification: Customary U.S. Units*, Fourth Edition with 2008 and 2009 Interim Revisions, Washington, D.C.

American Association of State Highway and Transportation Officials (AASHTO). 2010. *AASHTO LRFD Bridge Design Specifications*. Interim Revision. Fifth Edition, Washington, D.C.

Al-Mhaidib, A.I., and T.B. Edil. 1998. Model Tests for Uplift Resistance of Piles in Sand. *ASTM geotechnical testing journal*, Vol. 21, No. 3, pp 213-221.

American Society for Testing and Materials (ASTM)-D1143. 2007. Standard Test Methods for Deep Foundations Under Static Axial Compressive Load. PA.

American Society for Testing and Materials (ASTM)-D4945. 2008. Standard Test Methods for High-Strain Dynamic Testing of Deep Foundations. PA.

Balachowski, L. 2006. Scale Effect in Shaft Skin Friction from the Direct Shear Interface Tests. *Archives of Civil and Mechanical Engineering*, Vol. 6, No. 3, pp. 12–28.

Baycan, C. E. 1996. Field Performance of Expansive Anchors and Piles in Rock. PhD Dissertation, Monash University, Clayton, Victoria, Australia.

Bolton, M.D., and C. K. Lau. 1988. Scale effects arising from particle size. *Centrifuge 88*. Paris, pp 127-131.

Boulon, M. 1986. The Strength and Dilatancy of Sands. *Géotechnique,* Vol. 36, No. 1, pp. 65–78.

Boulon, M. and P. Foray. 1986. Physical and Numerical Simulation of Lateral Shaft Skin Friction along Offshore Piles in Sand. *Proceeding 3rd International Conference on Numerical Methods in Offshore Piling,* Nantes, pp. 127–147.

Bradshaw, A. S., B. Reyes, C. Devillers, and P. Sauco. 2016. A novel In Situ Test for the Design of Drilled Foundations. *DFI Journal – The Journal of the Deep Foundations Institute,* 10:1, 2-7, DOI: 10.1080/19375247.2016.1158383.

Brown, D. A., J. P. Turner, and R. J. Castelli. 2010. *Drilled Shafts: Construction Procedures and LRFD Design Methods.* NHI Course No. 132014, Geotechnical Engineering Circular No.10, National Highway Institute, U.S. Department of Transportation, Federal Highway Administration, Washington, D.C.

Desrues, J. 1991. An Introduction to strain localization in granular media. *Proc. Physics of Granular Media,* Winter School les Houches, Nova Sciences Publications, Hauppage, NY, pp. 127-142.

Fioravante, V. 2002. On the Shaft Friction Modelling of Non-displacement Piles in Sand. *Soils and Foundation,* Vol. 42, No. 2, pp 23–33.

Foray, P., L. Balachowski, and G. Rault. 1998. Scale Effect in Shaft Friction due to the Localisation of Deformations. *Proceedings of the International Conference Centrifuge 98,* Tokyo, Japan, September 23-25, pp. 211–216.

Frost, J. D., G. L. Hebeler, T. M. Evans and J. T. Dejong. 2004. Interface Behavior of Granular Soils. *Proceedings of Earth and Space 2004, ASCE International Conference on Engineering , Construction, and Operations in Challenging Environments,* Houston, pp. 65-72.

Garder, J., K. W. Ng, S. Sritharan, and M. Roling. 2012. *An Electronic Database for Drilled Shaft Foundation Testing (DSHAFT).* Final Report to Iowa Department of Transportation. Institute for Transportation, Iowa State University, Ames, IA.

Garnier. J. and D. König. 1998. Scale Effects in Piles and Nails Loading Tests in Sand. *Proceedings of the International Conference Centrifuge 98,* Tokyo, Japan, Vol. 1, pp. 205–210.

Hoteit, N. 1990. Contribution à l'étude de comportement d'interface sable-inclusion et application au frottement apparent. PhD dissertation, Institut National Polytechnique, Grenoble.

Lehane, B. M., C. Gaudin, and J. A. Schneider. 2005. Scale Effects on Tension Capacity for Rough Piles Buried in Dense Sands. *Géotechnique,* Vol. 55, N0. 10, pp. 709–719.

Lim, J. 2013. Time and scale effects on the shaft skin friction of displacement piles in sand. PhD dissertation. The University of Western Australia, Perth, Australia.

Lizzi, F. 1980. An experimental Approach to the Design of Large Diameter Floating Piles-the Similitude Method. *Ground Engineering,* Vol. 13, No. 2, pp. 17–19.

Lizzi, F. 1983. Ultimate Bearing Capacity of Friction Piles Calculated from Load Tests on Pilot Piles. *Ground Engineering,* Vol. 16, No. 5, pp. 41–45.

Lutenegger, J. A. and G. A. Miller. 1994. Uplift Capacity of Small Diameter Drilled Shafts from In Situ Tests. *Journal of Geotechnical Engineering,* Vol. 120, No. 8, pp. 1362–1380.

Marandi, S. M. and M. A. Karimzadeh. 2009. Analysis of the Effect of Pile Skin Resistance Versus Pile Diameter Based on Experimental Research. *American Journal of Applied Sciences,* Vol. 6, No. 1, pp. 114–123.

Meyerhof, G. G. 1983. Scale Effects of Ultimate Pile Capacity. *Journal of Geotechnical Engineering,* Vol. 109, No. 6, pp. 797–806.

Ng, W. K., S. Sritharan, and J. C. Ashlock. 2014. *Development of Preliminary Load and Resistance Factor Design of Drilled Shafts in Iowa*. Institute of Transportation, Ames, IA.

O'Neill, M. W. and L. C. Reese. 1999. Drilled Shafts: Construction Procedures and Design Methods. Publication No. FHWA-IF-99-025. Federal Highway Administration, Washington, D.C.

Osterberg, J. O. 1992. The Osterberg Load Cell for Testing Drilled Shafts and Driven Piles. Report to the Federal Highway Administration, Washington, D.C.

Osterberg, J. O. 1994. Recent Advances in Load Testing Driven Piles and Drilled Shafts Using the Osterberg Load Cell Method. Geotechnical Division, Illinois Section, ASCE, 79 pp.

Sinnreich, J. 2015. The scaling Effect of Bored Pile Radius on Unit Shear Capacity. *International Journal of Geotechnical Engineering,* Vol. 5, pp. 477–481.

Yu, H. S. and G. T. Houlsby. 1991. Finite cavity expansion in dilatant soils: loading analysis. *Géotechnique,* Vol. 41, No. 2, pp. 173–183.

Wernick, E. 1978. Skin Friction of Cylindrical Anchors in Non-Cohesive Soils. *Symposium on Soil Reinforcing and Stabilizing Techniques*, Sydney, pp. 201–219.

Yoshimi, Y and T. Kishida. 1981. Friction between Sand and Metal Surface, *10th ICSMFE*, Stockholm, pp. 831–834.

CHAPTER 5. DISPLACEMENT-BASED CAPACITY PREDICTION OF DRILLED SHAFTS USING THE FINITE ELEMENT METHOD

A paper to be submitted to the International Journal for Numerical and Analytical Methods in Geomechanics

Philippe Kalmogo, Sri Sritharan, Jeramy Ashlock

5.1 Abstract

The use of the finite element method to facilitate implementation of a displacement criteria into the design of axially-loaded drilled shafts is investigated in this study. Numerical modeling of the load-deformation response of three small-scale drilled shafts constructed and load tested in glacial till was conducted using the finite element program PLAXIS 2D. Soil parameters required for the implementation of the Mohr-Coulomb and Modified Cam-Clay constitutive models in the load test simulations were estimated from in-situ Cone Penetrometer Test (CPT) data and index properties from laboratory tests. Compared to measured load-deformation responses, simulation results indicate that the Mohr-Coulomb model can adequately predict drilled shaft field performance provided the correct soil parameters are used in the model. Poor predictions from the Modified Cam-Clay model indicate that the required parameters for the model should be directly measured from triaxial and isotropic consolidation tests rather than from empirical correlations as accomplished in this study.

5.2 Introduction

Prediction of drilled shaft field performance is subject to numerous uncertainties. In practice, the nominal overall geotechnical resistance of drilled shafts is commonly estimated using analytical methods that relate drilled shafts' known resistance to soil strength parameters. The required parameters can be directly measured or estimated from correlations to in-situ or laboratory soil specimen tests. Since these methods were developed from databases of load tests performed in a variety of locations with different geological conditions and using different strength criteria, accurate prediction of drilled shafts' performance at the local level is challenging considering the important effects of local geology and construction methods. Moreover, these methods are unable to provide the

magnitude of displacement corresponding to the estimated nominal resistance. Consequently, some design agencies conservatively chose to neglect the end bearing component of the drilled shaft's resistance since it requires higher displacements to be significantly mobilized compared to skin resistance. This practice, however, may be overly conservative in some cases. Shafts' deformations may be estimated using simple formulas or approximate closed-form solutions, but these methods do not cover layered soil profiles usually encountered in practice.

Field load testing on prototype shafts is relied upon to establish more reliable load-deformation characteristics and facilitate a displacement-based design. Test results can help minimize uncertainties associated with design methods, enable design optimization for the overall structure, and ensure that shafts' displacements under the anticipated loads are within acceptable limits. Due to the relatively high cost of performing such tests, only one or two load tests are generally conducted for a given project. Results are then used to design the entire foundation system of the project. This extrapolation of test shaft results to other production shafts, however, requires proper interpretation of load test results, appropriate subsurface characterization at the location of the production shafts, and adequate consideration of site variability, which are not often done correctly.

An alternate approach to displacement-based design of axially-loaded drilled shafts involving the use of the finite element method was investigated in this study. Accuracy of this approach to predict load-deformation response was examined using data from three small diameter drilled shaft load tests conducted as part of an investigation of shaft scale effect on skin resistance. The study focused on the development of axisymmetric models of the load tests using the soil-structure analysis program PLAXIS. Preliminary simulations of the load tests were conducted using the simple and easy to implement Mohr-Coulomb constitutive model. Then, the models were refined with the implementation of the more sophisticated Modified Cam Clay model, which is able to simulate strain hardening behavior of typical soils. All parameters needed for the implementation of both models were determined from empirical correlations using soil laboratory test and Cone Penetrometer Test (CPT) data.

Differences between predicted responses obtained from the models and actual shaft responses are discussed, and recommendations are provided to improve the accuracy of the models at simulating field performance.

5.3 Preliminary Analysis

Load tests were conducted at a site underlain by glacial till deposits. The subsurface was characterized using two conventional borings with Standard Penetration Testing and three CPT soundings including shear wave velocity measurements. Soil samples were also retrieved for relevant laboratory tests and appropriate classification of the geomaterial at the site. The test specimens included three drilled shafts with diameters of 1.5 ft (SP-18), 1.75 ft (SP-21), and 2 ft (SP-24) extending 17 ft below ground surface. Following construction using the dry method, the concrete was allowed sufficient time to gain strength, and the shafts were tested to geotechnical failure using ASTM D1143 recommended "Quick Test" procedure. The shafts were subjected to uplift compressive loading applied at the shaft tip so that end resistance could be avoided.

The 2D version of the finite element program PLAXIS was selected to attempt simulation of the completed load tests because it is relatively simple to use, includes several soil models, and is able to simulate soils' non-linear plastic behavior.
Preliminary modeling of the load tests was based on the Mohr-Coulomb model, and an undrained type was analysis was selected as the most appropriate to simulate load-deformation behavior the shafts in the glacial till. Three options are available in PLAXIS for undrained analyses using Mohr-Coulomb model including Undrained A, Undrained B, and Undrained C. While Undrained A and B enables effective stress analyses using effective strength parameters and total strength parameters, respectively, Undrained C is used for total stress analyses. Parameters necessary for implementation of the model are summarized in

Table 5.1 for all available types of analyses. Since undrained A analysis can over-predict the actual undrained shear strength, Undrained B with direct input of the glacial till undrained shear strength was selected for the preliminary model.

Table 5.1: Mohr-Coulomb model parameters

Undrained A	Undrained B	Undrained C
• Modulus, E'_{50} • Poisson's ratio, ν' • Cohesion, c' • Friction angle, φ' • Dilatancy angle, ψ'	• Modulus, E'_{50} • Poisson's ratio, ν' • Undrained shear strength, S_u	• Modulus, E'_u • Poisson's ratio, ν'_u • Undrained shear strength, S_u

The soil's modulus E_{50} was calculated as a function of depth from shear wave velocity measurements using Eq. (5.1).

$$E_{50} = 2G_{max}\left(\frac{G_{50}}{G_{max}}\right)(1+\nu) = 2\rho_T V_s^2\left(\frac{G_{50}}{G_{max}}\right)(1+\nu) \quad (5.1)$$

where,

E_{50} = Modulus at 50% strength level

G_{max} = Small strain shear modulus

G_{50} = Shear modulus at 50% strength level

ν = Poisson's ratio, 0.5 for undrained conditions

ρ_T = Total soil mass density

V_s = shear wave velocity

The reduction factor G_{50}/G_{max} was estimated as 0.2 from modulus reduction curves proposed by Fahey and Carter (1993). Shear strength values used for the analyses included peak and remolded state values. Remolded strength values were obtained from direct measurements of the cone sleeve friction, and peak strength values were estimated using Eq. (5.2) and an average cone factor of 14.

$$S_u = \frac{q_t - \sigma'_{v0}}{N_{kt}} \quad (5.2)$$

where,

S_u = Peak undrained shear strength

σ'_{v0} = Effective overburden stress

N_{kt} = Cone factor ranging from 10 and 20

Since direct laboratory measurements of the soil's unit weight as a function of depth were not available, an average value of 125 lb/ft^3 was assumed. The ground water table was conservatively assumed to be at 7.5 ft below ground surface for all shafts based on the CPT soundings.

PLAXIS provides the option to include interface elements to better model interaction between shaft and soil. The interface strength represented by the parameter R_{inter} can be assigned any values between 0 and 1 corresponding to flexible and rigid interfaces, respectively. A value of 1 indicates that the interface and the adjacent soil have the same strength whereas values smaller than 1 indicates a weaker interface. Brinkgreeve and Shen (2011) suggested that R_{inter} ranges between 0.7 and 1.0 for concrete-clay interaction, thus an average value of 0.85 was chosen for the analyses. A value of 0.01 was assigned to the soil layer at the shaft tip to prevent unrealistic tensile stresses from developing in the simulation. Summaries of the estimated soil layering and properties are presented in Table 5.2 through Table 5.4 for all CPT soundings.

Table 5.2: CPT Sounding 1

Layers	Thickness (ft)	γ (lb/ft^3)	Peak S_u (ksf)	Remolded S_u (ksf)	E'_{50} (ksf)	ν'	R_{inter}
Clay	0-4	125	2.5	1	629	0.40	0.85
Clay	4-10	125	3.3	1	1203	0.40	0.85
Clay	10-16	125	3.5	1	1657	0.40	0.85
Clay	16-17	125	4	2	1735	0.40	0.85
Clay	17-20	125	4	2	2180	0.40	0.01
Clay	20-24	125	4	2	2206	0.40	0.85
Clay	24-28	125	10	5.5	2750	0.40	0.85
Clay	28-32	125	3.5	3	4025	0.40	0.85

Table 5.3: CPT Sounding 2

Layers	Thickness (ft)	γ (lb/ft^3)	Peak S_u (ksf)	Remolded S_u (ksf)	E'$_{50}$ (ksf)	ν'	R_{inter}
Clay	0-4	125	2.75	2	300	0.40	0.85
Clay	4-10	125	3.8	1.5	719	0.40	0.85
Clay	10-16	125	4.5	1.7	1974	0.40	0.85
Clay	16-17	125	3.5	2.2	2539	0.40	0.85
Clay	17-20	125	4.3	2.2	2457	0.40	0.01
Clay	20-24	125	5.6	3.5	2407	0.40	0.85
Clay	24-28	125	4.5	1.5	3198	0.40	0.85
Clay	28-32	125	10	8.25	3096	0.40	0.85

Table 5.4: CPT Sounding 3

Layers	Thickness (ft)	γ (lb/ft^3)	Peak S_u (ksf)	Remolded S_u (ksf)	E'$_{50}$ (ksf)	ν'	R_{inter}
Clay	0-4	125	2	2	651	0.40	0.85
Clay	4-10	125	4.5	3.5	1136	0.40	0.85
Clay	10-16	125	5.5	2.25	1734	0.40	0.85
Clay	16-17	125	3.5	1.4	1620	0.40	0.85
Clay	17-20	125	3.5	1.4	1590	0.40	0.01
Clay	20-24	125	3.5	1.4	1800	0.40	0.85
Clay	24-28	125	3.5	1.4	1829	0.40	0.85
Clay	28-32	125	3.5	1.4	1994	0.40	0.85

The shafts were modeled as a non-porous linear elastic material with unit weight of 150 lb/ft^3, Poisson's ratio of 0.2 and appropriate composite stiffness values shown in Table 5.5.

Table 5.5: Shafts' composite stiffness

Shaft Diameter (ft)	E (ksf)
1.5	656870
1.75	647002
2	642834

Of the two element types available, the 15-node triangular element was selected to discretize the models. Upon conducting a convergence study on the influence of mesh and

domain size on the model results, a domain radius of 25 ft and depth of 32 ft were selected for all models. As shown in Figure 5.1, the sides of the soil domain were allowed to move vertically, while the bottom was restricted against movements in both vertical and horizontal directions. Mesh size in PLAXIS is defined by a coarseness factor, whose value ranges between 0 and 1. A finer mesh i.e., coarseness factor=0.1 was used within a 10-ft radius of the shaft, while a higher value of 0.5 was used for the rest of the domain.

Each drilled shaft load test was simulated in three phases using a displacement-controlled type of loading. During the initial phase, initial stresses in the model were established using K_o values generated by the program based on the input soil properties and ground water table.

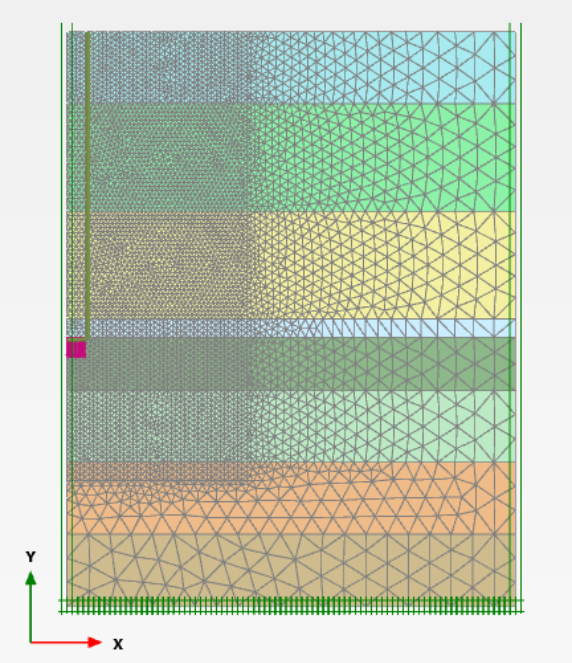

Figure 5.1: Plaxis model overview and mesh structure (SP-24)

Then, the shaft was wished in place by replacing the properties of the soil at the shaft's location with those of the shaft's material, and the interfaces between shaft and soil were activated. Finally, a prescribed upward displacement was applied at the shaft tip using small incremental steps. Since the CPT soundings were not performed at the exact shafts' locations, the simulations considered properties from individual soundings as well as average

values from the combination of two or all soundings. Predicted load-displacement responses obtained from the models are compared to the actual shafts' responses from the load tests in Figure 5.2 through Figure 5.7. Figure 5.2, Figure 5.4, and Figure 5.6 compare test results with simulated load-deformation responses using remolded shear strength for SP-18, SP-21, and SP 24, respectively. These figures indicate significant variability in the predicted shaft's response depending upon which CPT sounding is used to select the Mohr-Coulomb model parameters. For SP-18, models with CPT 2 and average of CPT 1 and 2 provided the best prediction of the shaft's load-deformation response. Using CPT 2 the model provided good agreement with the measured response up to a displacement value of 0.10 in. Between displacements of 0.10 in. and 0.50 in., the model slightly overestimated the shaft's capacity, and beyond 0.50 in. the model underestimated the shaft's resistance. Using average parameters from CPT 1 and 2, the simulated response was in good agreement with the measured response for displacement values smaller than 0.25 in. Beyond this value, the model under-predicted the measured shaft resistance. Assuming a strength criterion of 1 in. displacement, prediction errors of the actual shaft's capacity were 6% and 31% for CPT 1 and average of CPT 1 and 2, respectively.

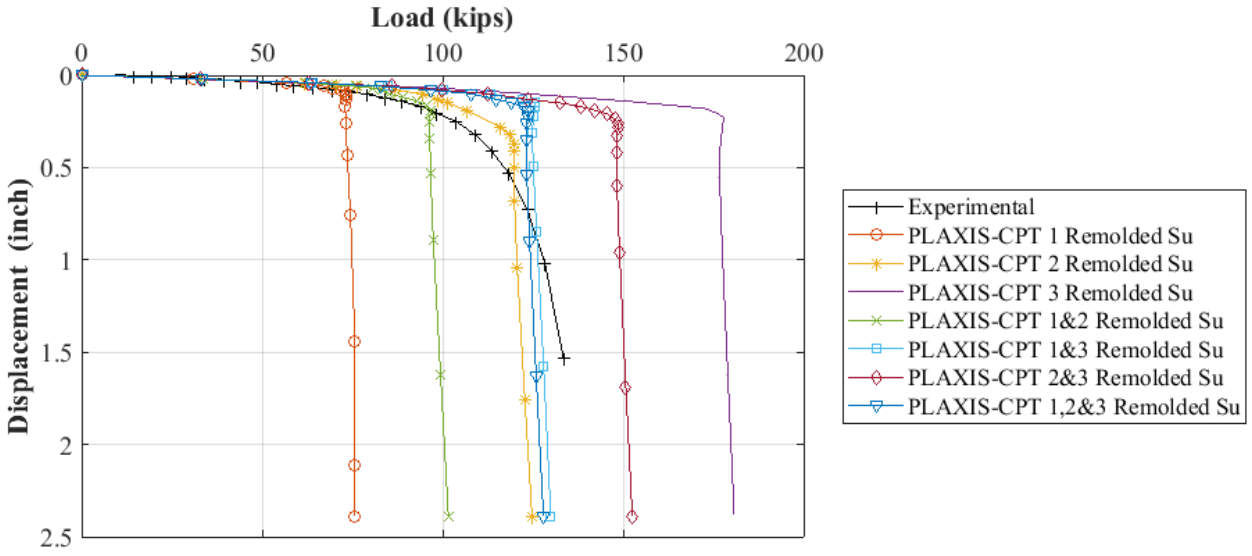

Figure 5.2: Measured vs. predicted load-displacement response for SP-18 shaft using remolded shear strength

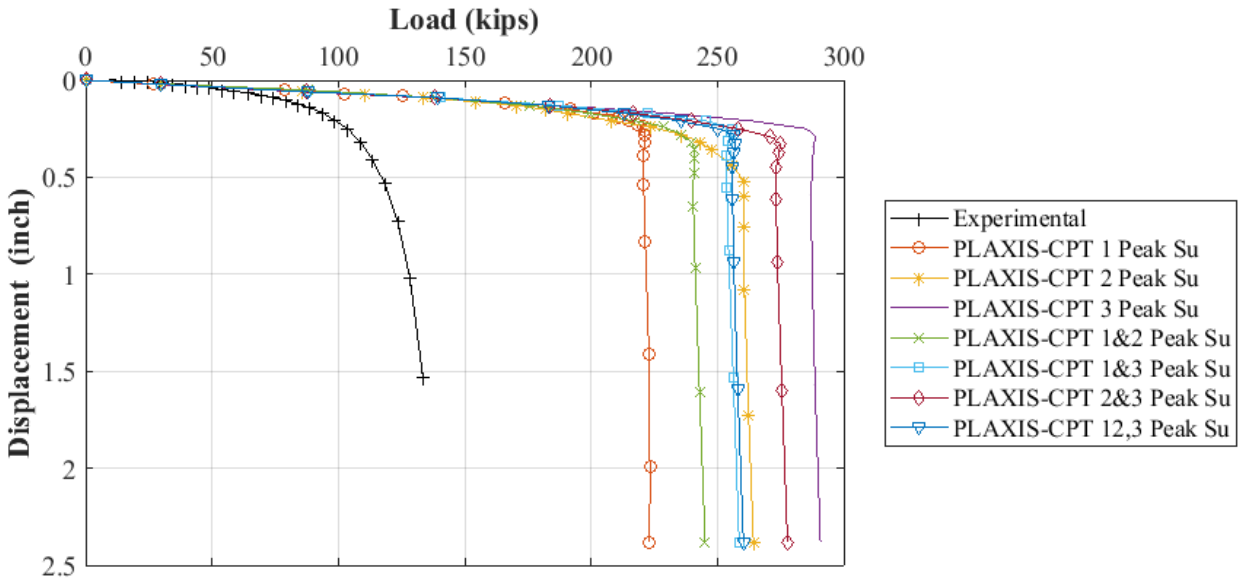

Figure 5.3: Measured vs. predicted load-displacement response for SP-18 shaft using peak shear strength

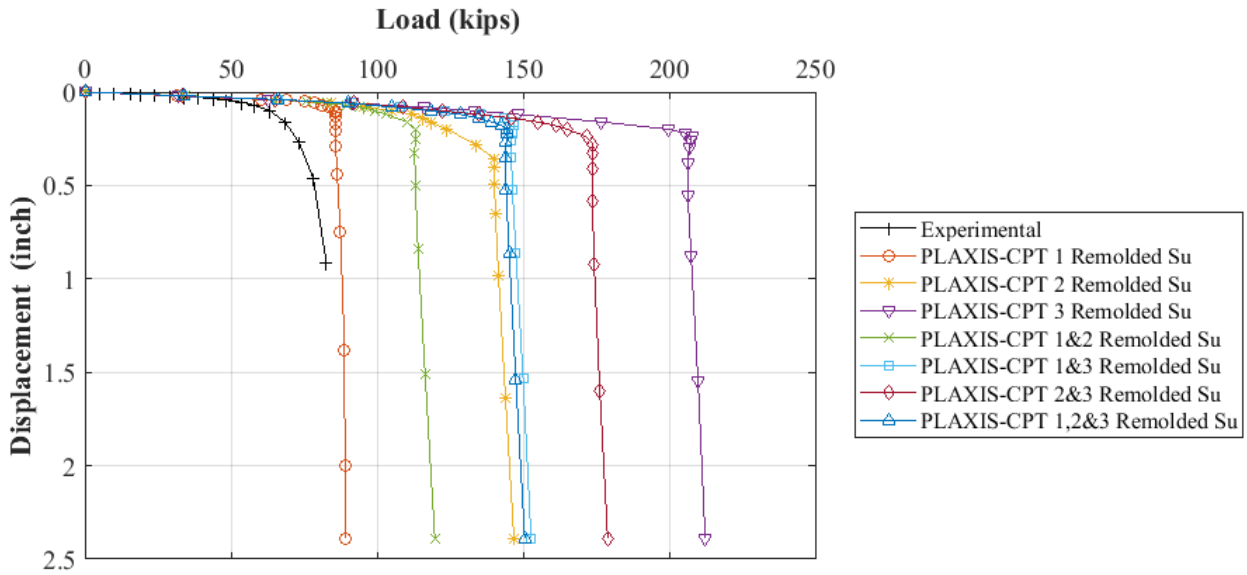

Figure 5.4: Measured vs. predicted load-displacement response for SP-21 shaft using remolded shear strength

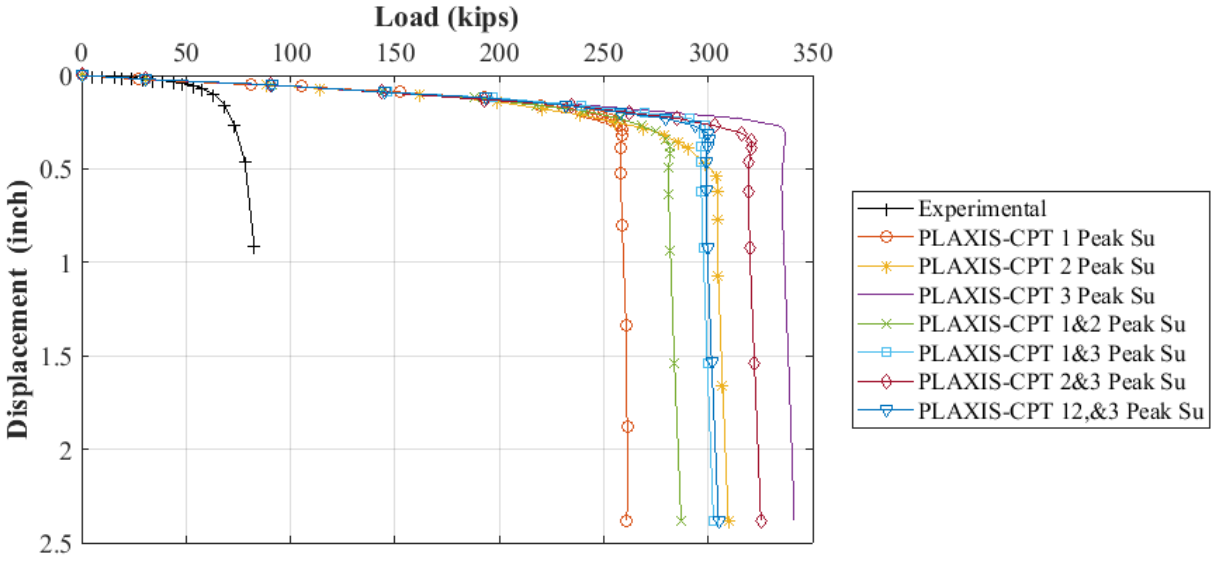

Figure 5.5: Measured vs. predicted load-displacement response for SP-21 shaft using peak shear strength

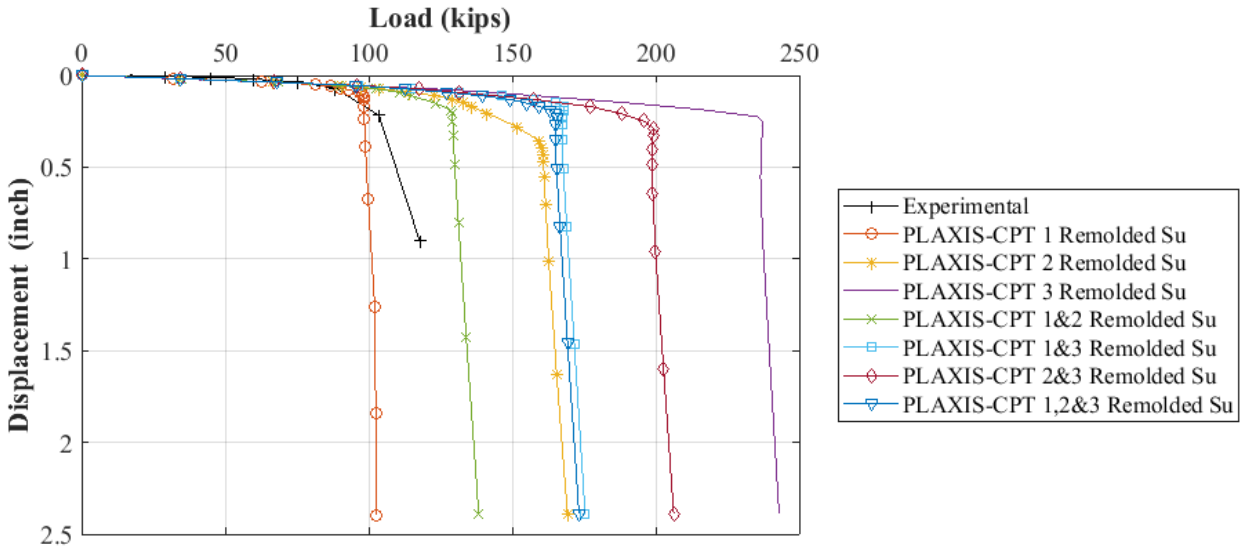

Figure 5.6: Measured vs. predicted load-displacement response for SP-24 shaft using remolded shear strength

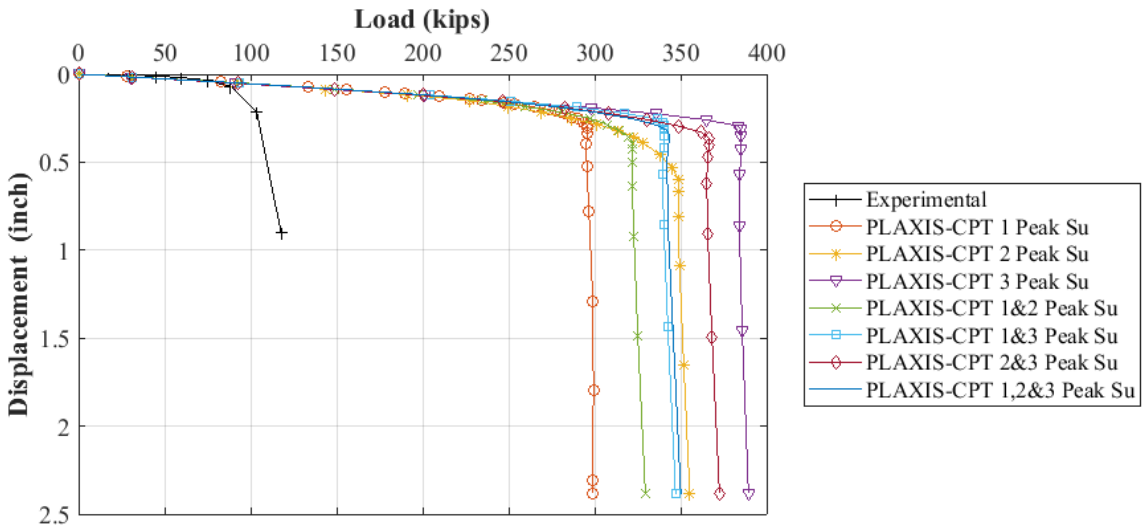

Figure 5.7: Measured vs. predicted load-displacement response for SP-24 shaft using peak shear strength

For SP-21, the closest match to the actual shaft's performance was obtained from CPT 1 data. However, the simulated load-displacement curve was stiffer than the measured response beyond a displacement value of 0.04 in. All other CPTs resulted in predicted responses that far exceeded the measured response. For a 1 in. displacement strength criterion, the model over-predicted the measured shaft's resistance by 7%.

For SP-24, CPT 1 data also provided the best estimate of the shaft's actual field capacity. Simulated and predicted responses were almost coincident up to a displacement value of 0.20 inch, beyond which the model underestimated the measured response. For a 1 in. displacement strength criterion, the model under-predicted the measured shaft's resistance by 18%.

Comparisons of measured load-deformation responses with simulated responses using peak shear strength are shown Figure 5.3, Figure 5.5, and Figure 5.7 for SP-18, SP-21, and SP 24, respectively. Similar to the predicted responses obtained using shear strength values at the remolded state, significant variability can be observed depending upon which CPT sounding is used to select model parameters. More importantly, these figures show that the peak shear strength significantly overestimates the actual shafts' field performance both in the elastic range and at ultimate.

Results from the finite element models indicate that the shafts' field capacity was closer to the remolded undrained shear strength rather than the peak strength of the glacial till. Model parameters determined from CPT 1 and CPT 2 provided the best predictions for all shafts. Although the models provided good predictions in early stages of loading, the bilinear elastoplastic Mohr-Coulomb model was unable to simulate the slight strain hardening behavior observed in the tests as loading progressed. This limitation of the model led to divergences between measured and predicted resistances at higher displacements.

5.4 Refined Modeling

To improve accuracy of the models at predicting the shafts' load-displacement responses observed in the field, the Modified Cam-Clay constitutive model was considered in the refined models. This cap plasticity type of soil model is based on Critical State theory, and it was developed based on the assumption of a logarithmic relationship between mean effective stress and void ratio of soil soft soil undergoing compression in isotropic stress conditions. In addition to its ability to model soil volume change more realistically, this type of model can also model softening and hardening behavior of soils.

Implementation of the undrained analysis using the Modified Cam-Clay model in PLAXIS requires five parameters including Poisson's ratio ν_{ur}, swelling index κ, compression index λ, tangent of the critical state line M, and initial void ratio e_{init}. As indicated by PLAXIS material models manual, the Poisson's ratio in this model is a real elastic parameter rather than a pseudo-elasticity constant as used in the Mohr-Coulomb model. A value of 0.20 was selected for the analyses based on the recommended range of 0.1 to 0.2. The compression and swelling index govern the soil's stiffness, and they can be determined from laboratory isotropic compression test on undisturbed soil samples. As shown in Figure 5.8, the compression index is the slope of the primary loading line and the swelling index that of the unloading line when the void ratio change is plotted as a function of the natural logarithm of the mean applied stress in an isotropic compression test. When compression index C_c and swelling index C_s from oedometer test are available, λ and κ can be calculated using Eq. (5.3) and (5.4).

$$\lambda = \frac{C_c}{2.3} \tag{5.3}$$

$$\kappa = \frac{2C_s}{2.3} \tag{5.4}$$

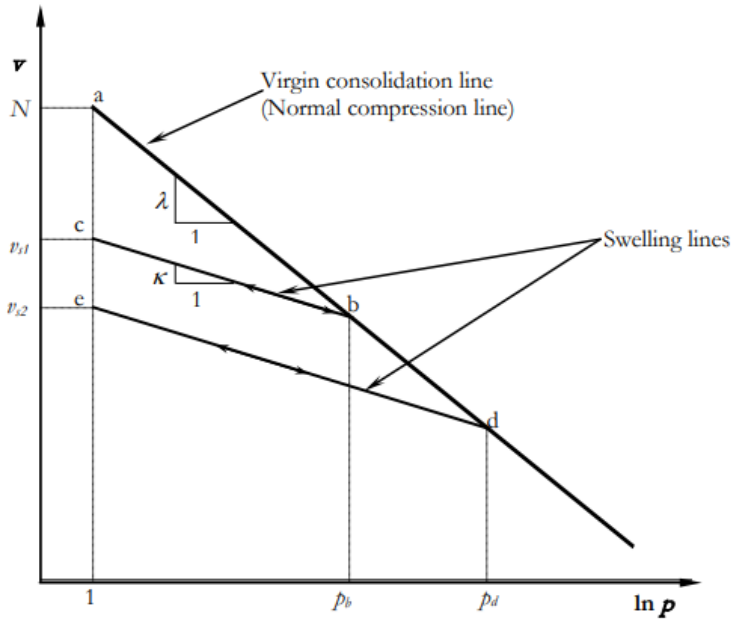

Figure 5.8: Definition of compression and swelling index parameters

Since data from either isotropic compression test or oedometer test were not available, λ and κ were estimated using C_c and C_s determined from the correlations proposed by Terzaghi and Peck (1967) (Eq. (5.5) and Nakase et al. (1988), respectively.

$$C_c = 0.009(LL - 10) \tag{5.5}$$

$$C_s = 0.00194(PI - 4.6) \tag{5.6}$$

where,

LL = Liquid Limit (%)

PI = Plasticity Index (%)

Based on the plastic and liquid limit data available, mean values of 0.07 and 0.02 were selected for λ and κ, respectively.

The tangent of critical state line parameter determines the soil shear strength. It is a function of the soil's friction angle, which should obtained from consolidated drained triaxial tests. For soil subjected to compression, M can be calculated using the friction angle φ as:

$$M = \frac{6 \sin \varphi}{3 - \sin \varphi} \tag{5.7}$$

In this study, the parameter M was calculated using CPT data and the friction angle correlation proposed by Kulhawy and Mayne (1990).

$$\varphi = 17.6° + 11.0° \log(q_{t1}) \tag{5.8}$$

where,

q_{t1} = $(q_t/\sigma_{atm})/(\sigma'_{v0}/\sigma_{atm})^{0.5}$

q_{t1} = Normalized cone tip resistance

q_t = Total cone tip resistance

σ_{atm} = Atmospheric pressure

σ'_{v0} = Overburden effective stress

The required initial void ratio parameter was estimated using correlation of moisture content to specific gravity as:

$$e_{init} = wG_s \tag{5.9}$$

where,

w = moisture content

G_s = Specific gravity

Based on the moisture content data and a specific gravity value of 2.8, a mean value of 0.40 was chosen for the model.

Interface strength in the Modified Cam-Clay model is defined in terms of the soil's cohesion, friction angle, and dilatancy angle.

Using preconsolidation stress estimates from Eq. (5.11) developed by Mayne and Brown (2003), cohesion was determined using Mayne and Stewart (1988) and Abdel-Ghaffar (1993) as:

$$c' \approx 0.02\sigma'_p \tag{5.10}$$

$$\sigma'_p = 0.101\sigma_{atm}{}^{0.102} G_0{}^{0.478} \sigma'_{v0}{}^{0.420} \tag{5.11}$$

where,

σ'_p = Preconsolidation stress

σ_{atm} = Atmospheric pressure

G_0 = Small strain shear wave velocity

σ'_{v0} = Overburden effective stress

Friction angle was determined from Eq. (5.8), and dilatancy angle was taken as the friction angle minus 30°. Estimated values for the model parameters are summarized in Table 5.6, Table 5.7, and

Table **5.8** for all CPT sounding. Interface strength at the shaft tip was set to nearly zero to prevent tensile stresses from developing. Although, the estimated values of M, c', φ, and ψ do not show significant variability with respect to depth and CPT location, the analyses considered all estimated values.

Table 5.6: Modified Cam-Clay model parameters from CPT 1 sounding

Layers	Thickness (ft)	λ	κ	M	e_{init}	ν_{ur}	c' (ksf)	φ	ψ
Clay	0-4			1.46				36	6
Clay	4-10			1.37				34	4
Clay	10-16			1.37				34	4
Clay	16-17	0.07	0.02	1.33	0.40	0.20	0.10	33	3
Clay	17-20			1.37				1	0
Clay	20-24			1.37				34	4
Clay	24-28			1.33				33	3
Clay	28-32			1.29				32	2

Table 5.7: Modified Cam-Clay model parameters from CPT 2 sounding

Layers	Thickness (ft)	λ	κ	M	e_{init}	ν_{ur}	c' (ksf)	φ	ψ
Clay	0-4			1.46				36	6
Clay	4-10			1.46				36	6
Clay	10-16			1.37				34	4
Clay	16-17	0.07	0.02	1.33	0.40	0.20	0.10	33	3
Clay	17-20			1.35				1	0
Clay	20-24			1.33				33	3
Clay	24-28			1.33				33	3
Clay	28-32			1.46				36	6

Table 5.8: Modified Cam-Clay model parameters from CPT 3 sounding

Layers	Thickness (ft)	λ	κ	M	e_{init}	ν_{ur}	c' (ksf)	φ	ψ
Clay	0-4			1.46				36	6
Clay	4-10			1.46				36	6
Clay	10-16			1.46				36	6
Clay	16-17	0.07	0.02	1.29	0.40	0.20	0.10	32	2
Clay	17-20			1.29				1	0
Clay	20-24			1.29				32	2
Clay	24-28			1.29				32	2
Clay	28-32			1.29				32	2

The simulation was performed following the same steps used in the preliminary analysis. Simulated and measured load-deformation responses are shown in Figure 5.9, Figure 5.10, and Figure 5.11 for SP-18, SP-21, and SP-24, respectively. It can be seen that model predictions deviate significantly from measured load-displacement responses for all shafts. In all cases, the simulated responses in the elastic range were less stiff than the actual responses observed. As expected from the estimated model parameters, there was negligible differences between simulated responses with respect to the CPT data used. Considering the 1 in. top displacement strength criteria, percent errors between model predictions and measured capacities were 294%, 106%, and 160% for SP-18, SP-21, and SP-24, respectively.

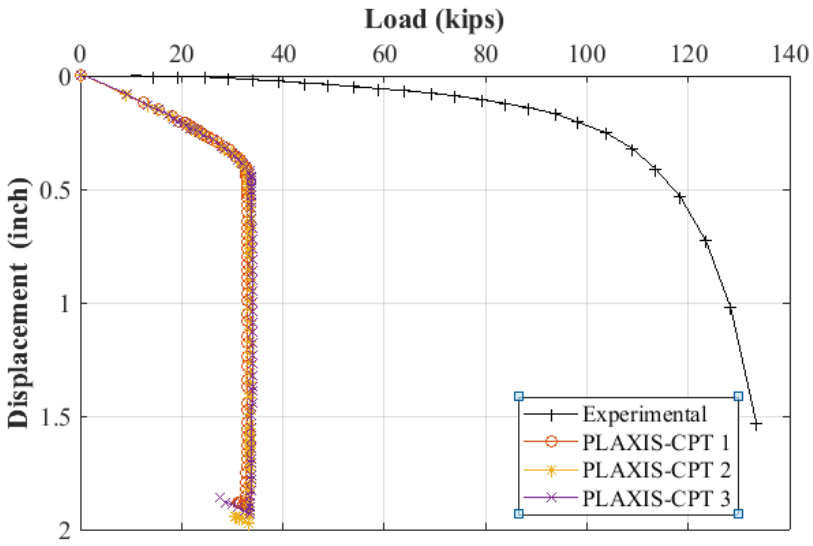

Figure 5.9: Measured vs. predicted load-displacement response for SP-18 shaft using Modified Cam Clay model

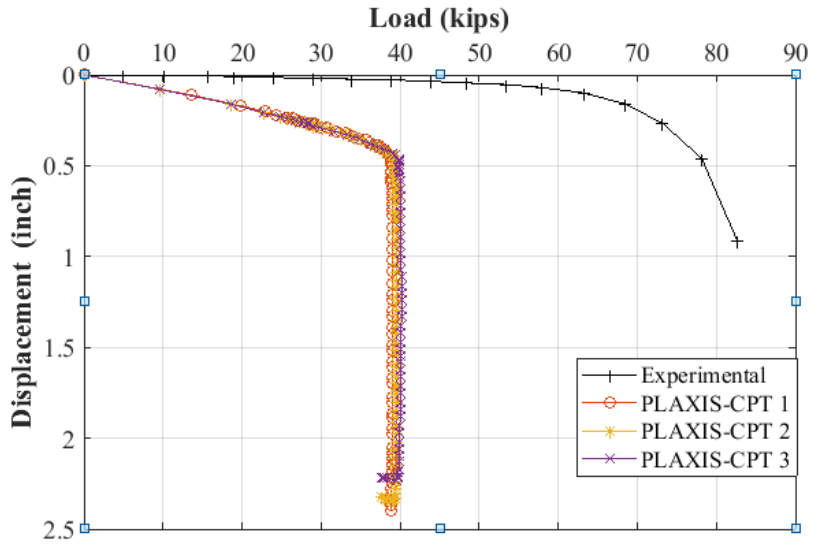

Figure 5.10: Measured vs. predicted load-displacement response for SP-21 shaft using Modified Cam Clay model

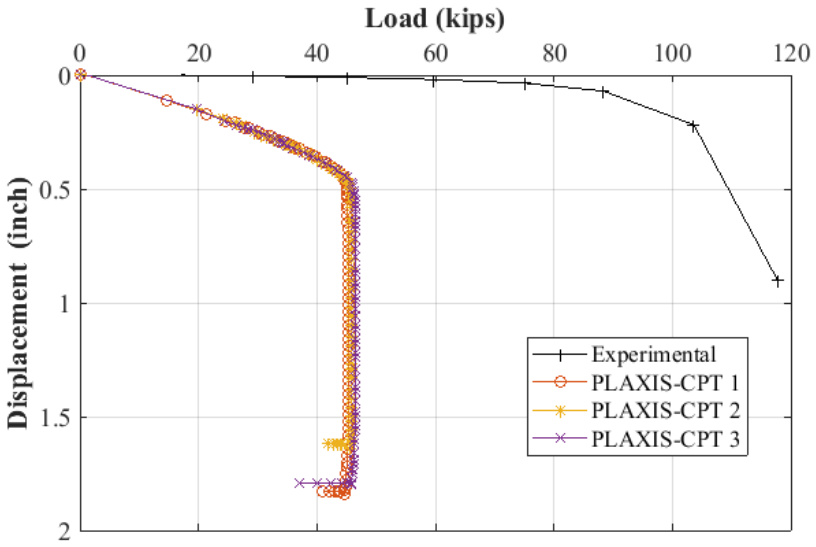

Figure 5.11: Measured vs. predicted load-displacement response for SP-24 shaft using Modified Cam Clay model

In some cases, formation of a gap at the interface between shaft and soil led to convergence issues that prevented full completion of the analysis. It can also be observed that, all simulated responses do not exhibit the same degree of strain hardening observed in the tests. Significant differences between model predictions and actual load-displacement responses can be attributed to inaccuracies involved in the procedure used to estimate the required model parameters. These parameters were determined from various correlations to CPT data and index properties since triaxial and isotropic consolidation test data were not available for direct measurements. These correlations may have led to model properties that are not representative of the site subsurface conditions.

5.6 Summary and Conclusions

The goal of the study presented herein was to investigate the use of the finite element method, via the soil-structure interaction program PLAXIS, to predict load-deformation behavior of drilled shafts and facilitate implementation of a displacement-based design. After using the simpler Mohr-Coulomb in a preliminary analysis, the Modified Cam-Clay model was considered in the refining stage of the models. Model parameters were estimated from correlations to CPT data and index properties determined in the laboratory. Assuming

undrained loading conditions for the glacial till, the load-deformation response of three shafts was simulated and compared to the measured response obtained from load test. The major findings can be summarized as follow:

- In the preliminary analysis, model prediction was greatly influenced by the location of the CPT sounding used to select model parameters. Simulated responses indicate that the actual capacity of the shafts was closer to the remolded rather than the peak undrained shear strength of the soil.
- Adequate predictions of the shafts' load deformation response were achieved in some cases. The most accurate predictions resulted from CPT 1 and 2 data. For SP-18, the models under-predicted the shaft's capacity by 6% and 31% for CPT 1 and average CPT 1 and 2, respectively, considering a strength criteria of 1 in. displacement. For SP-21 and SP-24, prediction errors were 7% and 18%, respectively.
- The use of the Modified Cam-Clay in the refined models did not improve prediction of the shafts' field behavior. In all cases, the models significantly under-predicted the shaft's capacity for a given displacement. This wide divergence between simulated and measured load-displacement responses is likely due to improper model parameters estimated from correlations to available data.
- Although the Mohr-Coulomb model is a simplified representation of soil's behavior, it was able to provide better predictions of the shafts' field behavior compared to the sophisticated Modified Cam-Clay model in this study. Model predictions could have been improved provided that CPT soundings were performed at the actual shaft's locations and interface properties were determined from laboratory direct shear testing of concrete and soil samples from the site. The Modified Cam-Clay model should not be used unless the required parameters can be appropriately determined from triaxial and consolidation test data.

5.7 References

AbdelSalam, S. S., K. W. Ng., S. Sritharan, M. T. Suleiman, and M. Roling. 2012. *Development of LRFD Design Procedures for Bridge Piles in Iowa – Recommended Resistance Factors with Consideration to Construction Control and Setup*. Final Report Vol. III. IHRB Project No. TR-573. Institute for Transportation, Iowa State University, Ames, IA. (http://www.intrans.iastate.edu/research/ reports.cfm).

Brinkgreeve, R. B. J., E. Engin, and W. M. Swolf. 2011. PLAXIS 2D version 2012 manual, Delf. the Netherlands.

Brinkgreeve, R. B. J., S. Kumarswamy, and W. M. Swolfs. 2018. PLAXIS 2D Manuals. Retrieved from https://www.plaxis.com/support/manuals/plaxis-2d-manuals/.

Burland, J. B. 1965. The yielding and dilation of clay. (Correspondence) *Géotechnique*, Vol. 15, pp. 211-214.

Davis, R. O. and A. P. S. Selvadurai. 2002. Chapter 7. Work hardening and modern theories for soil behavior. In *Plasticity and Geomechanics*. Illustrated, Cambridge University Press, ISBN 0521818303, 9780521818308, The Edinburg Building, Cambridge CB2 2RU, UK.

Gouw, T. 2014. Common Mistakes on the Application of Plaxis 2D in Analyzing Excavation Problems. International Journal of Applied Engineering Research, ISSN 0973-4562, Vol. 9, Number 21, pp. 8291-8311.

Kahlstrom, M. 2013. Plaxis 2D Comparison of Mohr-Coulomb and Soft Soil Material Models. MS Thesis. Lulea University of Technology, Lulea, Sweden.

Mayne, P. 2007. *NCHRP Synthesis 368: Cone Penetration Testing*. Transportation Research Board, Washington, D.C.

Nakase, A., T. Kamei and O. Kusakabe. 1988. Constitute parameters estimated by plasticity index. Journal of Geotechnical Engineering, Vol. 114, pp. 844-858.

Robertson, P. K. 2009. Interpretation of cone penetration tests-a unified approach. *Canadian Geotechnical Journal*, Vol. 46, pp. 1337-1355.

Wehnert, M. and P. A. Vermeer. 2004. Numerical analyses of load tests on bored piles. Ninth International Symposium on Numerical Models in Geomechanics-NUMOG IX, Ottawa, Canada, 25-27 August, 2004.

CHAPTER 6. DEVELOPMENT OF RELIABILITY-BASED REGIONAL RESISTANCE FACTORS FOR AXIALLY-LOADED DRILLED SHAFTS

A paper to be submitted to Georisk

Philippe Kalmogo, Sri Sritharan, Jeramy Ashlock

6.1 Abstract

Given the limitations of the American Association of State Highway Transportation and Officials (AASHTO) current specifications for Load and Resistance Factor Design (LRFD) of drilled shafts and the numerous benefits of a regional calibration, preliminary regional resistance factors for drilled shafts used for highway bridges in Iowa were calibrated by Ng et al. (2014) using the developed local database for Drilled Shaft Foundation Testing (DSHAFT). As part of the ongoing effort to develop a more comprehensive regional LRFD procedure for drilled shafts and to continuously refine the regional resistance factors, this study presents reliability-based analyses conducted on an expanded version of DSHAFT. Following the AASHTO LRFD framework and using the First Order Second Moment (FOSM) reliability method, resistance factors are calibrated for clay, sand, Intermediate Geomaterial (IGM), and rock for resistance prediction methods recommended by O'Neill and Reese (1999), Brown et al. (2010), and others. Limitations of the extrapolation methods developed by Ng et al. (2014) in the preliminary calibration are highlighted, and an alternate extrapolation procedure that relies on t-z analyses is proposed and implemented to estimate measured shaft resistance at the selected strength criteria including top displacements of 1 in. and 5% of the shaft diameter. With a focus on Strength I limit state, resistance factors are calibrated for individual side and tip resistance, and results are compared to other studies. Side resistance factors are calibrated using total and layered side resistance approaches, and differences are highlighted. It is shown that resistance factors calibrated using the total side resistance approach tend to be higher compared to those calibrated using the layered approach.

6.2 Introduction

Historically, drilled shafts were traditionally designed following the Allowable Strength Design (ASD) approach due to its relative simplicity. Even though the method

provided a way to incorporate uncertainties in design, its inability to quantitatively account for various sources of uncertainties made it a less desirable approach compared to the LRFD method. To provide a margin of safety against adverse performance of drilled shafts, ASD relies on a single factor of safety to account for the variability and uncertainty associated with the applied loads and geomaterial resistance. The factor of safety is largely dependent upon the designer's engineering judgment and long-term experience, and it could range from 1.2 to 6 depending on the project type and design method used (Withiam et al., 1998). As a result, ASD can lead to over-conservative and costly designs with unknown probability of failure. Additionally, superstructure design has longed moved to the more rational LRFD framework, and the use of ASD for substructure design can result in incompatible reliabilities across various components of a given structure.

Despite the fact that LRFD specifications for foundation design have been introduced in AASHTO code since 1994 to overcome the shortcomings associated with ASD, their adoption by the geotechnical engineering community had been a slow process. This has prompted the Federal Highway Administration (FHWA) to require the use of LRFD for all federally-funded bridges initiated after 2007. However, drilled shaft resistance factors recommended by AASHTO code based on the work of Allen (2005) were developed, as described in AASHTO (2014), "using either statistical analysis of shaft load tests combined with reliability theory (Paikowsky et al., 2004), fitting to allowable stress design (ASD), or both." Engineering judgment was also used to select the final resistance factor when calibration results from the two approaches were significantly different. A major limitation of current code recommendations is evident from the above statement. Current resistance factors recommended by AASHTO still rely on the factor of safety concept, therefore they fail to fulfill the fundamental goal of LRFD to achieve a consistent and compatible level of reliability between substructure and superstructure. Furthermore, statistical analyses were conducted on a general database that incorporated load tests from various regions with different soil conditions. Calibration based on such database may not always result in resistance factors that reflect geological conditions and construction practices specific to a given state or region.

Given the deficiencies associated with code recommendations, the FHWA has permitted and encouraged states to perform regional calibration of resistance factors consistent with AASHTO LRFD calibration framework using locally developed load test databases that take into account state-specific soil conditions and construction practices. While some states such as Iowa still use AASHTO resistance factors for LRFD of drilled shafts, others have transitioned to regionally established design guidelines that fully embody LRFD philosophy concepts. Calibration studies aimed at establishing regional resistance factors for drilled shafts have been conducted by several states including but not limited to Florida, Kansas, Louisiana, Missouri, and Nevada.

The state of Iowa efforts to develop a state-level LRFD procedure for the design and construction of drilled shafts were initiated with the development of the electronic load test database DSHAFT. Microsoft Office Access was used to gather and review various load tests from Iowa and several neighboring states. The initial version of DSHAFT included a collection of thirty two drilled shaft load tests performed in Iowa, Illinois, Minnesota, Missouri, Nebraska, and Tennessee. The database was later expanded to include nine additional load tests from Colorado, Kansas, Kentucky, South Dakota, and Nevada. The expanded database included 28 load tests with sufficient structural, subsurface, testing, and construction details needed for the resistance factor calibration. Using the FOSM reliability method, preliminary resistance factors were calibrated by Ng et al (2014) for skin friction and end bearing using O'Neill & Reese (1999) design methods as well as various analytical methods for end bearing from the literature.

As part of the ongoing effort to continuously refine regional resistance factors for drilled shafts design in Iowa, probability-based reliability analyses using an updated version of DSHAFT are conducted in this study. A total of 8 new O-cell load tests with sufficient information performed in Iowa were reviewed and included in DSHAFT for the new calibration. Limitations of the extrapolation procedures developed by Ng. et al (2014) and those associated with Loadtest procedure to generate equivalent top down load-displacement curve used in the preliminary resistance factors calibration are discussed. An alternative extrapolation method based on the t-z analysis approach is proposed and implemented in this study to quantify measured skin and tip resistance at various failure criteria. Drilled shafts

nominal capacities are predicted using design methods by O'Neill and Reese (1999) and Brown et al. (2010) and others from the literature. Then, statistical parameters required for the calibration are determined and used in the FOSM reliability method to develop resistance factors for side and tip resistance. Two different approaches are adopted in the calibration of resistance factor for side resistance. Results are compared to resistance factors from the preliminary calibration by Ng et al. (2014) and other values found in literature to highlight the improvements achieved from this calibration.

6.3 Sorting of DSHAFT

It is common procedure in calibration studies to group load tests in databases based on the predominant soil type present along the shaft at each load test. This categorization allows the calibration of resistance factors for specific geomaterial type and corresponding design methods. Load test sites are generally classified as clay, sand, mixed, IGM, or Rock. Because of the lack of clear guidelines recommended by AASHTO in this process of sorting load tests, a classification scheme termed the 70% rule was developed by Roling et al. (2010) in the regional calibration of resistance factors for driven piles in Iowa. Based on this criterion, a site is classified as sand or clay if 70% or more of the soil layers along the shaft length is composed of either geomaterial. Otherwise, the site is considered to be mixed. However, a classification based on an average soil profile or based on the most predominant type of soil ignores the true spatial variation of geomaterials which can introduce some errors in the calibrated factors. Additionally, this classification scheme is only applicable to soils, and it does not offer any directions on how to approach test sites underlain by a mix of rock or IGM and soil. Others have sometimes neglected skin friction of soils overlying the bedrock in calibration studies. However, resistance from the overburden soils is not always negligible, and it cannot be neglected without introducing some errors in the calibrated resistance factors.

To overcome these shortcomings, the analyses in this calibration focuses on a layered approach rather than an average soil profile. Strain gauges are routinely installed at soil layer interfaces in a test shaft to establish the load-deformation characteristic of individual soil layers. Using the strain gauge data, the soil profile at a given load test site can be divided into

several shear zones. The database is then sorted based on the geomaterial type in shear zones rather than along the entire shaft length. For instance the site shown in Figure 6.1 would be classified as mixed using an average soil profile classification scheme such as the 70% rule. A layered approach results in two shear zones (top of concrete-SG7, SG3-O-cell) classified as cohesive soil, and five shear zones (SG6-SG5, SG5-SG4, SG4-SG3, O-cell-SG2, SG2-tip) classified as cohesionless soil. Because of the presence of both sand and clay between SG7 and SG6, the shear zone between these strain gauges can be classified as mixed.

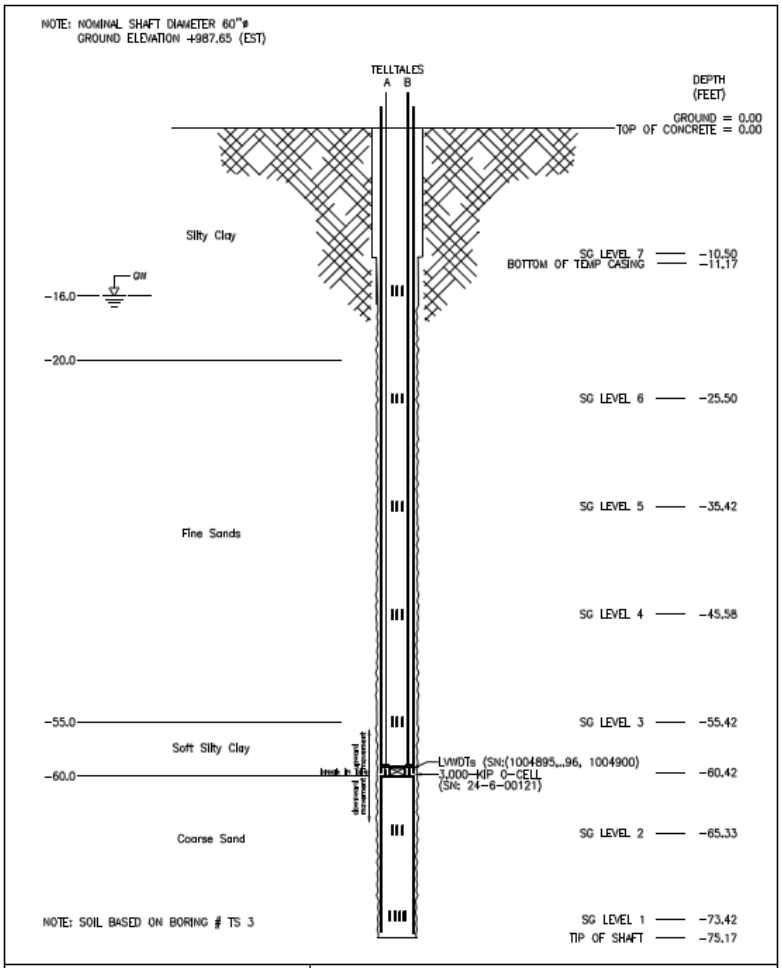

Figure 6.1: DST26 soil profile

Using this approach, DHSAFT results in 35 cohesive shear zones, 53 cohesionless, 27 cohesive IGM, and 22 rock that can be used to calibrate resistance factors for the various design methods recommended in O'Neill and Reese (1999) and Brown et al. (2010).

6.4 Shaft Measured Resistance

The nominal resistance of the shafts various shear zones and base from measured load-displacement curves are required for the calibration of resistance factors. Generally, the nominal resistance can be defined as the ultimate resistance established by one of the several methods available in literature, or as the resistance at a certain displacement of the shaft top. Available methods include but are not limited to Brinch-Hansen's, Butler and Hoy's, Chin's, Davisson's, De Beer's, and Hirany and Kulhawy Method. Since the Iowa DOT defines drilled shafts strength limit state in terms of shaft top displacement, the Iowa DOT 1-inch displacement criterion is used in this study. Resistance factors are also calibrated at the AASHTO criterion corresponding to 5% of the shaft diameter for top displacement so that a direct comparison can be made with code recommended resistance factors. Due to the fact that the majority of the load tests in DSHAFT are terminated before the target displacements are reached, extrapolation is needed to quantify the required resistances. Three different extrapolation procedures were developed by Ng et al. (2014) depending on whether ultimate resistance is achieved in side shear, end bearing, or neither. Case A represents a load test with side shear failure only, Case B a situation where only end bearing reaches ultimate, and Case C a load test in which failure is not achieved in either side shear or end bearing. Illustrations of these cases and respective extrapolation procedures are shown in Figure 6.2 through Figure 6.7.

Although the developed procedures can generate equivalent top load-displacement curve beyond the maximum displacement achieved during load testing, they have some limitations that should be highlighted. By relying on the various static design methods the proposed procedures introduce the uncertainty associated with these methods into the actual measured shaft capacities. The purpose of the calibration to evaluate the accuracy of the design methods at predicting the actual measured resistance is somewhat defeated when uncertainties from the design methods themselves are introduced into the measured resistance. Additionally, extrapolation of the equivalent top load-displacement curve in this fashion is not useful to the calibration of resistance factors using the layered approach. The proposed procedures are not able to provide any information on the load-displacement characteristics of each shear zone.

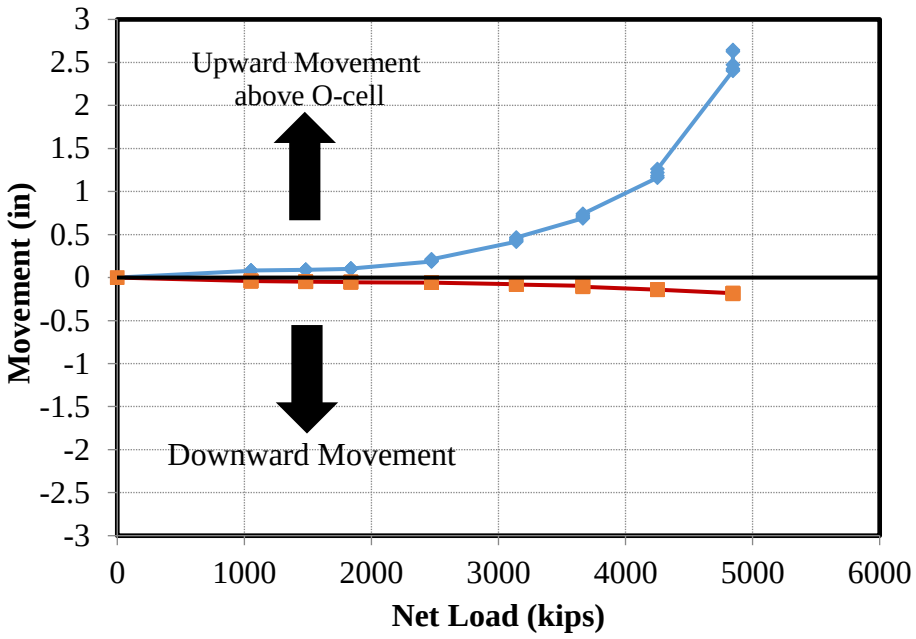

Figure 6.2: Case A, fully mobilized side shear in DST2

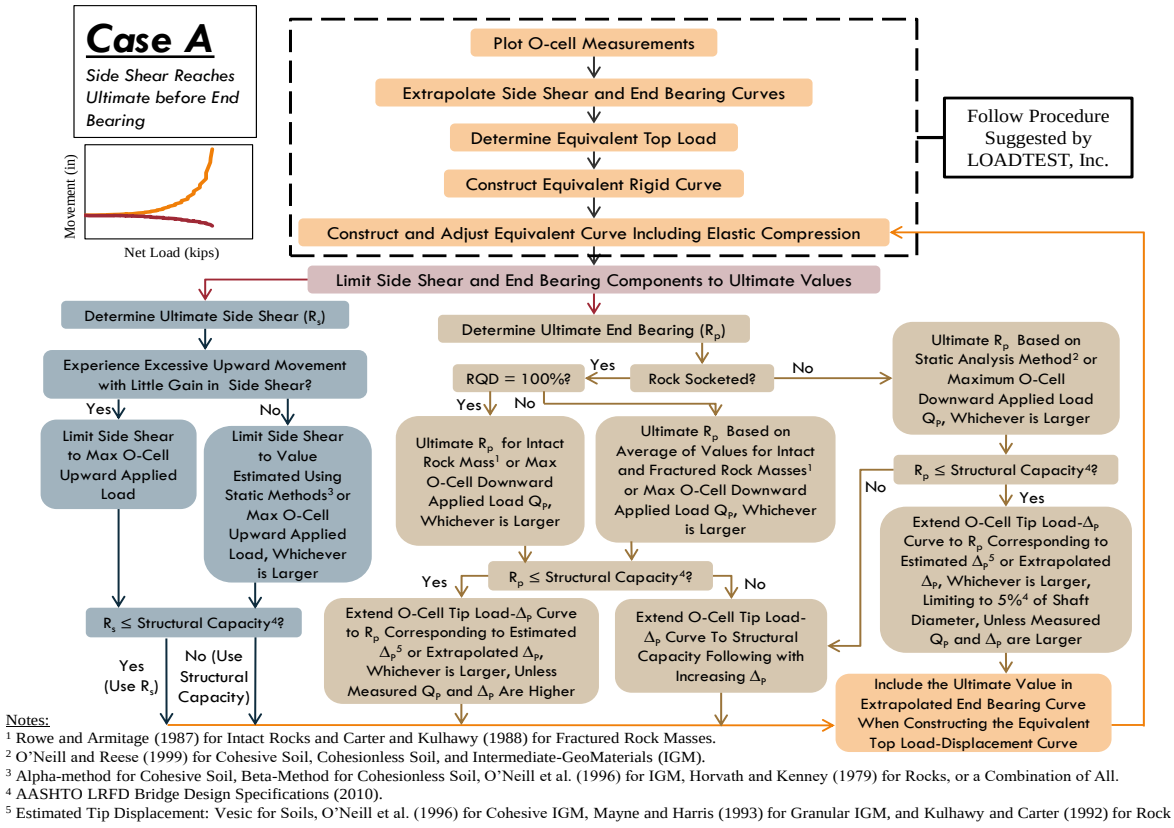

Figure 6.3: Proposed procedure to generate an equivalent top load-displacement curve for Case A (Ng et al. 2014)

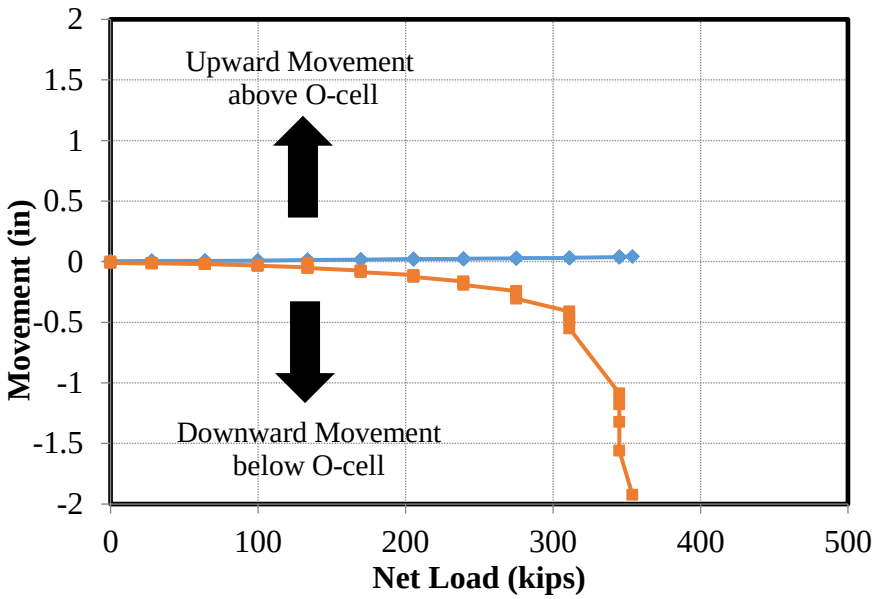

Figure 6.4: Case B, fully mobilized end bearing in DST6

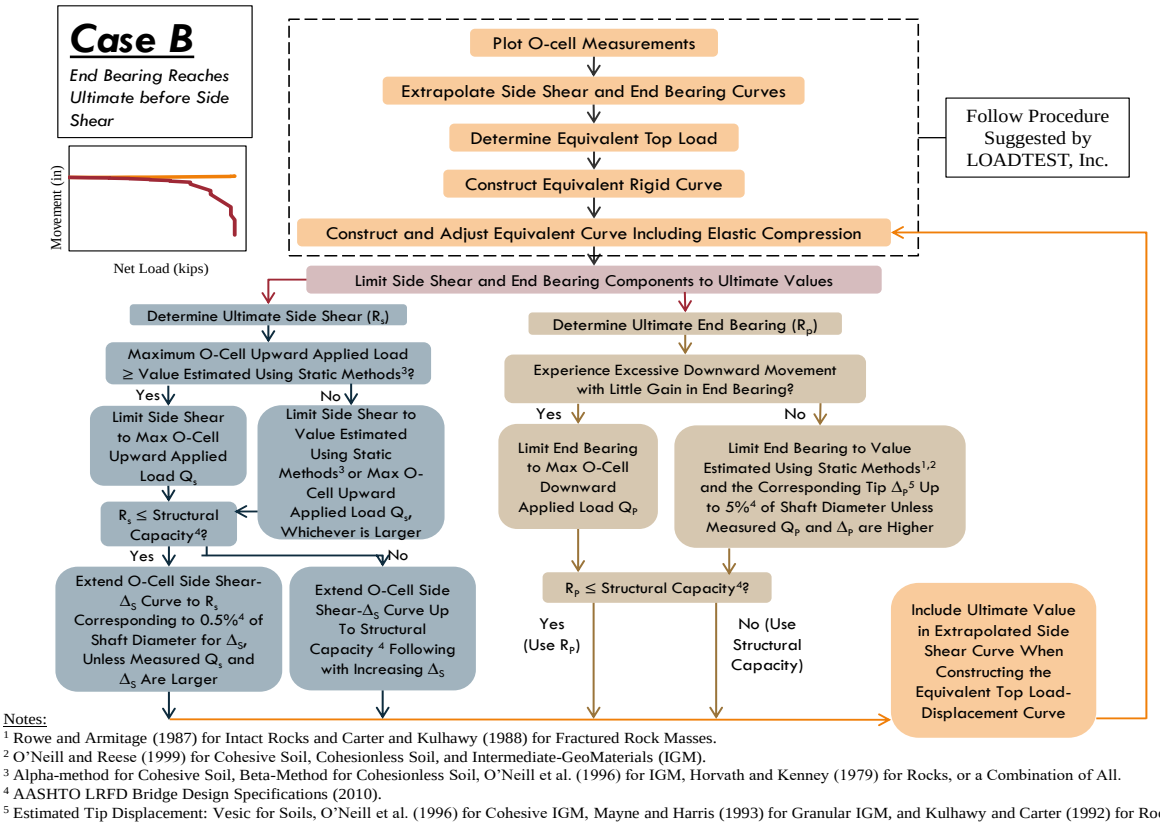

Notes:
[1] Rowe and Armitage (1987) for Intact Rocks and Carter and Kulhawy (1988) for Fractured Rock Masses.
[2] O'Neill and Reese (1999) for Cohesive Soil, Cohesionless Soil, and Intermediate-GeoMaterials (IGM).
[3] Alpha-method for Cohesive Soil, Beta-Method for Cohesionless Soil, O'Neill et al. (1996) for IGM, Horvath and Kenney (1979) for Rocks, or a Combination of All.
[4] AASHTO LRFD Bridge Design Specifications (2010).
[5] Estimated Tip Displacement: Vesic for Soils, O'Neill et al. (1996) for Cohesive IGM, Mayne and Harris (1993) for Granular IGM, and Kulhawy and Carter (1992) for Rock

Figure 6.5: Proposed procedure to generate an equivalent top load-displacement curve for Case B (Ng et al. 2014)

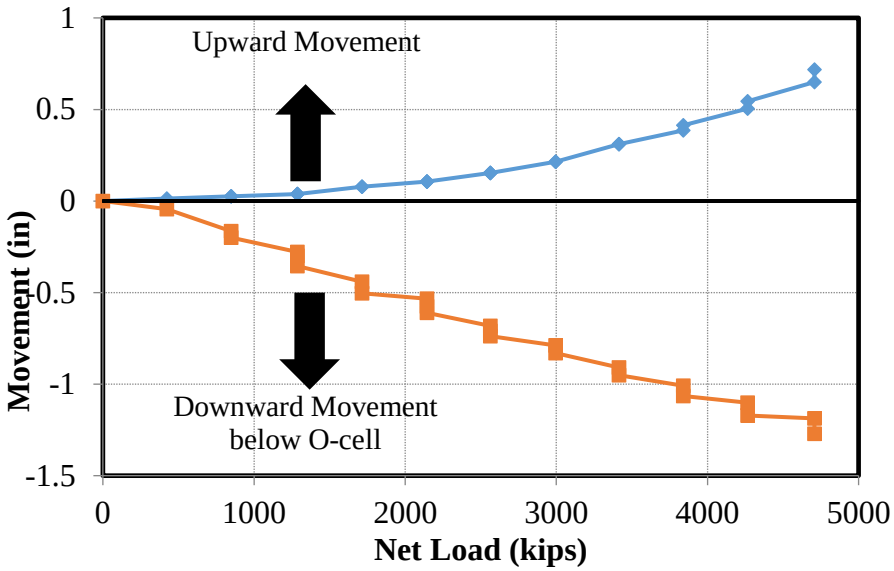

Figure 6.6: Case C, no failure achieved in either side shear or end bearing in DST39

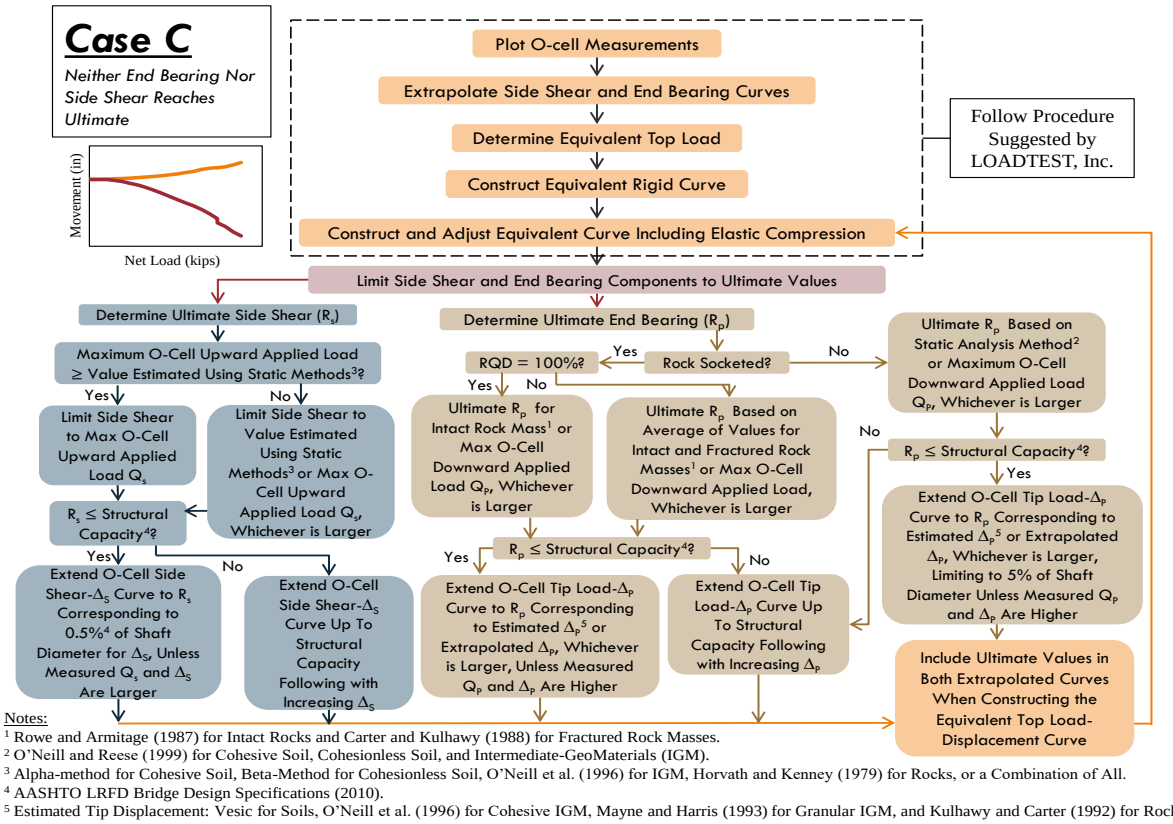

Figure 6.7: Proposed procedure to generate an equivalent top load-displacement curve for Case C (Ng et al. 2014)

To overcome this issue Ng et al. (2014) distributed the extrapolated total measured shaft resistance at a given top displacement among all layers based on their estimated contribution to the overall predicted shaft resistance. The uncertainties in the design methods are introduced once again into the measured capacities.

Given these limitations, a different approach to obtaining the required resistance values for the calibration is adopted in this study. This approach, which is based on the work of Lee and Park (2008) and Meyer et al. (1975), relies on t-z analyses using strain gauge data collected during load testing. Load-deformation behavior of all shear zones are established and used to quantify the mobilized resistance of each zone for a given top displacement with due consideration of the shaft elastic compression. For a given shaft segment i with an associated unit shear resistance t_i as illustrated in Figure 6.8, three governing equations are solved iteratively until convergence of the output and input loads and displacements. The same procedure is repeated for other segments until the complete shaft length is analyzed.

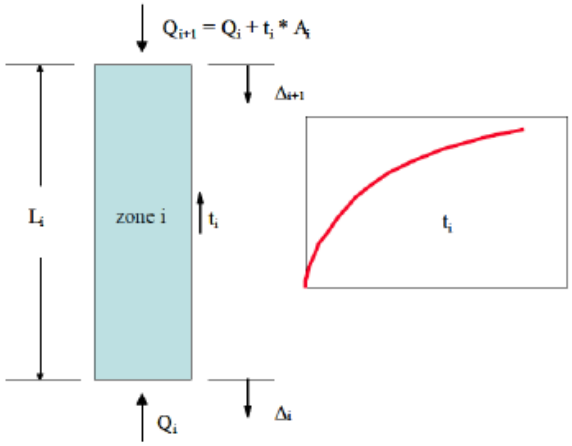

Figure 6.8: Sample shaft section in t-z analyses (Loadtest Inc. 2000)

$$\delta_i = \frac{(Q_i + Q_{i+1})L_i}{2A_iE_i} \tag{6.1}$$

$$\Delta_{i+1} = \Delta_i + \delta_i \tag{6.2}$$

$$Q_{i+1} = Q_i + t\left(\frac{\Delta_i + \Delta_{i+1}}{2}\right)A_i \quad (6.3)$$

where,

δ_i = Elastic compression of section i

Q_i & Q_{i+1} = Load at bottom and top of section i, respectively

Δ_i & Δ_{i+1} = Displacement at bottom and top of section i, respectively

A_i = Cross-sectional area of section i

E_i = Elastic Modulus of section i

It should be noted that the segment at the very bottom of the shaft also has an end resistance component, which must be taken into account in the analysis. When necessary, extrapolation of the unit skin friction or end bearing can be performed using one the functions recommended by Fellenius (2015) that best fit the measured data. Fitting functions include the Ratio Function, the Chin-Kondner Hyperbolic Function, the Exponential Function, the Hansen 80-% Function, and the Zhang Function. The Ratio Function and the Chin-Kondner Hyperbolic Function are best suited for geomaterials that exhibit a strain-hardening behavior. The increase in resistance with larger displacement is more pronounced in the Ratio Function compared to the Hyperbolic Function. The Hansen 80-% Function and the Zhang Function are strain-softening functions, and the Exponential Function is appropriate for geomaterials with an elasto-plastic trend. Because of the importance of the strain gauge data quality in this approach, not all load tests in the database could be used in the calibration.

6.5 Calibration Approach

The calibration requires development of a performance function that incorporates all random variables describing the failure mechanism of a drilled shaft. In the LRFD framework, the strength limit state of a drilled shaft is represented by the following:

$$\sum \gamma_i Q_{ni} \leq \varphi R_n \quad (6.4)$$

where,

γ_i = load factor for load type i

Q_{ni} = load type i

$\sum\gamma_i Q_{ni}$ = sum of factored load

φ = resistance factor

R_n = Nominal Resistance

Eq. (6.4) can be used to develop the performance function needed for the resistance factor calibration. Rearranging Eq. (6.4) and considering only dead load (Q_D) and live load (Q_L) leads to:

$$\varphi R_n - \left(\gamma_{Q_D} Q_D + \gamma_{Q_L} Q_L\right) \geq 0 \qquad (6.5)$$

where,

Q_D = Dead Load

Q_L = Live Load

γ_{Q_D} = Dead Load Factor

γ_{Q_L} = Live Load Factor

If the load and resistance are assumed to be random variables, then the performance limit function corresponding to Equation (2) can be written as:

$$g = R_m - Q_m \qquad (6.6)$$

where, g is a random variable representing the margin of safety, and Q_m and R_m are random variables representing the actual loads and resistance.

The variation of actual load and resistance values from predicted values can be expressed in terms of the bias λ, defined as the ratio of the measured to predicted values. Using this relationship between measured and predicted values, Equation (3) can be rewritten as:

$$g = \lambda_R R_n - \left(\lambda_{Q_D} Q_D + \lambda_{Q_L} Q_L\right) \qquad (6.7)$$

The minimum R_n required to satisfy the limit state design equation is obtained when Eq. (6.7) is equated to zero which represents the boundary line between satisfactory structure performance and adverse performance.

$$R_n = \frac{\gamma_{Q_D} Q_D + \gamma_{Q_L} Q_L}{\varphi} \tag{6.8}$$

Substituting Eq. (6.8) into (6.7) yields:

$$g = \lambda_R \frac{\gamma_{Q_D} Q_D + \gamma_{Q_L} Q_L}{\varphi} - \left(\lambda_{Q_D} Q_D + \lambda_{Q_L} Q_L\right) \tag{6.9}$$

Factoring out Q_L from each term in (6.9) gives:

$$\frac{g}{Q_L} = \lambda_R \frac{\gamma_{Q_D} \frac{Q_D}{Q_L} + \gamma_{Q_L}}{\varphi} - \left(\lambda_{Q_D} \frac{Q_D}{Q_L} + \lambda_{Q_L}\right) \tag{6.10}$$

Redefining g/Q_L as g, the performance function can be written as:

$$g = \lambda_R \frac{\gamma_{Q_D} \frac{Q_D}{Q_L} + \gamma_{Q_L}}{\varphi} - \left(\lambda_{Q_D} \frac{Q_D}{Q_L} + \lambda_{Q_L}\right) \tag{6.11}$$

where,

φ = Resistance factor

λ_R = Resistance bias

λ_{Q_D} = Dead load bias

λ_{Q_L} = Live load bias

Q_D = Dead load

Q_L = Live load

Appropriate values of load and resistance factors must be chosen such that the probability of undesired structure performance, i.e. P ($g < 0$), is less than a predetermined value. Graphically, the calibration consists in the selection of load and resistance factors to achieve a desired target reliability βt which, by definition, represents the number of standard deviations between the mean of the distribution of the performance function g and the failure line represented by $g = 0$ (Figure 6.9). The performance function g can be solved using

various reliability methods including the First Order Reliability Method (FORM), the First Order Second Moment (FOSM) method, or the more complex Monte Carlo simulation. As reported by Paikowsky (2004) and Allen (2005), the difference between the resistance factors calculated from these methods is within 10% with FORM and Monte Carlo simulation providing the highest values.

Upon developing the required performance function, the statistical characteristics of the load and resistance bias factors must be established in the next step of the calibration. The necessary parameters include the mean, standard deviation, and coefficient of variation (COV).

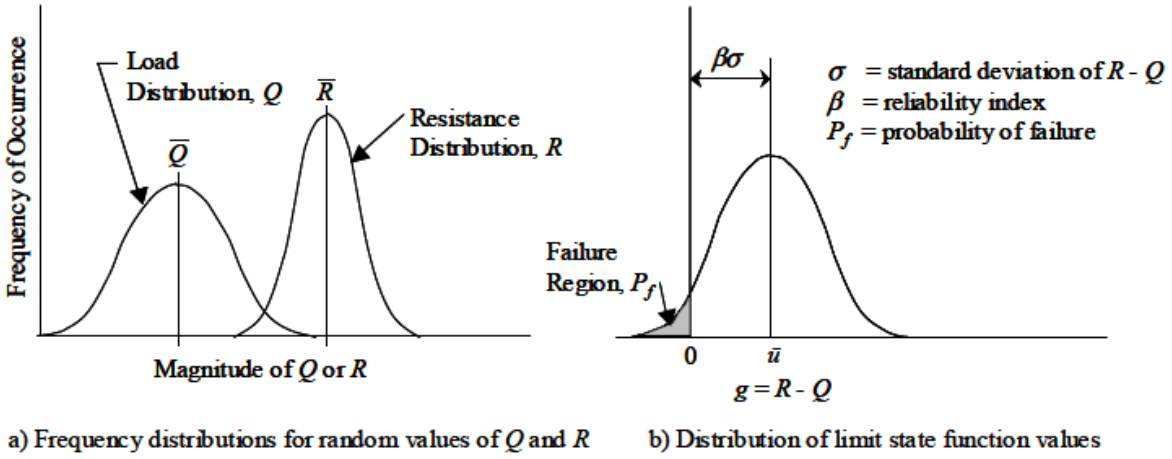

Figure 6.9: Probability of failure and reliability index (Withiam et al., 1998)

Additionally, an appropriate distribution type must be assigned to the load and resistance data upon comparing the shape of their respective histograms generated from observed values with existing theoretical frequency distribution types including but not limited to the normal and lognormal distributions. The assumed distribution type can then be verified using probability plots or statistical tests such as the Anderson-Darling (AD) (1952) normality method or the Pearson's chi-squared ($\chi 2$) test. Because of the lack of research on superstructure loads transfer to the foundation and the difficulty of obtaining such information, the characteristics of the load uncertainties used in superstructure analysis are also used for substructures. Consequently, load factors associated with the Strength I limit state condition recommended by AASHTO are used in this study. The dead and live load

random variables are assumed to follow a lognormal distribution with probabilistic characteristics presented in Table 6.1 (Nowak, 1999).

Table 6.1: Statistical parameters of dead load and live load

Load (Q)	Load Factor (γ)	Load Bias (λ)	Coefficient of Variation (COV_Q)
Dead (D)	1.25	1.05	0.1
Live (L)	1.75	1.15	0.2

The selection of a target reliability needed for the calibration is a function of several factors including but not limited to the desired failure probability, the amount of redundancy present in the foundation system, the level of reliability inherent in past ASD practices, the extent of damage and potential human loss in the event of undesired structure performance, and the design life of the structure. Maintaining a uniform level of reliability across all limit states is also an important aspect to be considered. Although, resistance factors for bridge structural components have been calibrated to achieve a reliability index of 3.5, reliability analyses by Barker et al. (1991) have shown that the previously used factors of safety for foundation design in the ASD framework resulted in reliabilities less than 3.5. Based on their findings, target reliabilities of 3.5, 2.5 to 3.0, and 2.0 to 2.5 were recommended for single shaft supported foundations, non-redundant systems, and highly redundant systems, respectively. Based on Paikowsky et al. (2004), a foundation system with five or more shafts in a group can be considered redundant. Otherwise it is classified as non-redundant. The higher reliability associated with highly redundant systems such as driven pile groups stem from the fact that the failure of a single component in a group may not automatically result in the collapse of the entire foundation. In contrast, a foundation composed of fewer components have a higher probability of failure in the event that a single element fails or is overloaded. In compliance with the above recommendations, AASHTO current resistance factors for drilled shafts were calibrated to achieve a target reliability of 3.0, thus this value is adopted in this study.

Another parameter required in the resistance factor calibration is the dead to live load ratio. This parameter is a function of the bridge span, and it could vary between 1.0 and 4.0. Though a range of 2 to 2.5 and a value of 3.0 were recommended by Paikowsky et al. (2004)

and Barker et al. (1991), respectively, this parameter has been found to have a negligible influence in the calibration. To confirm this observation, values of 2, 2.5 and 3.0 were investigated used in this study.

6.6 Resistance Bias Statistical Characterization

After sorting the database using the approach described in section 6.3 and obtaining the necessary measured and predicted resistances at the failure criteria considered, resistance biases were calculated for each category. Two different methods were used in calculating the resistance bias in the case of skin friction. Though a specific method of calculating the resistance bias has not been explicitly recommended in the AASHTO resistance factor calibration framework, the resistance bias is commonly calculated as the ratio of total measured skin friction to total predicted skin friction. This typical approach could not be used due to the nature of the database used in this study. The load test schematic shown in Figure 6.10 is used to describe the two methods used to compute the resistance bias for skin friction. The soil profile shown is composed of three clay shear zones and three IGM shear zones based on the soil classification and strength properties obtained from subsurface investigation. In the local approach, the resistance bias is calculated for each individual shear zone resulting in three different resistance biases for the clay soil category and three for the cohesive IGM category. The global approach follows the principle of total resistance commonly used in other calibration studies. It uses the sum of the resistance from shear zones of the same geomaterial category. For instance, instead of calculating three different bias values for the clay or IGM category shown in Figure 6.10, a single resistance bias can be calculated for each category as the sum of the measured skin friction to the predicted skin friction. The resistance bias datasets resulting from the two methods used in this study are presented in Table 6.2 and Table 6.3 for Iowa usable load tests only and Table 6.4 and Table 6.5 for all usable load tests. Similarly to Paikowsky et al. (2004), data points that were two standard deviations away from the mean were discarded from the calibration. A few observations can be made from the information presented in these tables. The sample sizes in Table 6.3 and Table 6.5 are considerably smaller than those presented in Table 6.2 and Table 6.4.

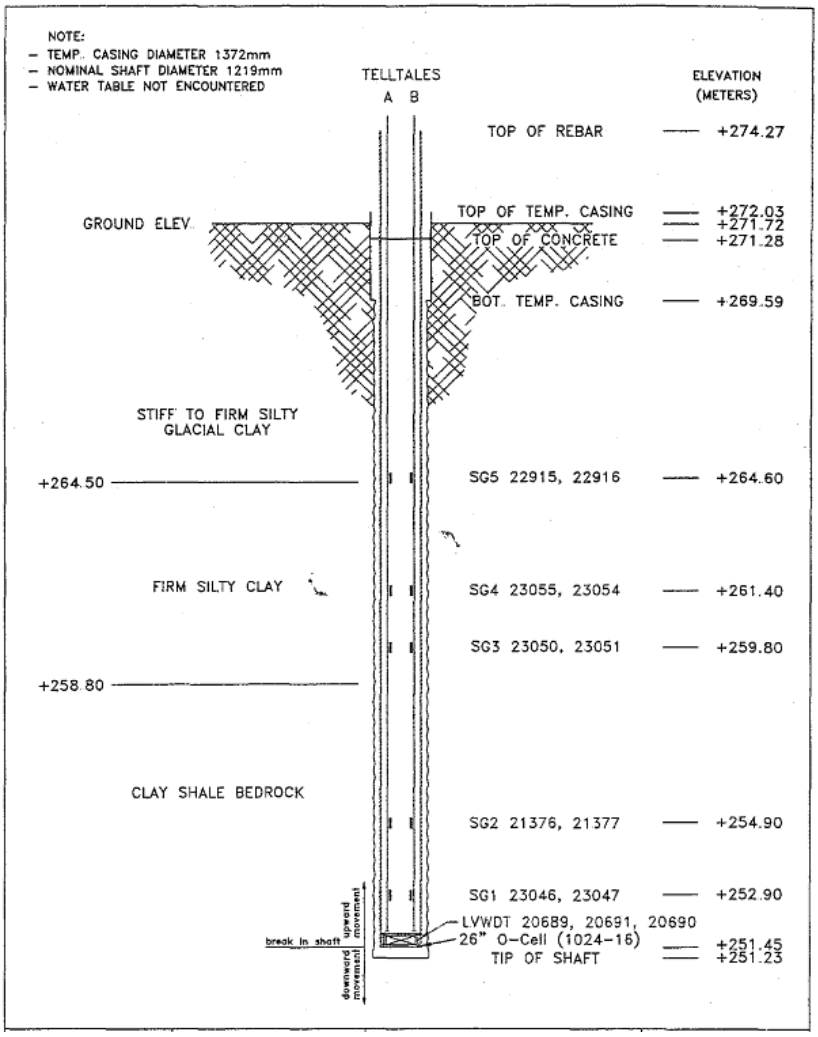

Figure 6.10: DST3 load test schematic

Generally, the two different approaches to the resistance bias calculation lead to different statistical characteristics although identical values were obtained in few cases. The mean values also indicate that all design methods have a tendency to underestimate the skin resistance, with the modified α-method being the most conservative. It can also be observed that resistance bias calculation using the sum of the resistance approach has the general effect of reducing the standard deviation and COV of the bias implying that the uncertainty associated with predicting the skin resistance of individual soil layers is greater than that associated with total skin resistance prediction. Resistance bias were also calculated for end bearing, and the estimated statistical parameters are presented in Table 6.6, Table 7.7, and Table 6.8.

Table 6.2: Skin friction statistical parameters from local approach using Iowa usable load tests

Design Method	1 inch Displacement				5%Diameter Displacement			
	Sample, N	Mean	Standard Dev	COV	Sample, N	Mean	Standard Dev	COV
α-Method	31	1.59	1.02	0.64	29	1.40	0.88	0.63
O'Neill & Reese (1999) β-Method	49	1.21	0.44	0.37	50	1.51	0.62	0.41
Brown et. al (2010) β-Method	51	1.18	0.43	0.37	51	1.44	0.56	0.39
O'Neill & Reese (1999) Modified α-Method	11	2.09	1.43	0.68	11	2.46	1.65	0.67
Horvath & Kenney (1979)	17	2.13	1.17	0.55	17	2.52	1.58	0.63
Kulhawy et al. (2005)	18	1.17	0.67	0.57	18	1.36	0.84	0.62

Table 6.3: Skin friction statistical parameters from global approach using Iowa usable load tests

Design Method	1 inch Displacement				5%Diameter Displacement			
	Sample, N	Mean	Standard Dev	COV	Sample, N	Mean	Standard Dev	COV
α-Method	11	1.31	0.51	0.39	11	1.28	0.53	0.41
O'Neill & Reese (1999) β-Method	9	1.23	0.29	0.24	9	1.51	0.32	0.21
Brown et. al (2010) β-Method	9	1.22	0.37	0.30	9	1.48	0.36	0.25
O'Neill & Reese (1999) Modified α-Method	5	1.88	0.81	0.43	5	2.50	1.63	0.65
Horvath & Kenney (1979)	7	2.10	0.72	0.34	7	2.30	0.99	0.43
Kulhawy et al. (2005)	7	1.06	0.23	0.21	7	1.17	0.40	0.34

Table 6.4: Skin friction statistical parameters from local approach using all usable load tests

Design Method	1 inch Displacement				5%Diameter Displacement			
	Sample, N	Mean	Standard Dev	COV	Sample, N	Mean	Standard Dev	COV
α-Method	31	1.59	1.02	0.64	29	1.40	0.88	0.63
O'Neill & Reese (1999) β-Method	49	1.21	0.44	0.37	50	1.51	0.62	0.41
Brown et. al (2010) β-Method	51	1.18	0.43	0.37	51	1.44	0.56	0.39
O'Neill & Reese (1999) Modified α-Method	25	2.58	1.57	0.61	26	2.85	1.62	0.57
Horvath & Kenney (1979)	21	2.14	1.12	0.52	21	2.52	1.47	0.58
Kulhawy et al. (2005)	21	1.11	0.63	0.57	22	1.29	0.78	0.61

Table 6.5: Skin friction statistical parameters from global approach using all usable load tests

Design Method	1 inch Displacement				5%Diameter Displacement			
	Sample, N	Mean	Standard Dev	COV	Sample, N	Mean	Standard Dev	COV
α-Method	11	1.31	0.51	0.39	11	1.28	0.53	0.41
O'Neill & Reese (1999) β-Method	9	1.23	0.29	0.24	9	1.51	0.32	0.21
Brown et. al (2010) β-Method	9	1.22	0.37	0.30	9	1.48	0.36	0.25
O'Neill & Reese (1999) Modified α-Method	10	2.26	1.15	0.51	11	2.94	1.59	0.54
Horvath & Kenney (1979)	10	2.00	0.74	0.37	10	2.22	0.97	0.44
Kulhawy et al. (2005)	10	0.94	0.30	0.32	10	1.05	0.42	0.40

For end bearing in soil, load tests were grouped in three different datasets including end bearing in clay, end bearing in sand without post-grouting, and end bearing in sand with post-grouting. The sample size is relatively small for all datasets and statistically insufficient for a reliable calibration. At the 1 in. top displacement criterion, there are two data points for end bearing in clay, three for end bearing in sand with no post-grouting, and three for end bearing in sand with post grouting. At the displacement criterion corresponding to AASHTO criterion, there are two data points for clay and for sand with no post-grouting, and only one for sand with post-grouting. Load tests with end bearing in cohesive IGM and rock are grouped into five datasets corresponding to five different design methods. As can be seen from Table 6.7 and Table 6.8, the sample size is relatively small as observed in the case of end bearing in soil. With the exception of the Carter and Kulhawy (1988) method, all design methods for end bearing in rock are on the unconservative side with a large variability in resistance prediction as evidenced by the high COV values. In the case of end bearing in IGM, all methods under-predicted the tip resistance except for the O'Neill and Reese (1999) method at the Iowa DOT 1 in. strength criterion. Similar to end bearing in rock, the COV values are high indicating a large variability in tip resistance prediction. It should be noted that the uncertainty in resistance prediction at the AASHTO strength criterion is generally less than that associated with resistance prediction at 1 in. top displacement.

Table 6.6: Statistical characteristics for end bearing in soil

Design Method	1 inch Displacement				5%Diameter Displacement			
	Sample, N	Mean	Standard Dev	COV	Sample, N	Mean	Standard Dev	COV
Clay, O'Neill & Reese (1999)	2	0.80	1.11	1.38	2	1.08	1.44	1.34
Sand, O'Neill & Reese (1999)	3	0.86	0.23	0.26	2	1.54	0.56	0.36
Sand with Base Grouting, O'Neill & Reese (1999)	3	1.84	0.39	0.21	1	n/a	n/a	n/a

Table 6.7: Statistical characteristics for end bearing in cohesive IGM

Design Method	1 inch Displacement				5%Diameter Displacement			
	Sample, N	Mean	Standard Dev	COV	Sample, N	Mean	Standard Dev	COV
Carter & Kulhawy (1988)	6	24.60	36.49	1.48	6	32.23	45.10	1.40
Ng et al (2014)	6	1.92	2.15	1.12	6	2.76	2.46	0.89
O'Neill & Reese (1999)	6	0.83	0.57	0.68	6	1.32	0.55	0.42
Rowe & Armitage (1987)	6	1.12	1.10	0.98	6	1.62	1.23	0.76
Sowers (1979)	6	2.79	2.74	0.98	6	4.06	3.06	0.76

Table 6.8: Statistical characteristics for end bearing in rock

Design Method	1 inch Displacement				5%Diameter Displacement			
	Sample, N	Mean	Standard Dev	COV	Sample, N	Mean	Standard Dev	COV
Carter & Kulhawy (1988)	6	7.92	10.79	1.36	6	37.17	68.48	1.84
Ng et al (2014)	6	0.33	0.19	0.58	6	0.67	0.37	0.55
O'Neill & Reese (1999)	6	0.31	0.21	0.67	6	0.56	0.21	0.37
Rowe & Armitage (1987)	6	0.26	0.21	0.83	6	0.44	0.20	0.46
Sowers (1979)	6	0.39	0.20	0.52	6	0.83	0.46	0.57

Various techniques were utilized to determine the distribution type that best suit the resistance bias for each data set. For each data set, histograms of observed values were generated and compared to theoretical normal and lognormal distribution fits. An example of such plot is presented in Figure 6.11 for resistance prediction in cohesive soils at the 1-inch strength criterion. The second technique consisted in generating plots of the cumulative distribution functions (CDF) for the calculated resistance bias as well as the theoretical

normal and lognormal distribution fit corresponding to each data group. When plotted against the standard normal variable, a normal distribution follows a straight line while a lognormal distribution follows a curve. The most appropriate distribution can be visually determined from this technique. An example of CDF is shown in Figure 6.12 for resistance prediction in cohesive soils at the 1-inch strength criterion. Using these two techniques, the lognormal distribution was found to be the most suited distribution type in most cases and was adopted for all categories.

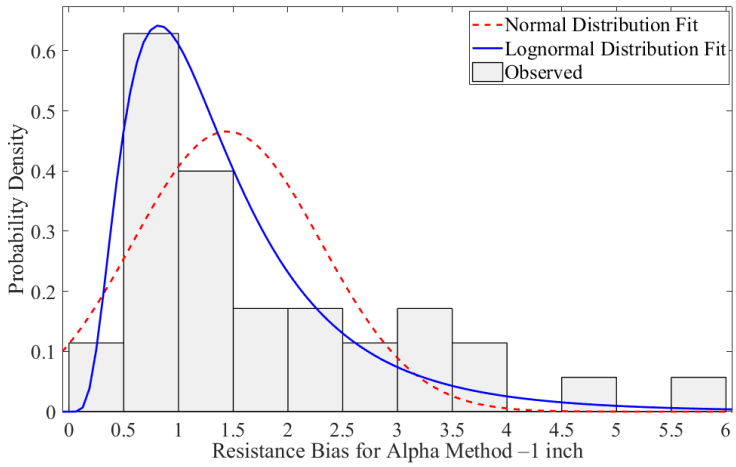

Figure 6.11: Probability density function for α-method at 1 inch strength criterion

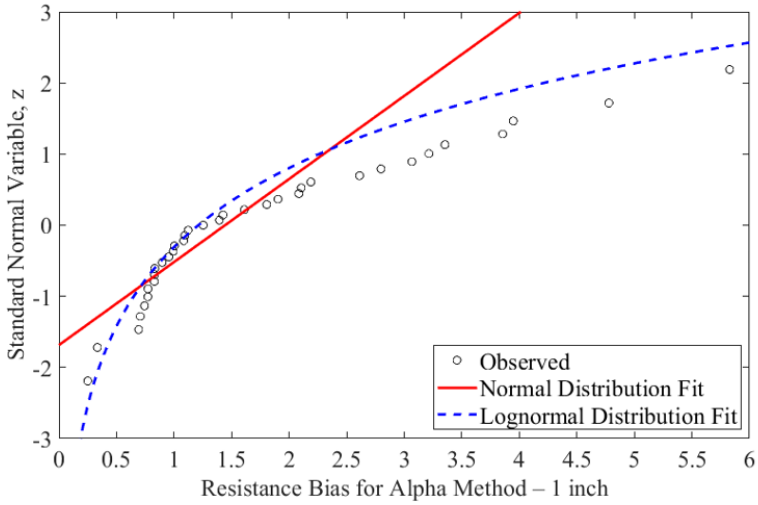

Figure 6.12: Cumulative distribution function for α-method at 1 inch strength criterion

6.7 Resistance Factors

After all required statistical parameters were estimated, resistance factors were calibrated to achieve a target reliability of 3.0 using the performance function and the FOSM reliability method. Efficiency factor defined as the ratio of the resistance factor to the mean resistance bias (φ/λ) was also calculated for each design method so that the true efficiency and economy of the design methods could be investigated.

6.7.1 Skin Friction

Table 6.9 presents resistance factors for skin friction calibrated using the local approach and considering load tests from the state of Iowa only. For skin friction in clay, the resistance factors were found to be 0.29 and 0.26 at the 1 in. top displacement criterion and the AASHTO criterion, respectively. Although a bit higher than the resistance factors established in the preliminary calibration by Ng et al. (2014), the newly calibrated factors do not show any improvements with regards to the code recommended value of 0.45.

For skin friction in sand using O'Neill and Reese (1999) β-method, the calibrated factors were 0.49 and 0.54 for the 1 in. and 5%D top displacement criteria, respectively. These values show an improvement compared to the value of 0.31 recommended in NCHRP 507 by Paikowsky et al. (2004), but they are lower than the resistance factors developed by Ng et al. (2014) in the preliminary calibration. This difference can be attributed to the difference in analysis procedures used. Resistance factors from Ng et al. (2014) were calibrated using the sum of the resistance approach, and the extrapolation technique used in that study differs from the one used in the study herein. For skin friction prediction in sand using the alternate β-method by Brown et al. (2010), the calibrated resistance factors were 0.47 and 0.55 for the 1 in. and 5%D criteria, respectively. Compared to AASHTO recommended value which was established based on a calibration by fitting to a factor of safety of 2.5, the calibrated values in this study do not show any improvement. Efficiency factors indicate that the Brown et al. (2010) method is slightly more efficient than the O'Neill and Reese (1999) method at the AASHTO criteria.

Table 6.9: Summary of resistance factors from local approach considering Iowa usable load tests

Design Method	Geomaterial	Failure Criteria	Resistance Factors at $\beta_T = 3.00$, φ						Efficiency, φ/λ		
			NCHRP 343[e]	NCHRP 507[b]	NHI 05-052[a]	NHI 05-052[c]	AASHTO (2016)[d]	Ng et al. (2014)	This Study	Ng et al. (2014)	This Study
O'Neill & Reese (1999) α-method	Cohesive Soil	Δ=1 in.	n/a	n/a	n/a	n/a	n/a	0.20	0.29	0.11	0.18
		Δ =5%D	0.65	0.36 (φ/λ=0.41)	0.55	0.60	0.45	0.22	0.26	0.12	0.19
O'Neill & Reese (1999) β-method	Cohesionless soil	Δ=1 in.	n/a	n/a	n/a	n/a	n/a	0.48	0.49	0.54	0.40
		Δ =5%D	n/a	0.31 (φ/λ=0.28)	0.52	n/a	n/a	0.47	0.54	0.53	0.35
Brown et al. (2010) β-method	Cohesionless soil	Δ=1 in.	n/a	n/a	n/a	n/a	n/a	n/a	0.47	n/a	0.40
		Δ =5%D	n/a	n/a	n/a	n/a	0.55	n/a	0.55	n/a	0.38
O'Neill & Reese (1999) modified α-method	Cohesive IGM	Δ=1 in.	n/a	n/a	n/a	n/a	n/a	0.63	0.34	0.30	0.16
		Δ =5%D	n/a	0.51 (φ/λ=0.41)	0.55	n/a	0.60	0.69	0.41	0.32	0.17
Horvath & Kenney (1979)	Rock	Δ=1 in.	n/a	n/a	n/a	n/a	n/a	0.55	0.50	0.49	0.24
		Δ =5%D	0.65	n/a	0.55	0.55	0.55	0.62	0.48	0.53	0.19
Kulhawy et al. (2005)	Rock	Δ=1 in.	n/a	n/a	n/a	n/a	n/a	n/a	0.26	n/a	0.22
		Δ =5%D	n/a	n/a	n/a	n/a	0.55	n/a	0.26	n/a	0.19

[a] – calibration by fitting to ASD; [b] – calibration performed using reliability theory (FORM); [c] – calibration performed using reliability theory (Monte Carlo Method); [d] – selected value among NCHRP 343, NCHRP 507 and Allen (2005); [e] – recommended value; n/a – not available; Δ – shaft top displacement; D – shaft diameter

Table 6.10: Summary of resistance factors from global approach considering Iowa usable load tests

Design Method	Geomaterial	Failure Criteria	Resistance Factors at $\beta_T = 3.00$, φ						Efficiency, φ/λ		
			NCHRP 343[e]	NCHRP 507[b]	NHI 05-052[a]	NHI 05-052[c]	AASHTO (2016)[d]	Ng et al. (2014)	This Study	Ng et al. (2014)	This Study
O'Neill & Reese (1999) α-method	Cohesive Soil	Δ=1 in.	n/a	n/a	n/a	n/a	n/a	0.20	0.48	0.11	0.37
		Δ =5%D	0.65	0.36 (φ/λ=0.41)	0.55	0.60	0.45	0.22	0.45	0.12	0.35
O'Neill & Reese (1999) β-method	Cohesionless soil	Δ=1 in.	n/a	n/a	n/a	n/a	n/a	0.48	0.73	0.54	0.59
		Δ =5%D	n/a	0.31 (φ/λ=0.28)	0.52	n/a	0.55	0.47	0.96	0.53	0.64
Brown et al. (2010) β-method	Cohesionless soil	Δ=1 in.	n/a	n/a	n/a	n/a	n/a	n/a	0.59	n/a	0.49
		Δ =5%D	n/a	n/a	n/a	n/a	0.55	n/a	0.85	n/a	0.58
O'Neill & Reese (1999) modified α-method	Cohesive IGM	Δ=1 in.	n/a	n/a	n/a	n/a	n/a	0.63	0.62	0.30	0.33
		Δ =5%D	n/a	0.51 (φ/λ=0.41)	0.55	n/a	0.60	0.69	0.44	0.32	0.18
Horvath & Kenney (1979)	Rock	Δ=1 in.	n/a	n/a	n/a	n/a	n/a	0.55	0.91	0.49	0.43
		Δ =5%D	0.65	n/a	0.55	0.55	0.55	0.69	0.77	0.53	0.34
Kulhawy et al. (2005)	Rock	Δ=1 in.	n/a	n/a	n/a	n/a	n/a	n/a	0.67	n/a	0.63
		Δ =5%D	n/a	n/a	n/a	n/a	0.55	n/a	0.51	n/a	0.43

[a] – calibration by fitting to ASD; [b] – calibration performed using reliability theory (FORM); [c] – calibration performed using reliability theory (Monte Carlo Method); [d] – selected value among NCHRP 343, NCHRP 507 and Allen (2005); [e] – recommended value; n/a – not available; Δ – shaft top displacement; D – shaft diameter

For skin friction in IGM, the calibrated factors of 0.34 and 0.41 show a decrease compared to values recommended by Paikowsky et al. (2004), Ng et al. (2014) and AASHTO.

For skin friction in rock using Horvath and Kenney (1979), the calibrated factors were 0.50 for the Iowa DOT criterion and 0.48 for AASHTO criterion. These values are lower than the resistance factors recommended by all other studies considered. Resistance factors for skin friction in rock using Kulhawy et al. (2005) were found to be 0.26 at 1 in. and 5%D criteria. These resistance factors are considerably smaller than AASHTO recommended value of 0.55. Efficiency factors indicate that the Horvath and Kenney (1979) method is slightly more efficient at the 1 in. criterion.

Considering the load tests from Iowa again, resistance factors were calibrated using the global approach, and the results are presented in Table 6.10. Generally, the resistance factors calibrated in this manner are higher than those calibrated using Approach I, and they show some improvement compared to Paikowsky et al. (2004), Ng et al. (2014) and AASHTO except for a few cases. For skin friction in clay using the α-method, the calibrated factors were 0.48 at the Iowa DOT strength criterion and 0.45 at the at the 5%D criterion. While the calibrated factor at the 5%D criterion was identical to the code recommended value of 0.45, the calibration achieved a 7% increase at the 1 in. displacement criterion.

For skin friction in sand using O'Neill & Reese (1999) β-method, the calibrated factors of 0.73 and 0.96 at the 1 in. and 5%D criteria, respectively, corresponded to a 33% and 75% increase compared to AASHTO value of 0.55. For skin friction in sand using Brown et al. (2010) β-method, the calibration resulted in a 7% increase at the 1 in. criterion and a 55% increase at the 5%D criterion. The O'Neill and Reese (1999) method had higher efficiency factors than the Brown et al. (2010) method.

For skin friction in IGM, the calibrated factor of 0.62 at the Iowa DOT criterion was 3% greater than AASHTO value of 0.60 while no improvement was observed at the 5%D criterion.

For skin friction in rock using Horvath and Kenney (1979), the calibrated factors showed significant improvements compared to AASHTO value of 0.55. The resistance factor

improved by 65% at the 1 in. criterion and by 40% at the 5%D criterion. For skin friction in rock using Kulhawy et al. (2005), the calibration improved the resistance factor by 22% at the Iowa DOT criterion, but no improvement was observed at the 5%D criterion. Efficiency factors indicate that the Kulhawy et al. (2005) is the economical method.

After considering exclusively the load tests from Iowa, resistance factors were recalibrated using all usable load tests in the database. The calibrated factors using the local approach and global approach are shown in Table 6.11 and Table 6.12, respectively. Since all usable load tests for the cohesive and cohesionless soil categories came from Iowa, the resistance factors remain unchanged from the previous analyses.

Following the local approach, the resistance factors obtained for skin friction in IGM were 0.51 and 0.64 at the Iowa DOT and AASHTO strength criteria, respectively, illustrating a 6.67% improvement at the AASHTO criterion. For skin friction in rock using Horvath and Kenney (1979) and Kulhawy et al. (2005) the calibrated factors did not show any improvements with respect to AASHTO recommendations. All resistance factors calibrated using Approach I were lower than those obtained from the preliminary calibration by Ng. et al (2014). Similar to the calibration that considered Iowa load tests only, Approach II leads to higher resistance factors compared to Approach I. For skin friction in cohesive IGM, the calibrated factor was identical to AASHTO value at the Iowa DOT criterion and 18.33% greater than AASHTO value at AASHTO criterion. The calibrated factors associated with Horvath and Kenney (1979) were 43.63% and 32.73% greater than AASHTO value at the Iowa DOT and AASHTO criterion, respectively. No improvement was observed for the Kulhawy et al. (2005).

6.7.2 End Bearing

Due to limited data available for end bearing in soil, reliable resistance factors could not be calibrated for tip resistance in clay and sand. Resistance factors for end bearing in cohesive IGM are presented in Table 6.13.

Table 6.11: Summary of resistance factors from local approach considering all usable load tests

Design Method	Geomaterial	Failure Criteria	Resistance Factors at $\beta_T = 3.00$, φ						Efficiency, φ/λ		
			NCHRP 343[e]	NCHRP 507[b]	NHI 05-052[a]	NHI 05-052[c]	AASHTO (2016)[d]	Ng et al. (2014)	This Study	Ng et al. (2014)	This Study
O'Neill & Reese (1999) α-method	Cohesive Soil	Δ=1 in.	n/a	n/a	n/a	n/a	n/a	0.20	0.29	0.11	0.18
		Δ =5%D	0.65	0.36 (φ/λ=0.41)	0.55	0.60	0.45	0.22	0.26	0.12	0.19
O'Neill & Reese (1999) β-method	Cohesionless soil	Δ=1 in.	n/a	n/a	n/a	n/a	n/a	0.48	0.47	0.54	0.40
		Δ =5%D	n/a	0.31 (φ/λ=0.28)	0.52	n/a	n/a	0.47	0.51	0.53	0.34
Brown et al. (2010) β-method	Cohesionless soil	Δ=1 in.	n/a	n/a	n/a	n/a	n/a	n/a	0.47	n/a	0.40
		Δ =5%D	n/a	n/a	n/a	n/a	0.55	n/a	0.54	n/a	0.38
O'Neill & Reese (1999) modified α-method	Cohesive IGM	Δ=1 in.	n/a	n/a	n/a	n/a	n/a	0.63	0.51	0.30	0.20
		Δ =5%D	n/a	0.51 (φ/λ=0.41)	0.55	n/a	0.60	0.69	0.64	0.32	0.22
Horvath & Kenney (1979)	Rock	Δ=1 in.	n/a	n/a	n/a	n/a	n/a	0.55	0.54	0.49	0.25
		Δ =5%D	0.65	n/a	0.55	0.55	0.55	0.62	0.54	0.53	0.21
Kulhawy et al. (2005)	Rock	Δ=1 in.	n/a	n/a	n/a	n/a	n/a	n/a	0.25	n/a	0.22
		Δ =5%D	n/a	n/a	n/a	n/a	0.55	n/a	0.26	n/a	0.20

(a) – calibration by fitting to ASD; (b) – calibration performed using reliability theory (FORM); (c) – calibration performed using reliability theory (Monte Carlo Method); (d) – selected value among NCHRP 343, NCHRP 507 and Allen (2005); (e) – recommended value; n/a – not available; Δ – shaft top displacement; D – shaft diameter

Table 6.12: Summary of resistance factors from global approach considering all usable load tests

Design Method	Geomaterial	Failure Criteria	Resistance Factors at $\beta_T = 3.00$, φ						Efficiency, φ/λ		
			NCHRP 343[e]	NCHRP 507[b]	NHI 05-052[a]	NHI 05-052[c]	AASHTO (2016)[d]	Ng et al. (2014)	This Study	Ng et al. (2014)	This Study
O'Neill & Reese (1999) α-method	Cohesive Soil	Δ=1 in.	n/a	n/a	n/a	n/a	n/a	0.20	0.48	0.11	0.37
		Δ =5%D	0.65	0.36 (φ/λ=0.41)	0.55	0.60	0.45	0.22	0.45	0.12	0.35
O'Neill & Reese (1999) β-method	Cohesionless soil	Δ=1 in.	n/a	n/a	n/a	n/a	n/a	0.48	0.73	0.54	0.62
		Δ =5%D	n/a	0.31 (φ/λ=0.28)	0.52	n/a	0.55	0.47	0.96	0.53	0.60
Brown et al. (2010) β-method	Cohesionless soil	Δ=1 in.	n/a	n/a	n/a	n/a	n/a	n/a	0.59	n/a	0.47
		Δ =5%D	n/a	n/a	n/a	n/a	0.55	n/a	0.85	n/a	0.57
O'Neill & Reese (1999) modified α-method	Cohesive IGM	Δ=1 in.	n/a	n/a	n/a	n/a	n/a	0.63	0.60	0.30	0.26
		Δ =5%D	n/a	0.51 (φ/λ=0.41)	0.55	n/a	0.60	0.69	0.71	0.32	0.24
Horvath & Kenney (1979)	Rock	Δ=1 in.	n/a	n/a	n/a	n/a	n/a	0.55	0.79	0.49	0.40
		Δ =5%D	0.65	n/a	0.55	0.55	0.55	0.69	0.73	0.53	0.33
Kulhawy et al. (2005)	Rock	Δ=1 in.	n/a	n/a	n/a	n/a	n/a	n/a	0.44	n/a	0.46
		Δ =5%D	n/a	n/a	n/a	n/a	0.55	n/a	0.39	n/a	0.37

(a) – calibration by fitting to ASD; (b) – calibration performed using reliability theory (FORM); (c) – calibration performed using reliability theory (Monte Carlo Method); (d) – selected value among NCHRP 343, NCHRP 507 and Allen (2005); (e) – recommended value; n/a – not available; Δ – shaft top displacement; D – shaft diameter

Table 6.13: Summary of resistance factors for end bearing in cohesive IGM

Design Method	Failure Criteria	Resistance Factors at β_T = 3.00, φ					Efficiency, φ/λ	
		NCHRP 507 [a]	NHI 05-052[b]	AASHTO (2016)[c]	Ng et al. (2014)	This Study	Ng et al. (2014)	This Study
Carter & Kulhawy (1988)	Δ=1 in.	n/a	n/a	n/a	1.71	0.69	0.22	0.03
	Δ=5%D	n/a	n/a	n/a	3.04	1.05	0.30	0.03
Ng et al. (2014)	Δ=1 in.	n/a	n/a	n/a	0.64	0.11	0.58	0.06
	Δ=5%D	n/a	n/a	n/a	0.84	0.26	0.62	0.10
O'Neill & Reese (1999)	Δ=1 in.	n/a	n/a	n/a	0.17	0.13	0.22	0.16
	Δ=5%D	0.57 to 0.65 (φ/λ= 0.44 to 0.48)	0.55	0.55	0.20	0.46	0.21	0.35
Rowe & Armitage (1987)	Δ=1 in.	n/a	n/a	n/a	0.32	0.09	0.33	0.08
	Δ=5%D	n/a	n/a	n/a	0.44	0.22	0.36	0.13
Sowers (1976)	Δ=1 in.	n/a	n/a	n/a	0.64	0.22	0.27	0.08
	Δ=5%D	n/a	n/a	n/a	1.06	0.54	0.33	0.13

[a] – calibration performed using reliability theory (FORM); [b] – calibration by fitting to ASD; [c] – selected value among NCHRP 343, NCHRP 507 and Allen (2005); LTR – load test report criterion; n/a – not available; Δ - shaft top displacement; D – shaft diameter.

Except for the resistance factor associated with O'Neill and Reese (1999) at the AASHTO criterion, all other resistance factors were considerably lower than those obtained in the preliminary calibration because of the differences in analyses and extrapolation procedures. Due to the overly conservative nature of the Carter and Kulhawy (1988) method, the calibration resulted in an unrealistic resistance factor greater than unity at the AASHTO strength criterion. The efficiencies of all methods are noticeably very low except for the O'Neill and Reese (1999). A comparison of the efficiencies, indicates that the O'Neill and Reese (1999) method would be the most economical design method with efficiencies of 0.16 and 0.35 at the Iowa DOT and AASHTO criterion, respectively. The resistance factor of 0.47 associated with this method at the AASHTO criterion is, however, lower than the values recommended by AASHTO (2016), NCHRP 343 (Barker et al. 1991), NCHRP 507 (Paikowsky et al. 2004) and NHI (Allen 2005).

Resistance factors for end bearing in rock are shown in Table 6.14. Similar to end bearing in cohesive IGM, resistance factors and efficiencies in this study were generally much lower than those obtained in the preliminary calibration with the exception of the

resistance factors associated with Carter and Kulhawy (1988). Efficiency values indicates that Sowers (1976) and O'Neill and Reese (1999) are the most efficient design methods at the Iowa DOT strength criterion and AASHTO criterion, respectively. For the Carter and Kulhawy (1988) the calibrated factors do not shown an improvement compared to values recommended by AASHTO (2016), NCHRP 343 (Barker et al. 1991), NCHRP 507 (Paikowsky et al. 2004) and NHI (Allen 2005).

Table 6.14: Summary of resistance factors for end bearing in rock

Design Method	Failure Criteria	Resistance Factors at $\beta_T = 3.00$, φ					Efficiency, φ/λ	
		NCHRP 507 [(a)]	NHI 05-052[(b)]	AASHTO (2016)[(c)]	Ng et al. (2014)	This Study	Ng et al. (2014)	This Study
Carter & Kulhawy (1988)	1-in Δ	n/a	n/a	n/a	0.22	0.28	0.04	0.03
	5%D for Δ	0.45 to 0.49 (φ/λ= 0.37 to 0.38)	0.55[(d)]	0.50[(d)]	0.31	0.36	0.04	0.04
Ng et al. (2014)	1-in Δ	n/a	n/a	n/a	0.36	0.07	0.41	0.20
	5%D for Δ	n/a	n/a	n/a	0.71	0.16	0.68	0.24
O'Neill & Reese (1999)	1-in Δ	n/a	n/a	n/a	0.22	0.05	0.29	0.15
	5%D for Δ	n/a	n/a	n/a	0.35	0.22	0.40	0.40
Rowe & Armitage (1987)	1-in Δ	n/a	n/a	n/a	0.10	0.03	0.30	0.10
	5%D for Δ	n/a	n/a	n/a	0.44	0.14	0.38	0.31
Sowers (1976)	1-in Δ	n/a	n/a	n/a	0.64	0.10	0.30	0.24
	5%D for Δ	n/a	n/a	n/a	1.06	0.19	0.38	0.23

[(a)] – calibration performed using reliability theory (FORM); [(b)] – calibration by fitting to ASD; [(c)] – selected value among NCHRP 343, NCHRP 507 and Allen (2005); [(d)] – based on Canadian Geotechnical Society (1985); LTR – load test report criterion; n/a – not available; Δ - shaft top displacement; D – shaft diameter.

6.8 Summary and Conclusions

The overall goal of the study presented herein was to refine the preliminary resistance factors for the design and construction of drilled shaft in axial compression for the state of Iowa. Following AASHTO LRFD framework, resistance factors were calibrated using an expanded version of DSHAFT. Limitations of the analyses and extrapolation procedures used in the preliminary calibration were highlighted, and a different procedure based on t-z analysis was used to quantify measured shafts' resistances at target top displacements of 1 in. and 5% of the shaft diameter. Using the FOSM reliability method, resistance factors were

calibrated at a target reliability of 3.0 for various skin friction and end bearing prediction methods. Two different procedures i.e., Approach I and Approach II were used in the calibration of skin friction resistance factors. The calibration initially considered load tests performed in Iowa only before including all usable load tests available in the database. The key findings of the study are summarized as follow:

- The statistical characteristics of the resistance bias and resulting resistance factor for skin friction were significantly influenced by the approach used in calculating the resistance bias. The global approach resulted in reduced variability in skin friction prediction as indicated by lower standard deviations. Consequently, the global approach led to higher resistance and efficiency factors compared to the local approach.

- All resistance factors calibrated using the local approach did not show any improvements over AASHTO LRFD Specifications-recommended values with the exception of the resistance factor for skin friction prediction in IGM at 5%D using the O'Neill and Reese (1999) modified α-method.

- For skin friction, the global calibration approach calibration increased the resistance factors at the 5%D strength criterion by 75% and 56% for the O'Neill & Reese (1999) β-method and the Brown et al. (2010) β-method, respectively. At the 1 in. strength criterion, the calibrated factors were 33% and 7% higher than AASHTO recommended values. Efficiency factors indicate that the O'Neill and Reese (1999) method is more economical than the Brown et al. (2010) method. For skin friction in cohesive soil using the α-method, the calibrated factor at the 1 in. criterion showed a 7% increase.

- For skin friction in cohesive IGM and rock, including load test data from other states in the global calibration approach led to lower resistance factors except for the O'Neill and Reese (1999) modified α-method at the 5%D criterion.
  For Iowa data only, the calibrated factors at the 1 in. criterion showed improvements of 3%, 65%, and 22% for the O'Neill and Reese (1999) modified α-method, the Horvath and Kenney (1979) method, and the Kulhawy et al. (2005) method,

respectively. At the 5%D criterion, the calibration increased the resistance factor for the Horvath and Kenney (1979) method by 40%.

For all load test data, the calibrated factors at the 1 in. criterion showed a 44% increase for the Horvath and Kenney (1979) method. At the 5%D criterion, the calibration increased the resistance factor for the O'Neill and Reese (1999) modified α-method and the Horvath and Kenney (1979) method by 18% and 33%, respectively. Efficiency factors indicate that the Kulhawy et al. (2005) method is more efficient than the Horvath and Kenney (1979) method.

- Additional load test data is needed to allow proper statistical characterization of the resistance bias and calibration of resistance factors for end bearing in cohesive and cohesionless soils.

- For end bearing in cohesive IGM and rock, calibrated factors and corresponding efficiency factors were generally low. Among the five methods considered, the most efficient at the 1 in. and 5%D criteria were the O'Neill and Reese (1999) method for cohesive IGM. For rock, the most efficient were the Sowers (1976) method at the 1 in. criterion and the O'Neill and Reese (1999) method at the 5%D criterion.

6.9 References

AbdelSalam, S. S., K. W. Ng., S. Sritharan, M. T. Suleiman, and M. Roling. 2012. *Development of LRFD Design Procedures for Bridge Piles in Iowa – Recommended Resistance Factors with Consideration to Construction Control and Setup*. Final Report Vol. III. IHRB Project No. TR-573. Institute for Transportation, Iowa State Univeristy, Ames, IA. (http://www.intrans.iastate.edu/research/ reports.cfm)

Allen, T. M. 2005. *Development of Geotechnical Resistance Factors and Downdrag Load Factors for LRFD Foundation Strength Limit State Design*. FHWA-NHI-05-052, Federal Highway Administration, U.S. Department of Transportation, Washington, D.C.

American Association of State Highway and Transportation Officials (AASHTO). 2010. *AASHTO LRFD Bridge Design Specifications*. Interim Revision. Fifth Edition, Washington, D.C.

American Association of State Highway and Transportation Officials (AASHTO). 2014. *AASHTO LRFD Bridge Design Specifications*. Interim Revision. Seventh Edition, Washington, D.C.

Barker, R., Duncan, J., Rojiani, K., Ooi, P., Tan, C., and Kim, S. (1991). *NCHRP Report 343: Manuals for the Design of Bridge Foundations*. Transportation Research Board, National Research Council, Washington, D.C.

Bloomquist, D., M. McVay, and Z. Hu. 2007. *Updating Florida Department of Transportation's (FDOT) Pile/Shaft Design Procedures Based on CPT & DTP Data*. Department of Civil and Coastal Engineering, University of Florida, Gainesville, FL.

Brown, D. A., J. P. Turner, and R. J. Castelli. 2010. *Drilled Shafts: Construction Procedures and LRFD Design Methods.* NHI Course No. 132014, Geotechnical Engineering Circular No. 10, National Highway Institute, U.S. Department of Transportation, Federal Highway Administration, Washington, D.C.

Fellenius, B. H. 2015. Using UniPile to fit t-z or q-z functions to load-movement records. Segundo Congreso Internacional de Fundaciones Profundas de Bolivia, Santa Cruz May 12-15, Lecture, 6 p, 2015.

Garder, J., K.W Ng, S. Sritharan, and M. Roling. 2012. *An Electronic Database for Drilled Shaft Foundation Testing (DSHAFT)*. Final Report to Iowa Department of Transportation. Institute for Transportation, Iowa State University, Ames, IA.

Goodman, R. E. 1980. *Introduction to Rock Mechanics*. Wiley, New York.

Green, D., K.W. Ng, K. Dunker, S. Sritharan, and M. Nop. 2012. *Development of LRFD Design Procedures for Bridge Piles in Iowa –Design Guide and Track Examples*. Final Report Vol. IV. Institute for Transportation, Iowa State Univeristy, Ames, IA.

Hassan, K.M, M. W. O′Neill, S. A. Sheikh, and C. D. Ealy. 1997. Design method for drilled shafts in soft argillaceous rock. *Journal of Geotechnical and Geoenvironmental Engineering*, ASCE, Vol. 123, No.3, pp. 272−280.

Horvath, R.G. and T. C. Kenney. 1979. *Shaft Resistance of Rock Socketed Drilled Piers*. Proceedings, Symposium on Deep Foundations, ASCE, New York, pp. 182-214.

Iowa Department of Transportation (Iowa DOT). 2011. *LRFD Bridge Design Manual* Section 6.3: Drilled Shafts. February 22. http://www.iowadot.gov/bridge/manuallrfd.htm

Kulhawy, F.H. and R.E. Goodman. 1980. *Design of Foundations on Discontinuous Rock*. Proceedings, International Conference on Structural Foundations on Rock, Vol. 1, Sydney, Australia, pp. 209–220.

Kulhawy, F. H., and K. K. Phoon. 2006. Some critical issues in Geo-RBD calibrations for foundations. *Proceedings, GeoCongress: Geotechnical Engineering in the Information Technology Age*, ASCE, Reston, VA.

Lee, J., and Y. Park. 2008. Equivalent Shaft Load–Head Settlement Curve Using a Bi-directional Shaft Load Test. *Computer and Geotechnics,* Vol. 35, Issue 2, pp. 124-133.

Meyer, P. L., D. V. Holmquist, and H. Matlock. 1975. Computer predictions for axially-loaded shafts with non-linear supports. *Proceedings of the 7th Offshore Technology Conference, Paper No. 2186, Houston, Texas.*

Ng, W. K., S. Sritharan, and J. C. Ashlock. 2014. *Development of Preliminary Load and Resistance Factor Design of Drilled Shafts in Iowa*. Project 11-410, Institute of Transportation, Ames, IA.

Nowak, A. 1999. *Calibration of LRFD Bridge Design Code*. NCHRP Report 368, Transportation Research Board, Washington, D.C.

O'Neill, M.W. and L.C. Reese. 1999. *Drilled Shafts: Construction Procedures and Design Methods.* Publication No. FHWA-IF-99-025. Federal Highway Administration, Washington, D.C.

Paikowsky, S.G. with Contributions from B. Birgisson, M. McVay, T. Nguyen, C. Kuo, G. Baecher, B. Ayyab, K. Stenersen, K. O′Malley, L. Chernauskas, and M. O′Neill. 2004. *Load and Resistance Factor Design (LRFD) for Deep Foundations*. NCHRP Report 507, Transportation Research Board, Washington, D.C.

Roling, M, S. Sritharan, and M. Suleiman. 2010. Development of LRFD Procedures for Bridge Pile Foundations in Iowa Volume I: An Electronic Database for PIle LOad Tests in Iowa (PILOT). IHRB Project No. TR-573. Institute for Transportation, Iowa State University, Ames, IA.

Rowe, R.K. and H.H. Armitage. 1987. A Design Method for Drilled Piers in Soft Rock. *Canadian Geotechnical Journal,* Vol. 24, pp. 126–142.

Sowers, G.F. 1976. Foundation Bearing in Weathered Rock. *Rock Engineering for Foundations and Slopes,* ASCE, New York, NY, pp. 32-42.

Turner, J.P. 2006. *Rock-Socketed Shafts for Highway Structure Foundations*. NCHRP Synthesis 360, Transportation Research Board, Washington, D.C., 148 p.

CHAPTER 7. CONCLUSIONS AND RECOMMENDATIONS

7.1 Introduction

The load and resistance factor design provides a rational framework to account for design uncertainty and reduce the failure probability of structures to an acceptable level. Given the departure of superstructure design from the formerly used allowable stress design in the early 80's, implementation of LRFD for substructures in general, and drilled shafts in particular, has become imperative to restore and ensure uniformity and consistency in design reliability. Since resistance factors recommended by AASHTO LRFD Specifications for drilled shaft design were not developed from calibration by reliability theory alone, they are not in full compliance with LRFD fundamental concepts. Moreover, these specifications were developed based on a database of load tests from a variety of regions with different soil conditions and construction practices. Consequently, the recommended factors may not accurately reflect conditions specific to any given region, and they may lead to unnecessary design conservatism. The goal of this research was to improve design reliability and efficiency of axially-loaded drilled shafts by developing probability-based regional resistance factors based on an appropriate load test database. The following sections provide a summary of the major findings of this study and recommendations for future research work.

7.2 Calibration Challenges

It was established that, if implemented successfully, a calibration at the regional level is expected to 1) lead to resistance factors that satisfy a consistent and uniform target level of reliability, 2) enable the development of resistance factors for design methods other than those provided by AASHTO specifications, and 3) increase design efficiency and thus reduce foundation cost. Result from calibration studies conducted by other states including Louisiana and Kansas showed, however, that regionally-calibrated factors can also be lower than code-recommended values contrary to one's assumed expectations. Several challenges encountered in the calibration presented in this study may prevent full realization of the expected benefits. These challenges included the following:

- Lack of good quality load test data needed to develop statistical characteristics of the resistance variable that adequately reflect local conditions.
- Need for extrapolation of load test data to estimate measured shafts' resistances needed in the calibration process resulting in additional uncertainty.
- Lack of laboratory testing for direct measurement of soil parameters needed to estimate shafts' resistances.
- Major differences in calibrated resistance factors depending upon whether a segmental or total resistance calibration approach is followed.

It is recommended that state DOTs ensure that future load tests are conducted to large displacements and full mobilization of the shafts' resistances to eliminate the need for extrapolation in the calibration. It is also recommended to dedicate additional resources to laboratory testing of adequate soil samples to determine relevant soil properties at the shafts' locations in order to reduce the use of correlations and facilitate the development of more efficient regional design methods.

7.3 Scale Effect on Skin Friction

The DSHAFT database developed for the resistance factor calibration contains load test data for drilled shafts of various diameter sizes, and it was analyzed to assess the dependency of skin friction on diameter. Plots of normalized shafts' resistances with respect to diameter were generated for geomaterial categories including cohesive soil, cohesionless soil, cohesive IGM, and rock. Significant scatter was observed in the plots, thus any strong correlation between skin friction and diameter could not be established.

Five instrumented small scale drilled shafts were constructed and load tested at two different sites to investigate the influence of diameter size on skin friction. Test data seem to agree with the general consensus that skin friction reduces with increasing shaft diameter. In cohesive soils, a power function fit to the 12 data points showed a strong correlation with a coefficient of determination of 0.81. In cohesionless soil, there were only three data points showing a linear relationship with a coefficient of determination of 0.57. Additional research is needed to further investigate the scale effect phenomena and develop a methodology to extrapolate test results to larger diameter shafts.

7.4 Numerical Modeling of Drilled Shaft Behavior under Axial Loading

The use of the finite element method to predict the behavior of axially-loaded drilled shafts was investigated. Numerical models of three small scale drilled shaft load tests in glacial till were created using the soil-structure analysis program PLAXIS. The models considered the Mohr-Coulomb and the Modified Cam-Clay constitutive models. Model parameters were determined directly and from empirical correlations to the available data including three CPT soundings and index properties from laboratory tests on soil samples. Simulation results showed that the shafts' capacities were closer to the remolded undrained shear strength rather than the peak. The Mohr-Coulomb model using CPT 1 and CPT 2 data provided adequate predictions of the shafts' field behavior. Errors between measured and predicted capacities at 1 in. displacement criterion ranged between 6% and 31%. However, the model was unable to replicate the slight strain hardening observed in the tests. The Modified Cam-Clay model, although more complex than the Mohr-Coulomb model, provided poor predictions. The model significantly underestimated the actual shafts' capacities as a result of possible inaccuracies in the estimated model parameters. It is recommended that the Modified Cam-Clay model should not be used unless the necessary stiffness and strength parameters can be measured from more appropriate laboratory tests including triaxial and isotropic consolidation tests.

7.5 Resistance Factors

Regional resistance factors for the design of drilled shafts in axial compression were calibrated in accordance with AASHTO LRFD framework using an expanded version of the DSHAFT database. It was necessary to use a segmental approach so that resistance factors could be calibrated according to geomaterial types and corresponding design methods. Considering strength criteria of 1 in. and 5%D displacement, resistance factors were calibrated to achieve a target reliability of 3.0. Skin friction resistance factors were calibrated using two different procedures i.e., Approach I and Approach II. The conclusions can be summarized as follow:

- For skin friction, resistance and efficiency factors obtained from Approach II calibration are higher than those from Approach I.

- Except for skin friction in IGM at 5%D using the O'Neill and Reese (1999) modified α-method, all resistance factors calibrated using Approach I did not show any improvement over AASHTO recommended values.
- Approach II calibration increased the resistance factors at the 5%D strength criterion by 75% and 56% for the O'Neill & Reese (1999) β-method and the Brown et al. (2010) β-method, respectively. At the 1 in. strength criterion, the calibrated factors were 33% and 7% higher than AASHTO recommended values. Efficiency factors indicate that the O'Neill and Reese (1999) method is more economical than the Brown et al. (2010) method. For skin friction in cohesive soil using the α-method, the calibrated factor at the 1 in. criterion showed a 7% increase.
- For Approach II calibration using Iowa data only, the calibrated factors at the 1 in. criterion showed improvements of 3%, 65%, and 22% for the O'Neill and Reese (1999) modified α-method, the Horvath and Kenney (1979) method, and the Kulhawy et al. (2005) method, respectively. At the 5%D criterion, the calibration increased the resistance factor for the Horvath and Kenney (1979) method by 40%. Considering all load test data, the calibrated factors at the 1 in. criterion showed a 44% increase for the Horvath and Kenney (1979) method. At the 5%D criterion, the calibration increased the resistance factor for the O'Neill and Reese (1999) modified α-method and the Horvath and Kenney (1979) method by 18% and 33%, respectively. Efficiency factors indicate that the Kulhawy et al. (2005) method is more efficient than the Horvath and Kenney (1979) method.
- For end bearing in cohesive IGM and rock, calibrated factors and corresponding efficiency factors were generally low. Among the five methods considered, the most efficient at the 1 in. and 5%D criteria were the O'Neill and Reese (1999) method for cohesive IGM. For rock, the most efficient were the Sowers (1976) method at the 1 in. criterion and the O'Neill and Reese (1999) method at the 5%D criterion.

7.6 Recommendation for Future Work

In light of the challenges and results of the work presented, the following recommendations are made for further investigation:

- The calibrated factors should be verified as additional load test data become available to ensure that they provide reliable and consistent designs.
- Additional load tests should be conducted in cohesive and cohesionless soils to enable calibration of resistance factors for end bearing in those geomaterials.
- Design efficiency may be further improved by developing design methods from load tests performed in Iowa only and properly determined soil parameters at the shafts' locations. This is particularly important for skin friction prediction in clay and cohesive IGM where efficiency factors were low.
- Given that the scale effect study was not totally conclusive, additional testing that overcome the shortcomings of the experimental field investigations presented here should be conducted. These tests should be executed in strict accordance with ASTM standards. Subsurface characterization should be performed at the planned location for each shaft to ensure any difference in soil conditions can be detected and accounted for in interpretation of test data. Testing should include diameter size ranging between 2.5 ft and 5.5 ft.
- Scale effect investigation should also consider other geomaterial types including cohesive IGM and rock, in which dilatant behavior and increase in normal stress at the shaft/soil interface tend to be more significant.
- The accuracy of the Modified Cam-Clay at predicting shaft's load-deformation responses should be further investigated using model parameters appropriately determined from laboratory tests. The Hardening Soil model should also be investigated as an alternative.